AGH UNIVERSITY OF SCIENCE AND TECHNOLOGY

Faculty of Materials Science and Ceramics

Empa
Materials Science and Technology

Doctoral dissertation

Carbon- and Copper- Based Composites for Virus Removal from Water

M.Eng. Kamila Domagała

Supervisors

Prof. Dr Thomas Graule

Prof. Dr habil. Eng. Dariusz Kata

Cracow, 2021

“If we knew what it was we were doing, it would not be called research, would it?”

– **Albert Einstein** –

Acknowledgements

I would like to express my sincere gratitude to my advisors Prof. Dr Thomas Graule and Prof. Dr hab. inż. Dariusz Kata for their continuous support, motivation and immense knowledge. Their guidance, comments and suggestions were invaluable.

Besides my advisors, I would like to thank Mario for insightful discussions and working together.

Special thanks are going to Caroline who was providing me positive energy, support and friendship.

I especially thank my mum who raised me and provided me with unconditional love and care.

Words fail me to express my appreciation towards my best friend and my love for always sticking by my side. I am grateful also to his family, who all have been supportive and caring.

Table of content

Abbreviations

AC – Activated Carbon

ACFs – Activated Carbon Fibres

BET – Brunauer-Emmett-Teller

BJH – Barrett-Joyner-Halenda

BSF – Biosand filter

CNTs – Carbon nanotubes

CVD – Chemical Vapour Deposition

CCVD – Catalytic Chemical Vapour Deposition

DAL – Double Agar Layer Method

DLVO – Derjaguin-Landau-Verwey-Overbeek theory

DSC – Differential Scanning Calorimetry

EA – Elemental Analysis

ELISA – Enzyme-Linked Immuno Sorbent

GAC – Granular Activated Carbon

HEPA – High Efficiency Particulate Air

ICP-MS – Inductively Coupled Plasma-Mass Spectrometry

IEP – Isoelectric point

IPCR – Immuno Polymerase Chain Reaction

IUPAC – International Union of Pure and Applied Chemistry

LRV – Log_{10} Removal Value

NP(s) – Nanoparticle(s)

MWCNTs – Multi-walled Carbon Nanotubes

NOM – Natural organic matter

PAN – Polyacrylonitrile

pH_{PZC} – Point of Zero Charge

PFU – Plaque Forming Units

POU – Point-of-use

ROS – Reactive Oxygen Species

SARS – Severe acute respiratory syndrome

SEM – Scanning Electron Microscopy

SPR – Surface Plasmon Resonance

SSA – Specific Surface Area

SWCNTs – Single-walled Carbon Nanotubes

qPCR – quantitative real-time Polymerase Chain Reaction

TEM – Transmission Electron Microscopy

TG – Thermogravimetric Analysis

TPD – Temperature Programmed Desorption

UN – United Nations

VdW – Van der Waals interactions

USEPA – United States Environmental Protection Agency

XPS – X-ray Photoelectron Spectroscopy

XRD – X-ray Diffraction

WHO – World Health Organisation

Abstract

Water is one of the most important substances on Earth, the lack of which would entail a real threat to all entities. Nowadays, the world faces many water-related problems, especially the means of to providing basic water services to people. Up to 2.2 billion people worldwide do not have access to clean, drinking water, i.e. free from contaminations like bacteria, viruses, protozoa, heavy metals or dyes [1]. Lack of drinking water, as well as low sanitation and hygiene levels, increase the spreading of waterborne diseases [1,2]. In 2016, 1.2 million people died due to diseases derived from inadequate water, sanitation and hygiene [3]. It is vital to emphasise the importance of investments in sanitation, development of water distribution networks and water treatment infrastructures. Many organizations, such as United Nations (UN) and World Health Organisation (WHO) create and lead programs for monitoring and improving sanitation and water services in the most affected countries. For water treatment purposes, central treatment plants are good solutions, there where exists the possibility of overcoming/ bypassing the limitations of low and middle-income countries (e.g. high cost, damaged piping systems) [4–6]. Another solution are Point-of-use (POU) systems, which allow for the treatment of water at point of the consumption [7]. Such solutions enable averting cross-contaminations. Although these technologies are already in use, there is still room for improvement. Many engineers and scientist around the world are looking for ways to not only improve but also create new solutions for treating water on an easily accessible, more efficient, affordable and easy to maintain manner.

The work presented within this PhD thesis was performed as part of the MultiCarboVir (Reusable multi-walled carbon nanotubes based water filter for virus pathogen removal in developing countries) project, conducted in the years 2018 - 2021, as a collaboration between three partners: the Laboratory for High Performance Ceramics of Empa Dübendorf, the Laboratory for Biointerfaces of Empa St. Gallen and the Department of Process Engineering of Eawag Dübendorf. The MultiCarboVir project aimed at designing and developing a novel adsorption material for water virus removal, testing under different water conditions, as well as providing fundamental understanding of the interactions occurring between the virus and fabricated composite material.

The objective of the following thesis was to develop a safe, economic and effective filtration material that is easy to reactivate and does not require consumables or electricity access for water purification applications in the field of virus removal at the household scale. Based on the assumed costs for material and assembly, the cartridge production cost can be calculated to

be 4000 Euro. The cost of treated water is estimated to be 0.001-0.01 Euro per litre. To this end, cost-effective and widely available substrates of carbon and copper species were utilised to fabricate material composites. Carbon substrates, such as multi-walled carbon nanotubes and activated carbon fibres exhibit high specific surface area and great sorption capabilities, appropriate for water treatment technologies [8–12], while copper species demonstrate antiviral characteristics [13–16]. Activated carbon is widely known and commonly applied in the field of water purification, especially for the removal of, e.g. heavy metals, dyes and odour substances [17–22]. Carbon nanotubes have been reported as a great adsorption material not only for heavy metals and organic contaminations but also for microbes [23–28]. Despite disputes on carbon nanotubes toxicity, promising results published regarding their great virucidal properties motivated us to utilise them in this study [24,29]. Additionally, carbon substrates provide strong Van der Waals interactions with virus particles due to their high Hamaker constant [30,31], which might be profitable in pathogens retention after initial contact [32]. Another advantage of carbon materials, such as activated carbon fibres and carbon nanotubes is the fact that they are useful supports for metal/ metal oxides due to their high chemical and thermal durability. The support structure can hinder or inhibit the release of the attached metal/ metal oxide into the water over long time periods, as well as reduce pressure drop caused by low packing densities [33,34]. Additionally, selected materials having unique thermal properties offer an easy way of composite material thermal regeneration, which can increase its lifetime. The combination of the two above-mentioned substrates, i.e. modifying carbon substrates with copper/ copper(I) oxide, enables attaining extraordinary adsorption properties with a high potential for water treatment technology applications in the form of Cu_2O/ MWCNTs and Cu/ ACFs composites. The assumed working principle of these composite materials is based on the electrostatic adsorption between the positively charged filter material and (mostly) negatively charged viruses [35–39]. The copper species will be vital in creating an enhanced amount of adsorption sites, whereas their positive surface charge provides appropriate electrostatic forces between the filter material and negatively charged viruses. As-received carbon materials and fabricated composites were tested not only for MS2 bacteriophages removal capacity but also for material conditioning and stability. This work provides crucial information on composite fabrication, including a necessary preliminary step of carbon materials functionalisation. Within this work, a two-step method of multi-walled carbon nanotubes purification and functionalisation (treatment with non-oxidative and oxidative acid) and functionalisation of activated carbon fibres by acid treatment followed by Soxhlet purification was developed. We performed three synthesis routes (adsorption of aqueous copper ion, adsorption of copper

hydroxide, and adsorption of copper complex) to obtain Cu_2O/ MWCNTs composites, as well as, one synthesis method (adsorption of aqueous copper ion) for development of Cu/ ACFs. Although the studied pristine MWCNTs were discovered to have discorded properties from those described in literature, they strongly supported the study in understanding mechanisms responsible for bacteriophages inactivation/ removal by MWCNTs-based composites. MWNCTs alone exhibited very low virucidal properties and were released into permeate from the filter. For this reason, more focus was put on activated carbon fibres. The mechanisms and conditions that influence copper ions adsorption onto ACFs were intensively studied. In presented study, as-received and functionalised+ Soxhlet activated carbon fibres exhibited a great potential toward MS2 bacteriophage removal, reaching higher virus removal than results published for granular or powder forms of activated carbon [40–42]. Figure 1 schematically summarises the experimental work performed within presented PhD thesis.

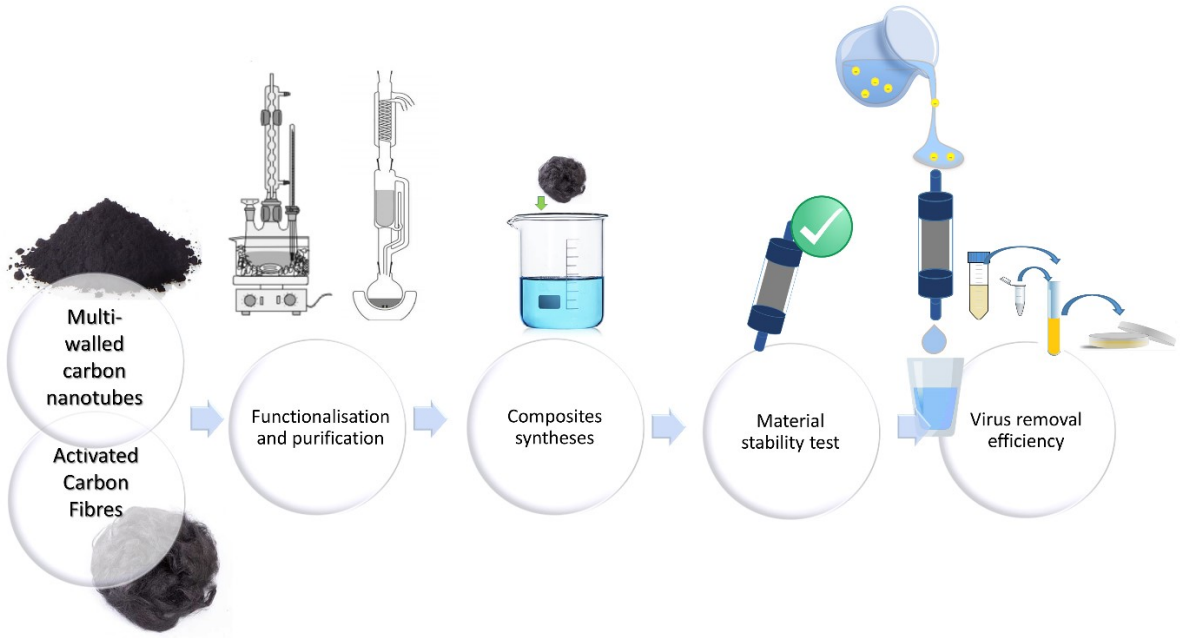

Figure 1 Scheme of performed work within PhD thesis;

The performed work allowed to revise the methods of testing filter or cartridge material for virus removal and procedure of virus concentration evaluation and conclude: (i) the necessity of material conditioning prior to application to obtain its stability, (ii) control the potential release of material elements that might affect material performance and lifetime, (iii) analysis of the time of permeate storage and its composition influence on virus concentration, (iv) analysis of possible mechanisms responsible for the virus inactivation/ removal by tested materials.

There were recognised different mechanisms responsible for virus removal or inactivation by tested materials: electrostatic interactions, Van der Waals forces, hydrophobic and steric repulsions, immediate inactivation of viruses by copper species presented on the material surface, and continued inactivation in permeate due to presence of dissolved copper species. Detailed determination of particular mechanism contribution is a complex process and needs further work. Nonetheless, it is certain that there is no single, dominating mechanism that is always in charge of virus removal.

Abstrakt

Woda jest jedną z najważniejszych substancji na Ziemi, jej brak może spowodować realne zagrożenie dla wszystkich żyjących organizmów. Obecnie świat zmaga się z wieloma poważnymi problemami związanymi z wodą, w szczególności z dostępem wody pitnej dla ludzi. Około 2.2 miliarda ludzi na świecie nie ma dostępu do czystej wody pitnej, tj. wolnej od zanieczyszczeń, takich jak bakterie, wirusy, pierwotniaki, metale ciężkie i barwniki [1]. Czynniki takie jak brak czystej wody pitnej, niski poziom warunków sanitarnych oraz higieny powodują wzrost rozprzestrzeniania się chorób przenoszonych przez wodzę [1,2]. W 2016 roku, 1.2 miliona ludzi zmarło z powodu chorób wywołanych zanieczyszczoną wodą oraz nieadekwatnymi warunkami sanitarnymi i brakiem higieny [3]. Należy podkreślić znaczenie inwestowania w sanityzację, rozwój sieci dystrybucji wody oraz infrastrukturę jej uzdatniania. Wiele organizacji, takich jak Organizacja Narodów Zjednoczonych oraz Światowa Organizacja Zdrowia, tworzą i prowadzą programy monitorowania i poprawy sanityzacji oraz infrastruktury dostarczania wody w krajach najbardziej dotkniętyc tym problemem. W celu oczyszczania wody, centralne stacje uzdatniania wody są dobrym rozwiązaniem, jeśli można przezwyciężyć ograniczenia istniejące w krajach nisko i średnio rozwiniętych (np. wysokie koszty, zniszczone instalacje wodociągowe) [4–6]. Innym rozwiązaniem są systemy Point-of-use (POU), które umożliwiają uzdatnianie wody bezpośrednio w miejscu konsumpcji oraz uniknięcie ponownego jej zanieczyszczenia [7]. Chociaż takie technologie są już stosowane, istnieje wiele możliwości ich dalszego usprawnienia i rozwoju. Wielu inżynierów i naukowców na całym świecie pracuje nad możliwościami nie tylko poprawiającymi obecne technologie, ale także tworzy nowe rozwiązania dla oczyszczania wody w sposób łatwo dostępny, bardziej wydajny, w przystępnej cenie i prosty w obsłudze.

Poniższe badania przedstawione w ramach pracy doktorskiej zostały wykonane jako część projektu MultiCarboVir (Re-usable multi-walled carbon nanotubes based water filter for virus pathogen removal in developing countries - Oparty na bazie wielościennych nanorurek węglowych filtr wodny wielokrotnego użytku do usuwania patogenów wirusowych w krajach rozwijających się), realizowanego w latach 2018 – 2021 w ramach współpracy pomiędzy trzema partnerami: Laboratorium High Performance Ceramics Empa w Dübendorf, Laboratorium Biointerfaces Empa w St. Gallen oraz Department of Process Engineering Eawag w Dübendorf. Celem projektu MultiCarboVir było zaprojektowanie oraz rozwój nowego materiału do filtracji wody usuwającego wirusy, testowanie jego działania w wodzie

pochodzącej z różnych źródeł oraz zrozumienie interakcji występujących pomiędzy wirusami oraz zsyntezowanym materiałem.

Celem poniższej pracy doktorskiej było opracowanie bezpiecznego, ekonomicznego i wydajnego materiału filtra do oczyszczania wody z wirusów możliwego do zastosowania w skali gospodarstwa domowego, łatwego w regeneracji i niewymagającego części eksploatacyjnych lub dostępu do elektryczności. Na podstawie zakładanych kosztów substratów i produkcji, szacowany koszt wytworzenia materiału to 4000 Euro. Przybliżony koszt oczyszczania jednego litra wody jest na poziomie 0.001-0.01 Euro. Stosunkowo tanie i łatwo dostępne substraty węgla i związków miedzi zostały wykorzystane do wytworzenia materiałów kompozytowych. Substraty węglowe, takie jak włókna węgla aktywnego (ACFs) oraz wielościenne nanorurki węglowe (MWCNTs) cechują się wysoką powierzchnią właściwą oraz świetnymi właściwościami sorpcyjnymi, odpowiednimi w technologii oczyszczania wody [8–12], z kolei związki miedzi wykazują charatkterystykę antywirusową [13–16]. Węgiel aktywny jest powszechnie znany i szeroko stosowany w dziedzinie oczyszczania wody, szczególnie w usuwaniu metali ciężkich, barwników oraz substancji zapachowych [17–22]. Nanorurki węglowe są uznawane za dobry materiał sorpcyjny, nie tylko dla metali ciężkich, zanieczyszczeń organicznych ale także dla mikroorganizmów [23–28]. Pomimo kontrowersji na temat toksyczności nanorurek węglowych, ostatnio opublikowane, obiecujące wyniki potwierdzające świetne właściwości antywirusowe nanorurek stanowiły motywację do zastosowania ich w poniższych badaniach [24,29]. Dodatkowo, substraty węglowe wykazują silne wiązania Van der Waalsa z wirusem, z powodu wysokiej wartości stałej Hamakera [30,31], co może być korzystne w przypadku zatrzymywania patogenów po pierwszym kontakcie materiału z wirusem [32]. Kolejną zaletą substratów węglowych, takich jak włókna węgla aktywnego oraz nanorurki węglowe, jest wysoka wytrzymałość. Sprawia to, że są one użyteczną strukturą pomocniczą dla metali/ tlenków metali. Struktura pomocnicza może w długim okresie czasu zahamować lub zwolnić uwalnianie przyłączonego do węgla metalu/ tlenku metalu do wody a także zredukować spadek ciśnienia spowodowany małą gęstością upakowania materiału [33,34]. Dodatkowo, wybrane substraty węglowe posiadają wyjątkowe właściwości termiczne oferując tym samym łatwy sposób regeneracji termicznej materiału, co może zwiększyć jego żywotność. Połączenie dwóch, powyżej wspomnianych substratów, tj. modyfikowanie węglowego materiału miedzią/ tlenkiem miedzi(I) w postaci kompozytów Cu_2O/ MWNCTs oraz Cu/ ACFs, umożliwia uzyskanie wyjątkowych właściwości mających wysoki potencjał zastosowania w technologii uzdatniania wody. Zakładana zasada działania kompozytów bazuje na adsorpcji wywołanej oddziaływaniami elektrostatycznymi pomiędzy

materiałem filtra o ładunku pozytywnym, a wirusami mającymi ładunek ujemny [35–39]. Związki miedzi są kluczowe w tworzeniu zwiększonej ilości aktywnych miejsc, oraz zapewnieniu pozytywnego ładunku, co prowadzi do występowania sił elektrostatycznych pomiędzy materiałem filtra, a negatywnie naładowanymi wirusami. Substraty węglowe oraz zsyntezowane kompozyty zostały przetestowane nie tylko pod kątem wydajności usuwania bakteriofagów MS2 ale także w aspekcie kondycjonowania materiału filtra i jego stabilności. Poniższa praca prezentuje kluczowe informacje w zakresie syntezy kompozytów, włączając konieczny, wstępny krok sfunkcjonalizowania substratów węglowych. W toku pracy została opracowana dwustopniowa metoda oczyszczania i funkcjonalizowania wielościennych nanorurek węglowych (działanie odpowiednio nieutleniającym, następnie utleniającym kwasem) oraz funkcjonalizowania włókien węgla aktywnego poprzez działanie kwasem i oczyszczanie aparatem Soxhleta. Opracowano trzy sposoby syntezy (adsorpcja jonu miedzi, adsorpcja wodorotlenku miedzi, adsorpcja kompleksu miedzi) otrzymywania kompozytu Cu_2O/ MWNCTs, a także jedną metodę syntezy (adsorpcja jonu miedzi) dla kompozytu Cu/ ACFs. Mimo, że nanorurki węglowe wykazały właściwości niespójne z informacjami opisanymi w literaturze, mocno wsparły badania w zrozumieniu mechanizmu odpowiedzialnego za inaktywację i usuwanie bakteriofagów przez kompozyty, do syntezy których zostały użyte. Wielościenne nanorurki węglowe wykazały słabe właściwości antywirusowe i były wymywane z materiału filtra do filtratu. Z tego powodu skupiono się na włóknach z węgla aktywnego. Zbadano mechanizm oraz warunki wpływające na adsorpcję jonów miedzi na włókna węgla aktywnego. Niezmodyfikowane oraz sfunkcjonalizowane włókna węgla aktywnego wykazały wysoki potencjał usuwania bakteriofagów MS2, uzyskując wyższe wartości usuwania wirusów niż opublikowane wyniki dla węgla aktywnego w postaci granulek lub proszku [40–42]. Figura 2 przedstawia prac eksperymentalnych wykonanych w ramach poniższej pracy doktorskiej.

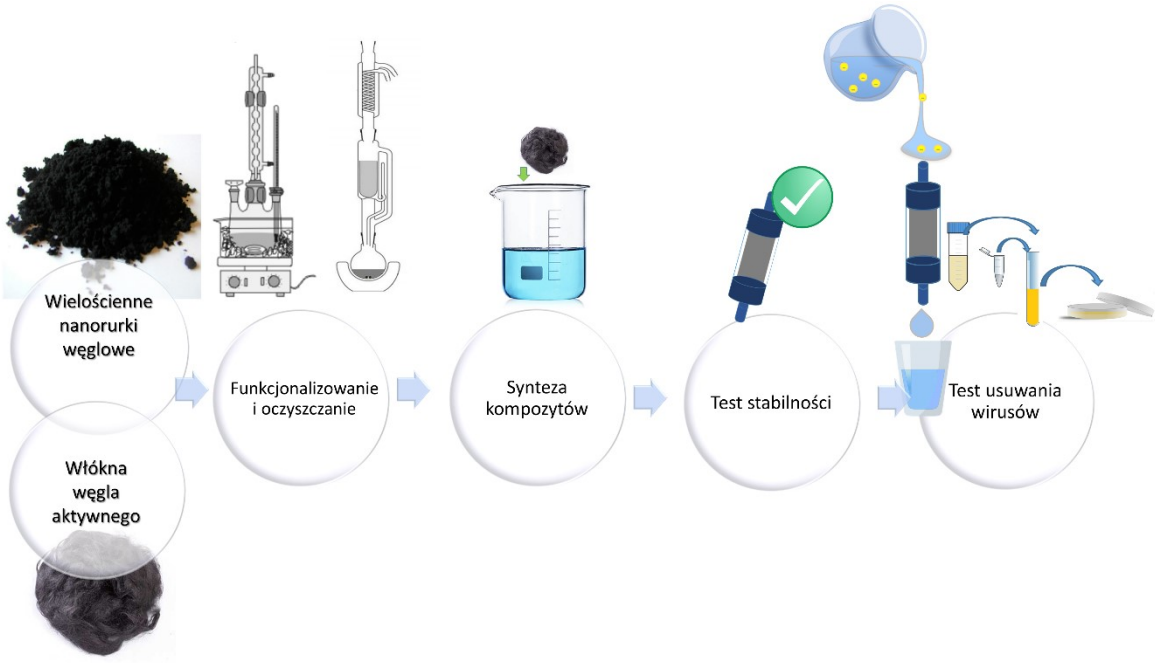

Figure 2 Schemat pracy wykonanej w ramach poniższej pracy doktorskiej;

Wykonane badania pozwoliły zrewidować metody testowania materiału filtracyjnego w aspekcie usuwania wirusów oraz procedury oceny stężenia wirusów. Można wywnioskować: (i) konieczność kondycjonowania materiału przed właściwym zastosowaniem by osiągnąc jego stabilność, (ii) kontrolę potencjalnego uwalniania elementów kompozytu, które mogą wpływać na wydajność i żywotność materiału; (iii) ocenę wpływu czasu przechowywania oraz składu filtratu na stężenie wirusów, (iv) analizę mechanizmów odpowiedzialnych za dezaktywację/ usuwanie wirusów przez testowane materiały.

W wyniku badań zostały rozpoznane różne mechanizmy odpowiedzialne za usuwanie oraz inaktywację wirusów poprzez testowane materiały: elektrostatyczne interakcje, siły Van der Waalsa, hydrofobowe oraz steryczne oddziaływania, bezpośrednia inaktywacja wirusów ze związkami miedzi obecnymi na powierzchni kompozytu, ciągła inaktywacja w filtracie z powodu obecności wymytych związków miedzi. Dokładne określenie udziału poszczególnych interakcji jest skomplikowanym procesem i wymaga dalszych badań. Niemniej jednak, jest pewnym, iż nie istnieje jeden dominujący mechanizm, który jest odpowiedzialny za usuwanie wirusów.

I Theoretical Review

1. Problems with drinking water around the world

Water is an essential and substantial ingredient for all beings, as well as core of socio-economic world development. It is the most important resource that connects every aspect of life and guarantees that our environment can work properly.

Water is an abundant resource on earth, 97.5 % of it constitutes saline water, while only 2.5 % of water is fresh. 68.7 % of fresh water is locked up in glaciers and less than 0.5 % of fresh water is available for humans [43]. Figure 3 presents the global distribution of water indicating that limited water quantities are accessible for consumption. Global water resources are threatened due to strong climate change that affects water availability and its temporal and spatial distribution [3]. Such changes lead to an increasing number of water-related disasters, e.g. droughts, floods, landslides and storms, strongly impacting water availability and also introduces contaminants into the water [3,44]. Around four billion people experience water scarcity for at least one month per year due to the situation exacerbated by climate change [3].

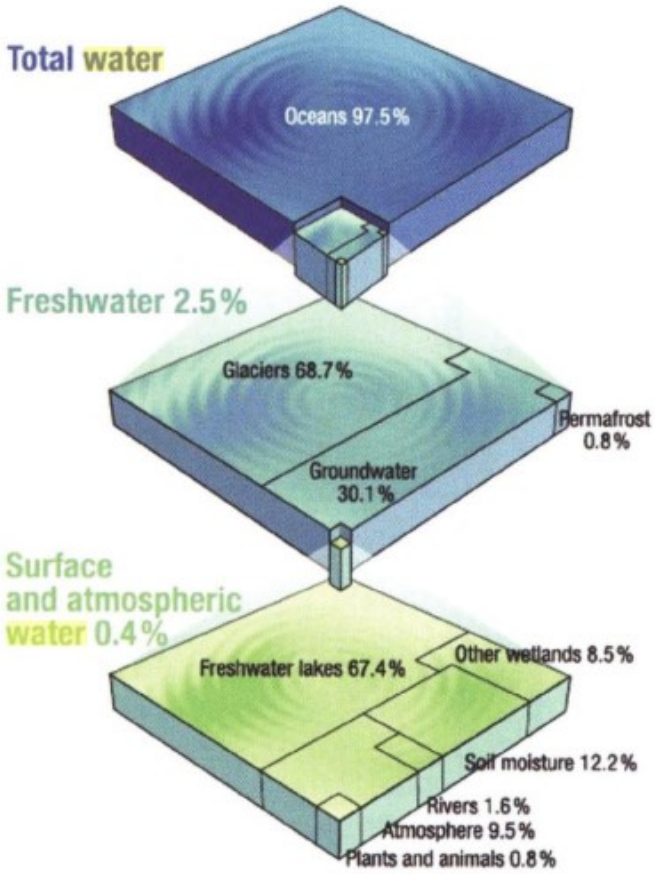

Figure 3 Global distribution of the world's water [43];

Despite the enormous improvement in life quality, awareness about health, environment concern and continuous development of water supplies, billions of humans still do not have access

to the clean drinking water. Furthermore, global water use has increased by factor of six over the past 100 years and continuous to grow of about 1 % per year, due to increasing population, economic development and shifting consumption patterns [3].

Moreover, the world's fresh water resources pollution is increasingly exposed to organic waste, pathogens, fertilizers and pesticides, heavy metals and emerging pollutants [3]. The source of organic matter pollutants is continuously growing, due to municipal and industrial wastewater discharge, agriculture intensification and reduction in water dilution capacity. Pathogen contamination is the most common water quality problem in developing countries caused by unsafe water and low sanitation [3].

According to the report (Figure 4) published by World Health Organization in 2017, nearly 29 % of the global population lacks access to safely managed drinking water services [1].

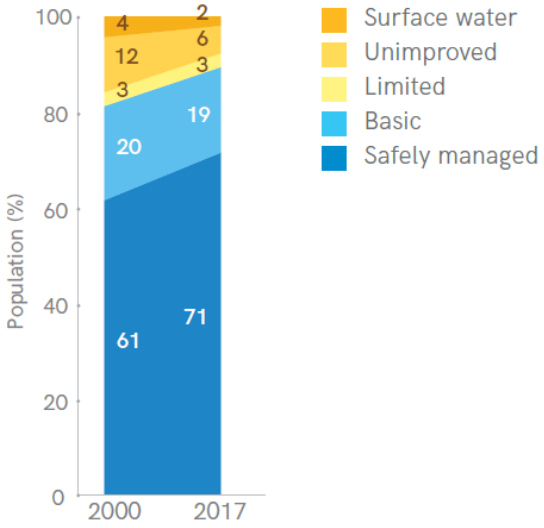

Figure 4 Global drinking water coverage 2000-2017 (%) [1];

Safely managed drinking water services stand for accessible on premises (located within the dwelling, yard or plot), available when needed (sufficient amount of water available for at least 12 h per day) and free from contaminations (compliant with standards for faecal, chemical contaminations) [1]. The mentioned number means that eight out of ten people used improved sources with water available when needed, three out of four people (5.4 billion) used improved sources located on premises and free from contaminations [1]. 435 million people take water from unprotected wells and springs, while 144 million people are dependent on untreated surface water (lakes, ponds, rivers, streams) [1]. It is estimated that at least 2 billion people use a drinking water source contaminated with faeces [1].

Figure 5 presents data regarding the sanitation and handwashing level globally in 2017. According to that study, only 45 % of population (3.4 billion) use safely managed sanitation facilities, while 9 % (627 million people) still practise open defecation. 60 % of global population have basic handwashing facilities with soap and water available at home. Contaminated water together with poor sanitation and improper wastewater treatment are a source of wide spreading water-related diseases and deaths. Bacteria and viruses present in water cause the occurrence of many waterborne diseases such as diarrhea, cholera, hepatitis A and polio. It was estimated that 3.2 % of global deaths are caused by unsafe water [1]. Bacteria are widely considered as a source of diseases, however viruses are less acknowledged to have an impact on human health [45]. Viruses are the smallest pathogens, which infective dose is very low, making them difficult to detect and inactivate [44].

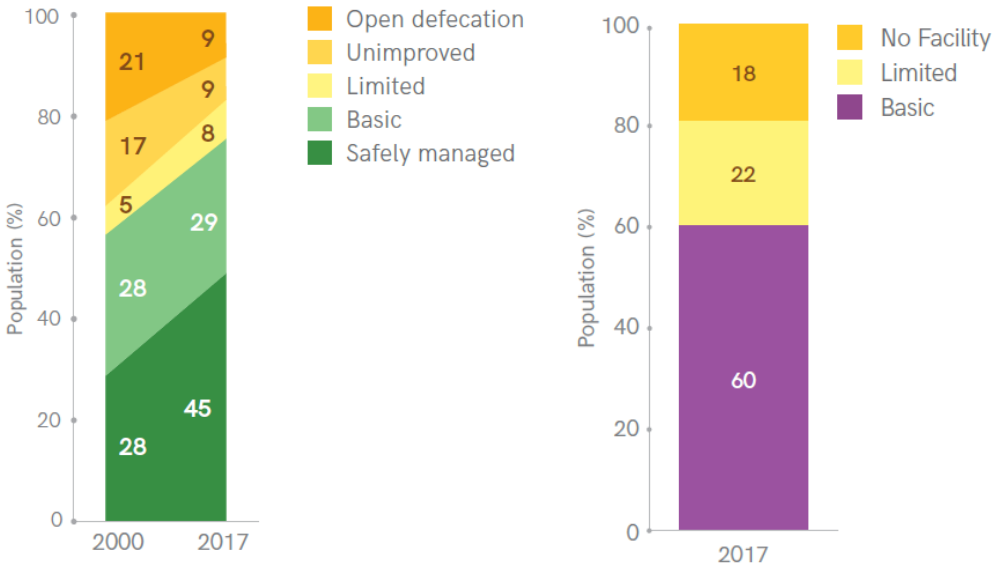

Figure 5 Global sanitation (right) and handwashing (left) coverage in 2017 [1];

2. Viruses

2.1. Virus characteristics

The first entry regarding viruses appeared 120 years ago and was described as a transmissible agent that causes disease in animals and plants [45]. Figure 6 schematically depicts a virus structure. Viruses consist of a capsid (protein coat), which encircles nucleic acid (RNA or DNA).

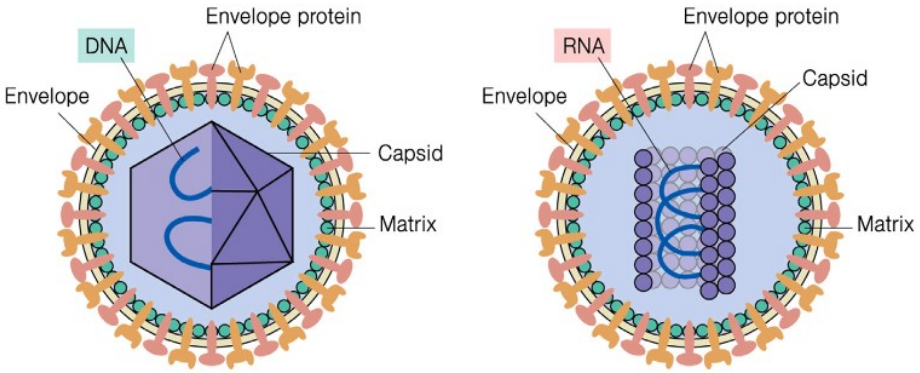

Figure 6 Schematic diagram of virus particles (left – a typical envelope virus particle with a spherical capsid and DNA viral genome; right – a typical envelope virus particle with a helical capsid and RNA viral genome) [46];

The amino acids in protein coat contain weakly acidic and basic groups, like carboxyl and amino groups, which determine the virus particle amphoteric nature [47]. The capsid plays a protective role, sequestering the genome material from physical and chemical damaging agents [46]. Another function is to recognise the cellular receptor for the entry and delivery of the viral genome to the site of genome replication. There are two shapes of capsid structure, i.e. spherical and helical. Some pathogens additionally have an outer envelope composed of a lipid bilayer, which is derived from cell membranes, and virally coded envelope proteins [46].

Viruses are the smallest pathogens (Figure 7) (~10-300 nm) and thereby the most difficult to remove from water [48,49]. Their size is about 10-100 times smaller than bacteria.

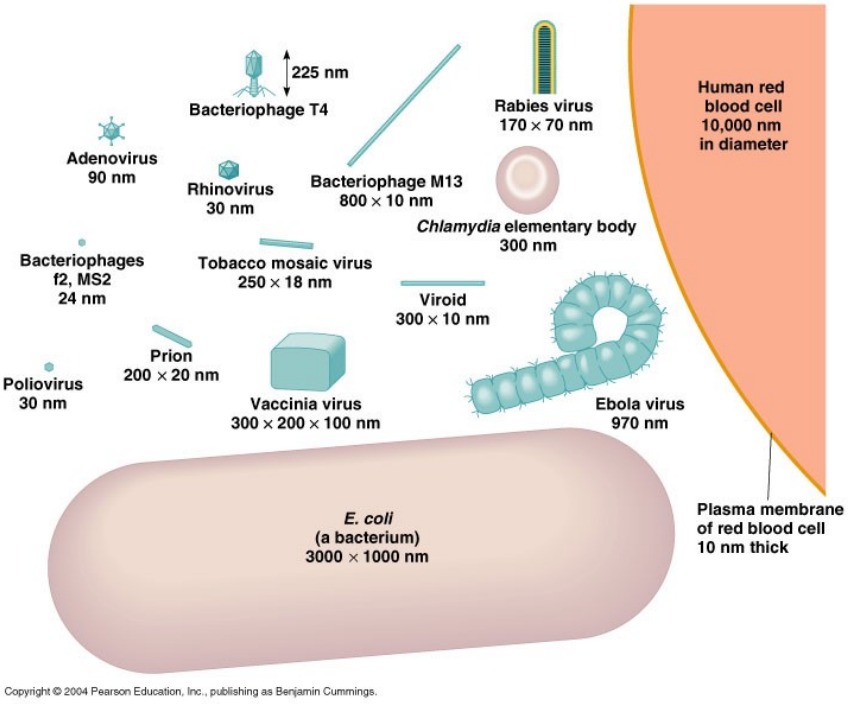

Figure 7 Comparison of the size of viruses [44];

Viruses possess five main features, where they: (i) replicate only inside living cells, (ii) are an infectious agent meaning that it is transmissible from an infected host to uninfected hosts, (iii) propagate themselves via the assembly of their components in infected cells, (iv) rapidly cope with environmental changes (e.g. drug, antibodies, host cell), (v) deliver their genomes to the host cells via infection [45]. Viruses can be divided based on the genome type as presented in Figure 8.

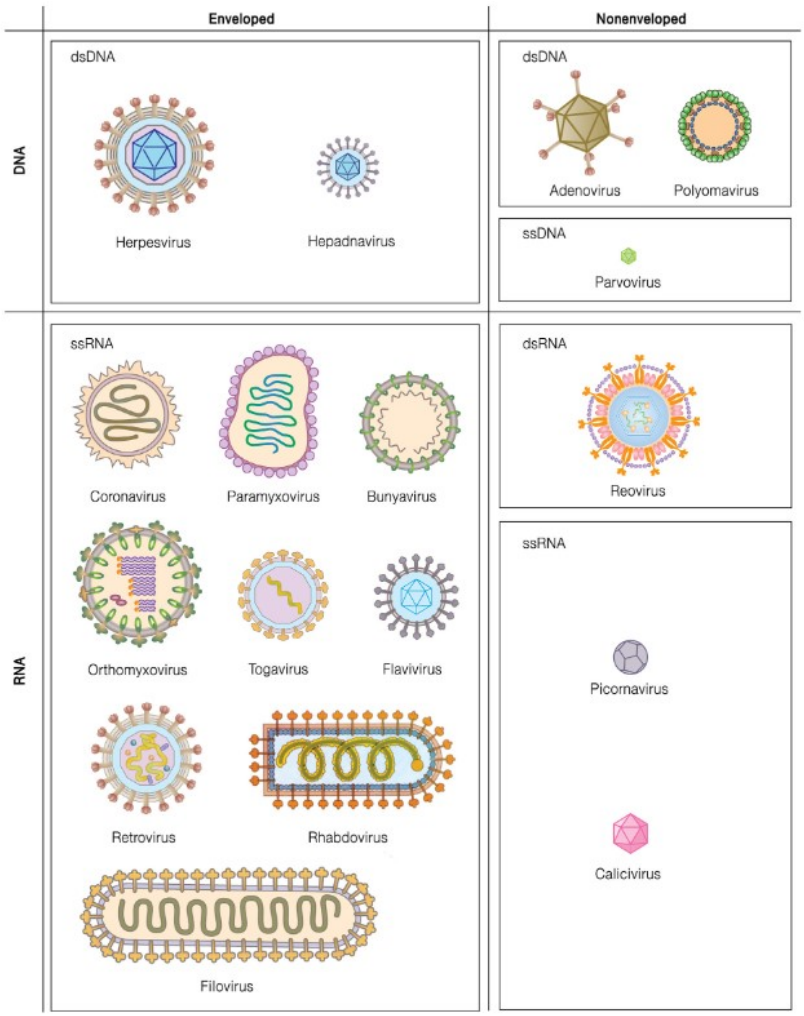

Figure 8 Classification of viruses by the nature of the nucleic genome [38];

Water-transmitted viral pathogens are classified by the WHO having a moderate to high health significance [48]. The moderate health significance is ascribed to Adenoviruses and Astroviruses, while to the high one belong Enteroviruses, Hepatitis (A and E) virus, Norovirus, Rotaviruses and Sapoviruses [48]. Table 1 presents the most commonly detected viruses in water.

Table 1 Common enteric viruses detected in water [50–53];

Virus family	Genome	Genera	Size, nm	IEP	Disease
Piccornaviridae	ssRNA	Poliovirus	32	4.1-8.3	Paralysis, meningitis, fever
		Enterovirus	28-30	4.7-6.7	Paralysis, meningitis, fever
		Hepatitis A	27	2.8	Hepatitis
Adenoviridae	dsDNA	Adenovirus	94	4.5	Gastroenteritis, respiratory, disease, conjunctivitis
Caliciviridae	ssRNA	Norovirus	40	5.6-6.0	Gastroenteritis, fever
		Astrovirus	27-30	-	Gastroenteritis
		Hepatitis E	27-30	-	Hepatitis
Reoviridae	dsRNA	Reovirus	75	3.8-3.9	Unknown
		Rotavirus	80	8.0	Gastroenteritis

2.2. Source of virus infections

Diverse microbial contaminations present in all environments are concern to the public health. Among them, the greatest anxiety comes from the prevalence of enteric viruses in water [3,48]. Figure 9 presents potential transmittance routes of pathogens [48,54].

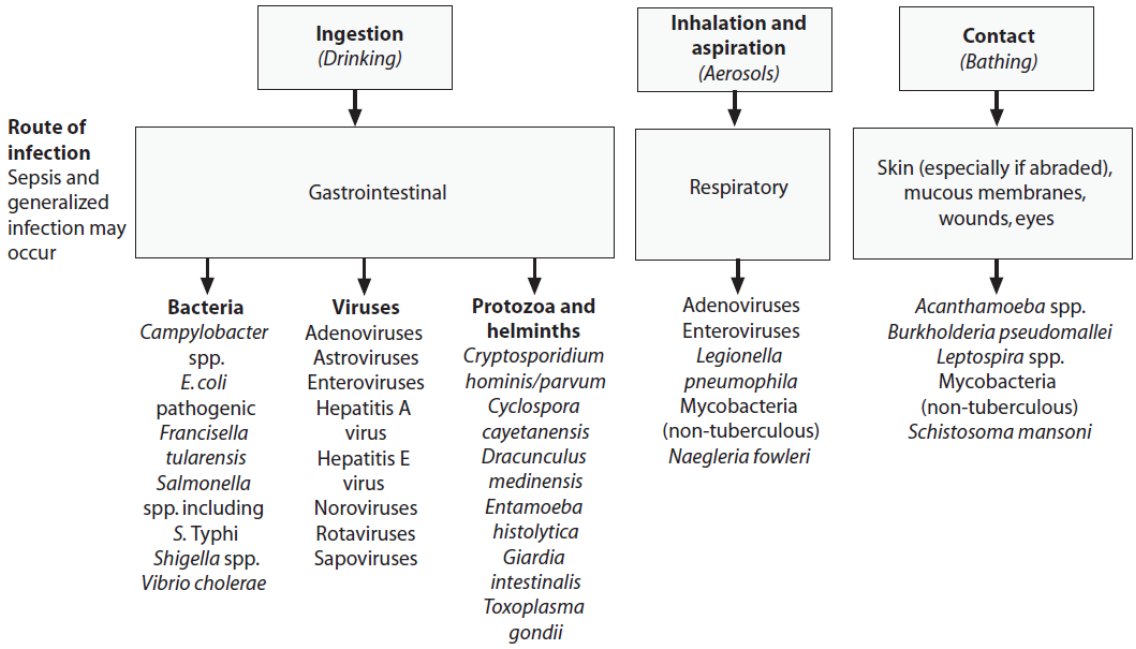

Figure 9 Transmission pathways and examples of water-related pathogens [48];

Microbial enteric pathogens may enter human organisms via many potential routes of transmissions, such as ingestion, contact and inhalation/ aspiration [48]. The source of waterborne pathogens is mostly sewages, which contains faeces contaminated with pathogenic viruses [55]. Crops could be irrigated with wastewater or fertilised with sewage containing animal and human faeces. Viruses shed by animals that can also cause disease in humans, are called zoonotic viruses. In this way, the water and food distribution systems are the main source of virus pollutions. The viruses are ingested by drinking fouled water and eating contaminated food. Recreational waters polluted with sewages lead to contact infections by skin, mucous membranes, wounds or eyes. Another transmission pathway is inhalation, which is more about airborne pathogens. Airborne viruses, such as novel SARS-CoV-2, are spreading through both person-to-person contact and droplet infection. Tiny droplets containing virus particles, distributed by infected people by breathing, talking, sneezing or coughing, are carried by water vapour and suspended in the air are easily transmitted.

Studies have reported that one virus particle is enough to cause an infection and lead to serious diseases [56]. The effects of exposure to pathogens are not the same for all individuals, or as a consequence, for the entire population [57]. It depends on the individual's immunity, age, sex, state of health and living conditions. An important factor is also the persistence of the pathogen in environment that is influenced by many factors, e.g. temperature, salinity and pH in case of an aqueous environment, humidity in case of air environment, nutrient or host availability. Viruses are able to survive for extended period of time in the environment under a wide range of pH and temperatures [48,55].

2.3. Air filtration vs water filtration

Bioaerosols refer to particles of biological origin present in air, such as viruses, bacteria, fungi and pollen [58]. Exposure to airborne viruses in any environment may lead to many adverse health hazards for society. In light of recent events, it is worth mentioning the COVID-19 (coronavirus disease) pandemic caused by the novel SARS-CoV-2 virus, where first infection cases were detected in December 2019 in Wuhan, China [59]. Up until the end of 2020, the pandemic has resulted in over 75 million cases worldwide with a mortality rate of approximately 2 %. The origin of this disease was found to be in bats [60]. SARS-CoV-2 belongs to the Coronaviridae family and human coronaviruses were firstly discovered in the 1960s [61]. Initially, it was thought that they cause common-cold-like, self-limiting respiratory infections, however, since human coronaviruses have been discovered, it transpired that they lead to serious, and even fatal respiratory complications [61,62]. In addition COVID-19, there are other known human

coronaviruses, e.g. SARS-CoV, MERS-CoV, HKU1-CoV, HCoVNL63, HCoV-OC43, and HCoV-229 that have seriously impacted public health [63].

These outbreaks lead to research towards the more intensive recognition of airborne virus transmission routes, their dynamics, as well as conditions that support virus' survival. Not all viruses are contagious in the same manner, e.g. droplet, contact or smear infection. Airborne viruses spread through both person-to-person contact and droplet infection. Their survival is dependent on air temperature, humidity (either absolute and relative [64]), pressure, velocity and even direction of the wind [65,66]. The temperature influences the state of virus proteins and genome [66]. Generally, viruses with lipid envelopes will tend to survive longer at lower (20 – 30%) relative humidity, while non-lipid enveloped viruses are prone to preserve longer in higher (70 – 90 %) relative humidity conditions [66].

Removal of viruses from an aerial environment is a relevant point not only in the field of public health but also for special applications, e.g. pharmaceuticals operations [67]. Conventional methods involve filtration using an appropriate and efficient filter material [58,68]. A number of air-filtration devices have been made over the years to eliminate microbes. They are applied in various ways, including personal facemasks/ respirators and central heating, ventilating, and air-conditioning (HVAC) systems of buildings [69].

One of the discovered solutions for fine particles were HEPA (High Efficiency Particulate Air) filters, which are a complex wave of fibres that carry an electrostatic charge that attracts passing particles. Their removal effectiveness specification is 99.97 % for particles with size >0.3 μm. HEPA exhibit high bacteria removal efficiencies, however, in the case of viruses, they are only able to capture part of the viruses present in the air [68,70]. Typical filters work based on conventional mechanical mechanisms (i.e. impaction, interception, and diffusion) and their efficiency can be improved by applying electric fields and/or charging particles [69]. Usually, filter materials consist of various fibres made of e.g. carbon, glass, polymer [67,68]. Next to filter material selections, an aerosolized microbes inactivation technology is needed, where current solutions include air ionizers, heaters, dryers, chemical treatments, photocatalytic oxidation and ultraviolet irradiation processes [69].

Water filters for virus removal application are working based on different mechanisms. The first one includes the physical removal of size exclusion determined by the filter material' pore size. The second one is driven by electrostatic attraction, Van der Waals (VdW) forces, hydrophobic interactions and steric effects [71,72]. Factors that strongly influence virus removal, beyond the properties of filter material and viruses, are the properties of the water, i.e. water

pH, ionic strength, and presence of natural organic matter. Since the greater driving force is electrostatic interaction, the point of zero charge of viruses and the selected material is a factor that plays a great role. The water pH affects the charge density and may alter it for both the virus and material, and ultimately, impact the adsorption. Organic matter varies for water type and quality. It interferes with virus adsorption by accumulating on the filter's surface and competes with viruses on adsorption sites [73].

Another important aspect of virus removal by filters, besides their adsorption, is their inactivation. Effective virus inactivation can be done by blocking or destroying of host-cell receptors on the virus and inactivating the nucleic acid [38].

2.4. Waterborne viruses - standards to control their removal

Due to the high risk of infection and special condition requirements, permissions and validation of water treatment solutions in terms of virus removal were introduced. Based on the studies over a range of enteric viruses, regulations are determined for each disinfectant on the basis of an appropriate dose to adequately inactivate the most resistant viruses [54]. United States Environmental Protection Agency (USEPA) recommend viral removal or inactivation of 99.99 %, which represents 4 $\log_{10}$ units, by approved treatment techniques [54,74,75]. The Log_{10} removal value (LRV) is a way to express the removal or inactivation efficiency for a specific target such as an organism, particulate or surrogate. A removal value of 1 $\log_{10}$ represents a 90 % reduction in abundance of the target component, 2 LRV equals 99 % reduction etc. [49].

In 2014, WHO published recommendations for the evaluation of household treatment technologies. Examination is based on multilevel approach to define targets of three levels of performance to remove pathogens (Table 2) [76]. For viruses, the target value is ≥ 5 $\log_{10}$ reduction, which represents 99.999 % removal.

Table 2 Criteria of evaluation household treatment solutions according to WHO [76];

Pathogen type	Comprehensive protection	Advanced protection	Satisfying protection	Below expectations
Bacteria ($\log_{10}$)	≥4	≥2	meets requirements on at least advanced protection level for two pathogens	meets no criteria
Virus ($\log_{10}$)	≥5	≥3		
Protozoa ($\log_{10}$)	≥4	≥2		

For the rapid detection and water quality assessment, bacteriophages are applied as model viruses to assess the behaviour and survival of enteric viruses in the environment and to evaluate the resistance to water treatment and disinfection processes, e.g., MS2, ϕX174, Qβ, PM2, PRD1

[77,78]. Bacteriophages are virus surrogates, i.e. they have similar physical, chemical and biological properties (size, shape, morphology, modes of replication, surface properties). Like viruses, phages consist of a nucleic acid molecule surrounded by a protein coat, and some have lipid envelope and additional structures, such as tails and spikes [78]. Moreover, bacteriophages are non-pathogenic for humans, animals and plants, and have no impact on the environment. There is no one bacteriophage that accurately represents the behaviour of all enteric viruses for all waters disinfection/ purification methods [54]. Bacteriophages that are of interest in water quality assessment can be classified into six families, according to the morphology and nucleic acid content (Figure 10) [78]. Among phages, the F-RNA (Family Leviviridae) are theoretically the best surrogates for enteric viruses, as they originating from the faeces of humans and warm-blooded animal and they fail to multiply in the environment, additionally, they resemble structure, size and composition close to human enteric viruses [78].

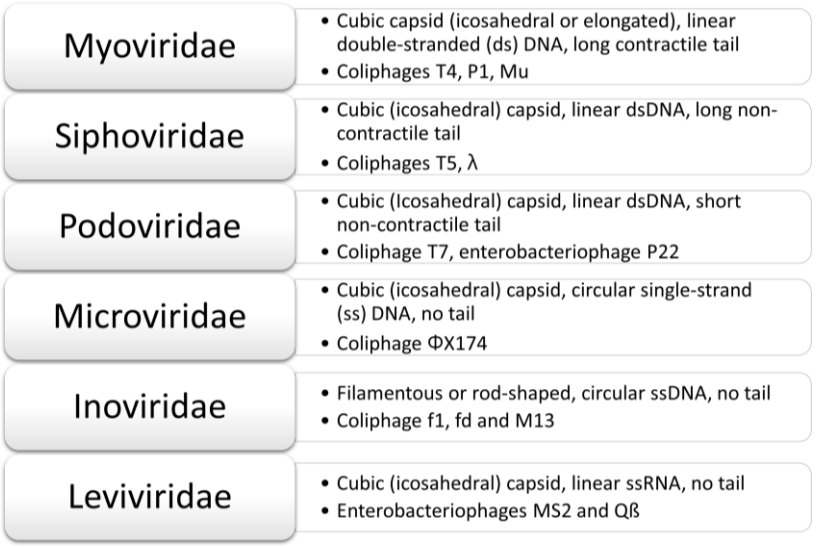

Figure 10 Bacteriophages classification for interest of water quality assessment [78];

Phages and enteric viruses replicate only inside host cells, which are metabolise host bacteria and mammalian cells, respectively [79]. Phages infect only certain bacteria, which is determined by receptor sites (protein molecules) on the bacteria surface. Only specific phages will recognise these receptor sites and will attach to them, resulting in bacterial infection [78].

A major advantage of phages is that, compared to viruses, they are detectable by simple, inexpensive and rapid techniques [78], while methods for virus detection usually require time, advanced laboratories, expertise and expensive equipment [54]. Detection is important in monitoring water quality, through surveillance and quantitative microbial risk assessment [44].

Various evaluation and characterisation procedures can be applied for the detection and quantification of pathogens in drinking water. Such methods include enumeration or quantal assays of total viable, active, or infectious viruses [80]. Examples of methods used for pathogen identification in water samples: water microbiology (e.g. plaque assays, colorimetric and fluorescence methods), immunological methods (e.g. enzyme-linked immunoSorbent assay (ELISA), surface plasmon resonance (SPR)), generic methods (e.g. quantitative real-time quantitative polymerase chain reaction (qPCR), immuno- polymerase chain reaction (IPCR), DNA sequencing, mass spectrometry, microarrays) [81]. However, the main methods used for virus quantification or virus infectivity are: molecular method such as PCR and virological methods. such as plaque assays and end-point dilution [82]. PCR-based methods allow for rapid measurements, however, they do not distinguish infectious versus non-infectious viral particles [54]. Plaque assay is the easiest one from above mentioned, although it is time-consuming and only enables measuring infectious virus particles as number of plaque forming unit - PFU (one PFU is considered either an isolated virus particle or an aggregated of several infectious viruses) in a given sample [74,83]. Specifically, a confluent monolayer of host cells is infected with a virus at varying dilutions and covered with a semisolid medium, such as agar, to prevent the virus infection from spreading indiscriminately [82]. The virus infected cell spreads the infection to adjacent cells. As the infection cycle is repeated, the infected cell area forms a plaque, visible to the naked eye. The PFU/mL result represents the number of infectious particles in the sample, assuming that each plaque represents a single infectious virus particle [82].

3. Methods for water purification

Supplying water suitable for drinking entails ensuring availability and accessibility to water resources and adequate treatment of wastewater, which are sometimes limited in many countries. Creating water treatment infrastructures are labour and capital-intensive, and require long-term planning. There are many different technologies that can be applied either on a household scale or on a community scale to purify water and deactivate microorganisms present within [4].

3.1. Central treatment

According to the report published by WHO in 2017, 2.2 billion people worldwide had access to piped water systems. In urban regions, central treatment plants are typically available, consisting of a multi-step treatment process. Combined treatment includes coagulation, flocculation, sedimentation, filtration and disinfection (Figure 11). In the coagulation step, chemicals (e.g. aluminium sulphate) are added to promote particle binding. Flocculation involves mixing of the solution, leading to the formation of larger clumps, called flocs. Next, the mixture of flocs and water enter a settling tank, where the flocs settle to the bottom of the tank as sedimentation. Afterwards, the water goes through an array of filters to remove unsettled flocs, particles, contaminants and pathogens. The final step consists of disinfection to inactivate any remaining pathogens and to prevent their re-growing in the distribution system. Centralised water treatment plants ensures high treatment efficiency and water quality.

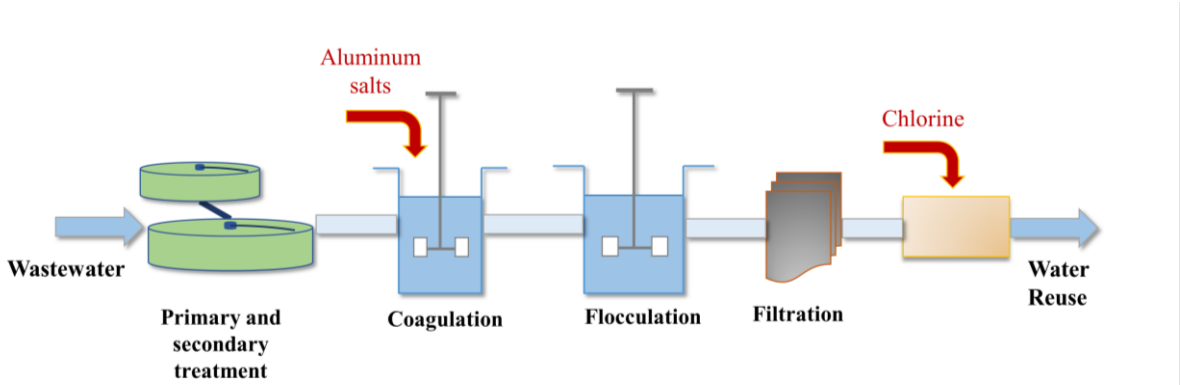

Figure 11 Scheme of centralised water treatment plant [84];

However, central treatment installations are not present in low- and middle-income countries, due to limitations, including insufficient technical capacities to build and maintain such infrastructure and low household density for installing distribution systems [4–6]. Furthermore, the cost of building, operating and maintaining water treatment infrastructures are significant, going beyond the means of many regions worldwide. System components need to be high quality and constant system surveillance is required, as so to quickly locate defects, such as degradation of pipe protective coatings, pipe cracks, leakages and blockages that may appear over time. If these rigorous requirements are not met, contaminants will enter the water system, making the water no longer safe for consumption [5,6].

3.2. Point-of-use systems

Taking into account limitations occurring in low- and middle-income countries, decentralized systems provide basic sanitation conditions. For communities that do not have access to centralised water treatment facilities, Point-of-use (POU) systems are key solutions. Such systems have potential in places, where piped systems are not possible to install and are not free from leakage or where people rely on contaminated water sources or where stored water becomes contaminated due to unhygienic handling [48]. POU systems allow treating the water at the point of consumption either for common and individual use. Household water treatment technologies comprises of a range of options that enable treating collected water or contaminated piped water to remove or inactivate microbial [48]. Such systems are able to remove bacteria and protozoa from water, however, in some cases, virus removal is still a challenge [7]. Point-of-use systems are user-friendly, low-cost and do not require high maintenance [6]. Commonly applied POU methods include three categories: thermal and solar technologies (i.e. solar irradiation, UV radiation), chemical treatment (i.e. chlorine disinfection, chemical coagulation, flocculation) and physical treatment (i.e. sedimentation, filtration) [7].

3.2.1. Thermal and solar treatment

In thermal technologies, the mechanism behind microbe destruction in water is heat produced by fuel burning. Methods differentiate boiling and heating up to pasteurisation temperatures. Boiling (100 ºC) is the most known, effective and accessible method of water disinfection. Heating up to ~60 ºC (pasteurisation temperature) for a period of minutes destroys most waterborne pathogens. The recommended procedure for the former is to raise the temperature so that rolling boil is achieved, removing from heat and allowing the water to cool naturally. Unfortunately, this method has a high probability of recontamination after prolonged storage. This process is effective against all waterborne pathogens. The disadvantage of this solution is the constant need of a fuel source, its availability and cost.

There are also technologies that use solar irradiation to inactivate microbes in either dark or opaque containers by relying on heat from sunlight energy [48]. Solar water disinfection (SODIS) systems consist of clear plastic containers that allow UV radiation penetration from sunlight. They rely on the combined action of the UV radiation, oxidative activity associated with dissolved oxygen, and heat [48]. This method is simple, low-cost and requires no or low maintenance. It provides effective disinfection, however, it is dependent on weather conditions and

geographical location. This method requires pre-treatment of highly turbid water and is not able to remove chemical pollutants from water [6].

UV disinfection inactivates microorganisms by damaging their intracellular proteins and nucleic acid, thus impairing their ability to replicate [85]. The effectiveness of the UV method depends on the delivered dose, which is determined by the intensity and exposure time, as well as water turbidity and the suspended matter. UV-light technologies using lamps are applied in households or small-scale water treatment plants. Typically, in this technology, water is stored in vessels or flows through pipes exposed to UV radiation from the UV lamps. This method is simple to use, does not introduce chemicals or causes the production of harmful disinfection by-products in water [7]. Although UV disinfection is simple to use, it possess some limitations. UV systems require pre-treatment step, e.g. pre-filtration to remove colour, turbidity, and particles that may shield microorganisms from the UV source [86]. Additionally, regular maintenance and constant access to electricity is needed to operate and clean the UV lamps. Furthermore, a reliable supply chain is required and the relative cost of treatment is high [87]. Unfortunately, UV treatment is not always efficient for virus removal, e.g. the adenovirus is highly resistant to inactivation by UV light [48,88]. Moreover, this method does not prevent water recontamination or microbial regrowth after treatment [7].

3.2.2. Chemical treatment

Chemical disinfection deactivates microorganisms by oxidising their biochemical building blocks and disrupting vital cell functions [85]. Such methods includes the application of any chlorine-based technology, such as chlorine, chloramines, ozone and chlorine dioxide. Disinfection of household drinking-water is done primarily with free chlorine, either in liquid form, as hypochlorous acid or in the dry form of calcium hypochlorite or sodium dichloroisocyanurate. These substances are relatively safe and inexpensive. However, in the case of an emergency, more dangerous substances may be used for household application, such as sodium trichloroisocyanurate and chlorine dioxide [48]. Treatment at a household level is difficult and the availability of chlorine tablets, as well as occurring taste- and odour problems hinder its application [4,54]. Furthermore, harmful or even carcinogenic chlorinated by-products may form during the disinfection step, especially in the case of water contaminated by organic matter [89,90]. The advantage of chemical treatment is the residual protection against re-contamination (ozone-based treatment being an exemption). Such systems require a reliable supply chain and quality control of products [87]. The efficiency of chlorine disinfection is dependent on water quality characteristics (presence of organic and inorganic matter, pH, temperature and

turbidity), reactivity against specific microorganisms, dose and contact time [85]. It is important to properly adjust the dose and monitor the treated water and the presence of free residual chlorine [85].

Coagulation and flocculation are low energy processes that result in turbidity in water that cause the reduction of supportive structures for microorganisms [6]. Coagulation is the destabilisation of smaller particles and the formation of larger particles, while flocculation aggregates suspended and larger contaminations into flocs [6]. These processes are not effective in microorganism removal and have to be supported by other treatments. Popular coagulants are aluminium or iron salts. Single-use coagulant/ flocculent sachets, which combine flocculent and disinfection together are available on the market (Rubicon, Prideco Holdings), as well as devices that combines coagulation and flocculation with filtration (e.g. Blue Q, Amway Corporation) [6,85].

3.2.3. Physical treatment

Physical water treatment typically consist of sedimentation and different filtration techniques. Sedimentation is any method, which involves the settling of suspended particles to remove them from water. This method can be either applied as a stand-alone for water treatment process, where it is usually preceded by coagulation and/or flocculation or as a pre-treatment step for other treatments, e.g. solar or chemical disinfection. It is a simple and cost-effective technology that allows to reduce water turbidity and remove large microbes.

Filtration is a simple method that allows removing colloids, solids and pathogens [6]. Filters rely on the physical straining through a single or multiple structured porous surfaces to physically remove and retain microbes by size exclusion [48]. Particles retained in a filter medium are smaller than the size of the filter material. Particles are trapped and adhere to the filter medium. Figure 12 presents the membrane filtration spectrum, which is rejection-characteristic dependent. Other processes occurring in filtration technologies are electrostatic adsorption between oppositely charged materials and Van der Waals interactions.

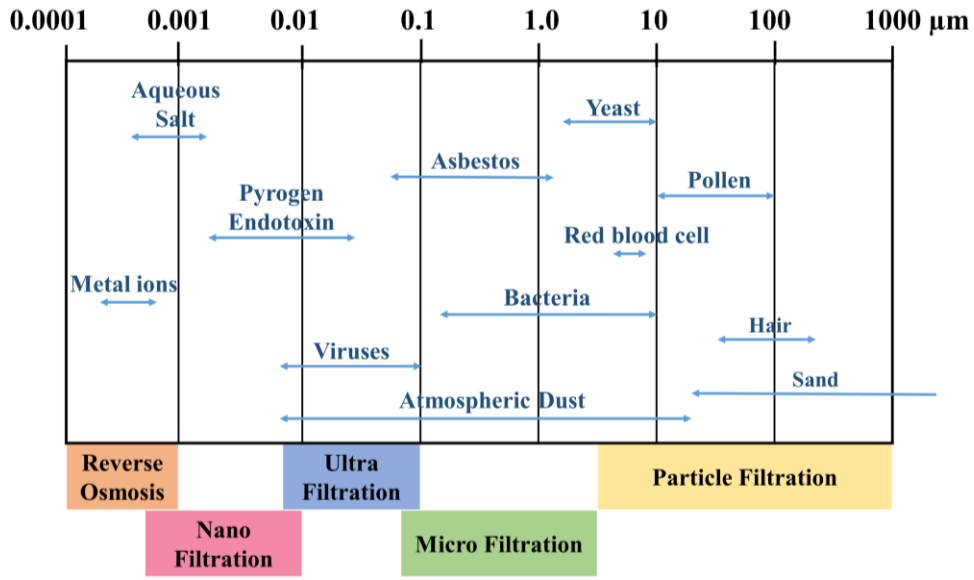

Figure 12 Schematic illustration of membrane filtration spectrum [91];

To effectively remove viruses, a material with suitable pore size (nanometric) is required, which is often the limiting factor of this technology [92]. In membrane filtration, typically an external driving source is required to meet high pressure requirements to achieve the desired flow rate to initiate and enhance filtration process. Further drawbacks of filtration are high filter production costs and the necessity of regular maintenance due to the formation of a fouling layer and clogs that block filter surfaces. Backwashing removes reversible fouling, while chemical cleaning discards biofouling and scaling [6]. The advantages include no need of power source and simplicity of usage, however, a minimal likelihood of water contamination or change in taste of water can occur [85]. Filtration technologies implemented in POU systems are mainly (bio)sand filters (BSF), textile fibres, ceramic and membrane filters [6].

Biosand filters (BSF) can be easily produced with locally available raw materials [6]. They differ from standard sand filters in the placement of the outlet point [6]. The outlet point in biosand filters is located higher, allowing for the saturation of sand layer with water during operation and the formation of biofilm layer, which can help with microorganism and colloids removal from contaminated water [6]. It has been shown that the depth of the filter plays a role in microorganism removal, e.g. Wang et al. obtained 3.4 LRV of MS2 using filter with 5.4 cm filter depth, while with 54.3 cm filter depth 6.7 LRV [93]. Bradley et al. have obtained 5 LRV of MS2 using biosand filter modified with Fe_2O_3 [94]. Glass fibre coated with hematite nano-

particles revealed good removal of MS2 bacteriophages and Rotavirus depending on the conditions, while pristine glass fibre showed no removal [95]. Other granular materials applied in filtration include anthracite, crushed sandstone or other soft rock and charcoal [7].
Textile fibres are mainly made of polymers or biopolymers, such as cellulose, wool, polyacrylonitrile, polyethylene terephthalate and polyamide [91]. Although most textile fibres are used for the adsorption of dyes and metals from water, some of them, modified with metal oxides, have been found to be good materials for virus removal. Szekeres et al. have described that Cu-coated nanofibrillated cellulose filters are effective in microorganism removal [35]. Trepper et al. have shown that nanoalumina fibre filters based on glass fibre and nanoalumina fibres called Argonide, are efficient in removing bacteria and viruses [96]. There are some commercial solutions available on the market, such as electropositive adsorptive filters, including (i) charged depth filter Zeta Plus EXT (3M) made of cellulose fibre that allows to reach up to 6 LRV of virus removal [97]; (ii) cellulose - diatomaceous earth charged modifies resin filter (series S, Zeta Plus, AMF Cuno) that efficiently adsorb polio virus from tap water [98].

Ceramic filters are simple to use, require a one-time capital cost and can be locally manufactured using available resources, for example clay soil or fine organic materials (e.g. sawdust, rice hulls) [87,92]. The material is sintered to obtain pores and increase its strength, which together with the generated surface area, determines the material's efficiency. Ceramic filters require regular cleaning, receptacles and maintenance of spare parts [87]. Such filters usually work against bacteria and protozoa, exhibiting limited performance against viruses [48]. Ceramic filters are additionally coated with metal to enhance disinfection [92]. Brown et al. studied non-modified ceramic filters and reached less than 2 LRV for MS2 bacteriophages [99]. Ceramic depth filters modified with MgO have shown MS2 bacteriophage retention exceeding 4 LRV [37], while ceramic microfilters modified with Y_2O_3 [100] or ZrO_2 [101] reach 4 LRV.

Common products for water filtration offered commercially for households, such as those produced by e.g. Brita, Home Master, iSpring, Whirpool, 3M, GE Smart Express Water are mostly carbon-based. Those filters are mainly utilised for the reduction of taste- and aroma-impairing substances (e.g. chlorine), adsorption of metal (such as lead, copper, and iron), reduction of limescale and hardness of water, more rarely the removal of herbicides, pesticides and pharmaceuticals. There are also products, which are aimed to have bactericidal and virucidal properties. They work via multi-stages filtration that includes other filtration systems than carbon-based, such as UV filters (products offered by ESP Water) or other combined technologies. It is worth

mentioning that such solutions are usually expensive and sometimes not affordable in developing areas. WHO have tested a few commercial products to check whether they fulfil the criteria of efficient microbiological performance and whether they can be used in places exposed to contaminated water [87]. Two products produced by the Lifestraw SA company, relying on ultrafiltration (0.02 μm hollow fibre) met the criteria and were capable removing up to 5 LRV of viruses and 8 LRV of E. coli. Smaller viruses and bacteria, however, were able to pass through the filter [87].

4. Carbon materials: origin, structure and application

4.1. Elemental carbon

Carbon is the chemical element number 6 denoted with symbol C in the periodic table. Carbon has seven isotopes, the main ones being ^{12}C (98.89 %) and ^{13}C (1.11 %) [102]. According to the IUPAC, isotope ^{12}C is the basis for atomic weights due to its large abundance and stability. Carbon is often bonded to itself in chains or rings with single (C-C) or multiple bonds (C=C, C≡C). Carbon is found free in nature in four allotropic forms: diamond, graphite, fullerenes and amorphous [102]. Carbon allotropes are bonded together, principally via sp^2 and sp^3 hybridisations.

In diamond (Figure 13a), each carbon atom is bonded to four carbon atoms (C-C bond distance is 0.1544 nm) forming a regular tetrahedron using 2s, $2p_x$, $2p_y$ and $2p_z$ orbitals in sp^3 configurations. Diamond claves along the (111) planes [103].

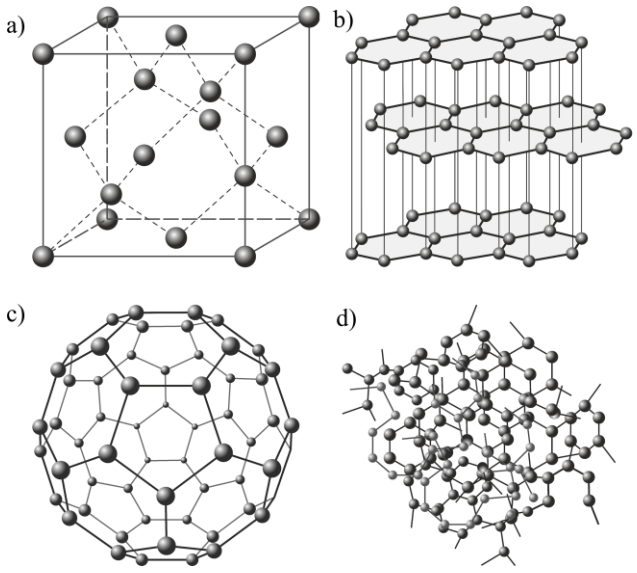

Figure 13 Structure of a) diamond; b) graphite; c) fullerene; d) amorphous carbon. Images not to scale;

Graphite has a parallel stack layer structure (Figure 13b), where every carbon atom within the layer plane is bonded with σ and π bonds to three other atoms with distance 0.1415 nm [104]. The distance between graphite layers is approximately 0.335 nm, which indicates that bonding forces between layers are rather small, leading to easy slippage of layers or their separation [104]. Graphite claves along (001) planes and exist in two forms alpha (hexagonal) and beta (rhombohedral) [104].

Fullerenes (Figure 13c) consist of carbon atoms bonded through single or double bonds to each other to form closed or partially closed cage-like fused- ringpolyclinic system [105]. Fullerenes are the zero dimensional form of graphitic carbon [106]. The molecule can be either a hollow sphere, ellipsoid, cylindrical (carbon nanotube) etc. Fullerenes have a number of carbon atoms C_{2n} (n>~12). Various forms of fullerene have been found, the most stable being fullerene C_{60} (buckminsterfullerene), composed of 12 pentagons and 20 hexagons of sp^2 bonded carbon atoms [106].

Amorphous carbon (Figure 13d) is a carbon with a short-range crystalline order without the presence of a long-ranged one, with deviations in the interatomic distances and/ or interbonding angles [105]. It has a disordered network of carbon atoms that are mostly bonded by sp^2 bonds, small amounts of sp^3 bonds and almost no sp^1 bonds [107]. The ratio between sp^2 to sp^3 bonding and the hydrogen content define the short-range order in amorphous carbon. Amorphous carbon includes chars, cokes, activated carbon etc.

4.2. Multi-walled Carbon Nanotubes

Carbon nanotubes were described by Iijima and Bethune as nanoscale cylinders with a radius of a few nanometres and several micrometres of length [12,108]. Carbon nanotubes form a hexagonal lattice of carbon atoms with hybridisation sp^2 capped in fullerene-like structures that form these walls of tubes [12,106,109–111]. Based on the number of layers, CNTs are categorised into single-walled carbon nanotubes (SWCNTs) and multi-walled carbon nanotubes (MWCNTs). SWCNTs consist of a single- layer of graphene with a diameter of 0.4-2 nm [111]. Multi-walled carbon nanotubes (Figure 14) are made of at least two concentric cylindrical shells of graphene sheets coaxially having a hollow area in the centre and spacing between the layers [12]. MWCNTs' outer diameters range from ~2 nm up to even 100 nm, depending on the number of walls [109,111,112]. MWCNT tip ends are usually closed by being capped by half-fullerene molecules [109]. The lengths usually differ, from 1 μm up to a few centimetres [109]. MWCNTs exist in two structural models, namely the Russian Doll, where the carbon nanotube has another carbon nanotube inside it and the outer nanotube has a greater diameter than those

inside of it, and the Parchment model, where a single graphene sheet is wrapped around itself multiple times [109].

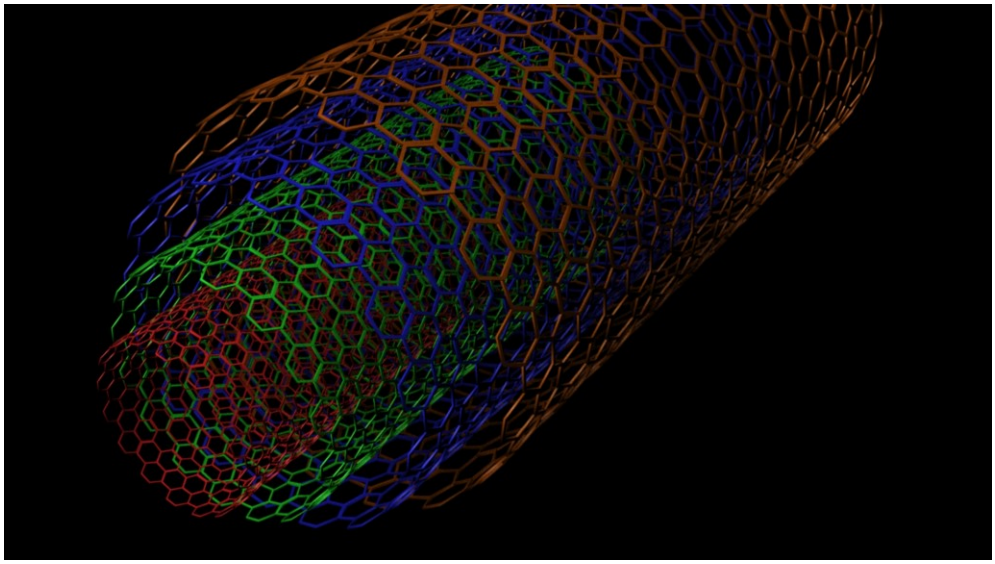

Figure 14 3D model of multi-walled carbon nanotube [113];

CNTs were initially manufactured via high- temperature synthesis procedures, like carbon arc discharge, laser ablation, however these processes were substituted by low-temperature ones [109]. Currently, the most common CNT synthesis techniques include chemical vapour deposition (CVD) and its derivative, catalytic chemical vapour deposition (CCVD) [109]. These methods aim to dissociate hydrocarbon molecules catalysed by the metal and following saturation of carbon atom in the catalyst particle [110,114]. Within the furnace, a catalyst is placed or fabricated in situ to initiate the dissociation process. Catalyst include materials, such as nanosized transition metal particles (Ni, Mo, Fe, Co) or their oxides, as well as alumina, silica, quartz or magnesium oxide as supports [109,115]. Next, a gas mixture of hydrocarbon source (methane, natural gas, acetylene, or benzene [116]) and inert gas is passed over the catalyst bed at temperature of 500-1100 ºC [114]. Next, the furnace is set to cool down to room temperature and the product is collected. The advantage of such a process is being able to choose the growth mechanism to produce a variety of forms (e.g. powder or forest) and shapes (straight, curved, planar-spiral and helix) of CNTs [114].

Figure 15 depicts possible furnace configuration that is horizontal or vertical. In horizontal configuration, a catalyst is placed in ceramic or quartz boat and the produced nanotubes are collected from the quartz tube. The vertical configuration is used for the continuous production of

nanotubes. Here, the catalyst and source of hydrocarbon are placed at the top of the furnace, while the grown product is collected in the chamber.

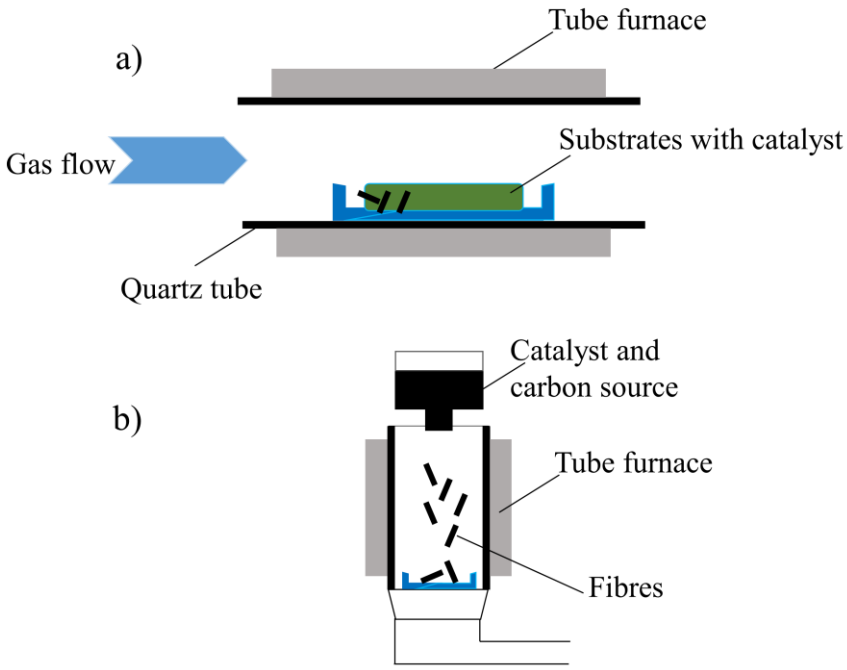

Figure 15 Scheme of a) horizontal; b) vertical furnace for multi-walled carbon nanotubes production;

CCVD method perquisite is a possibility to obtain large amounts of nanotubes with higher quality [110,116]. CNTs manufacturing technology is developing to be "greener", retaining the process efficiency, mitigating environment impact and production of side-products [117]. Moreover, the cost of CNT manufacturing is also decreasing. The price per gram in the year 2000 was $150 and decreased to $50 in 2010 [118]. Nowadays, carbon nanotubes are sold by even for a few dollars per gram.

MWCNTs are not usually characterised by high purity, as they contain various contaminants, such as metals and/ or carbonaceous particles, which can affect some of the material's properties (optical, electrical and mechanical) [119]. The most critical impurities in terms of water purification applications are metal residuals, that could have adverse biological effects [119,120]. Therefore, it is necessary to implement a purification step. As MWCNTs are hydrophobic, there is a need for additional enhancements to improve their properties and chemical reactivity for further treatment [121]. The typical functionalisation process of MWCNT surfaces is oxidation by incorporating – OH, – COOH, – CHO groups [122–124]. The methods of oxidation include treatment with oxidation gases, e.g. ozone, cold oxygen plasma, as well as the reaction with oxidising acids, such as HNO_3, $KMNO_4$, H_2SO_4: H_2O_2 or H_2SO_4: HNO_3 [120,121,123,125–

127]. Concentrated nitric acid exhibits the highest oxidation efficiency among all mentioned media, which can be enhanced at higher temperatures [120,121].

CNTs have gained a lot of interest over the last years and have become an important topic of scientific research due to their remarkable strength, optical activity, thermal stability, thermal and electrical conductivity [8,106,111,128]. Such outstanding properties enable CNTs to find applications in many different scientific fields and innovative technologies, such as optoelectronics, semiconductors and biotechnology [12,111].

CNTs have also been considered as a viable option in water filtration due to their exceptional properties, such as small diameters, high specific surface area, beneficial sorption capability and sorption efficiency [8,9]. Moreover, their needle-like shape allows to form an entangled layer on the filter's support structure, leading to decreased membrane pore size, and in turn, increased virus retention without impairing the filter's flux [129]. In comparison to existing filter material alternatives, CNTs can additionally capture the virus due to strong Van der Waals bonding on the basis of the high Hamaker constant [32,130]. Additionally, during contact with microbes, the sharp ends of the nanotubes can cause irremissible damage to the cells [8]. Moreover, CNTs have been noted to be good agents for heavy metal [27,131], organic contaminations [26,132] and dyes removal [28,111] from water. The affinity of the heavy metal ions towards CNTs is highly dependent on the solution's pH, ionic strength (total amount of ions multiplied by their charge), as well as material's functional groups [8]. Organic removal is affected by the physicochemical properties of the material, such as surface area and presence of functional groups, which is linked with hydrophobic/ hydrophilic nature of material [8]. It has been reported that functionalised MWCNTs adsorb 2-7 times more benzene, toluene etc. than pristine nanotubes [133]. Dyes removal is dependent on dye type, its initial concentration, solution's pH, and temperature [28].
CNTs have been reported to be good antimicrobial agents [25,129]. The geometry of carbon-based nanomaterials may have an influence on their deposition and their interactions with microorganisms [8]. Numerous studies have discussed the antibacterial properties of CNTs, however, only a few of them describe their antiviral activity [24,134,135]. Brady-Estévez et al. presented that filters made of SWCNTs supported on PVDF membranes are effective in the removal of E. coli bacteria [25]. Yang et al also proved that MWCNTs with smaller diameters have stronger toxicity to bacteria than those with larger diameters [136]. Shorter tubes having

many more ends per part of material, make that there are significantly more interactions between microbes and these ends [136]. The study of the virucidal properties of SWCNTs demonstrated values of 7 LRV, depending on water pH and chemistry [137]. In the work of Ahmed et al., SWCNTs exhibited MS2 bacteriophages removal equal to 3 LRV [138]. According to Brady-Estévez et al., MWCNTs exhibited MS2 inactivation of 1.5 to 3 LRV higher compared to SWCNTs, reaching up to 8 LRV [129]. Srivastava et al. have reported good removal of the polio virus using MWNCTs [24].

The above mentioned studies have proven that pristine MWCNTs are very promising for virus removal, however, their further modifications can increase their sorption capabilities and virucidal activity [8,12,111]. Certain chemical modifications, such as the dispersion of MWCNTs in polymers or incorporation of metal or metal oxide particles on the surface of CNTs, have led to the formation of more effective composites for water treatment when compared to the raw materials [12,36]. Carbon nanotubes are useful supports for metal oxides due to their high chemical durability [33,34]. The support structure can hinder or inhibit the release of the attached metal oxide into the water over long time periods, as well as reduce potential pressure drops caused by low packing density [33,34]. MWCNT modification with metals and metal oxides is well known and is used for different applications [139–144]. Following metals and/ or their oxides are good virucide: Fe [145], MgO [146], CuO [13], Cu_2O [14–16,147] and Ag [148,149]. The combination of MWCNTs support with virucidal metal oxide gives an alternative material for virus removal applications.

MWCNTs possess many advantages for water treatment applications, such as high specific surface area, favourable sorption capability, ease of modification, profitable support structure that proves low-pressure drops, low packing density, and high permeability. High Hamaker constant [32,130] and antimicrobial affinity will additionally provide enhanced interactions with viruses. In addition, MWCNTs are marked by unique thermal properties that offer ease of filter material thermal regeneration, enhancing material lifetime.

4.3. Activated Carbon Fibres

Activated carbon (AC) is a common term describing carbon-based materials, which have a well-developed pore structure and extended surface area. The external surface area is relatively small with respect to the area of the pores, with the specific surface area of AC varying from hundreds to more than a thousand m^2/g [17–19,150]. Approximately 90-95 % of the total surface area consists of micropores [150]. According to the IUPAC classification, pores can be divided into three categories, namely micropores, with pore size <2 nm, mesopores (pore size 2-50 nm) and

macropores characterised by pore size >50 nm [151]. AC, apart from being porous is an amorphous, carbonaceous material containing hydrophobic graphene layers and hydrophilic functional groups. Moreover, it is possible to distinguish different forms of AC, i.e. powder, granular, extruded, fibres and cloth (Figure 16) [18].

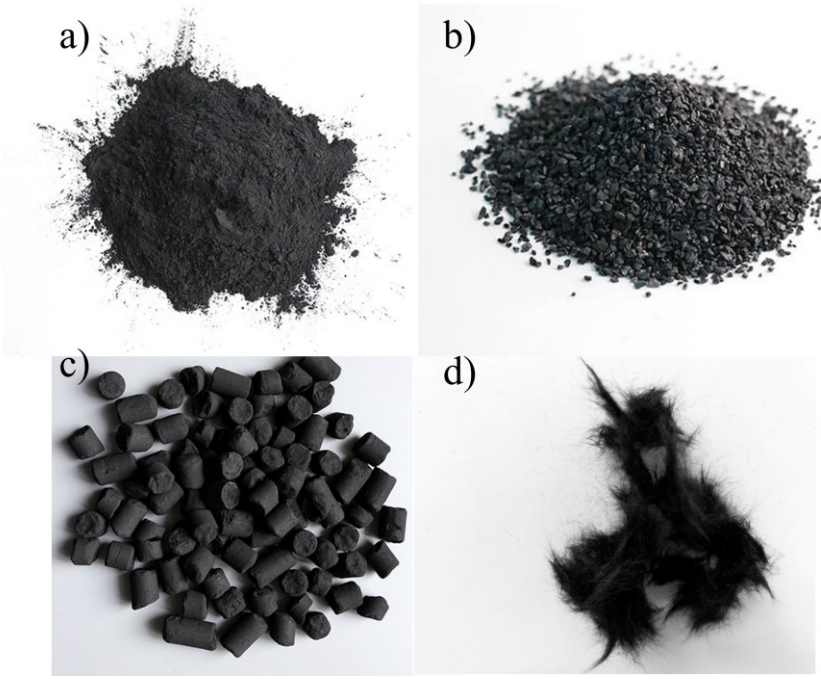

Figure 16 Activated carbon types: a) powder; b) granule; c) extruded; [152] d) fibre;

AC is recognized as one of the most widely used adsorbent materials, especially in water purification technologies [17,18,22]. It has the capability of removing various pollutants from water, such as compounds responsible for taste, odour, pesticides, dyes, organic contaminations (dissolved organic matter, organic micropollutants) and heavy metals [18–22]. Activated carbon is applied in its powdered form (particle diameter <40 μm) in slurry reactors or as a granule in fixed-bed adsorbers (particle diameter 0.5-4 mm) [22]. Powdered activated carbon offers a larger specific surface area and faster adsorption kinetics, while the granular form more quickly reaches its saturation point [153]. Granular AC is characterised by easier regeneration in comparison to the powder version.

Studies have proved that activated carbon fibres (ACFs) have 2-50 higher adsorption rates than granular activated carbon (GAC), due to smaller diameter, higher microporosity and larger surface area [154–156]. This makes the fibres' surfaces more accessible and leads to higher reactivity. Additionally, ACFs offer advantage of capability to be easily molded into the shape of

the adsorption system and producing low hydrodynamic resistance [18]. Activated carbon fibres are a unique material characterised by a large adsorptive capacity and extremely high specific surface area, which is attributed to high microporosity, low mesoporosity and mostly absence of macroporosity [10,11]. Additionally, ACFs are characterised by high stiffness, mechanical strength, and electrical conductivity [157].

The synthesis process for producing activated carbon is responsible for such properties. AC and ACFs are synthesised in a three-step procedure (Figure 17) consisting of stabilisation, carbonisation and activation [10]. Additionally, in ACFs production process, a step o fibres formation has to be included e.g., spinning, that usually take part before stabilisation. [10,155]. The substrates need to have high carbon and low ash content, high density and low volatile content. The precursors for ACFs production include carbonaceous materials, synthetic and natural one, such as rayon, pitch, saran, polyacrylonitrile (PAN), phenolic resin, as well as biomass [10,154,155]. The choice of substrate depends on the pore characteristics, required surface chemical properties and targeted application [10].

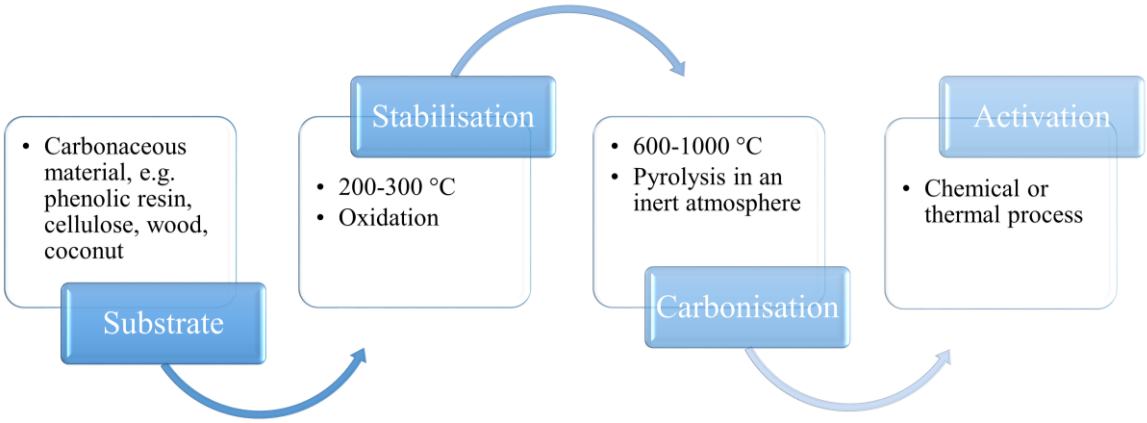

Figure 17 Scheme of activated carbon synthesis;

The stabilisation process (oxidation at 200-300 ºC) aims to prevent the melting of the precursor during carbonisation, which is especially crucial for PAN and pitch substrates [10]. Next, AC is carbonised (600-1000 ºC), e.g. by pyrolysis in an inert atmosphere [154]. During this process dehydrogenation, condensation and isomerisation takes place, the free atoms of elementary carbon are grouped into organised crystallographic formations known as elementary graphite crystallites [158]. Carbonaceous materials give rise to graphitic carbon only if they pass through a liquid stage, which allows large aromatic molecules to form nematic disc-like liquid crystals,

forming the mesophase precursor of the graphitic structure [159]. The last step in the manufacturing process is activation, which enlarges the surface area and porosity of the carbon material by increasing the number of micro and mesopores [11,150]. This can be done either by means of chemical or via thermal processes in a controlled atmosphere [11]. Chemical treatment usually utilises chemical agents, e.g. KOH, NaOH, $ZnCl_2$ or H_3PO_4, which are used as dehydration agents that influence the pyrolytic decomposition and inhibit the formation of tar, thus enhancing the yield of carbon [11,160]. The main assets of chemical activation are obtaining mostly a powder-form product, higher yield and lower temperatures, shorter activation time, higher porosity obtained in comparison to thermal treatment [11]. The biggest drawback of chemical treatment is the need of a washing stage and carbon instability originating from degradation [11]. Most of the activated carbon used in water treatment technologies are activated via thermal processes [22]. During thermal treatment, AC are heated in an oxidising atmosphere of steam, air or carbon dioxide at temperature range 700-1000 ºC [10,155]. The carbon activation burn-off can be easily controlled.
Biomass usage as a ACFs' precursor is an interesting point, leading to lower production cost and making the technology greener [10]. Application of synthetic precursors might be expensive, the manufacturing cost of activated carbon depends on many factors (e.g. raw material, activation route, plant capacity) and can vary from $1 to around $10 per kg [161].

ACFs have found application not only as an adsorption material for wastewater treatment, but also as a storage media for natural gas, air purification, separation of gases, adsorption of volatile organic compounds or toxic gases, and as electrodes [10,11,162].
Their properties, such as high adsorption volume, high adsorption and desorption capabilities, and ease of reactivation are advantageous for water filtration purposes [163]. Problem with channelling during filtration, characteristic when using granules, can be avoided as ACFs can form woven or nonwoven mats [11].

There are different approaches for modifying AC to improve its sorption capacity for water treatment applications. The most common is modifying their surface chemistry, which can be done through oxidation by acid treatment, base treatment, plasma treatment, microwave treatment, ozone treatment etc. [17,164,165]. Many examples of activated carbon modified with metal/ metal oxides have been described for diverse purposes, e.g. Cu/ AC for cyanide removal from water [166], Cu/ AC for humic acid removal [167], Fe-Ag/ AC for Cr(VI) adsorption from aqueous solution; AC impregnated with Ag/Cu to remove Pb from water [168], Co/ ACFs for

SO_2 removal [169], TiO_2/ ACFs for degradation of organic pollutants in water [170], Fe/ ACFs for gaseous volatile organic compounds removal [171] and carbon nanofibers grown on ACFs for phenol and led removal from water [172].

Published study on activated carbon antiviral properties show very low performance toward virus filtration: Hijnen et al. revealed low removal of MS2 bacteriophages for GAC, equal to 0.2-0.7 LRV [41], Shimabuku et al. noted 0.32 LRV for GAC, while Cookson et al. observed removal lower than 1 LRV [42], obtaining only 18 % coverage of carbon surface [40]. GAC modified with Al_2O_3 resulted in low efficiency of MS2 removal [173], while GAC modified with Ag and CuO exhibited 3 LRV for T4 bacteriophages [42].

ACFs were studied for bactericidal properties, Ag/ ACFs revealed strong activity against E. coli S. cerevisiae and P. pastoris bacteria [174,175], while carbon nanofibers grown on ACFs and modified with Cu,Au or Cu/ Au demonstrated inhibition of E.coli and Staphylococcus Aureus bacteria growth [176].

There are plenty of reasons for selecting ACFs as the substrate material, the most important being: well-developed micropore structure and extended surface area beneficial for sorption capacity, and ease of functionalisation for enhancing material chemical reactivity. Furthermore, thermal resistivity is profitable for filter material thermal regeneration and lifetime. High value of activated carbon Hamaker constant ($6 \cdot 10^{-20}$ J) is also favourable for virus adsorption and retention [30]. An advantage of activated carbon fibres over other forms like powder or granules is lower packing density, higher permeability and higher stability regarding regeneration temperature. According to literature, activated carbon in water purification is mainly used in their pristine forms or functionalised by surface oxidation. Although AC finds its main application in the removal of heavy metals, dyes and organic pollutants from water, it is not so widely used for microorganism removal, also viruses [41]. So far, the adsorption of viruses by activated carbon fibres, functionalised fibres or fibres modified with metal/ metal oxides have not been thoroughly addressed. This work brings the novelty of utilising ACFs for virus removal application.

5. Copper and its oxides

Copper is a chemical element denoted with atomic number 29 and symbol Cu. It is an abundant metal, probably the first time discovered in prehistoric times [177]. Copper oxides exist in two stable forms, i.e. cuprous oxide Cu_2O and cupric oxide CuO. The basic properties of Cu, Cu_2O and CuO are summarised in Table 3.

Table 3 Properties of copper and its oxides [102,177–184];

Property	**Cu**	**Cu_2O**	**CuO**
Density, g/cm^3	9.0	5.7 - 6.1	6.6
Crystal system	cubic	cubic	monoclinic
Point/ Space group	$O_h^5/Fm\bar{3}m$	$T_h^2/Pn\bar{3}$ or $O_h^4/Pn\bar{3}m$	$C_{2h}^6/C2/c$
Melting point, °C	1085	1508	1630
Electric properties	conductor	semiconductor	semiconductor
Band gap, eV	-	2.2	1.0 - 1.7
Dielectric constant	-	7.1	18.7
Refractive index	-	2.7	2.9
IEP*	9.8	5.0 - 11.5**	4.0 - 9.9**
Colour	reddish brown	red	black

*According to the literature
**Depends on measurement technique

The most stable phase among copper species in the Cu-O system, at room temperature and under normal pressure is CuO (Figure 18).

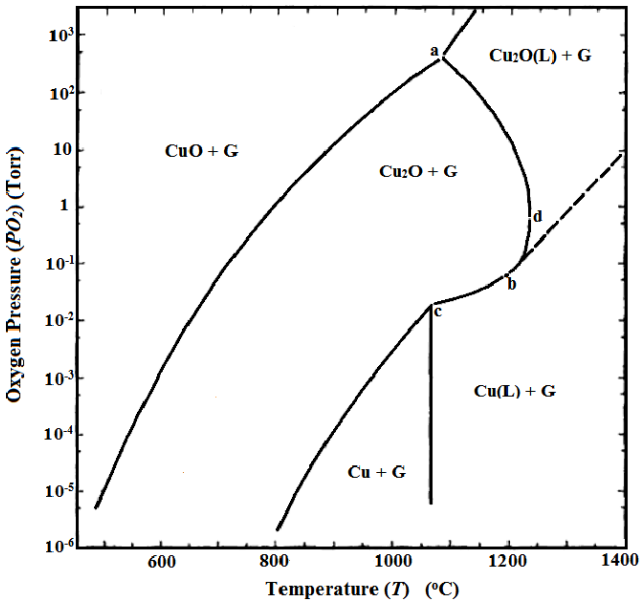

Figure 18 Cu-O phase diagram [185];

The solubility of copper species is a very important property when considering their application in water treatment. The Pourbaix diagram describes the conditions of copper species stability (Fig. 19). Copper solubility in water depends on the temperature, pH, dissolved oxygen, concentration of dissolved copper, as well as on the presence of ions [186,187]. Precipitation-dis-

solution, complexation and acid–base reactions govern copper speciation in water [186]. Temperature affects the different stability areas of immunity, passivity and corrosion. Immunity (metal stability) and passivity (oxides formation) decrease with increasing temperature. The corrosion area for acidic pH range increases with the increase in temperature, due to the decrease in passivity and immunity, while the corrosion area at alkaline pH increases [187]. Immunity and passivity areas increase with higher concentration at elevated temperature, while the corrosion area decreases [187]. The Pourbaix diagram for copper shows that copper is a noble metal above the H^+/H_2 line. Nevertheless, in an oxidising environment at acidic conditions copper dissolves and forms copper(I) ions, which at a higher potential is further transferred into Cu^{2+}. An oxidising environment in an alkaline pH oxidises Cu to $Cu(OH)_2^-$.

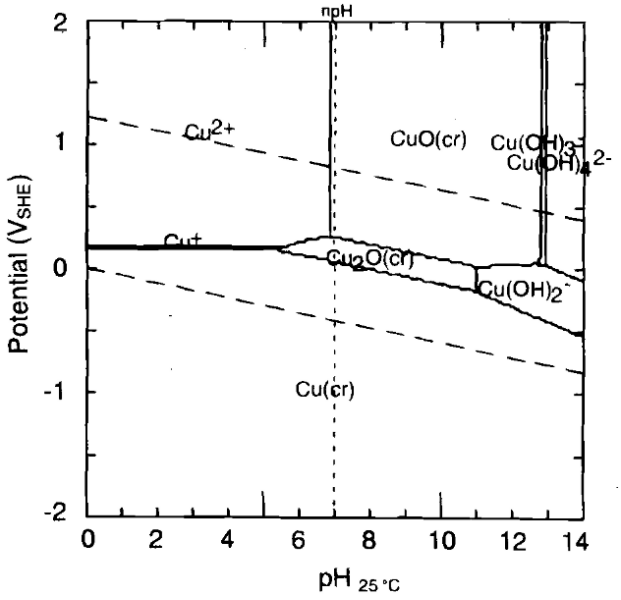

Figure 19 Pourbaix diagram of copper at 25 °C for $[Cu_{(aq.)}]_{tot}=10^{-6}$ mol/kg [187];

According to Figure 20, CuO (tenorite) is more soluble than Cu_2O (cuprite) under normal conditions within a wide pH range. Under alkaline conditions, an opposite trend is observed. Cuprite is stable from pH 7.5 to 8.5, tenorite from 8 to 11, while the correlation between $Cu_2(CO_3)(OH)_2$ (malachite) and $Cu(OH)_2$ (cupric hydroxide) is similar. The copper ion is stable in solution for pH<7.0, also at that time a formation of the ion occurs from the oxide state [188].

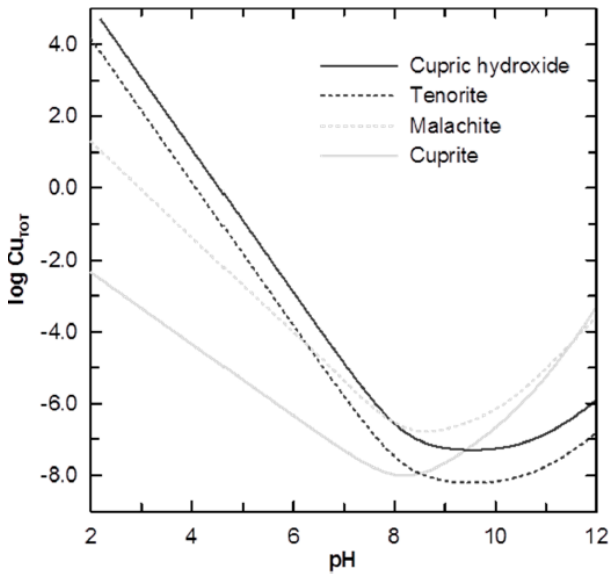

Figure 20 Solubility of copper species depending on water pH [186];

When applying copper in water treatment, it is important to consider its concentration in drinking water and its influence on the health of humans. The pH of drinking water is typically in the range from 6.5 to 8.5, while in case of natural waters (rain water, ground water) the pH may be lower (even equal to 4 [189]), due to e.g. acid rain [190]. These factors, in turn, may affect some stages of water purification and, in this case, potential release of copper [190]. Trace amounts of copper are vital for human diet, however, the ingestion of copper could induce acute and chronic effects, with long-term overexposure potentially resulting in liver damage due to copper accumulation [186]. WHO established a value of maximum copper concentration in drinking water equal to 2 mg/L [191]. Some countries have decided to set more strict limits, e.g. Switzerland 1 mg/L [192].

Copper is known since ancient times as an effective disinfecting agent. It was utilised to manufacture primitive medical instruments, as well as to be pressed to wounds to avoid infection spreading [177]. Current studies distinguish antibacterial [14,15,147,193] and antiviral [13–16,147] properties of copper and its species. Copper inactivation mechanism of bacteria is explained in a contact killing concept [194].

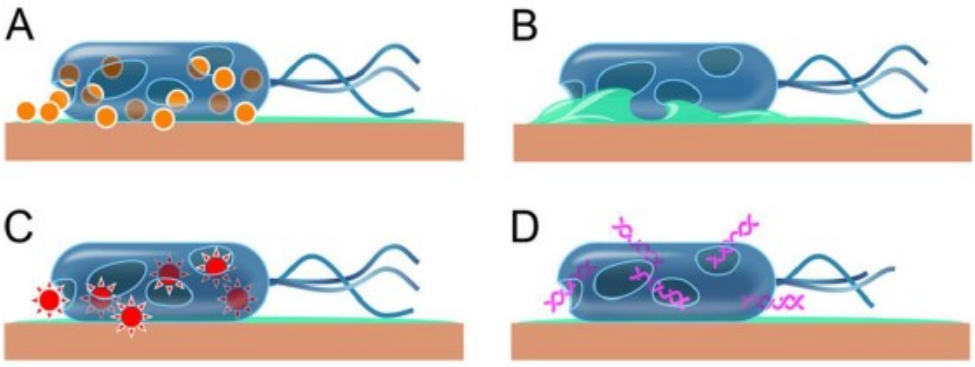

Figure 21 Scheme of the contact killing mechanism of bacteria; a) copper dissolution and cell damage; b) cell membrane rupture due to copper and other stress phenomena; c) copper ion induction or reactive oxygen species, which cause further cell damage; d) DNA degradation [194];

In this mechanism (Fig. 21), copper ions interact with the microbe cell membrane causing its damaging. Copper ions induce the generation of reactive oxygen species (ROS). Emerging hydroxyl radicals (Eq. 1) lead to the oxidation of amino acids – components of many lipids and proteins (Eq. 2 and Eq. 3) Oxidation stress triggered by copper redox reactions cause further cell damage. As a result, the DNA of bacteria is damaged.

$$Cu^{+} + H_2O_2 \rightarrow Cu^{2+} + OH^{-} + OH^{\cdot} \quad \text{Eq. 1}$$

$$2Cu^{2+} + 2RSH \rightarrow 2Cu^{+} + RSSR + 2H^{+} \quad \text{Eq. 2}$$

$$2Cu^{+} + 2H^{+} + O_2 \rightarrow 2Cu^{2+} + H_2O_2 \quad \text{Eq. 3}$$

Nonetheless, it is not fully understood, which factors exactly influence contact killing. It was proven that copper ions and factors influencing their solubility affect process efficiency [194]. It has been reported that bacteria can establish a defence mechanism against copper, e.g. by producing proteins able to complex metal ions, reducing permeability of bacteria membranes to copper [194].

There are no systematic studies regarding the correlation between the bactericidal and virucidal characteristics of copper, as well as their bacteria/ virus removal mechanisms. The difficulty comes from the differences in viral structure, presence of outer capsids, as well as secondary reactions [195]. In literature, there is limited information regarding exact virucidal behaviour of copper species. Furthermore, varieties of test conditions are presented to determine the antimicrobial properties of copper and its oxides [13,16,196,197]. Applied experimental conditions vary between experiment types, e.g. contact or flow, water pH and composition, type and concentration of tested microorganism/ virus, exposure time, etc.

Sunada et al. presented three origins of copper compounds virucidal behaviour: formation of ROS, release of copper ions and immediate contact with the material surface [16]. ROS role

was questioned owing to the fact of no metabolic virus activity that cannot produce superoxide or hydrogen peroxide, which aim to form hydroxyl radicals in reaction with copper ions. Influence of released copper ions was also contradicted due to the fact that permeate, which contained released ions of Cu^{+} and Cu^{2+}, exhibited very low reduction. Opposite, Armstrong et al. observed reduction of MS2 increased with increasing doses of copper equal to 1.8 LRV of MS2 within 6 hours due to 0.3 mg/L of dissolved ionic copper [196].

Nieto-Juarez et al. discussed inactivation of MS2 phages in advanced oxidation process, influenced by presence of H_2O_2, copper concentration, $HO^{\cdot}$ production and sunlight in natural waters, concluding that hydrogen peroxide concentration in natural waters might be too low as well as the complexation of the trace metals by organic matter may lead to its reduced activity [198]. Copper acting in Fenton reactions was also reported in many other publications [199–201].

Thurman et al [38] discussed the molecular mechanism of copper ion disinfection of viruses, which can be effectively done by blocking or destroying of host-cell receptors or the nucleic acid and proposed impact of toxic metals in general. Overall, the metal ion may inactivate viruses by reacting outside or inside the virus directly or indirectly [38]. Lund et al revealed that heavy metals exhibit oxidation power and might react with proteins or nucleic acid of viruses [38,202]. Copper can facilitate hydrolysis or nucleophilic displacement either directly, through polarization of the substrate and subsequent external attack by the nucleophile (hydroxide radical), or indirectly, through generation of a coordinated reactive nucleophile (reactive base reagent), while hydroxylated metal oxides may undergo nucleophilic attack [38,203]. Martin et al., Hutchinson et al. and Wong et al. reported complexation of RNA by copper that exhibited affinity for either O, N and S sites of RNA, leading to its degradation [38,204–206]. Rifkind et al. found copper affinity to phosphates groups of nucleic acid caused its disordering [38,207]. There were also proposed two contradiction models describing copper binding to DNA resulting in its destabilisation [38,208,209].

Copper and its oxide besides being virucide, possess other properties crucial in water treatment applications. Copper is an abundant element, cost-effective and a less toxic material in comparison to other metals [197]. Copper and its species have a positive surface charge derived from base-range isoelectric points. This makes copper an attractive choice for the targeted application, as its presence provides a positive surface charge of synthesised composites and supports, achieving more active adsorption sites for virus removal.

6. Adsorption process in context of study application

Adsorption is a process of enrichment of one or more components on interfacial layer. It can be distinguished for two processes: chemisorption and physisorption, depends on involved forces. Physisorption is a process related to the condensation of vapour, which may form multilayer. This is a reversible process, exothermic, where the energy of physisorption is equivalent of the energy of condensation (usually <50 kJ/mol). Physisorption reaches fast equilibrium and decreases with temperature increase. Chemisorption comprises the chemical bonds formation between adsorbent and adsorbate, leading to monolayer formation. The process is irreversible with the same magnitude of energy change as chemical reaction, absorption usually increases with increasing temperature.

Adsorption processes are widely used in water treatment. Depending on the adsorbent type used different type of contaminations can be removed from water, e.g. organics substances, inorganic ions [22].

In described PhD thesis, adsorption in liquid phase, as well as an electrostatic adsorption found an application. The first one helps to explain phenomena that take place during composites synthesis, while the second one describes filter material working principle and the interactions between the filter material and viruses.

6.1. Adsorption in liquid phase- application in composites synthesis

In the liquid phase adsorption, a solute form of dilute solution onto a solid surface is observed as an exchange process between the solute in solution and molecules adsorbed on the surface. The adsorption process is affected by solvent (that impacts mobility of adsorbed solute molecules), the interaction between solvent and solute, the interactions between solute molecules both in the bulk solution and on the surface, as well as the surface properties of roughness, porosity and heterogeneity.

All the isotherm equations for gas phase adsorption can be extended to liquid phase (except capillary condensation theory) by replacing the pressure term with concentration and corresponding changes in the units of the parameters. The liquid phase adsorption is more complex regard gas one, due to presence of solvent molecules and formation of micelles [210]. Despite monolayer coverage occurrence, the adsorbed molecules are not necessarily tightly packed with the same orientation.

Reaching and describing adsorption equilibrium is crucial to assess the adsorption process and design of adsorbent. The adsorption equilibrium is described by adsorbate concentration, adsorbed amount and temperature. Temperature is kept as constant and equilibrium relationship is expressed as: $q_{eq} = f(c_{eq})$, T=const.

The Langmuir model is generally suitable for describing the chemisorption process when ionic or covalent chemical bonds are formed between the adsorbent and the adsorbate [211]. In this work, the Langmuir model is established to describe adsorption of Cu^{2+} ions from aqueous solution onto carbon substrates. The model assumes (i) energy homogeneity of adsorbent surface, (ii) one surface active site being occupied by one molecule (the monolayer formation), (iii) no interactions between adsorbate molecules. This model is an interpretation of Type I isotherm. The kinetic derivation of Langmuir model has the following form [212]:

$$\theta = \frac{bC}{1+bC} \qquad \text{Eq. 4}$$

where: θ – fraction of sites already filled, b – constant, C – solution concentration, p – pressure.

To understand the adsorption process of aqueous Cu^{2+} onto carbon a speciation of copper ions in aqueous solution is necessary. Various factors affect the adsorption of metal ions from aqueous solution, including metal ions concentration, their speciation, solution pH, contact time, temperature, adsorbent dosage and its surface functionality [213]. In dilute solutions of metal ions, hydrogen bonding in the solvent and hydration of ions is more significant than surface heterogeneity. In the case of carbon based material, surface chemistry means oxygen-containing functional groups (i.e. carboxyl, carboxylic anhydrides, lactone, lacto and phenolic hydroxyl groups), which determines the point of zero charge [214].

Equation 5 presents the general hydrolysis reaction of metallic cations, while Table 4 summarises hydrolysis constants for copper.

$$xM^{z+} + yH_2O = M_x(OH)_y^{(xz-y)+} + yH^+ \qquad \text{Eq. 5}$$

Table 4 Summary of copper ion hydrolysis at 298 K* [215];

Species	Log K_{xy}	A	Bm_x
$Cu(OH)^+$	<-8.0	-1.022	+0.25
$Cu(OH)_2$	<-17.3	-1.022	+0.20
$Cu(OH)_3^-$	<-27.8	0.000	-0.40
$Cu(OH)_4^{2-}$	-39.6	2.044	-0.16

*Log β_n = Log k_n + $AI^{1/2}/(1+I^{1/2})+Bm_x$

(β_n, k_n, overall formation quotient and formation constant for a hydrolysis product formed by reaction with water, m_x molality of OH^- in all its forms; I ionic strength), m_x=1.0

Taking into account above mentioned, it is possible to calculate speciation of $Cu^{2+}_{(aq)}$ ions in solution, which is presented on Figure 22. For calculations, ChemEQL v.3.2 software was applied. The low solution concentrations used in this study do not allow precipitation to occur, and, therefore, the speciation diagrams can be constructed from the hydrolysis equilibria of mononuclear hydroxides using hydrolysis constants. It is clearly visible that Cu^{2+} ions start to hydrolyse at pH ~ 6, in case of more dilute solution (0.02 mmol).

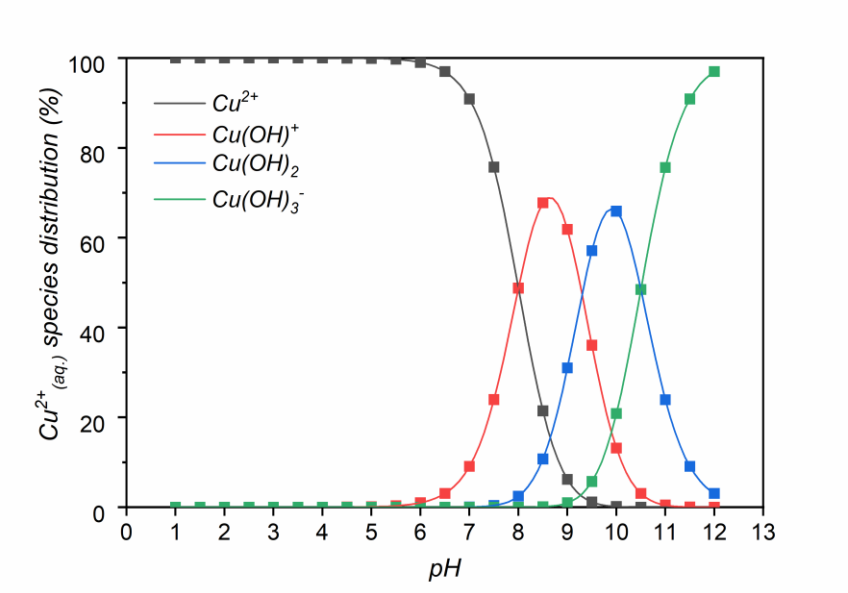

Figure 22 Speciation of $Cu^{2+}_{(aq.)}$ ion species in dilute aqueous solution;

The mechanism of metal ions adsorption has been widely discussed, however not fully explained. It is complex and attributed to chemical and physical adsorption between adsorbent and metal ion [211]. Chemical adsorption includes chelating formation, electrostatic attraction, and ion exchange, while physical adsorption provides Van der Waals forces and hydrogen bond interaction.

Van der Waals forces include repulsion and attraction forces and have three major contributions like dipole-dipole attraction, dispersion force and induction force [211]. Hydrogen bond interaction occurs for hydrogen atoms (present in functional groups, i.e. hydroxyl, carboxyl) that react with the electronically negative atoms, such as O, S, N, F, Cl, of the adsorbate molecules by lone pair electron [211]. Chelation is a bonding type between metal ions and molecules. It involves formation of more than two separate coordination bonds between a single central atom and multiple bonded ligand [211]. Generally, these ligands refer to organic compounds. Electrostatic interaction concerns electrostatic force of long-range interaction taking place between the attractive electrostatic adsorption in aqueous solution of differently charged particles and

solid adsorbent. Ion exchange refers to atom exchange between adsorbent atoms and solute ions via ionic bonds. The adsorbent has functional groups (e.g. hydroxyl, carboxyl or amino) that are ion exchanged with electrolyte cation or anion in aqueous solution reaction.

For carbon based adsorbents with functional groups and Cu^{2+} aqueous ion, we can take into consideration electrostatic attraction, ion exchange and Van der Waals force that take place during synthesis process.

Variety of interactions between metal ions and the adsorbent material surface (here carbon) could occur [213]:

(i) Formation of surface complexes

$$2(COH) + M^{2+} \overset{K_1^{`}}{\leftrightarrow} (CO^-)_2M^{2+} + 2H^+ \quad \text{Eq. 6}$$

$$or\ 2(CO^-) + M^{2+} \overset{K_1^{`}}{\leftrightarrow} (CO^-)_2M^{2+} \quad \text{Eq. 7}$$

$$2(COH) + MOH^+ \overset{K_2^{`}}{\leftrightarrow} (CO^-)_2MOH^+ + 2H^+ \quad \text{Eq. 8}$$

$$or\ 2(CO^-) + MOH^+ \overset{K_2^{`}}{\leftrightarrow} (CO^-)_2MOH^+ \quad \text{Eq. 9}$$

$$2(COH) + M(OH)_2 \overset{K_3^{`}}{\leftrightarrow} (CO^-)_2M(OH)_2 + 2H^+ \quad \text{Eq. 10}$$

$$or\ 2(CO^-) + M(OH)_2 \overset{K_3^{`}}{\leftrightarrow} (CO^-)_2M(OH)_2 \quad \text{Eq. 11}$$

$$2(CO^-) + M(OH)_3{}^- \overset{K_4^{`}}{\leftrightarrow} (CO^-)_2M(OH)_3{}^- \quad \text{Eq. 12}$$

(ii) Ion-exchange processes

$$-OH + M^+ + X^- = -OM + X^+ + X^- \quad \text{Eq. 13}$$

$$-OH + M^+ + OH^- = -OM + H_2O \quad \text{Eq. 14}$$

The adsorption mechanism of most metal ions at low concentration can be described as the ion exchange between protons and metal ions. At higher concentration, a more complex reactions might be considered [150].

(iii) Redox reactions with a change of metal valence

Cu^+ cation is rather unstable in aqueous solution, therefore redox reactions can take place under presence of complexing agents that would stabilise Cu(I).

6.2. Filter working principle and DLVO Theory

Assumed working principle of fabricated composites for virus removal is based on the electro-static adsorption between positively charged filter material and negatively charged viruses [35,38,95,98]. Sobsey et al. revealed that positively charged filters are more efficient in virus removal under water conditions, where the net charges of the virus particles and filter media

are opposite [98]. According to the theory, viruses can be attracted to an oppositely charged material and adsorbed on it. The majority of enteric viruses carry a negative charge in natural pH conditions, the isoelectric point is in the range 1.9-8.4, depending on the species [50,216]. Carbon substrates modified with copper species will provide positive surface charge (isoelectric point, measured in other work performed within MultiCarboVir Project, of Cu, Cu_2O and CuO is 7.4, 11 and 9.5, respectively [217]) of Cu_2O/ MWCNTs and Cu/ ACFs composites (Fig. 23). Moreover, the high Hamaker constant of graphitised substrates may lead to irreversible virus particles bonding due to Van der Waals attraction after initial contact. Metal-virus interactions may damage the virus protein capsid or genome, resulting in non-reversible inactivation of the viruses [218,219].

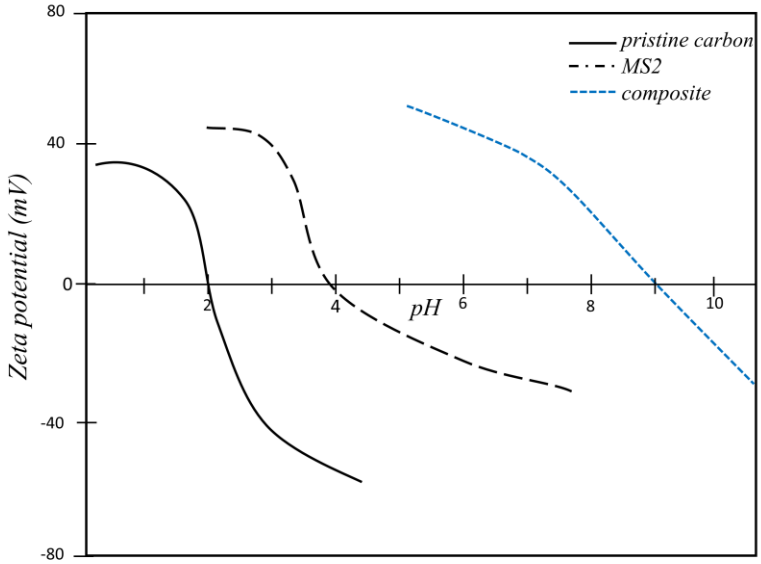

Figure 23 Scheme of carbon-copper composite material working principle;

The Derjaguin-Landau-Verwey-Overbeek (DLVO) theory was originally formulated to determine the colloidal system stability, taking into account attractive long-range Van der Waals forces and repulsive electrostatic interactions [212]. The basic hypothesis assumes that the forces (and potentials) between considered surfaces are additive and do not influence each other mutually [220]. The DLVO theory is often used in a broader sense, including other forces under the assumption of their additivity [220]. It is applied to describe forces between colloid and surface, thus it can be used to explain adsorption phenomena based on overall assumed electrostatic interactions and Van der Waals attraction between virus and solid material [221]. This basic framework in understanding the mechanism and forces governing virus adsorption has to be broadened taking into account role of the other forces.

The DLVO theory has been related to smooth particles with ideal geometry and uniform properties. At particle scale, adsorption/ desorption phenomenon is governed by attractive and repulsive forces that takes places between virus and material. These interactions include electrical double layer attraction/repulsions, London-Van der Waals forces, short-range forces as hydration and steric repulsions [72]. Interactions are dependent on the isoelectric point of virus and its hydrophobic/ hydrophilic nature, isoelectric point of material and environmental physical (flow velocity, viscosity of fluid) and chemical conditions (pH, ionic strength of solution, and presence of organic matter). pH affects the net charge, while ionic strength influences the double layer compression/expansion, leading to attraction/repulsion [71].

The electrical double layer potential energy (ϕ^{DL}) corresponds to the overlapped, charged surfaces diffusion, surrounding ion to balance charges [72]. There are two parallel layers, the first one (0.1 nm) is the surface charge, formed by ions adsorbed on the object due to chemical interactions. The second layer (0.5 nm) consists of oppositely charged ions attracted to the surface via the Coulomb force, electrically screening the first layer. Coulomb interactions are very strong and of long range, although much weaker in water [212,222]. The double layer is sensitive to solution chemistry.

London- Van der Waals forces (ϕ^{vdW}) are due to dipole-dipole instantaneous interactions between surfaces [72]. They depend on the polarizability of interacting surfaces and the solution, as well as surfaces surface area. Changes in the solution chemistry (pH, ionic strength) have no influence on those forces. Van der Waals forces are anisotropic (exception between two noble gas atoms) meaning depend on the orientation of the molecules. VdW interactions are characterised by Hamaker constant, characteristic of material. This value depends on polarizability, density of material, dielectric properties of the medium surrounding the particles. It can be positive or negative for specific types of material/ medium pairs [222]. Negative value means that VdW interactions are repulsive. Van der Waals forces are essentially electrostatic interactions and refer to the induction force, the orientation force and the dispersion force. Induction force describes the attraction between two polar molecules, each of which has the electric dipole moment and is temperature dependent [223]. The orientation force arises between permanent dipoles and induced dipoles (the molecule with a permanent dipole repels another molecule's electrons), as well as induced and permanent dipoles (not temperature dependent) [223]. Dispersive forces (London forces) are generally long-range forces, however, depending on the situation they can act on large distances (>10 nm) and short ones (~0.2 nm) [222]. Those forces occur between any pair of molecules, including non-polar atoms. They can be repulsive or attractive. Dispersive forces do not only bring the molecules together but tend to mutually align

or orient them (effect is weaker then with dipolar interactions). Those forces are not additive, meaning that the force between two bodies is affected by the presence other bodies nearby [222]. The short-range forces (<10 nm) are not well explained, but it is assumed that they are caused by hydration or steric/structural repulsion. Such forces could have large impact on the colloidal system properties, and even sometimes dominate [212]. They define primary minimum of finite depth (ϕ_{min1}), their effect is defined in two ways: minimum separation distance related to the shear plane distance and the thickness of the layers of hydrated water between surfaces; as well as the Born potential energy (ϕ^{Born}) [72]. Hydrophobic effect results in a free energy gain in the system, where the interfacial area between water and apolar surfaces is minimised by adsorption. This effect is increasing with increasing apolarity. Hydrogen bonds are formed between donating and accepting moieties on the virus and adsorbent surfaces, however, they are likely suppressed in aqueous systems [71]. Steric repulsions occur at very small interatomic distances, when the electron clouds of atoms overlap. Those forces determine how close two atoms/ molecules can approach each other [222]. The structuring of solvent molecules is determined primarily by the geometry of molecules [222,224], so steric effects might come from topographies of both virus and adsorbent [71]. Those forces depend not only on the properties of the intervening liquid medium but also on the chemical and physical properties of the surfaces, e.g. hydrophilic or hydrophobic, smooth or rough, amorphous or crystalline (atomically structured), homogeneous or heterogeneous, natural or patterned, rigid or fluid-like [222]. When a surface is approached by a second surface, the ordering of liquid molecules in between is disrupted as they are confined in a very small space [224]. This phenomenon of ordering change gives rise to the solvation force, called also hydration force, when the solvent medium is water [224].

The total potential energy (ϕ^{Total}) is a sum of electrical double layer interactions, Van der Waals forces and the Born potential energy, dependent on the distance between two surfaces, as depicted on Figure 24.

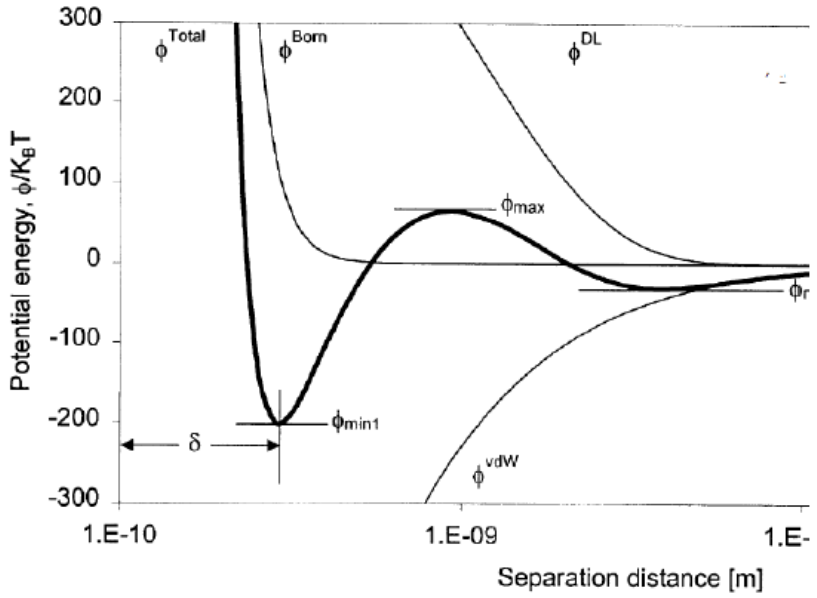

Figure 24 DLVO potential energy as a function of separation distance between colloid and surface;

When the interactions between oppositely charged virus and surface are considered, the London- Van der Waals potential energy and double layer potential energy become negative (the corresponding double layers of two charged bodies approach overlap, the local ion concentration increases compared to the bulk, thus creating an osmotic pressure, and therefore, a corresponding repulsive force) and separation distance decrease. Thus, the total potential energy is negative or favourable, characterised only by the primary minimum (ϕ_{min1}) and there is no energy barrier. Here the critical role plays high value of graphitised material Hamaker constant that help to irreversibly adsorb pathogen particle after the initial contact.

In case of interaction between like-charged virus and surface, when their double layers overlap, the double layer potential energy increases with decrease of the separation distance. This phenomenon is due to the repulsion between charges. The counter ions are forced into a smaller space, decreasing their entropy and giving rise to a repulsive interaction force [212]. The total potential energy is characterised by a minimum at low distance (ϕ_{min1}). With increasing separation distance the potential energy exhibits repulsive energy barrier (ϕ_{max}) and a local secondary minimum at ϕ_n. The potential energy secondary minimum takes place when Van der Waals attraction exceeds the repulsion of the electrical double layers.

It is assumed that electrostatic repulsions between virus and like-charged adsorbent inhibit or hinder adsorption [225,226]. However, in the study of Armanious et al. it is suggested that adsorption of viruses is feasible, but weak. Its occurrence is governed by the contribution from the hydrophobic effect in addition to VdW interactions and a steric effect [71].

Above mentioned proves the complexity in understanding all the forces involved in mechanism of virus adsorption onto solid material. It is important to consider carefully the role and impact of particular forces on relationship between virus and adsorbent. This can be helpful in designing and developing efficient material for water purification.

II Experimental Part

7. Objectives of the Experimental Part

The main goal of this PhD work was to develop an efficient adsorption material for water treatment with a focus on virus removal at the household scale. To do so, carbon substrates of multi-walled carbon nanotubes and activated carbon fibres were selected and their surfaces were functionalised and purified through oxidation, then modified via different synthesis routes to obtain composite materials of Cu_2O/ MWCNTs and Cu/ ACFs.

First, multi-walled carbon nanotubes and activated carbon fibres were treated within purification and functionalisation steps. MWCNTs treatment aimed to remove heavy metal contaminations (catalyst) and incorporate functional groups onto MWCNTs surfaces using a two-step process of (i) non-oxidative treatment with diluted HCl and (ii) oxidation with hot concentrated HNO_3 [227]. Incorporation of functional groups onto ACFs surfaces was done via oxidation using concentrated HNO_3, followed by Soxhlet purification to remove acid residuals. Carbon substrates were fully characterised before and after functionalisation to understand the process's influence on the physical and chemical properties of the material. The following techniques were used to characterise the functionalised MWCNTs and ACFs:

- SEM for ACFs, TEM for MWCNTs to determine the surface morphology;
- Elemental analysis to determine the contents of carbon, hydrogen, nitrogen and oxygen;
- Raman spectroscopy to identify defects in material structure;
- XPS to detect the types of functional groups;
- Acid/base titration to qualitatively and quantitatively determine functional groups;
- pH drift method to measure the point of zero charge;
- ICP-MS to determine the amount of removed catalyst from MWCNTs;
- Specific surface area and porosity measurement using adsorption of N_2 (77 K) and CO_2 (273 K);

Functionalised carbon substrates were utilised for composites preparation. Cu_2O/ MWCNTs composites manufacturing procedures included the following syntheses:

(i) Adsorption of aqueous copper ion;
(ii) Adsorption of copper(II) hydroxide;
(iii) Adsorption of copper complex;

While the preparation of Cu/ ACFs composites comprised of:

(iv) Adsorption of aqueous copper ion;

The obtained MWCNTs composites were utilised in the form of a membrane filter, while ACFs composites were placed in cartridges. The manufactured composites were first conditioned to examine their stability and the potential release of copper species. The conditioning test was an important prerequisite to understand the long-term viability of the material for water treatment and virus removal.

Further studies included a virus removal efficiency test, where MS2 bacteriophage was applied as a virus surrogate. The virus removal study was performed by passing the MS2 bacteriophage solution (at pH 5 and 7) through the as-prepared filters or cartridges at a constant flux. Virus removal efficacy was assessed for as-received and functionalised carbon materials, as well as synthesised composites. The concentration of MS2 in the permeate was tested with time control (checked directly after permeate collection t=0 h, and after two hours of storage t=2 h), followed by copper concentration evaluation in the permeate to determine the presence of desorbed/ dissolved copper and its effect on virus inactivation.

However, further studies performed within the MultiCarboVir project by its project partner - Eawag, suspected (however does not quantify) a MWNCTs release from the filter into the permeate. Such a phenomenon is not acceptable for water treatment technology, as it increases negative health impact risks. Nonetheless, studies performed using MWCNTs gave a deeper insight into important aspects of virus removal investigation. Based on that, a decision was made to divert further studies form MWCNTs and focus on other, more promising carbon substrates, such as ACFs.

8. Material characteristics

8.1. Properties of as-received carbon materials

Multi-walled Carbon Nanotubes

Commercial Multi-walled Carbon Nanotubes 20-30 nm were purchased from Cheap Tubes company (Lot 030104, CAS 308068-56-6). According to the data sheet provided by the supplier, the material was characterised by a declared purity >95 wt.%, outer diameter 20-30 nm, length 10-30 µm, SSA 110 m^2/g. MWCNTs were grown by means of CCVD on iron and nickel catalysts.

Figure 25 presents TEM images of as-received MWCNTs, which are highly agglomerated and form a bundled network. The measured outer and inner diameters are in the range of 10-30 nm and 3-5 nm, respectively, varying along the given tube length. The multi-walled structure of MWCNTs is clearly visible on TEM images (Fig. 25) and the wall thickness is in the range of

2-4 nm. The measured specific surface area is 117 m^2/g, which, together with measured diameter, are in accordance with the data given by the supplier.

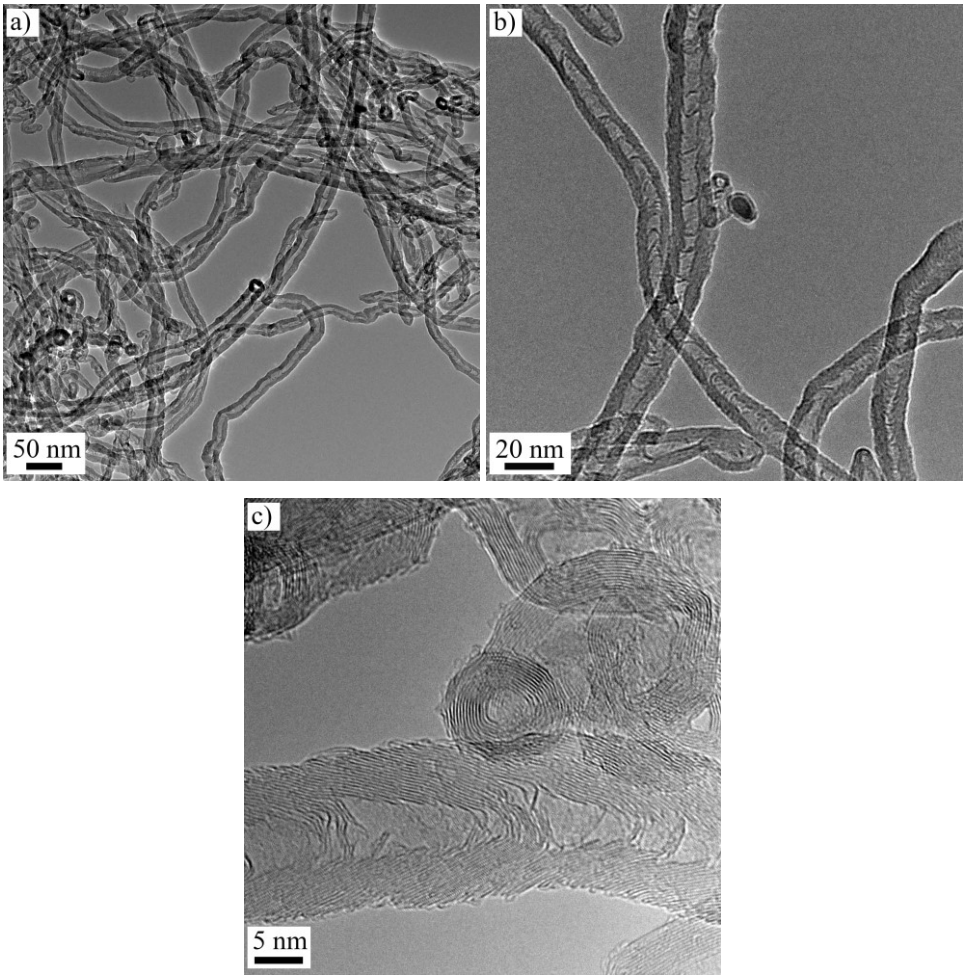

Figure 25 a, b and c) A series of TEM images of as-received multi-walled carbon nanotubes;

The Raman spectrum presented in Figure 26 shows the characteristic bands of the as-received MWCNTs. The D band at 1345 cm^{-1} is associated with the defect in the carbon with sp^2 hybridization [1]. The peak is prominent indicating a high defective level of the material' structure [2]. There are observed a two overlapping bands at ~1600 cm^{-1}, the G band at ~1580 cm^{-1} and D' band at~1612 cm^{-1}. The G band is associated with the graphitisation of the sample, circumferential displacement, and in-plane vibration of the C-C bond in all sp^2 carbon materials [1]. The D' band provides information about atomic displacement along the nanotube axis [1]. The G*, G', D+G and 2D' bands are also visible at 2450 cm^{-1}, 2690 cm^{-1}, 2930 cm^{-1} and 3210 cm^{-1}, respectively, whose intensities increase with the number of defects [3]. Additionally, the ratio

between the area of the D and G bands is relatively high (D/G=1.55), proving that the as-received MWCNTs have many defect points, which may potentially lead to easier surface modification.

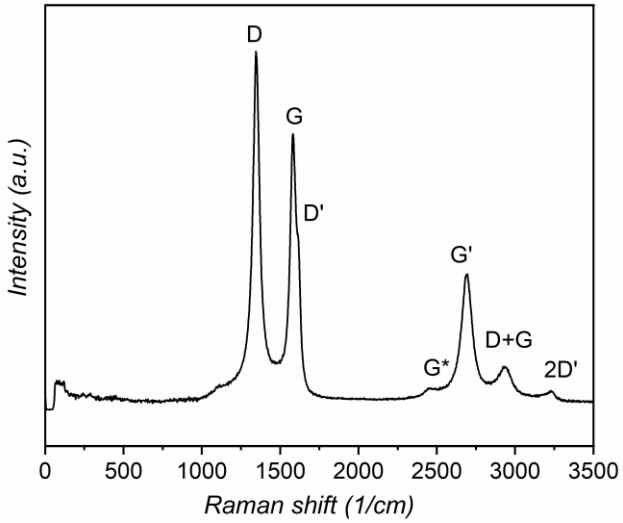

Figure 26 Raman spectrum of as-received multi-walled carbon nanotubes;

Activated Carbon Fibres

Commercial activated carbon fibres, type ACF-1603-20, were bought from Kynol Europa GmbH. Characteristics given by the supplier are the following: fibre length: 3±1.5 mm, diameter 9 μm, moisture content 45-55 %, pore volume 0.8 cm^3/g, micropore diameter 21-27 Å. The fibres were made of phenolic resin and were activated by carbonization at high temperature. Further details regarding the carbonization and activation steps were not disclosed by the supplier.

Figure 27 presents the SEM images of the as-received ACFs. The images indicate a heterogeneity of the material (Figure 27a, and 27b). Some of ACFs have smooth, fine and regular surface, however, some of them have grooves on their surfaces, which could be interpreted as micropores. The fibres have a uniform diameter and fibre shape. The measured diameter is in the range 9-18 μm, with a length of 1.5-4.5 mm. On some fibres, surface contaminations were observed, which were recognised with EDX as carbon particles. The cross-section of as-received fibres (Figure 27c and 27d) revealed that the fibres have something resembling and shell, which looks porous. Due to the limited resolution of the microscope, there is no possibility to observe a nanoporous structure, however, it was possible to determine the presence of porosity via BET/ BJH studies.

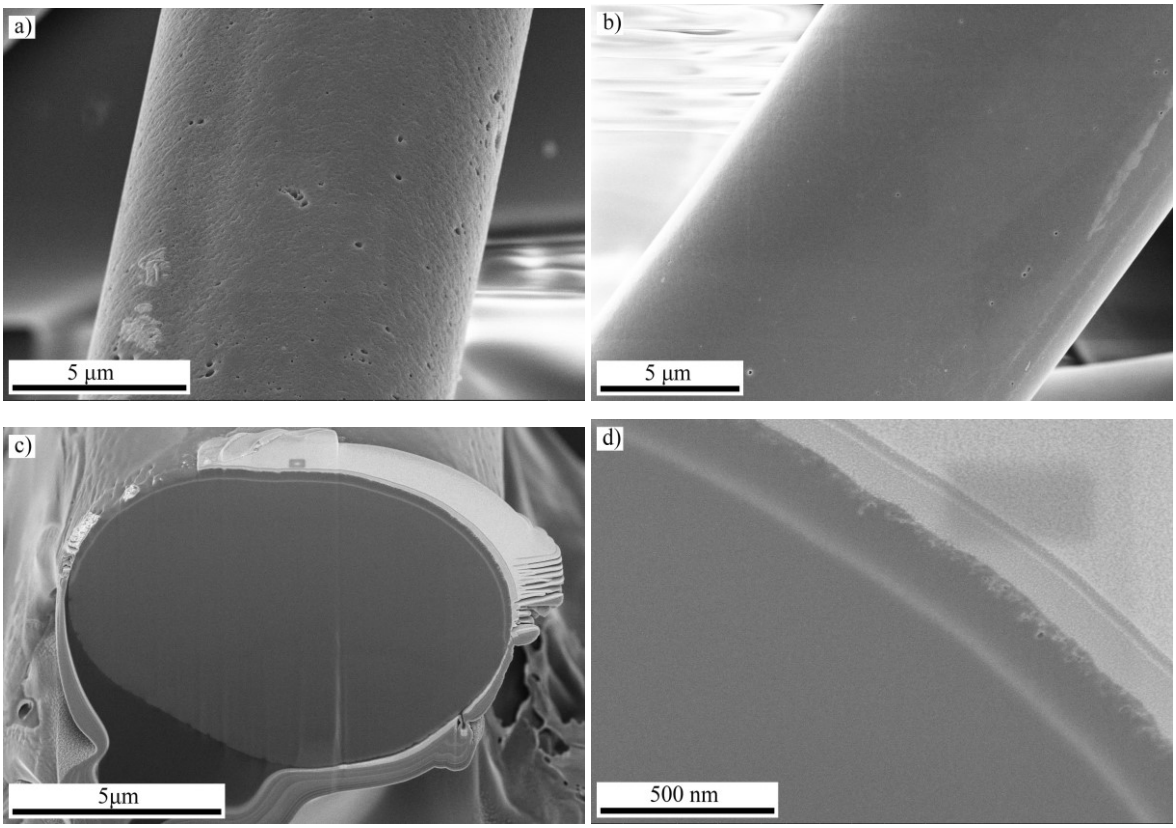

Figure 27 a, b, c, d) SEM images of as-received activated carbon fibres;

The Specific surface area of as-received ACFs is equal to 1677 m^2/g, while total pore volume V_{N2}=0.453 cm^3/g, and micropore volume V_{CO2}=0.108 cm^3/g. The calculated mean radius of the micropore from N_2 at 77 K and CO_2 at 273 K adsorption is 1.08 nm and 0.26 nm, respectively. Raman spectroscopy of ACFs shown in Figure 28 presents the characteristic carbon bands. The D and G bands, observed at 1344 cm^{-1} and 1599 cm^{-1}, respectively, are typical for activated carbon fibres. The G band corresponds to graphitic in-plane vibrations with E2g symmetry, while the D band is believed to arise from the presence of defects and disorders, such as the presence of in-plane substitutional heteroatoms, grain boundaries, aliphatic chains, etc., which serve to lower the symmetry of the quasi- infinite lattice [228]. Both peaks are prominent and narrow, indicating a low defective level of the material's structure [229]. The second order frequency, which splits into three bands, was detected: the G', D+G and 2D' bands visible at 2715 cm^{-1}, 2920 cm^{-1} and 3200 cm^{-1}, respectively. Split bands occur for highly ordered crystalline materials [229].

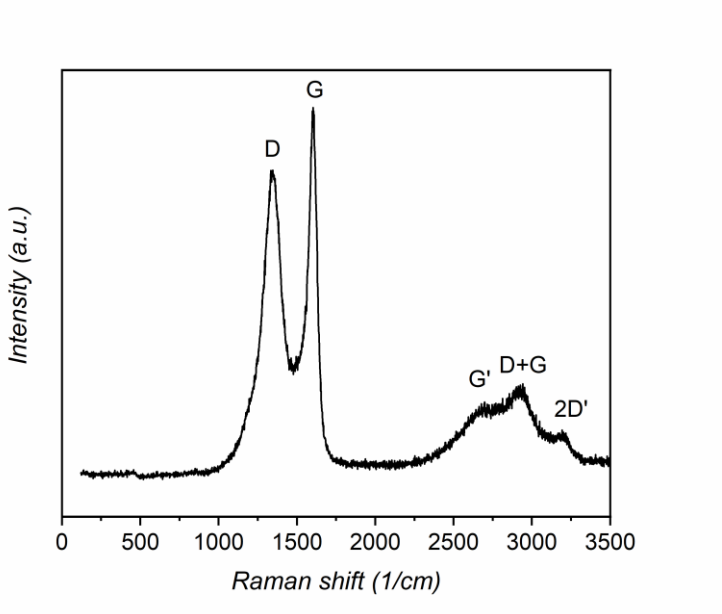

Figure 28 Raman spectrum of as-received activated carbon fibres;

8.2. Gases and other reagents

A variety of gases and reagents were used through the duration of presented work. Their specifications and applications are listed in Table 5.

Table 5 The gases and reagents used in the study;

Name	Formula	Supplier	Specification	Application
Gases:				
Carbon dioxide	CO_2	Pangas	99.995%	Porous structure characterisation
Hydrogen/ Argon	H_2/Ar	Pangas	2 vol.% H_2 in Ar 99.995%	Composite synthesis
Nitrogen	N_2	Pangas	≥99.995%	Composite synthesis, samples degassing, porous structure characterisation
Reagents:				
Ammonium hydroxide	NH_4OH	Merck	Ph. Eur., ~25%	Composite synthesis
Bacteriological Agar	$(C_{12}H_{18}O_9)_n$	Merck	For microbiology	DAL method
Calcium chloride	$CaCl_2$	Merck	Ph. Eur.	DAL method

Name	Formula	Supplier	Specification	Application
Copper(II) acetate monohydrate	$Cu(CH_3COO)_2 \cdot H_2O$	Merck	p.a., ≥99.0% (RT)	Composite synthesis
Copper nitrate trihydrate	$Cu(NO_3)_2 \cdot 3H_2O$	Merck	p.a., ≥99.5%	Composite synthesis
Ethanol	C_2H_5OH	Alcosuisse	p.a., ≥99.8%	Filters preparation
Glucose anhydrous	$C_6H_{12}O_6$	VWR Chemicals	For microbiology	DAL method
Hydrochloric acid	HCl	Carl Roth	35%, supra quality	Functionalisation
Hydrochloric acid	HCl	Carl Roth	0.05 M, volumetric standard solution	Acid/base titration
Hydrochloric acid	HCl	Carl Roth	0.1 M, volumetric standard solution	Acid/base titration
Hydrogen peroxide	H_2O_2	Merck	30%	MWCNTs digestion
Magnesium sulphate heptahydrate	$MgSO_4 \cdot 7H_2O$	Fluka	p.a., ≥98.0%	DAL method
Nanopure water	H_2O	MicroPure UV, Thermo Scientific	18.2 MΩ·cm	Applied in all works
Nitric acid	HNO_3	Carl Roth	Supra-quality, 65%	Functionalisation, MWCNTs digestion
Nitric acid	HNO_3	Carl Roth	0.1 M	Composite synthesis
Phenolphthalein	$C_{20}H_{14}O_4$	Carl Roth	p.a., ≥99.0%	Acid/base titration
Potassium sodium tartrate tetrahydrate	$C_4H_4KNaO_6 \cdot 4H_2O$	Carl Roth	p.a., ≥99.0%	Composite synthesis
Sodium phosphate monobasic monohydrate	$NaH_2PO_4 \cdot H_2O$	Merck	p.a., ≥99.0%	DAL method
Sodium bicarbonate	Na_2CO_3	Merck	p.a., ≥99.7%	Acid/base titration
Sodium hydrogen carbonate anhydrous	$NaHCO_3$	Merck	p.a., ≥99.5%	Acid/base titration
Sodium chloride	NaCl	VWR Chemicals	p.a., ≥99.0%	DAL method pH drift method

Name	Formula	Supplier	Specification	Application
Sodium chloride	NaCl	Merck	p.a., ≥99.0%	Point of zero charge
Sodium hydroxide	NaOH	Carl Roth	0.05 M, volumetric standard solution	Acid/base titration
Sodium hydroxide	NaOH	Carl Roth	0.1 M, volumetric standard solution	Acid/base titration
Sodium hydroxide	NaOH	Merck	Pellets p.a., ≥98.0%	Composite synthesis
Streptomycin	$(C_{21}H_{39}N_7O_{12})_2 \cdot 3H_2SO_4$	PanReac AppliChem ITW Reagents	Activity: min. 720 I.U./mg	DAL method
Tris(hydroxymethyl) aminomethane	$NH_2C(CH_2OH)_3$	VWR Chemicals	Ultra Pure	DAL method
Tryptic Soy Agar		Difco	For microbiology	DAL method
Tryptic Soy Broth		Merck	For microbiology	DAL method
Tryptone		Carl Roth	For microbiology	DAL method
Yeast extract		Carl Roth	For microbiology	DAL method

9. Methods and procedures

9.1. Carbon material purification and functionalisation

Multi-walled Carbon Nanotubes

MWCNTs purification and functionalisation steps consisted of (i) the non-oxidative treatment with diluted HCl and (ii) oxidation process with hot, concentrated HNO_3 [227]. The reason for a two-step process is the fact that HCl has been reported to be a good agent to remove Fe, Ni (catalysts) and carbon impurities [122,123], while concentrated HNO_3 is effective in MWCNTs surface oxidation [121]. Treatment with only HNO_3 will not result in effective purification (Fe and Ni removal), which is crucial for water treatment application [119,120]. Application of concentrated HNO_3 does not lead to catalyst removal [122], as it causes iron and nickel passivation [230,231].

The first step of MWCNTs purification was done by dispersing the MWCNTs in 10 % HCl (0.01 g/mL) by 5 minutes sonication in a water bath (DT106, Bandelin Electronics). The dispersion was constantly stirred at 300 rpm for 24 h at room temperature. Subsequently, the MWCNTs were rinsed with nanopure water until a neutral pH value of the filtrate was reached,

followed by drying in an oven (FD-115, Binder) at 120 °C for 2 h. In the second step, the purified MWCNTs were treated with concentrated HNO_3. Firstly, the MWCNTs were immersed in 65 % HNO_3 (0.01 g/mL), after which 45 min of sonication in an iced water bath was applied. Next, the dispersion was heated for 6 h at 120 °C under reflux conditions. After that process, the MWCNTs were filtered and washed with nanopure water until a neutral pH was achieved. At the final step, the oxidised MWCNTs were dried overnight in an oven (FD-115, Binder) at 120 °C.

Activated Carbon Fibres

The surface of ACFs is chemically unreactive, which may lead to the inadequate bonding of material during modification [157,164]. An available method for reactivity enhancement is surface treatment via oxidation. In literature, besides plasma treatment and gamma irradiation, chemical oxidation is proposed [164,165]. Treatment can be performed either in gas or liquid phase. Gas phase oxidation includes using oxidising agents, such as O_2, NO_2, O_3, while liquid phase processing includes HNO_3, H_2O_2, $(NH_4)_2S_2O_8$, H_2SO_4, $HClO_4$ [214,232,233]. Efficiency on the oxidation process is dependent on the concentration of oxidative medium, treatment time, temperature and fibres itself [164]. Functionalisation causes many modifications of ACF surfaces, e.g. decrease in specific surface area, increase in surface roughness, as well as micropores [164,234]. Functional groups, such as carboxylic, carbonyl and hydroxyl are incorporated onto the material's surface, increasing thereby chemical reactivity [17,164,165,234,235].

As-received ACFs (ACF_{AR}) were immersed in 65 % HNO_3 (0.015 g/mL) and then heated for 60 minutes at 90 °C under reflux conditions. Subsequently, the resulting functionalised ACFs (ACF_{FUN}) were removed from the suspension and washed with nanopure water until reaching neutral pH, following by drying overnight in an oven (FD-115, Binder) at 60 °C. Additionally, a portion of functionalised ACFs were extracted using a Soxhlet apparatus ($ACF_{FUN+SOX}$) to remove any acidic residuals. The ACFs were placed in an extraction thimble (Cellulose thimbles 603, Whatman) and washed with boiled water (water-refluxed). Extraction via boiling was carried out for around 72 h, until the pH of the water rinsed fibres remained unchanged. Afterwards, the $ACF_{FUN+SOX}$ were dried in an oven at 60 °C (FD-115, Binder) for 48 h. Additionally, as a reference, a sample of as-received fibres purified with Soxhlet (ACF_{AR+SOX}) was prepared.

9.2. Composites synthesis routes

Multi-walled carbon nanotubes-based composites

Adsorption of aqueous copper ion (composite 1)

0.285 M copper acetate monohydrate solution was added to a suspension of functionalised MWCNTs in water (0.2 g/100 mL nanopure water, sonicated 10 min in a sonication bath). The addition was carried out under constant stirring (300 rpm) and when it was completed, the system was kept under stirring for 2 h. Then, the suspension was filtered (PVDF membrane 0.1 µm, 47 mm, Hawach Scientific Co., Ltd) and the collected solid product was dried overnight in an oven at 120 °C. Next, a calcination process in a N_2 atmosphere at 300 °C for 2 h in a tube furnace (GHC 120900, Carbolite Gero GmbH & Co. KG) was performed to obtain Cu_2O. Figure 29 shows the synthesis routes of *composite 1*.

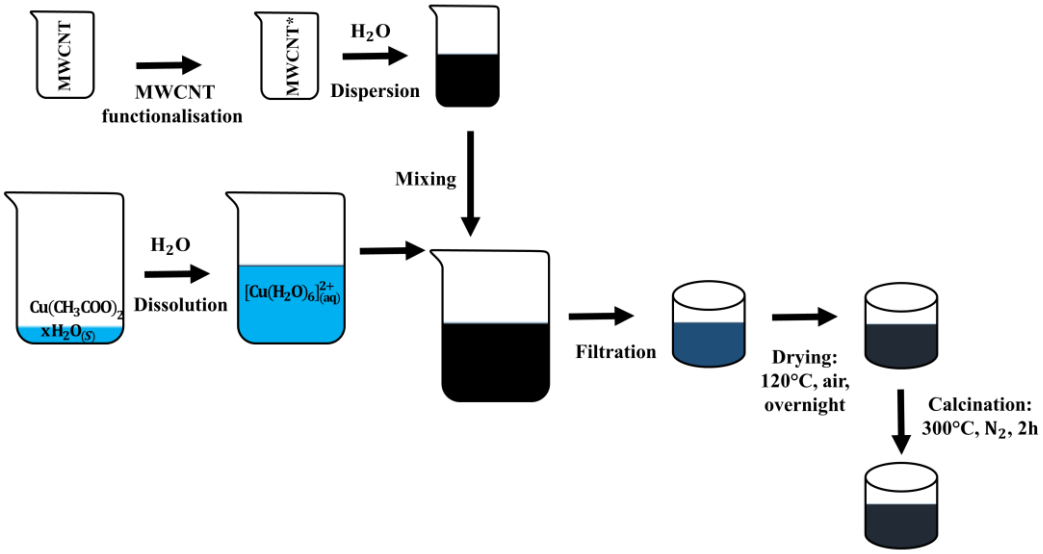

Figure 29 Scheme of the copper ion adsorption synthesis (route 1);

Adsorption of copper hydroxide (composite 2)

The solution of copper acetate and the dispersion of functionalised MWCNTs were prepared according to the same procedure as described above. Once both were mixed, an ammonium hydroxide solution (2 mol NH_4OH) was gradually added in a stoichiometric OH/Cu ratio in order to obtain $Cu(OH)_2$ precipitation. The suspension was continuously stirred (300 rpm) for 2 h and filtered, then the solid product was dried in an oven overnight at 120 °C. Next, a thermal treatment in a N_2 atmosphere at 300 °C for 2 h in a tube furnace was performed to attain Cu_2O. Figure 30 presents the scheme of synthesis of *composite 2* and *3*.

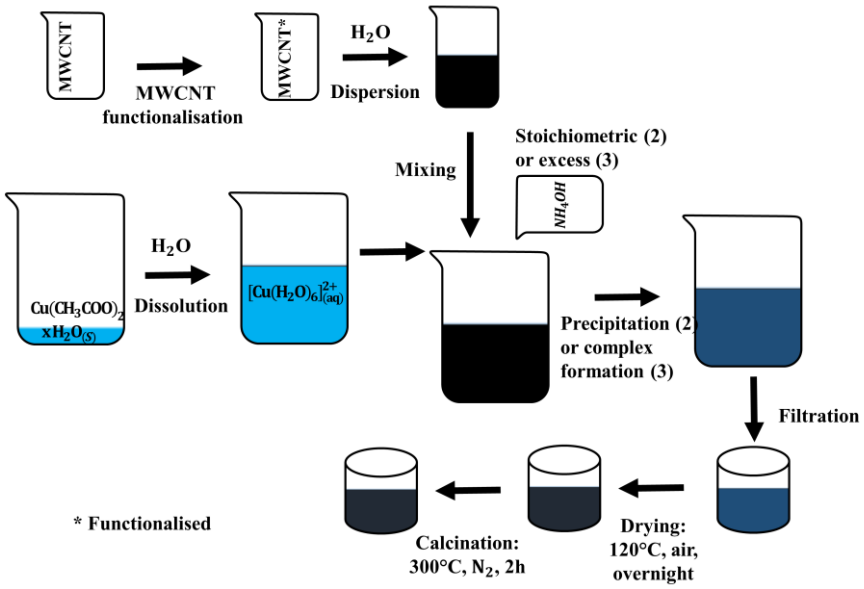

Figure 30 Scheme of the copper hydroxide adsorption (route 2) and copper complex adsorption (route 3) synthesis procedures – intermediate products;

Adsorption of copper complex (composite 3)

Composite 3 was prepared following the same procedure as for the copper hydroxide precipitation with the exception that instead of stoichiometric ratio of ammonium hydroxide an excess was used to form the $[Cu(NH_3)_4]^{2+}$ complex.

Activated carbon fibres-based composites

Adsorption of aqueous copper ions

Based on ACFs characterisation, only functionalised+ Soxhlet ACFs were selected for copper-adsorption studies. Additionally, the as-received ACFs were also subjected to copper-adsorption, and used as a reference specimen to understand the advantages of both functionalisation and oxidation-Soxhlet treatments.

50 mg of ACFs (as-received or acid-treated+ Soxhlet) were immersed in 25 mL of a $Cu(NO_3)_2 \cdot 3H_2O$ solution with different concentration of copper ions (C_{init}: 0.05, 0.1 0.5, 1, 2, 2.5, 5, 10, 20 mmol). The suspensions were continuous stirred (200 rpm) to equilibrate for 24 h (the equilibration time was selected based on the preliminary test evaluating the time impact on adsorption efficiency). Subsequently, the suspension was vacuum filtered (PVDF membrane 0.1 µm, 47 mm, Hawach Scientific Co., Ltd) and the permeate was collected. Blank samples (initial solutions) and permeates were tested with ICP-MS (Agilent 7500CE, Agilent) to determine the copper concentration. In order to investigate displacement of the protons from the functional groups on the activated carbon fibres' surfaces by the adsorption of metal ion species,

the pH values of the solutions were measured before and after adsorption using a pH meter (FiveEasy, Mettler Toledo). A series of initial pH conditions (pH_{init}: unmodified, 4.0, 2.0, (only for $ACF_{FUN+SOX}$) and 1.0) were tested during the adsorption process.

The resulting optimal combination of Cu^{2+} concentration of 20 mmol and initial pH equal 4.0 were applied for the preparation of a series of six composites, as follows: (i) two Cu-impregnated sample, dried at 60 ºC in air for 24 h ($CuACF_{AR}$ and $CuACF_{FUN+SOX}$); (ii) two N_2 thermal treated samples (GHC 120900, Carbolite Gero GmbH & Co. KG) ($NCuACF_{AR}$ and $NCuCFN_{FUN+SOX}$) at 350 °C in a N_2 atmosphere for 2 h with a heating rate of 5 ºC/min; (iii) two H_2 treated samples ($HCuACF_{AR}$ and $HCuACF_{FUN+SOX}$) at 350 °C in a H_2/Ar atmosphere for 2 h with a heating rate of 5 ºC/min.

9.3. Filter and cartridge preparation

MWCNTs materials were tested as thin filters, utilising small amounts of material. To prepare the filters of as-received MWCNTs and MWCNTs-based composites, the following procedure was applied: 20 mg of as-received MWCNTs/ material composite was suspended in 20 mL of 95 % EtOH via 5 minutes sonication in a sonication bath. The suspension was uniformly deposited on a glass fibre filter (47 mm, 0.4 µm, Macherey-Nagel) by applying vacuum filtration. The as-prepared filter was placed in a supporting plastic filter holder (Figure 31a). The obtained filter loading was 1.15 mg/cm^2.

ACFs (as-received and functionalised+ Soxhlet) and ACFs composites were tested in the form of cartridges. The glass cartridge (Figure 31b) was specially designed and made at Empa, having following dimensions: d_{in}=8 mm, d_{out}=14.4 mm, l=35 mm. In the polymer inlet and outer caps of the cartridge, cut glass fibre filters (0.4 µm, Macherey-Nagel) were placed to avoid fibres being released from the system. 300 mg of ACFs/ ACFs composite were placed in the cartridge.

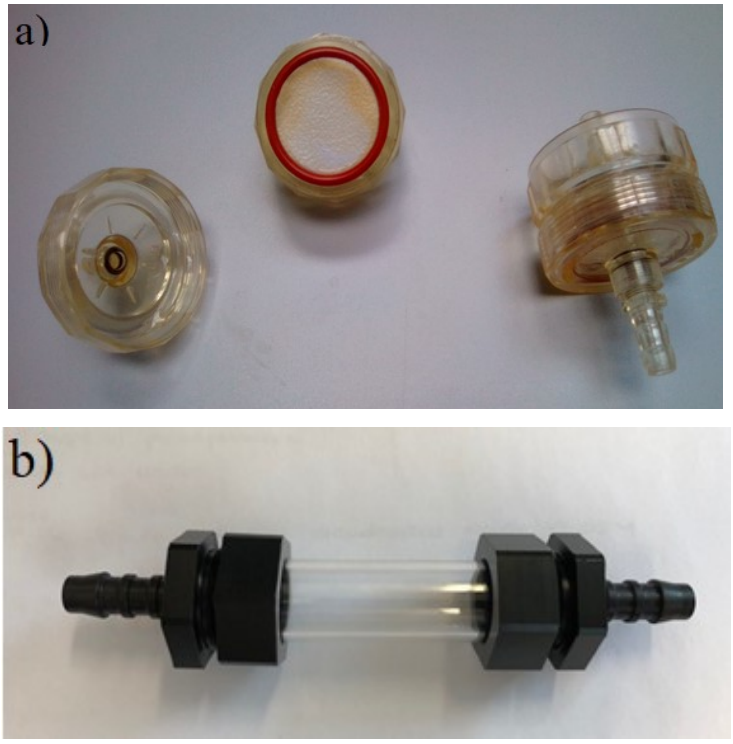

Figure 31 Photographs of a) filter holder; b) cartridge for virus removal tests;

9.4. Stability test of composites - filter conditioning and copper release test

The composites, as well as basic carbon substrates were conditioned at pH 5.0 and 7.0, as the filter material must be able to withstand both common and harsh water pH ranges. This is supported by the enhanced solubility of copper species at low pH, which, if released, might impact material efficiency in MS2 removal, its lifetime, as well as bring some health concerns [186,190,199]. Since the pH of natural waters often exceeds 7.0, further testing at higher pH values would be required prior to the potential implementation of the proposed materials [189,190].

MWCNTs-based composites

After day 1 of the MS2 bacteriophage removal test, the as-prepared MWCNTs-based filters were flushed with 0.01 M NaCl solution with pH values of either to 5.0 and 7.0 (consistent with the experimental pH) for 24 h at the same flux (160 $L/m^2 \cdot h$). The permeate samples were regularly collected and the concentration of released copper in the permeate during filtration was analysed via inductively coupled plasma-mass spectrometry (ICP-MS 7500 CE, Agilent).

ACFs-based composites

Here, in contrast to MWCNTs-based composite study, first, the stability tests and conditioning of the synthesised materials were performed, followed by the virus removal studies.

The as-prepared cartridges were rinsed with 0.01 M NaCl solution with pH values of 5.0 and 7.0 for 24 h at the flow rate of 150 mL/h. Permeate samples were regularly collected. The concentration of the released copper in permeate during filtration, was analysed via ICP-MS (ICP-MS 7500 CE, Agilent).

9.5. MS2 bacteriophages and virus removal experiment

MS2 are non-enveloped enteric virus surrogates, F-specific RNA bacteriophages, and have similar morphologies and structural resemblances to waterborne viruses, like enteroviruses, caliciviruses, astroviruses and Hepatitis A and E virus [74,236]. They are commonly used as model bacteriophages in water purification studies [77,237]. MS2 is round in shape and has a diameter of 25 nm, [50,238]. MS2 are hydrophobic in character [47] and possess an isoelectric point equal to ~4 [50]. The advantage using MS2 bacteriophages is the possibility to prepare larger quantitates at a high concentrations, which enables to demonstrate even 11 LRV removal [74].

9.5.1. Media preparation and bacteria/ virus growth

In this study, two MS2 stock solutions and their Escherichia coli (E. coli) hosts from two different sources were applied. The bacteriophage MS2 and E. coli host used in the MWCNTs test were purchased from the German Collection of Microorganisms and Cell Cultures (DSMZ 13767 and 5695, respectively). The ready-to-use MS2 bacteriophage stock, as well as E. coli host applied in the ACFs test were bought from Culture Collection of Switzerland (CCOS).

The E. coli stock from DSMZ was grown from a single bacterium to form a colony. Briefly, the cotton pellet containing the E. coli was rehydrated in broth, then the suspension was streaked out onto a hard agar plate with a sterile loop. Subsequently, the hard agar plate was incubated overnight at 37 °C (Climo-Shaker ISF1-X, Adolf Küchner AG). On the next day, the selected single colony was inoculated into broth and the culture was grown until reaching an optical density (OD) (UV-VIS measurement at 600 nm, Libra S4+ Visible Spectrophotometer, Biochrom) equal to 0.4-0.6. Reaching such a value provides the appropriate growing state of E. coli. Next, the bacteria were regrown using the same methodology until reaching an OD= 0.2. Then, 15 % of a sterile glycerol solution was added to the E. coli culture and 100 µL samples were pipetted into sterile Eppendorf tubes and stored at -80 °C.

The MS2 bacteriophages from DSMZ were propagated with E. coli as a host, then purified and concentrated according to the DSMZ protocol. The MS2 bacteriophage were revitalized with the E. coli solution obtaining the first stock of MS2. Subsequently, it was amplified by the addition of the first MS2 stock into the 1 L solution of E. coli. The obtained second stock was

centrifuged, and then the supernatant was filtered through a 0.22 µm PES filter (Millex GP, Merck) unit and the filtrate was collected in an autoclaved glass bottle. This step allowed to remove any remaining E. coli. The last purification step consisted on filtrating the low molecular weight molecules out of the virus stock solution in order to increase the virus concentration, which was done using Amicon™ Ultra Centrifugal Filter Units 100 kDa (Merck Millipore). The obtained MS2 filtrate was diluted in a virus dilution buffer and stored in a fridge at 4 °C. The MS2 and E. coli from CCOS were ready to use without any further preparations.

9.5.2. Determination of MS2 concentration

Virus concentration was quantified using the Double Agar Layer (DAL) method [239] and measured as a number of plaque forming units (PFU) per mL. The solutions were prepared according to the protocol and their compositions were summarised in Table 6 and Table 7.

Table 6 Composition of solutions used with DAL method with MS2 bought from DSMZ;

Antibiotic (2 mg/mL stock)			
Nanopure H_2O, mL		Streptomycin, g	
100		0.20	
Soft Agar (0.7 %)			
Nanopure H_2O, mL	Tryptic Soy Broth, g	Bacteriological Agar, g	Antibiotic, mL
1000	30	7	1
Hard Agar (1.5 %)			
Nanopure H_2O, mL	Tryptic Soy Broth, g	Bacteriological Agar, g	Antibiotic, mL
1000	30	15	1
Broth			
Nanopure H_2O, mL	Tryptic Soy Broth, g		Antibiotic, mL
1000	30		1
Virus Dilution Buffer (VDB)			
Nanopure H_2O, mL	$NaH_2PO_4 \cdot H_2O$, g		NaCl, g
1000	0.78		0.58

The inequalities in solution compositions come from the differences in media used for MS2 and E. coli propagation by companies. To avoid contamination during the experiments, all solutions except antibiotic were autoclaved at 121±1 ºC for 20 minutes before their utilisation. The used equipment was either sterile, cleaned with 70 % ethanol (e.g. surfaces) or autoclaved. All described steps of the DAL procedure were done in the presence of a Bunsen Burner.

Table 7 Composition of solutions used with DAL method with MS2 bought from CCOS;

Soft Agar (0.7 %)						
Nanopure H_2O, mL			Tryptic Soy Agar, g			$MgSO_4$, g
1000			32			0.60
Hard Agar (1.5 %)						
Nanopure H_2O, mL			Tryptic Soy Agar, g			$MgSO_4$, g
1000			40			0.60
Broth						
Nanopure H_2O, mL	Trypton, g	Yest extract, g	NaCl, g	Glucose, g	$CaCl_2$, g	$MgSO_4$, g
1000	1	0.10	0.80	0.10	0.03	0.015
Virus Dilution Buffer (VDB)						
Nanopure H_2O, mL			$NH_2C(CH_2OH)_3$, g			$MgSO_4$, g
1000			2.50			0.60

DAL protocol encompass a three-day procedure. Day 1 consisted of inoculating the E. coli in 15 mL of broth and placing it overnight in a shacking incubator at 37 °C. Next, soft agar (0.7 % agar) and hard agar (1.5 % agar) solutions were prepared and autoclaved. Day 2 involved re-growing the overnight E. coli culture by putting 200 µL of it into 15 mL of broth. The new culture was placed into a shaking incubator until visible turbidity was achieved. Next, series of MS2 solution dilutions were made. The virus stock and analysed samples should be diluted according to the procedure presented in Figure 32.

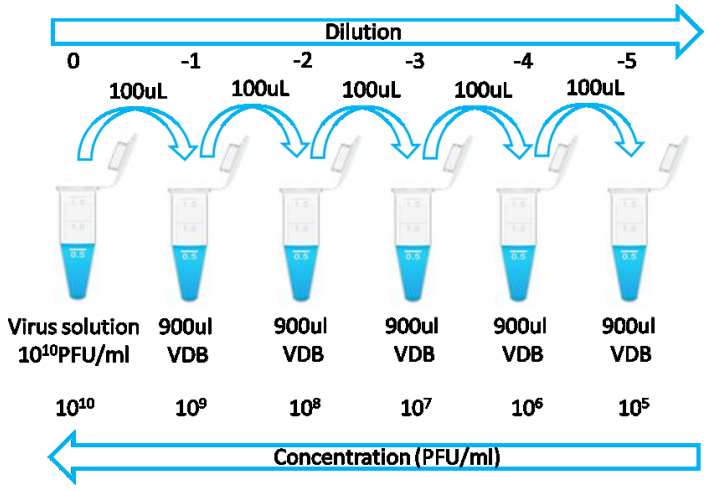

Figure 32 Scheme of dilution procedure in the plaque assay method;

The next step was the preparation of soft agar tubes and hard agar plates. 6 mL of soft agar was poured into autoclaved vials and then they were kept in a water bath (WNE 45, Memmert GmbH Co. KG) at 50 °C to avoid solidification. 7 mL of hard agar was poured with a sterile pipette onto a petri dish and uniformly distributed. The final step is plating (Figure 33), where: 100 µL of filtration permeate containing MS2 was mixed with 200 µL of E. coli suspension and 5 mL of molten soft agar, which was then poured onto a solidified hard agar plate and incubated overnight at 37 °C.

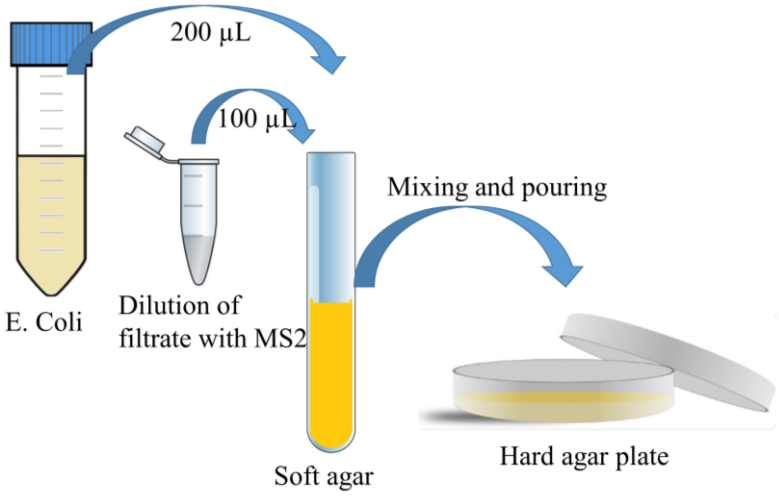

Figure 33 Scheme of DAL procedure;

On day 3, plaque-forming units (PFU) were counted (transparent circles representing one colony, caused by phage infection, (Figure 34) on each plate.

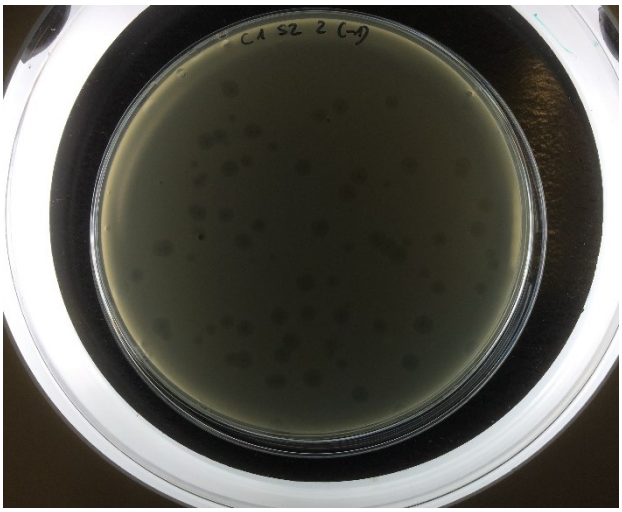

Figure 34 Image of petri dish with MS2 assay, transparent circles represent one colony;

The virus concentration (I_f), considering dilution (D), was calculated using the following formula (Eq. 15):

$$I_f = \frac{PFU \cdot D}{0.1} \left[{}^{PFU}/_{mL} \right] \quad \text{Eq. 15}$$

9.5.3. MS2 bacteriophage removal experiment

The virus removal study (flow-experiment) was performed by passing the MS2 bacteriophage solution through the as-prepared filters or cartridges at a constant water flow using a peristaltic pump. Filter permeate samples were collected and the virus concentration was determined using the DAL method. Plating was done directly after permeate collection (t=0 h), and after two hours of storage (t=2 h) to evaluate if additional removal with time is observed. The collected permeates were tested for Cu concentration with ICP-MS (ICP-MS 7500 CE, Agilent)

The MS2 removal test was done at two different pH values. All experiments were performed in duplicate, the use of duplicates was based on prior studies and methods [129,239].

In the MWNCTs study, the used MS2 concentration was equal to 10^8 PFU/mL, with an applied flux equal to 160 L/m^2·h (which refers to ~280 mL/h). The MS2 removal test was done at pH 5.0 and 7.0 before and after the filter had been conditioned for 24 h.

In the ACFs study, the applied MS2 concentration was 10^5 PFU/mL, while the flow was set to 150 mL/h. Here, applying the conclusions from the MWCNTs study, the virus removal test was performed at pH 5.5 and 7.3 only after material conditioning.

MS2 $\log_{10}$ removal (LRV) was calculated using the following formula:

$$LRV = log(\frac{I_i}{I_f}) \quad \text{Eq. 16}$$

where: I_i - the initial MS2 concentration (PFU/mL), and I_f - the MS2 concentration in filtrate (PFU/mL).

Negative and positive controls were performed alongside every experiment. The controls behaved as expected, no effect of the filter permeate on the DAL assay was observed.

10. Equipment used and characterisation methods

10.1. Carbon substrates

Electron Microscopes

The size and morphology of MWNCTs were determined using transmission electron microscopy (TEM, JEOL JEM-2200FS). Samples were prepared by dispersing a small amount of material in 95 % ethanol via 5 minutes sonication in a sonication bath and then placing one droplet of suspension onto TEM grids (Lacey Carbon Film on Cu Mesh, S166-2, Plano GmbH). Ethanol was evaporated by drying at room temperature. The samples were analysed in normal mode and in high resolution mode, with an applied tension 200 kV.

The surface morphology of the ACFs was analysed using scanning electron microscopy (SEM) (FIB/SEM System FEI Helios 660 G3 UC, FEI). ACFs were directly placed on carbon double-side adhesive tape and analysed. Samples were not additionally dried or coated prior the analysis. Imaging was done using secondary electron (SE) mode. Chemical composition evaluation of contaminations present on ACFs was performed using a Tescan VEGA3 (Tescan Instruments) equipped with energy-dispersive x-ray spectroscopy (EDX) XFlask 6I10, Bruker. Esprit 2.0 software was applied for data analysis.

Elemental analysis (EA)

The elemental analysis of carbon substrates were analysed using a CHNS/O Flash Smart, Thermo Scientific instrument. Based on the analysis of Methionine reference samples, the analytical method was calibrated. Samples (approx. 0.4 mg) for CHNS analysis were weighed in tin crucibles and then loaded into the Flash Smart analyser.

For oxygen content analysis, reference samples of the BBOT standard (2,5-Bis(5-tert-butyl-2-benzo-oxazol-2-yl)thiophen) were prepared and used for equipment calibration. Samples (approx. 1 mg) were weighed in silver crucibles and loaded into the Flash Smart analyser.

X-ray photoelectron spectroscopy (XPS)

XPS spectra were recorded using a hemispherical analyser EA15 (PREVAC) equipped with a dual anode X-ray source RS40B1 (PREVAC). The measurements of MWCNTs were performed using Al Kα (1486.6 eV) radiation and an analyser pass energy of 100 eV while for ACFs, measurements were performed using Mg Kα (1254 eV) radiation and an analyser pass energy of 100 eV. The measurements were performed in normal emission geometry with an energy resolution of 0.9 eV and under ultra-high vacuum (UHV) conditions ($8 \cdot 10^{-10}$ mbar for MWCNTs and $1 \cdot 10^{-9}$ mbar for ACFs). The analysis area and depth were approx. 3 mm^2 and 10 nm, respectively.

For MWCNTs the powder samples were pressed into indium foil, while for ACFs, bunch of fibres were used for measurements. The samples were mounted and positioned in a dedicated holder and pumped down to high vacuum then transferred into the UHV chamber. The survey and high resolution spectra were acquired for every sample. The spectra were analysed with the use of CasaXPS 2.3.15 software. The electron binding energy (BE) scale was calibrated for the Fermi edge at 0.0 eV. The Shirley type spectrum background was used. The highly resolved spectra were deconvoluted with Voigt function (Gauss to Lorentz profile ratio of 70:30). The spectra were compared in relation to the background level.

The atomic concentration was calculated for the respective thickness of the surface layer of MWCNTs (h = 9.9, 5.0, and 3.8 nm respectively for C, Fe_2O_3, and NiO) and ACFs (h = 9.9 nm for C) samples. The calculations of elements at the sample surface were performed with QUASES-IMFP-TPP2M Ver 2.2 software according to S. Tanuma et al. [240]. The calculations take into account 95 % of the photoelectrons emitted from the surface. The accuracy of the calculation is ±3 %. Deconvolution of the components spectrum was done according to the work by J.A. Leiro et al. [241].

XPS has been used to characterise the functional groups on carbon. This method is sensitive to sample chemical speciation. There is also possible to determine the atomic ratio of oxygen to carbon on the surface of the analysed carbons [242].

Acid/base titration

Acid/ base titration was applied to determine the effectiveness of the carbon material functionalisation process and to quantify the amount of incorporated functional groups on the carbon surfaces. Boehm titration is used for the identification and quantification of carbon surface functionalities [243]. This method relies on the concept that oxygen groups on carbon surfaces possess different acidities, whereby bases with different strengths neutralise the different acidic

groups [227,243,244]. In the method, bases with increasing strength are used, e.g. $NaHCO_3$, Na_2CO_3, NaOH. It is assumed that NaOH reacts with carboxyl, lactone and phenolic groups, Na_2CO_3 neutralizes carboxyl and lactones, whereas $NaHCO_3$ only reacts with carboxyl groups [244]. The number of individual groups was calculated as follows:

(i) carboxyl groups = groups titrated with $NaHCO_3$

(ii) lactone groups = groups titrated with Na_2CO_3 minus those titrated with $NaHCO_3$

(iii) phenol groups = groups titrated with NaOH minus those titrated with Na_2CO_3

The surface basicity is less understood than acidic functional groups. It is assumed that the basicity of carbon is relatively weak. Its origin may be associated with the presence of oxygen functional groups or the existence of pyrone-type structures on the edges of polyaromatic layers [245].

Acid/base titration of MWCNTs and ACFs [243,244,246] was done by preparing a suspension of 250 mg of carbon material in 25 mL of three reaction bases of 0.05 M NaOH, 0.05 M $NaHCO_3$ and 0.05 M Na_2CO_3. The samples were agitated for 24 h to reach equilibrium state for both carbon materials [247]. Subsequently, the suspensions were filtered (PVDF membrane 0.1 µm, 47 mm, Hawach Scientific Co., Ltd) and 10 mL aliquots of filtrate were collected. Then, the aliquots were acidified by the addition of standardised 0.05 M HCl. 20 mL of 0.05 M HCl for aliquots of the NaOH, $NaHCO_3$ reaction base and 30 mL of 0.05 M HCl for Na_2CO_3. Different volumes were used to ensure complete neutralization of the Na_2CO_3 base, which requires two protons vs the one proton required by the NaOH and $NaHCO_3$ reaction bases [244]. The as-prepared acidified samples were degassed via bubbling with N_2 for 2 h to expel dissolved CO_2. Next, the acidified samples were back- titrated with a standardised solution of 0.05 M NaOH, while being continually saturated with N_2. The endpoints were determined using a pH Meter (FiveEasyPlus, Mettler Toledo) and phenolphthalein as an indicator. All steps were performed at room temperature.

Point of Zero Charge of MWNCTs and ACFs

The point of zero charge (pH_{pzc}) was measured according to the method described by Stoeckli et al. for various activated carbons by the so called pH drift method [232]. In this method, the proton concentration in the solution is adjusted to shift the equilibrium of acidic group dissociation or to shift the equilibrium of basic functional groups adsorbing protons. If the solution pH is above the pH_{PZC} the carbon surfaces release protons into solution, while if the solution pH is lower the pH_{PZC} the carbon surfaces adsorb protons in solution. A final point is reached when the solution pH does not change, which means that the acids groups are in equilibrium with

protons in solution. Since carbon surfaces contain a variety of acidic and basic functional groups, the pH at the point of zero charge corresponds to an effective pKa. At the point of zero charge, all surface charges are effectively neutralised so that the net surface charge of the carbon is zero [248,249].

The pH of a solution of 0.01 M NaCl was adjusted from 1-12 by adding either HCl or NaOH. The solutions were degassed by bubbling with N_2 gas at 298 K to remove dissolved carbon dioxide until the initial pH stabilised. 50 mg of MWCNTs or 75 mg of ACFs were added into 25 mL of the 0.01 M NaCl solution. After 24 h, the final pH was recorded. The graph of final versus initial pH was used to determine the point at which the initial pH and final pH values were equal. This value was taken as the point of zero charge.

Raman spectroscopy

MWCNTs were analysed with Raman spectroscopy with backscattering geometry to determine their purity level as well as presence of disorders. An Alpha 300 R Confocal Raman Microscope (WITec) equipped with a RayLine laser (WITec) working at λ= 532 nm was applied to the record Raman spectra of MWCNTs sample in the range of 0-3500 cm^{-1}. Measurement parameters: 5 % of laser power (75 mW), exposure 60 s time, 1 accumulation per measurement. Prior the analysis, MWCNTs were suspended in 98 % EtOH (1 g/L) using sonication bath and a droplet was placed on glass disc.

For the analysis of ACFs, a Renishaw inVia dispersive Raman System H45383 equipped with a Spectra-Physics laser (λ= 514 nm) was used. Spectra were recorder in the range of 120-3500 cm^{-1}. The applied measurement parameters were: 10 % of laser power (24 mW), exposure 30 s time, 1 accumulation per measurement. ACFs substrates were placed on glass disc and directly measured.

OriginPro 2018 software was used for the raw spectra peak fitting applying Lorentz function.

Thermogravimetric analysis (TG) and Differential Scanning Calorimetry (DSC)

Simultaneous thermal analysis (STA 449 F3 Jupiter, Netzsch) was used to determine the influence of the functionalisation step on the burning temperature of MWCNTs. TG and DSC was performed simultaneously on a sample with mass ~4 mg, which was heated from room temperature to 800 ºC with a heating rate of 5 K/min in air. For the measurement, a DSC/ TG Al_2O_3 crucible was used.

Porous structure and specific surface area characterisation

The specific surface areas (SSA) of the MWCNT substrates were determined from a 5-point N_2 adsorption isotherm obtained from Brunauer-Emmett-Teller measurements using a SA 3100 Surface Area Analyser (Beckman Coulter). Prior to analysis each sample was introduced to the glass sample holder and the sample was degassed at 180 °C in synthetic air (Carbagas) for 2 h using a SA-PREP Surface Area Outgasser (Beckman Coulter, Germany).

The surface area, pore volumes of ACFs were determined using an ASAP 2020 (Micrometrics) apparatus. The micropore volumes were obtained from the data for adsorption of CO_2, at 273 K, while the total pore volumes and specific surface areas were obtained from the adsorption of N_2, at 77 K.

Approximately 100 mg of each sample was placed in a sample tube. The sample chamber was heated to 150 °C, then evacuated to a pressure of 13 μbar and the samples were outgassed for a few hours. Next, the samples were allowed to cool down to room temperature and weighted to determine their dry weight. Afterwards, the heating mantles were replaced by a Dewar filled with an appropriate coolant, such as ice/water, at 273 K for CO_2 adsorption and liquid nitrogen at 77 K for N_2 adsorption.

For each sample, the physical properties, such as surface area, pore volumes, pore size distributions were extracted from the experimental isotherms data by applying the below explained equations.

The Brunauer, Emmett and Teller (BET) model is usually used for multilayer adsorption of gases on a wide range of porous and non-porous adsorbents for obtaining specific surface areas adsorbents from adsorption isotherms. According to the assumption deriving from the Langmuir equation, the BET model assumes that the first adsorption layer (the monolayer) is localised on the surface sites of uniform adsorption energy and that the second and subsequent layers (the multilayer) build up by a process analogous to condensation of the liquid adsorbate. The original adsorbed model proposed by Brunauer, Emmett and Teller [250].

$$\frac{V}{V_m} = \frac{cX}{1-X}\sum_{n=1}^{\infty}\beta_n\left(\frac{1-(n+1)X^n+nX^{n+1}}{1+(c-1)X-cX^{n+1}}\right) \qquad \text{Eq. 17}$$

where: V – molar amount adsorbed, V_m – amount of adsorptive required to cover the surface as a monolayer (monolayer capacity), X – relative pressure (p/p^0), c - BET constant.

Equation 17 reduces to the Langmuir equation by putting $n= \beta_n = 1$. With assumption of $\beta_n = 1$ and $n= \infty$, it forms:

$$\frac{X}{V(1-X)} = \frac{1}{V_m c} + \frac{(c-1)}{V_m c}X \qquad \text{Eq. 18}$$

For each point designated for surface area calculations, the BET transformation is calculated with the least-squares method. V_m and c can be obtained from the slope, an intercept of the straight line plot of X(V(1-X)) vs X. The surface area of adsorbents can be obtained from V_m.

$$s = \frac{c-1}{V_m \cdot c} \quad \text{Eq. 19}$$

$$i = \frac{1}{V_m \cdot c} \quad \text{Eq. 20}$$

$$c = \frac{s}{i} + 1 \quad \text{Eq. 21}$$

$$V_m = \frac{1}{s+i} \quad \text{Eq. 22}$$

where: s – slope, i – intercept

$$BET = L\sigma \cdot V_m \Leftrightarrow BET = 4.35 \cdot V_m \quad \text{Eq. 23}$$

where: L - Avogadro constant (mol^{-1}), σ – molecular cross sectional area of N_2 (nm^2)

Langmuir total pore volume was calculated with a least-squares method using following equation [251]:

$$V_{N2} = \frac{P}{P_0} * \frac{1}{V} \quad \text{Eq. 24}$$

where: V – the volume adsorbed at equilibrium pressure (cm^3/g STP)

The Dubinin-Radushkevich equation was applied for calculating the micropore volume from carbon dioxide adsorption, with a least-squares method [252]:

$$\log(V) = \log(V_0) - D\left[log\frac{P_0}{P}\right]^2 \quad \text{Eq. 25}$$

$$D = 0.4343B(T/\beta)^2 \quad \text{Eq. 26}$$

where: V – the volume adsorbed at equilibrium pressure (cm^3/g STP), V_0 – the micropore capacity (cm^3/g STP), P_0 – saturation vapour pressure of gas at temperature T (mmHg), P – equilibrium pressure (mmHg), B – a constant, β – the affinity coefficient of analysis gas relative to P_0 gas (0.35 for CO_2) [253], T – analysis bath temperature (K).

The intercept, $\log(V_0)$ can be found by performing the least-squares fit on the designated pairs. Assuming the adsorption of gas is restricted to a monolayer, V_0 is the monolayer capacity. Based on this assumption, the following are calculated:

$$V_0 = 10^i \quad \text{Eq. 27}$$

where: i – intercept (cm^3/g STP).

Inductively coupled plasma mass spectrometry (ICP-MS)

ICP-MS (ICP-MS 7500CE, Agilent) was applied to determine heavy metal concentrations in as-received and functionalised MWNCTs. MWCNTs were acid digested using a microwave digestion system ultraCLAVE (MLS GmbH) prior to analysis. Digestions were performed in 4 mL HNO_3 (65 %) and 0.5 mL H_2O_2, (30 %), for 5 mg of MWCNTs samples. The ultra-CLAVE ran using the following steps: Step 1: 25 °C to 160 °C in 10 min.; Step 2: 160 °C to 240 °C in 9 min.; Step 3: 240 °C for 10 min. After cooling down, the solution was removed and filled up to 50 mL with nanopure water.

10.2. Composites

Electron Microscopy

The size and morphology of synthetized MWNCTs composites were determined using TEM (JEOL JEM-2200FS). The measurement and the sample preparation were done in the same manner as for MWCNTs substrates.

The surface morphology of the ACFs-based composites was analysed using SEM (FEI Nano-SEM 230). Material samples were placed onto a carbon double-side adhesive tape attached to SEM sample holder. Excess of material was removed by using compressed air. Next, the samples were sputtered with a layer of conductive carbon to avoid sample charging during measurement. Microscope was working in high vacuum mode, voltage of 5-10 kV an immersion mode with TLD detector.

X-ray photoelectron spectroscopy

The X-ray photoelectron spectra of ACFs-based composites were recorded and analysed in the same manner as activated carbon fibres substrates.

X-ray diffraction

The phases of the obtained composites were determined by means of an X-ray diffraction (XRD) (PANalytical X'Pert PROh–2h, PANalytical) scan system equipped with a Johansson monochromator (Cu Ka1 radiation, 1.5406 Å) and an X'Celerator linear detector. The scans were acquired in the 2θ range of 5−80° with a step size of 0.016° and a scanning speed of $0.021°s^{-1}$. Phase compositions of the spectra were analysed with HighScore Plus Software. Crystallite sizes (S) were determined using the Scherrer equation [254]:

$$S=k\lambda/\beta\cos\Theta \qquad \text{Eq. 28}$$

where: k – shape factor (0.9), λ – X-ray wavelength, β – full width at half-maximum intensity (radians), and θ – Bragg angle (radians).

Point of Zero Charge of ACFs-based composites

The point of zero charge of ACFs-based composites was measured according to the method described above for ACFs substrates.

Porous structure and specific surface area characterisation

The specific surface areas of the as-prepared MWCNTs composites were determined in the same way as for MWCNTs substrates.

The surface area, pore volumes of ACFs composites were determined from adsorption of nitrogen at 77 K and carbon dioxide at 273 K, using a Micrometrics ASAP 2020 apparatus. Samples were prepared for analysis in the same way as non-modified ACFs.

III Results and discussion

11. Characterisation of functionalised carbon substrates

11.1. Functionalised Multi-Walled Carbon Nanotubes

The multi-walled carbon nanotubes functionalisation was done using two-step method consisted of (i) the non-oxidative treatment with diluted HCl and (ii) oxidation process with hot concentrated HNO_3 [227]. The aim was to remove heavy metals contaminations and incorporate functional groups onto MWNCTs' surface in order to increase their reactivity.

TEM images (Figure 35) present functionalised multi-walled carbon nanotubes. Strong oxidation conditions caused degradation of MWCNT structures resulting in tube breaking and shortening, which endings were jagged. In comparison to as-received MWCNTs (Figure 25), the functionalised ones have a lower degree of agglomeration and shorter tube lengths, while the tube diameter remains unaffected. No significant differences were observed in the morphology of functionalised MWCNTs in regard to as-received ones.

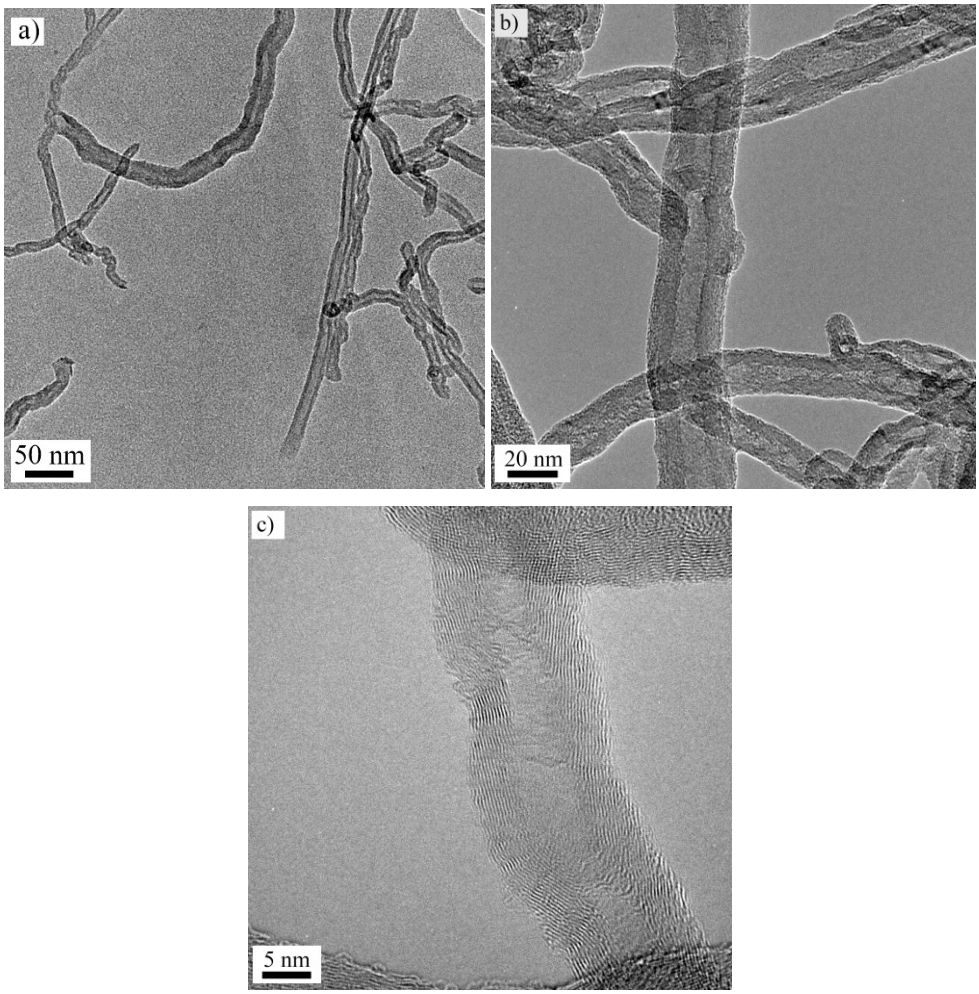

Figure 35 a, b, c) TEM images of functionalised multi-walled carbon nanotubes;

Table 8 presents the elemental analysis (EA) outcome of as-received and functionalised multi-walled carbon nanotubes. The results indicate an increase in nitrogen (from 1.06 to 3.97 wt.%) and hydrogen (from 0.19 to 0.30 wt.%) content for functionalised MWCNTs. The amount of carbon decreased (from 96.47 to 90.90 wt.%), while oxygen remains the same (6.25 wt.%), which could point out that the total oxygen content in the sample volume remains unchanged, as well as the O/C atomic ratio. This can indicate that during treatment, carbon oxidised to CO. The treatment increases the N/C atomic ratio by factor of 4x, denoting the incorporation of nitrogen residuals.

Table 8 Elemental analysis of multi-walled carbon nanotubes;

MWCNTs type	C, wt.%	H, wt.%	N, wt.%	O, wt.%	N/C	H/C	O/C
As-received	96.47	0.19	1.06	6.25	0.011	0.002	0.065
Functionalised	90.90	0.30	3.97	6.25	0.044	0.003	0.069

The XPS study allowed for a qualitative characterisation of the type and amount of functional groups present on the uppermost surface of MWCNTs (depth of analysis ~10 nm). Survey spectra of MWCNTs representing the total concentration of the elements at the sample's surface (Figure 36a, Table 9a), revealed that the O/C atomic ratios are 0.019 and 0.069 for as-received and functionalised MWCNTs, respectively. This leads to the conclusion that the treatment caused surface oxidation. However, in comparison to EA, a higher discrepancy between O/C ratio is observed, which can be linked with measurement technique that analyse entire sample or only surface. The MWCNTs were manufactured via CCVD process and primarily contained iron and nickel, which were applied as catalysts. XPS study allowed to conclude a decrease in heavy metals atomic ratio, especially nickel (from 0.11 at.% to 0.00 (value below the detection limit) for as-received and functionalised MWCNTs, respectively). Here, an increase in nitrogen atomic concentration (from 0.02 to 0.18 at.%) is observed within the acid treatment. Figure 36 and Table 9 present further XPS peaks of C 1s (Fig. 36b and Table 9b) and O 1s (Fig. 36c and Table 9c) of the as-received and functionalised MWCNTs. The oxidation treatment led to a concentration increase in hydroxyl (B peak in Fig. 36b and B peak in Fig. 36c), carbonyl (C peak in Fig. 36b) and carboxylic (D peak in Fig. 36b) groups. Additionally, the X peak (Fig. 36b) associated to the C-Metal decreased, which confirms that the oxidation treatment removes the catalysts (Fe, Ni) from the end points of MWCNTs.

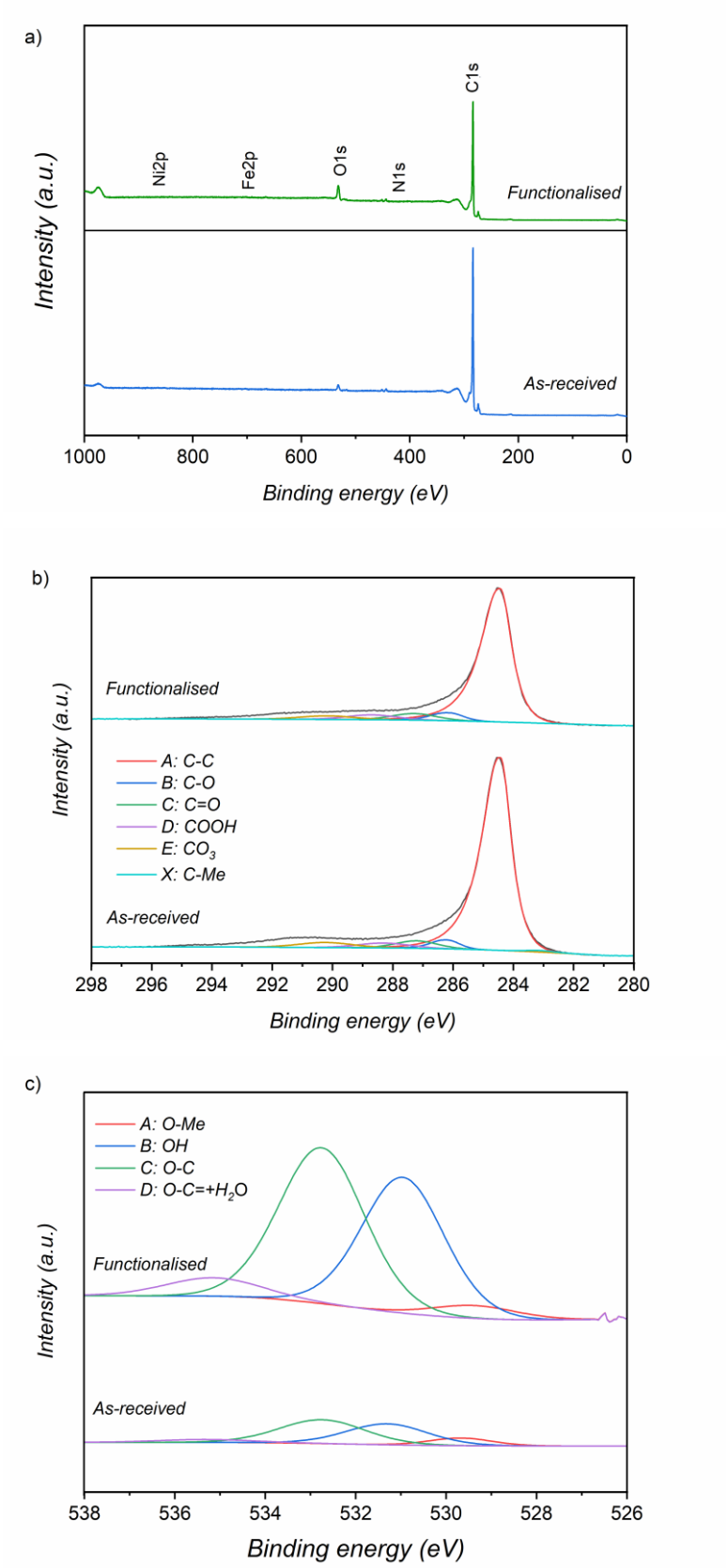

Figure 36 XPS spectrum a) Survey; b) C 1s; c) O 1s of as-received and functionalised multi-walled carbon nanotubes;

Table 9 Data describing the XPS spectra of multi-walled carbon nanotubes presented in Figure 36: a) survey spectra; b) C 1s and O 1s;

a) Survey spectra

Survey	As-received		Functionalised	
Name	pos., eV	at.%	pos., eV	at.%
C1s	283.84	97.84	283.84	93.32
O1s	532.84	1.88	532.09	6.45
N1s	404.84	0.02	404.59	0.18
Fe2p	732.09	0.01	727.59	0.01
Ni2p	864.49	0.11	882.09	0.00
O/C	0.019		0.069	
N/C	0.000		0.002	

b) C 1s and O 1s spectra

Name	As-received			Functionalised		
	C 1s					
	pos., eV	FWHM, eV	%area	pos., eV	FWHM, eV	%area
A: C-C	284.43	0.863	84.91	284.44	0.899	82.14
B: C-O	286.20	0.979	3.46	286.13	1.114	4.72
C: C=O	287.21	1.611	4.09	287.29	1.735	5.20
D: COOH	288.30	2.009	3.31	288.70	1.983	4.40
E: CO_3	290.24	2.123	3.65	290.19	2.123	3.55
X: C-Me	283.11	1.073	0.58	283.75	1.073	0.00
	O 1s					
	pos., eV	FWHM, eV	%area	pos., eV	FWHM, eV	%area
A: O-Me	529.68	1.617	10.61	529.38	2.222	4.02
B: OH	531.31	2.109	37.83	530.96	2.142	40.85
C: O-C	532.75	2.224	45.42	532.76	2.224	48.73
D: O-C=+H_2O	535.32	2.478	6.14	535.15	2.479	6.39

Acid/ base titration allowed to quantify the amount of functional groups and confirmed the trend and information given by XPS. The obtained results are presented in Table 10. It was observed that an increase in concentration of carboxylic (-COOH), phenolic (-OH) and lactone (-C=O) groups after oxidation process occurs. The phenolic groups were not detected for as-received MWCNTs. There can be a few explanations: (i) a relatively low amount of phenolic groups [255] or (ii) carbonyl groups (presence confirmed with XPS) with neighbouring phenol groups

may transform into lactone groups [256]. The functionalisation step was efficient in oxidising the surface of MWNCTs.

Table 10 Functional groups concentrations determined by acid/ base titration of multi-walled carbon; nanotubes;

MWCNTs type	Phenolic, mmol/g	Lactone, mmol/g	Carboxylic, mmol/g	Total amount, mmol/g
As-received	0.00	0.08	0.31	0.39
Functionalised	0.22	0.16	0.79	1.17

Figure 37 presents graph of final pH_f vs initial pH_i for multi-walled carbon nanotubes. The point of zero charge for as-received MWCNTs is 4.5, while for functionalised one it is 2.7. The functionalisation process leads to a decrease of the point of zero charge, due to the incorporation of acidic functional groups.

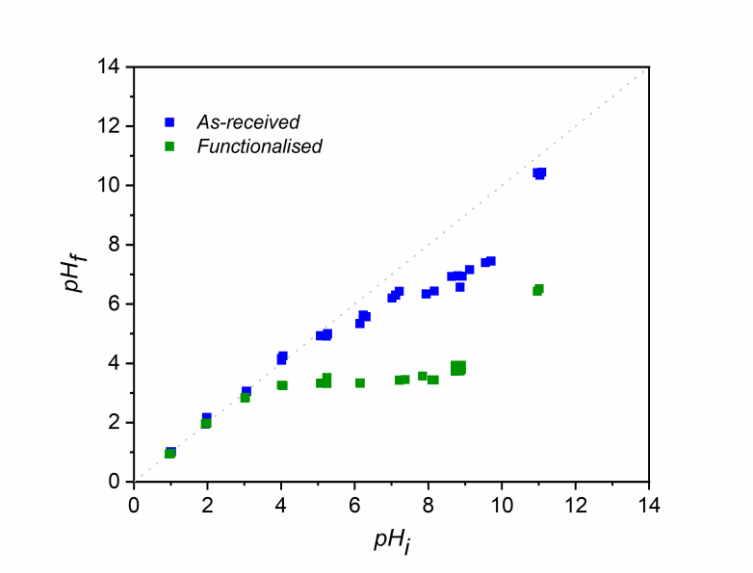

Figure 37 Graph of final pH versus initial pH of multi-walled carbon nanotubes;

To further prove trace metal removal, their presence and concentration was measured using ICP-MS (Figure 38a). A nearly 90 wt.% decrease in catalyst concentration was observed after the functionalisation process, confirming the high efficiency of the two-step applied methodology. Additionally, TG-DSC studies (Figure 38b) revealed that the functionalisation step caused a shift of combustion temperature from ~600 to 625 °C for as-received and functionalised MWCNTs, respectively, due to the decrease in catalysts content (Fe, Ni) [257]. Furthermore, a

continuous mass loss was noted from 50 until 500 °C, which can be explained by the dehydration of adsorbed water and -OH, -CHO and -COOH groups generated during the oxidation process.

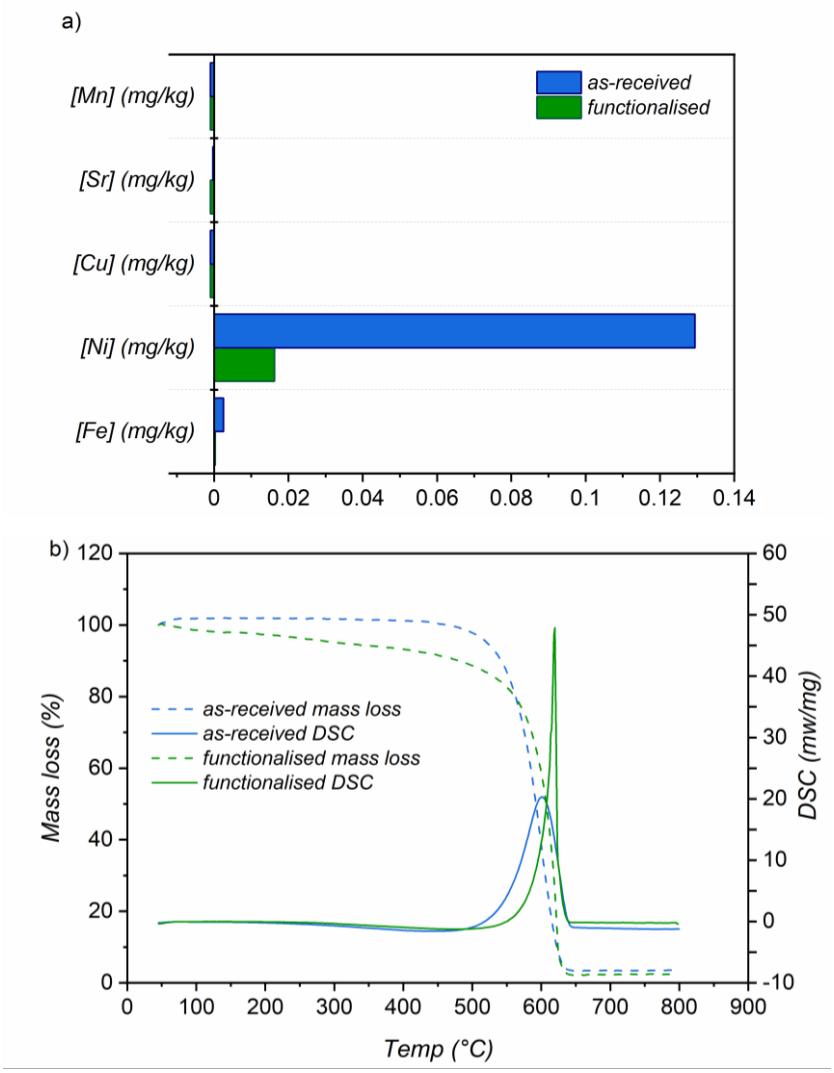

Figure 38 a) ICP-MS results; b) TG-DSC data of as-received and functionalised multi-walled carbon nanotubes;

The SSA of the as-received and functionalised material was compared and an increase from 116 m^2/g to 265 m^2/g was observed. This increase was assigned to the incorporation of functional groups, as well as tube shortening and deagglomeration [258]. Moreover, the functionalised MWCNTs were more dispersible and formed a slurry with higher stability in comparison with the as-received material. This is linked with the presence of functional groups at the MWCNTs' surface, which create hydrogen bonds with water molecules [257].

The comparison of total oxygen content obtained via different methods is presented in Table 11. For EA, the oxygen concentrations were taken as measured, for acid/ base titration the quantities of detected surface groups were summarised and multiplied with the molecular weight of oxygen per functional group [247]. For XPS, the value was taken from the survey spectra and recalculated to wt.%.

Table 11 Comparison between the oxygen concentrations (wt. %) obtained by different techniques;

MWCNTs type	Elemental analysis	Acid/ base titration	XPS
As-received	6.50	1.25	2.48
Functionalised	6.50	3.39	8.36

Although EA represents oxygen content of the whole sample, it shows the same oxygen content for as-received and functionalised samples. Taking into account only XPS results, it can be concluded that functionalised MWCNTs have oxygen located mainly in the uppermost surface layer while as-received one contains oxygen in bulk. However, acid/ base titration and XPS follow the same trend indicating that nitric acid treatment resulted in the incorporation of oxygen on MWCNTs surfaces.

As the result of the MWCNTs functionalisation process, a degradation of carbon nanotubes structure was observed. The nanotubes were broken and shorten, while their diameter remains unchanged. XPS study and acid/ base titration confirmed incorporation of functional groups onto MWCNTs' surface. ICP-MS technique together with XPS revealed a significant reduction of catalysts presence. The point of zero charge of as-received MWCNTs decreased from 4.5 to 2.7 for functionalised MWCNTs, due to presence of functional groups. The SSA of as-received and functionalised MWNCTs increased from 116 m^2/g to 265 m^2/g, respectively.

11.2. Functionalised Activated Carbon Fibres

Activated carbon fibres were functionalised by a tailored combination of HNO_3 oxidation and Soxhlet extraction. The aim of the treatment was to introduce functional groups onto fibres' surface, increase microporosity, as well as enhance reactivity and the amount of active sites.
Figure 39 presents the SEM images of functionalised ACFs. Nitric acid oxidation did not markedly affect the macro structural morphological features of the activated carbon fibres. The func-

tionalised ACFs exhibit after acid treatment either a smooth surface or surface with some defects in the form of roughness and groves, which are clearly visible. No change in fibre diameter and length after oxidation was observed.

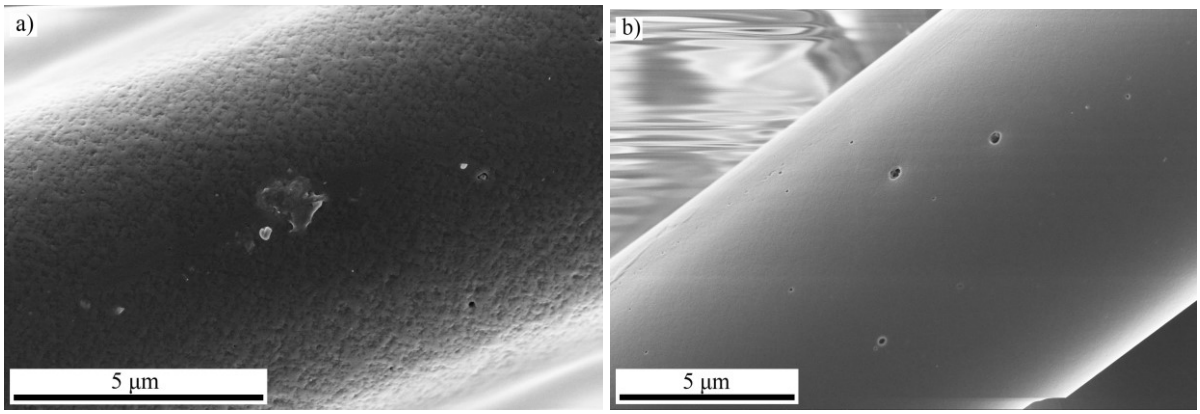

Figure 39 a, b) SEM images of functionalised activated carbon fibres;

Raman spectroscopy measurements were carried out to investigate the changes in material structure after acid oxidation and Soxhlet purification step. Figure 40 presents Raman spectra of all activated carbon fibres, which resemble one another, indicating that the applied treatment has no significant effect on materials structure.

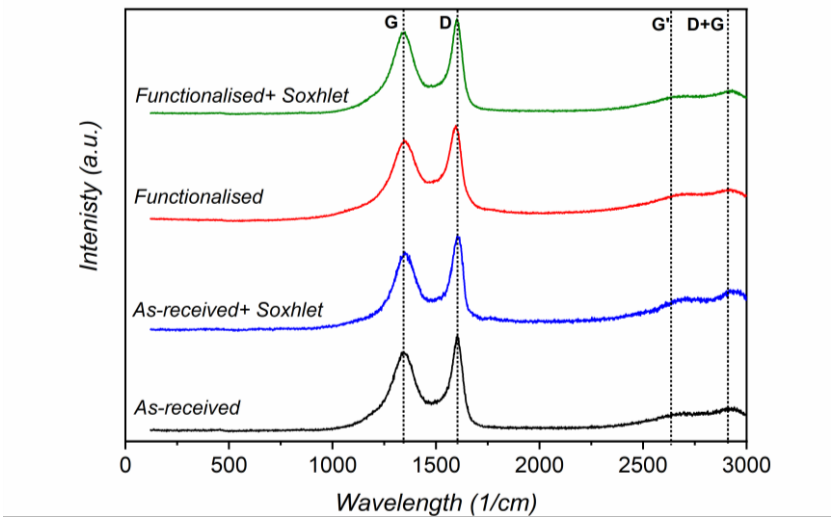

Figure 40 Raman spectroscopy of all activated carbon fibres;

Table 12 presents the analysis of Raman spectra. No significant differences are observed between the G band positions caused by the applied treatment. However, a slight shift of the D band to higher wavelength numbers was noted within the acid functionalisation, while Soxhlet treatment brought it back to previous position. The intensity ratio of the two first-order bands

slightly decreases for acid treatment, while the Soxhlet step caused its increase. It is assumed that the increase in I_D/I_G is associated with the increase in material disorder (e.g. substitutional) [259]. It is important to underline that the I_D/I_G ratio not only represents exact changes in structuring order, but also the contribution of heteroatoms introduced during functionalisation (O, H, N) that heavily influence Raman response [260–262].

Table 12 Peak intensity ratio, peak area ratio, half of the maximum peak width, peak position values of the first-order D and G band of activated carbon fibres;

ACFs type	I_D/I_G	A_D/A_G	WD, cm^{-1}	WG, cm^{-1}	D-Peak position, cm^{-1}	G-peak Position, cm^{-1}
As-received	0.87	2.12	159.0	64.5	1344.0	1599.0
As-received + Soxhlet	0.82	1.81	159.0	71.7	1351.7	1600.3
Functionalised	0.84	1.90	177.6	78.7	1352.3	1595.7
Functionalised + Soxhlet	0.92	2.08	147.0	61.6	1342.0	1599.0

For calculating the carbon structural parameters from XRD analysis, such as the relative carbon nano-crystal thickness (L_c), and apparent crystallite diameter (L_a) the Scherrer equation (Eq. 28) was used [254]. The first peak (centred around $2\theta = 23°$) corresponds to the (002) reflection of graphite assigned to the stacking order of the graphene layers, while $2\theta = 44°$ represents the (100) reflection attributed to the in-plane structure of graphitic crystallites [263]. The interlayer space (d_{002}) was determined through Bragg's law equation (Eq. 29) [264,265].

$$n\lambda_{XRD} = 2d_{002}\sin(\Theta_{002}) \qquad \text{Eq. 29}$$

where: λ_{XRD} - the wavelength of the incident X-ray radiation, d_{002} - the interlayer space, θ_{002} - the position of the (002) peaks.

All results are summarised in Table 13.

Table 13 Crystallite thickness L_c, interlayer distance d_{002}, and crystal diameter L_a determined from XRD spectra of activated carbon fibres;

ACFs type	Crystallite thickness, L_c, Å	Interlayer distance, d_{002}, Å	Crystal diameter, L_a, Å
As-received	6.3	1.9	32.7
As-received + Soxhlet	9.2	2.1	22.3
Functionalised	8.6	1.9	58.1
Functionalised + Soxhlet	10.5	1.9	38.5

The interlayer spacing of as-received fibres is relatively low in comparison to the graphite value equal to 3.4 Å [259]. Within the acid treatment, the interlayer distance does not changing. The L_a value increases, which suggests an increase in crystallites size [259].
Various correlations between the I_D/I_G ratio and L_a parameter are given in the literature, they are dependent on analysed material properties, e.g., crystallite size (<2 nm, 2-7 nm or >7 nm), type of disorder, chemical composition [262]. Such correlations are not fully applicable here due to effect of incorporated heteroatoms (O, H, N).

The results of EA are presented in Table 14. A significant change of carbon content for as-received and functionalised ACFs is noted, which prove that a majority of the fibres' surfaces oxidised. Nitric acid oxidation increases the H/C, O/C and N/C atomic ratios in carbon fibres from 0.006, 0.089 and 0.000 to 0.017, 0.507 and 0.009 of as-received and functionalised ACFs. This means that the functionalisation process resulted in an increase in oxygen (approx. 4 times) and nitrogen content (from 0 to 0.59 wt.%). The Soxhlet purification step caused a slight decrease in content of O, H and N. The last observation might indicate either that Soxhlet purification was performed not long enough to effectively remove nitric acid residuals or that the N-containing groups are strongly bonded to ACFs that were not expelled.

Table 14 Elemental analysis of activated carbon fibres;

ACFs type	C, wt.%	H, wt.%	N, wt.%	O, wt.%	N/C	H/C	O/C
As-received	90.65	0.50	0.00	8.07	0.000	0.006	0.089
As-received + Soxhlet	91.20	0.73	0.00	5.59	0.000	0.008	0.061
Functionalised	64.84	1.11	0.59	32.85	0.009	0.017	0.507
Functionalised + Soxhlet	65.02	0.96	0.44	29.67	0.007	0.015	0.456

Various techniques can be applied to determine the presence of functional groups on carbon surfaces [266,267]. Following that, in the presented study, XPS, acid/ base titration and pH_{PZC} measurements were utilised. Figure 41a and Table 15a present a XPS survey spectra of all four ACFs types, where nearly a three times increase in oxygen and two times increase in nitrogen content of functionalised and functionalised+ Soxhlet ACFs vs as-received ACFs. The O_{1s}/C_{1s} atomic ratios (Table 15a) at the samples surface are 0.069, 0.089, 0.229, 0.219 for as-received,

as-received+ Soxhlet, functionalised, functionalised+ Soxhlet, respectively. The XPS study revealed oxidation of the uppermost ACFs surface.

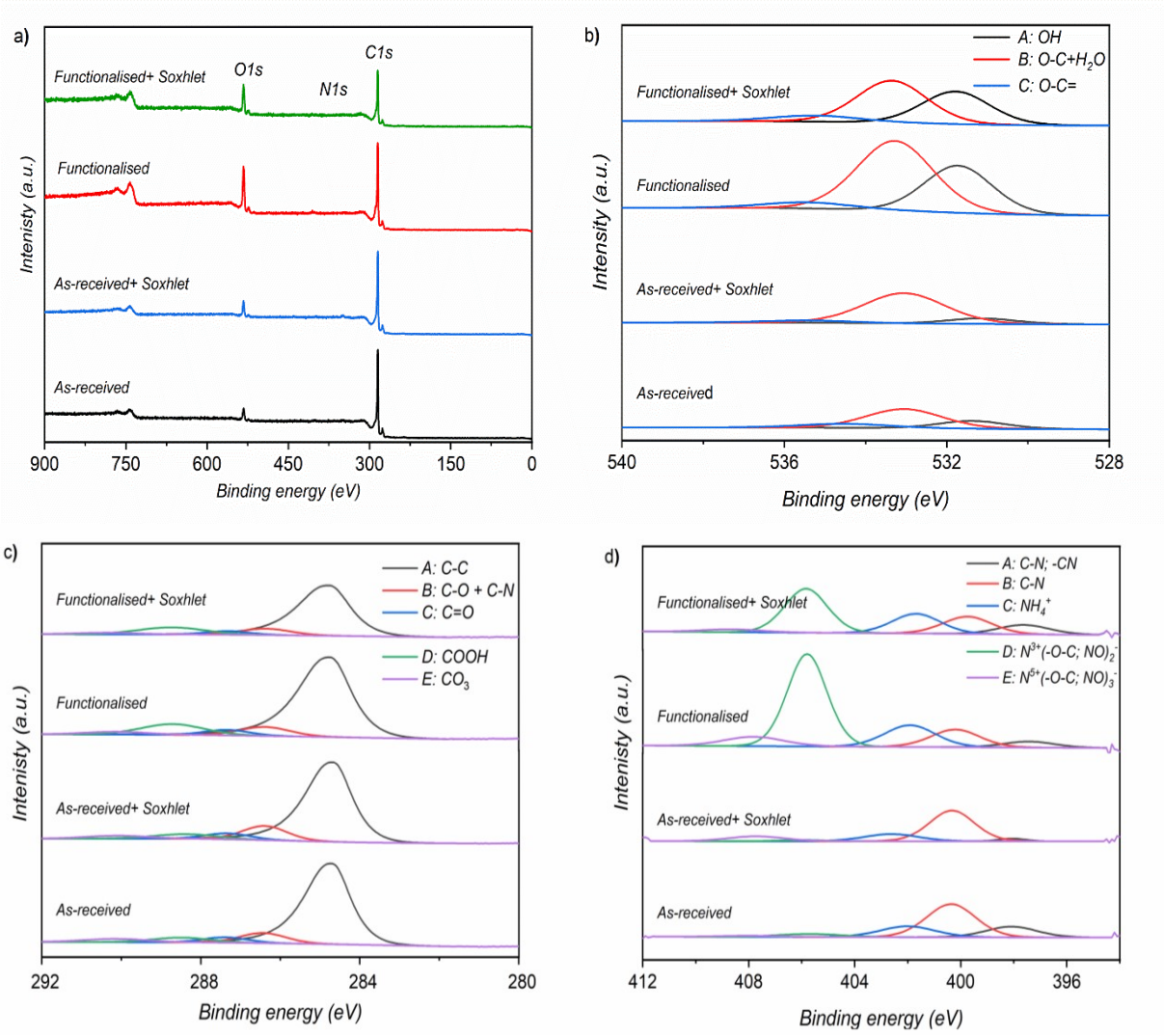

Figure 41 XPS spectrum a) Survey; b) C 1s; c) O 1s; d) N 1s of activated carbon fibres;

The functionalisation step led to a concentration increase in carboxylic (D peak in Figure 41c) and hydroxyl groups (A peak in Figure 41b, B peak in Figure 41c) on ACFs surfaces. However, the increase in hydroxyl groups might not be clear at first glance, as the growth of peak B in Figure 41c is not prominent because its value represents two functional groups. This peak is assigned to alcohol or ether groups plus amines, while each of mentioned groups is also represented by A peak in Figure 41b and B peak in Figure 41d. A peak in Figure 41b makes up hydroxyl groups, which concentration is increasing, B peak in Figure 41d constitutes of amine groups, which amount strongly decreases after acid treatment. Functionalisation with HNO_3 also introduces a small amount of surface nitrogen functional groups, which can be observed as nitrogen content increases, visible in Figure 41a. The N_{1s}/C_{1s} atomic ratios at the sample

surface are 0.011, 0.008, 0.028, 0.213 for as-received, as-received+ Soxhlet, functionalised, functionalised+ Soxhlet, respectively. After both treatment steps, a decrease in concentration of nitrile and amine groups was noted and increase in concentration of N^{3+}-O-C; NO_2^- and nitrate(III) groups bonded to organic chains, which were probably trapped in the pores [268]. Again, this shows that the Soxhlet purification step is not sufficient to completely remove nitric acid residuals as still N-containing groups are observed (Fig. 41a and 41d).

Table 15 Data described XPS spectra presented in Figure 41: a) Survey spectra; b) C 1s; c) O 1s; d) N 1s spectra of activated carbon fibres;

a) Survey spectra

Survey	**As-received**		**As-received+ Soxhlet**		**Functionalised**		**Functionalised+ Soxhlet**	
Name	pos., eV	at.%	pos., eV	at.%	pos., eV	at.%	pos., eV	at.%
C1s	284.75	92.58	284.75	91.20	285.00	79.53	285.00	80.57
O1s	532.50	6.38	533.00	8.08	532.75	18.25	532.75	17.62
N1s	399.75	1.03	398.75	0.72	405.75	2.22	406.00	1.82
O/C	0.069		0.089		0.229		0.219	
N/C	0.011		0.008		0.028		0.023	

b) C 1s spectra

C 1S	**As-received**			**As-received+ Soxhlet**			**Functionalised**			**Functionalised+ Soxhlet**		
Name	pos., eV	FWHM, eV	%area	pos., eV	FWHM, eV	%area	pos., eV	FWHM, eV	%area	pos., eV	FWHM, eV	%area
A	84.70	1.09	77.17	284.67	1.11	74.52	284.67	1.25	74.64	284.76	1.24	73.13
B	286.44	1.36	9.02	286.40	1.32	11.78	286.39	1.48	7.39	286.37	1.48	8.08
C	287.38	1.35	4.72	287.33	1.35	5.84	287.34	1.35	4.12	287.32	1.31	4.08
D	288.49	1.69	5.23	288.37	1.84	5.34	288.72	1.85	11.05	288.74	1.99	12.16
E	290.15	1.83	3.87	290.10	1.83	3.32	290.12	1.83	2.80	290.35	1.83	2.55

c) O 1s spectra

O 1S	**As-received**			**As-received+ Soxhlet**			**Functionalised**			**Functionalised+ Soxhlet**		
Name	pos., eV	FWHM, eV	%area	pos., eV	FWHM, eV	%area	pos., eV	FWHM, eV	%area	pos., eV	FWHM, eV	%area
A	531.38	1.97	22.30	531.13	1.97	12.40	531.72	1.97	35.36	531.78	1.97	38.89
B	533.06	2.21	62.19	533.06	2.35	81.37	533.28	2.21	58.64	533.36	2.03	51.76
C	534.50	2.58	15.50	535.39	2.52	6.22	535.43	2.58	6.00	535.23	2.58	9.35

d) N 1s spectra

N 1S	As-received			As-received+ Soxhlet			Functionalised			Functionalised+ Soxhlet		
Name	pos., eV	FWHM, eV	%area	pos., eV	FWHM, eV	%area	pos., eV	FWHM, eV	%area	pos., eV	FWHM, eV	%area
A	398.09	2.27	18.21	398.07	1.19	3.42	397.43	2.26	4.77	397.62	2.26	11.11
B	400.37	2.17	53.66	400.33	1.98	63.76	400.21	2.17	13.33	399.75	2.17	19.95
C	402.01	2.43	19.73	402.62	2.40	17.93	401.92	2.27	17.16	401.69	2.14	22.05
D	405.69	2.83	6.31	405.98	1.91	2.37	405.80	1.75	56.51	405.84	1.89	43.43
E	407.98	2.65	2.10	407.72	2.45	12.52	407.81	2.65	8.63	407.81	2.64	3.81

A comparison between the XPS and EA techniques reveals that the results follow the same trend regarding changes in elements concentration, however, value discrepancies can be observed and they come from the fact that XPS allows only to study the upmost sample surface, while EA the bulk. Nevertheless, it can be concluded that oxidation takes place uniformly through the fibres, as the same tendency occurs. However, the reaction with nitric acid seems to be more dominant on the outermost surface than inside of the ACFs, as the amount of nitrogen analysed in functionalised ACFs is higher in the XPS study than for EA.

Recently published studies have proposed possible mechanism responsible for oxidation of activated carbons and revealed that it is similar to the reaction involving the oxidation of aromatic hydrocarbons (i.e. 9,10-dihydrophenanthrene and diphenylmethane) with nitric acid [267–269]. The formation of the dicarboxylic group is assumed to occur on the aliphatic side of the molecule especially if the side chains consist of more than one carbon atom, as presented in Figure 42, reaction a). The reaction is initiated by the splitting of the C–C bond at the a-position of the benzylic carbon atom [269]. Oxidation involving a methylene ($–CH_2–$) group would result in the formation of a ketone as shown in reaction b), Figure 42 [268]. The mechanism would form the highly reactive nitronium ion (NO_2^+), which will ultimately cause the formation of the nitrated product as shown in reaction c), Figure 42 [267]. In the case of oxidised carbons, however, the nitrated product would appear in small quantities due to the limited amount of the nitronium ions, as their formation is promoted by the presence of acid catalyst (e.g. sulphuric acid) [267].

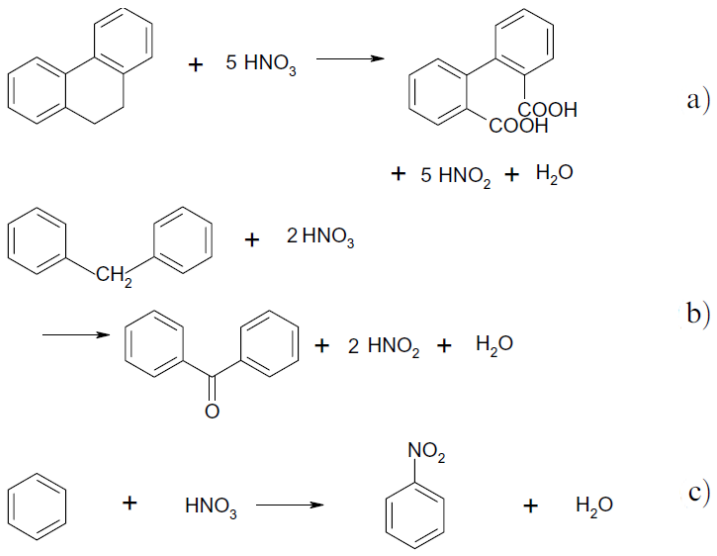

Figure 42 Scheme of three reactions occurring during oxidation of activated carbon surface with nitric acid [267,268];

Acid/ base titration (Table 16) revealed that the functionalisation process led to a six fold increase in the total amount of functional groups (0.46 mmol/g for as-received ACFs vs 3.31 mmol/g for functionalised one). There, a higher increase in carboxylic group concentration was observed, from 0.10 to 2.26 mmol/g. It is highly profitable for the following treatment steps, due to the high affinity of carboxylic groups to metal ions adsorption from aqueous solutions [270]. Thereby, functional groups enhance the hydrophilic character of the carbon surface, thus promoting metal adsorption.

Table 16 Functional groups concentrations determined by acid/ base titration of activated carbon fibres;

ACFs type	Phenolic, mmol/g	Lactone, mmol/g	Carboxylic, mmol/g	Total amount, mmol/g
As-received	0.36	0.00	0.10	0.46
As-received + Soxhlet	0.11	0.31	0.30	0.72
Functionalised	0.04	1.01	2.26	3.31
Functionalised + Soxhlet	0.83	0.61	2.04	3.48

The point of zero charge is an important parameter to understand material surfaces properties in solutions. The pH drift method was applied to measure the pH at the point of zero charge of all activated carbon fibres. Figure 43 shows the curves of final pH_f against initial pH_i for all activated carbon fibres used.

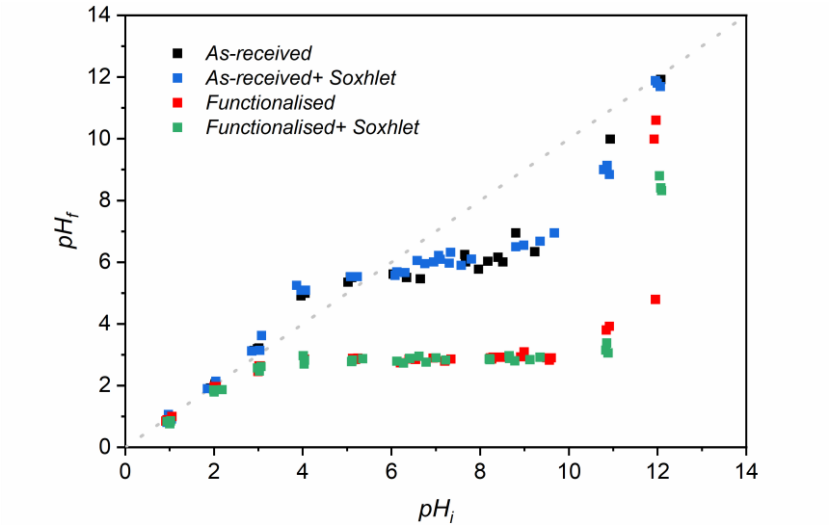

Figure 43 Final pH versus initial pH of activated carbon fibres;

The comparison of pH_{PZC} of as-received fibres shows that these ACFs have similar pH_{PZC} values equal to 5.8 and 5.6 for as-received and as-received+ Soxhlet, respectively. Oxidation with concentrated nitric acid caused the shift of point of zero charge to the lowest value of 1.9 for functionalised ACFs. The lower pH_{PZC} implies that the ACFs surface has a net negative charge in aqueous solution, due to the presence of acidic functional groups that release protons into the solution, which leaves the carbon surfaces negatively charged. The dissociation of the carboxylic groups can be the reason for the shift of pH_{PZC} for functionalised samples, which presence was confirmed with other techniques (XPS, acid/ base titration) [268]. Purification with Soxhlet slightly decrease pH_{PZC}, which is equal to 1.5 for functionalised+ Soxhlet ACFs. A correlation between pH_{PZC} and the oxygen content is presented in Figure 44. The pH_{PZC} decreases with increasing oxygen content. Acidic functional groups on carbon surfaces affect the material point of zero charge, leading to its lower value [271].

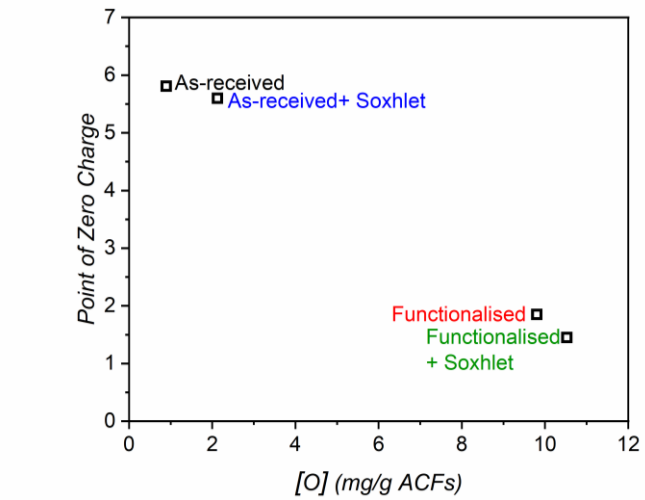

Figure 44 Variation of pH_{PZC} with oxygen content of activated carbon fibres;

The specific surface area and porous structure characteristics of as-received and functionalised ACFs were assessed by CO_2 at 273 K and N_2 adsorption at 77 K, as the material is assumed to be highly microporous. Figure 45a) presents the isotherms for CO_2 adsorption on all used ACFs. The micropore volume is well represented by CO_2 measurement at 273 K. The Dubinin- Radushkevich equation was applied to the CO_2 adsorption isotherm data for all ACFs to calculate the micropore volume (V_{CO2}).

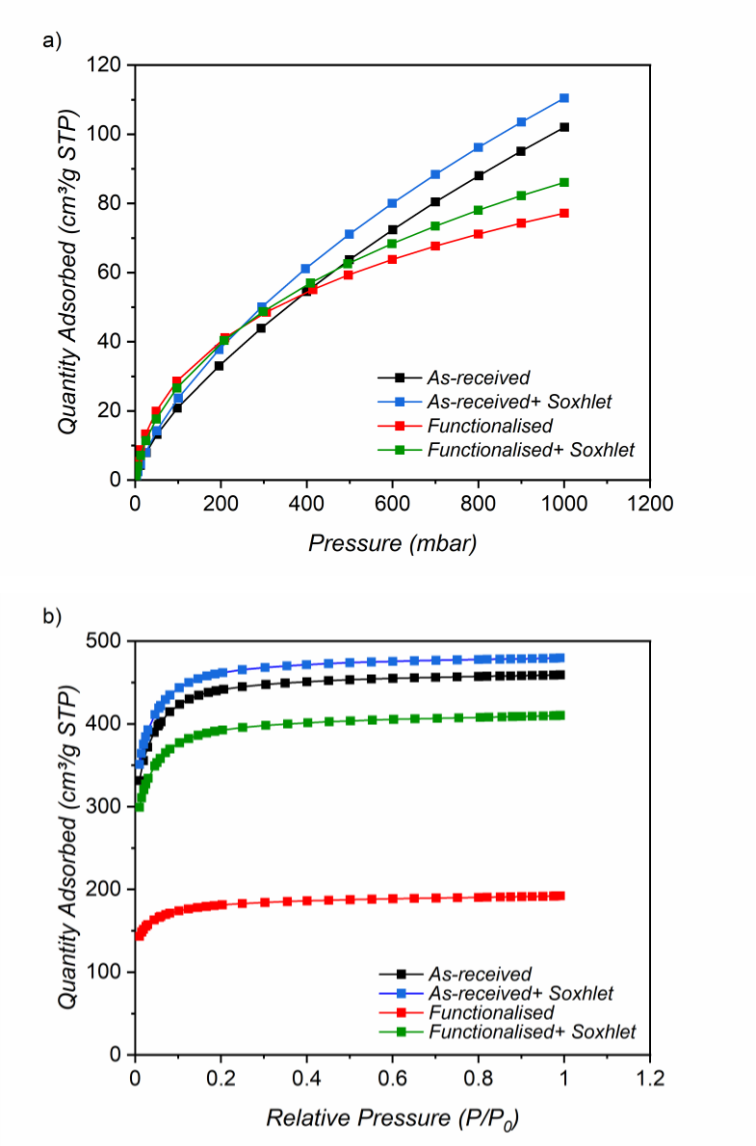

Figure 45 a) CO_2 adsorption isotherm; b) N_2 adsorption isotherm of activated carbon fibres;

The micropore volume is equal to 0.108 cm^3g^{-1} and 0.130 cm^3g^{-1}, for as-received and as-received+ Soxhlet, respectively. It shows the higher CO_2 uptake at low pressure for the oxidised samples (0.137 cm^3g^{-1}, 0.141 cm^3g^{-1} for functionalised and functionalised+ Soxhlet, respectively), which indicates microporosity increase of ~25 % in comparison to the as-received

ACFs. The results also prove that Soxhlet extraction is opening up the porosity and at the same time does not greatly change the porous structure between Soxhlet purified samples.

The nitrogen isotherms at 77 K of all tested activated carbon fibres are present on Figure 45b). According to the IUPAC classification, the isotherms for N_2 adsorption are type I, reaching a plateau that defines the maximum amount adsorbed [151]. The Langmuir equation was used to determine the maximum adsorbed and the total pore volume (V_{N2}) of carbon materials, which is 0.453 cm^3/g^{-1} and 0.468 cm^3/g^{-1} for as-received and as-received+ Soxhlet ACFs, respectively. Nitric acid oxidation treatment reduces the total pore volume and additionally enhances microporosity. After oxidation, the total volume is equal to 0.186 cm^3g^{-1}. This phenomenon can be explained by pore blockage by small structure changes, involving the incorporation of functional groups on ACF surfaces. However, Soxhlet purification causes the enablement of pores, increasing pore volume V_{CO2}= 0.141 cm^3g^{-1} and V_{N2}= 0.397 cm^3g^{-1} for as-received+ Soxhlet sample.

Table 17 gives the porous structure parameters and specific surface areas of activated carbon fibres. The specific surface area of as-received is equal to 1677 m^2/g, which is lower than one for as-received purified by Soxhlet extraction (1769 m^2/g). BET surface area was affected by acid treatment, where a 60 % reduction to 698 m^2/g for functionalised ACFs is observed. According to literature, such a decrease is a result of increased blocking of micropores caused by newly introduced surface oxygen complexes or the formation of humic substances, as indicated by other researchers [268,272]. Other studies suggest that this outcome is due to surface smoothing by excessive oxidation [273,274] or collapse of the pore walls due to strong treatment [214,275]. Soxhlet purification significantly increases SSA up to 1652 m^2/g for functionalised+ Soxhlet sample.

Micropore radius calculated based on N_2 adsorption remain almost unchanged independent of the treatment. Its average size is around 1 nm. Values obtained based on CO_2 adsorption revealed an increase in micropore mean radius from 0.26 nm to 0.79 nm for as-received and functionalised ACFs, respectively. The micropore diameter of fibres given by the supplier was estimated to 2.1-2.7 nm.

The ratio of V_{CO2}/V_{N2} increases with both oxidation and Soxhlet treatment. It confirms process impact on microporosity increase.

Table 17 Pore volumes and specific surface areas of activated carbon fibres;

ACFs type	Pore volume, cm^3g^{-1}		V_{CO2}/V_{N2}	x_0^c, nm	x_0^d, nm	SSA, m^2g^{-1}
	V_{CO2}[a]	V_{N2}[b]				
As-received	0.108	0.453	0.238	1.08	0.26	1677
As-received + Soxhlet	0.130	0.468	0.279	1.06	0.29	1769
Functionalised	0.137	0.186	0.740	1.06	0.79	698
Functionalised + Soxhlet	0.141	0.397	0.356	0.96	0.34	1652

a obtained from an intercept of DR plot
b obtained from Langmuir model at $p/p^0 = 1$
c mean radius of the micropore (N_2 at 77 K)
d mean radius of the micropore (CO_2 at 273 K)

It is important to compare the results of total oxygen content obtained via different methods, Table 18 presents such a summary of analyses. For EA, the oxygen concentration was taken as measured. For acid/ base titration quantities of detected surface groups were summarised and multiplied with the molecular weight of oxygen within functional groups giving the total oxygen concentration [247].

Table 18 Comparison between the oxygen concentrations (wt.%) obtained by different techniques;

ACFs type	Elemental analysis	Acid/ base titration	XPS
As-received	8.07	0.90	8.31
As-received + Soxhlet	5.59	2.13	10.47
Functionalised	32.85	10.52	22.84
Functionalised + Soxhlet	29.67	9.80	22.11

For the XPS the value was taken from the survey spectra and recalculated to wt.%. In elemental analysis the whole sample is probed, meaning that not only oxygen present on the surface was taken into account but also oxygen from interior of the sample [247], therefore, it provides higher oxygen values than other methods.

As a result of the functionalisation process, no significant effect on the carbon fibres' structure and morphology was observed. The fibres diameter and length remained unaffected. Significant amount of oxygen and nitrogen were introduced on the fibres' surface, which was confirmed with EA and XPS techniques. Acid/ base titration and XPS attested incorporation of functional

groups onto surface. The pH_{PZC} of fibres decreased from 5.8 to 1.9 for as-received and functionalised ACFs, respectively. Within the treatment, a 25 % increase in fibres microporosity was observed in comparison to the as-received ACFs, while the specific surface area decreased by nearly 60 % from 1677 m^2/g to 698 m^2/g for as-received and functionalised ACFs, respectively.

11.3. Conclusions of carbon substrates functionalisation

The two- step functionalisation and purification process of multi-walled carbon nanotubes resulted in degradation of carbon nanotubes' structure leading to the tube breaking and shortening, while their diameter remains unaffected. Data obtained from acid/ base titration and XPS spectra proved increase in the functional groups content (carboxylic, carboxyl and hydroxyl). Taking into account results of XPS, EA and acid/ base titration techniques, it can be concluded, that the MWCNT' surface was more oxidised than a bulk. ICP-MS and XPS studies confirmed reduction of catalysts content by nearly 90 wt.%. Functional groups presence affected the point of zero charge of as-received multi-walled carbon nanotubes, which was shifted from 4.5 to 2.7 for functionalised MWCNTs. The measured specific surface area of the as-received and functionalised MWCNTs increased more than two times, from 116 m^2/g to 265 m^2/g, respectively.

Activated carbon fibres were functionalised by a tailored combination of nitric acid oxidation and Soxhlet extraction. Oxidation process did not affect significantly the macro structural morphological features of carbon fibre, which was confirmed with SEM and Raman measurements. A slight decrease in I_D/I_G ratio was observed, which is associated with material disorder and introduction of N, H and O heteroatoms. EA together with XPS confirmed significant increase in oxygen and nitrogen content with oxidation. XPS study and acid/ base titration revealed incorporation of functional groups, with major contribution of carboxylic ones. The pH_{PZC} of fibres decreased from 5.8 to 1.9 for as-received and functionalised ACFs, respectively, due to presence of acidic functional groups. A 25 % increase in fibres microporosity for functionalised fibres was noted in comparison to the as-received ACFs. Also a 60 % decrease in specific surface area was observed, exhibiting values of 1677 m^2/g and 698 m^2/g for as-received and functionalised ACFs, respectively.

12. Synthesis and characterisation of obtained materials

12.1. Composites based on Multi-walled Carbon Nanotubes

MWCNTs-based composites were fabricated via three distinctive synthesis routes: (i) adsorption of aqueous copper ion (*composite 1*), (ii) adsorption of copper(II) hydroxide (*composite 2*), (iii) adsorption of copper complex (*composite 3*).

In the copper ion attachment synthesis (route 1), the copper ions formed by hydrolysis of copper salt (Eq. 30) attach to the functional groups formed on MWCNTs surfaces during the functionalisation step due to electrostatic interactions [276]. Additionally, because of opposite charges Cu^{2+} ions can also be adsorbed directly onto the MWCNTs surface [233]. Then during the thermal treatment, the Cu_2O-NPs nucleate directly on the surface of the MWCNTs.

$$Cu(CH_3COO)_{2(s)} \xrightarrow{H_2O} [Cu(H_2O)_6]^{2+}_{(aq)} + 2CH_3COO^-_{(aq)} \qquad \text{Eq. 30}$$

For the second synthesis route (copper precipitation synthesis), an addition of stoichiometric amount of ammonium hydroxide led to the formation of copper(II) hydroxide precipitates (Eq. 31), which resulted in a composite with high ratio of copper species to MWCNTs. The calcination step caused decomposition of copper hydroxide to copper(I) oxide.

$$[Cu(H_2O)_6]^{2+}_{(aq)} + 2NH_{3(aq)} \rightarrow Cu(OH)_{2(s)} + 2NH^+_{4\,(aq)} \qquad \text{Eq. 31}$$

In the copper complex attachment synthesis (route 3), water molecules are replaced with ammonia, forming a tetraaminediaqua copper(II) solution (Eq. 32). The complex can react with the carboxylic groups present on MWCNTs' surface, leading to the formation of amide intermediate product of MWCNT-CONH-$Cu(NH_3)_3^{2+}$ [277]. During the thermal treatment, complex decomposes forming Cu_2O/ MWCNTs composite.

$$[Cu(H_2O)_6]^{2+}_{(aq)} + 4NH_{3(aq)} \rightarrow [Cu(NH_3)_4(H_2O)_2]^{2+}_{(aq)} + 4H_2O \qquad \text{Eq. 32}$$

XRD patterns of the obtained composites are presented in the Figure 46. Cu_2O was the dominant phase obtained in *composites 1*, *2* and *3* while some traces of CuO were detected in *composite 1* and *2*. The intensity ratio between the Cu_2O (I_{Cu2O}) and C (I_C) peaks (I_{Cu2O}/I_C ratio) were 2.3, 49.1 and 1.5 for *composite 1*, *composite 2* and *composite 3*, respectively. The average crystallite sizes of Cu_2O, calculated using the Scherrer equation, were 40, 36 and 36 nm for composites *1*, *2* and *3*, respectively. Taking into account that carbon content in all composites is the same, as well as calculated crystal sizes are in the same range, the changes in I_{Cu2O}/I_C ratio are attributable to changes in Cu_2O mass, which is dependent on synthesis route. *Composite 2* has the highest I_{Cu2O}/I_C ratio due to the precipitation synthesis, where all of the copper

used was precipitated to copper hydroxide. The small difference I_{Cu2O}/I_C ratio between *composite 1* and *3* is caused by the first synthesis step, which is limiting factor (Figure 47). The free Cu^{2+} ions (synthesis route 1) interact with functional groups and MWCNTs surfaces with less steric and reaction limitation than formed amide groups between the amine complex and the MWCNTs carboxylic groups (synthesis route 3) [277].

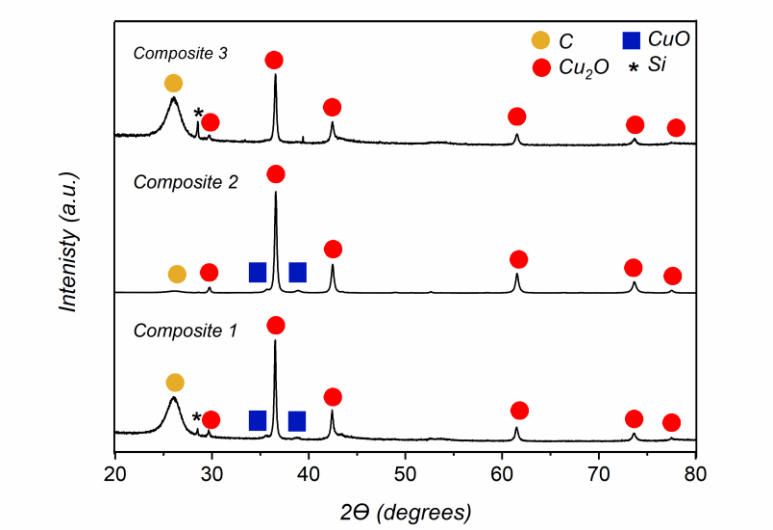

Figure 46 XRD patterns of obtained MWCNTS-based composites after calcination (Si peak comes from the sample holder);

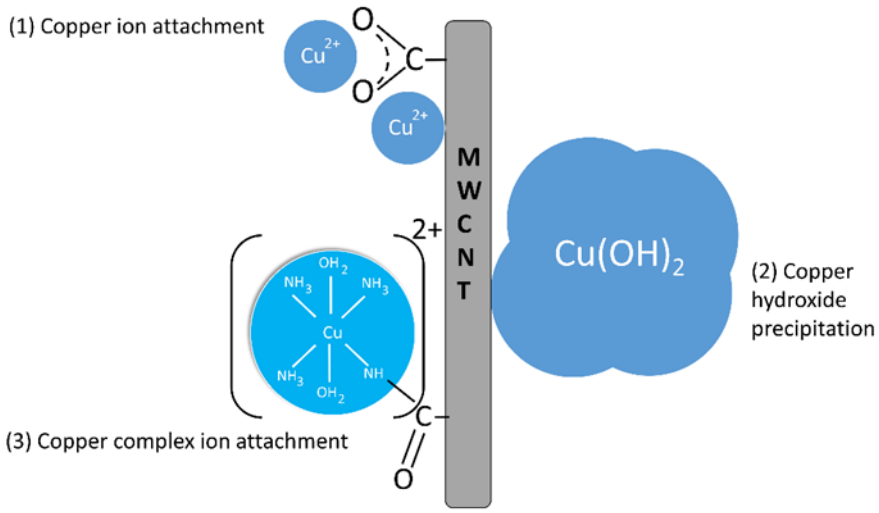

Figure 47 Scheme of the interactions of copper species with the multi-walled carbon nanotubes during the first step of the syntheses;

Figure 48 presents TEM images of obtained composites, where spherical Cu_2O nanoparticles are deposited onto MWCNTs. For *composite 1*, the diameter of Cu_2O varied from 12 to 55 nm and the NPs are randomly distributed along the carbon nanotube. In *composite 2*, cuprous oxide

nanoparticles in the range of 5-85 nm are agglomerated, probably due to the high Cu_2O:MWCNTs ratio as a consequence of the precipitation reaction. In *composite 3*, MWCNTs are uniformly coated with single Cu_2O particles in the size range of 8-60 nm.

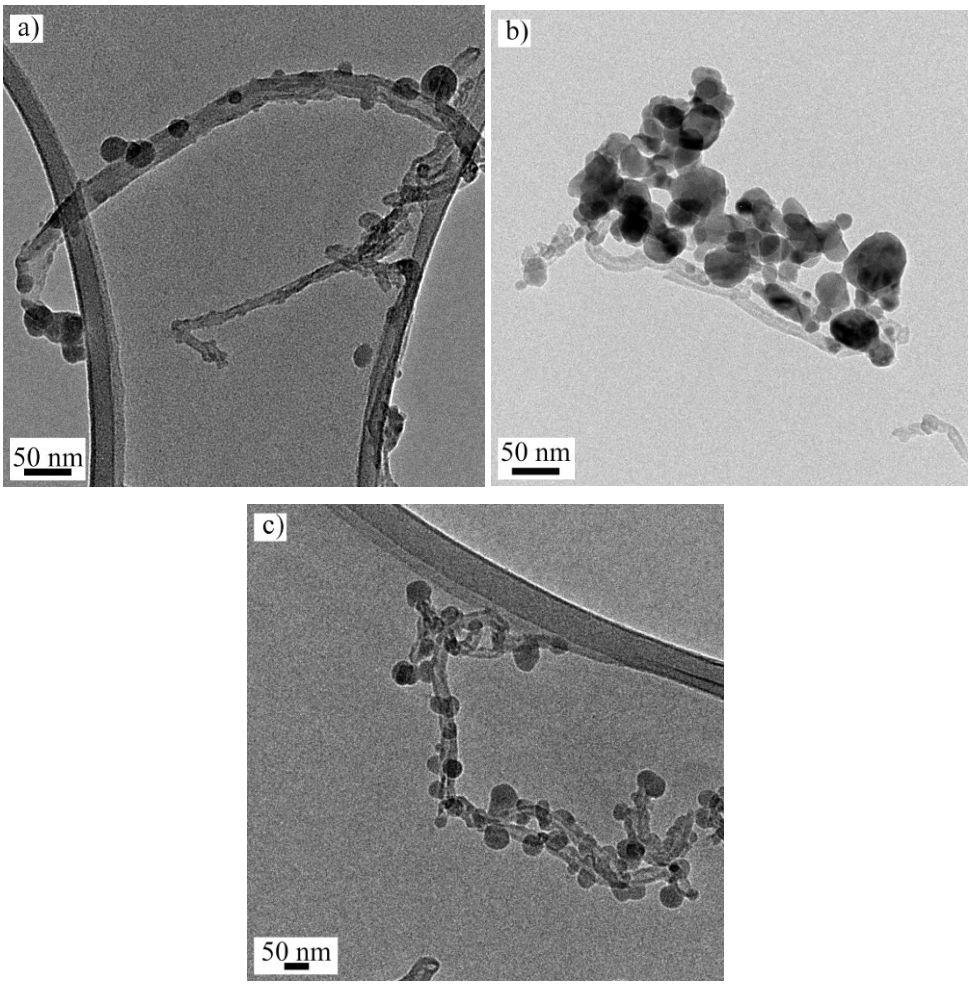

Figure 48 TEM images of obtained a) *composite 1*; b) *composite 2*; c) *composite 3;*

Characteristic of composites: I_{Cu2O}/I_C ratio, crystallite size, interval of nanoparticle (NP) diameter and SSA, is summarised in Table 19.

Table 19 I_{Cu2O}/I_C ratio, crystallite size, nanoparticle (NP) diameter and SSA of the three synthesised MWCNTs-based composites;

Composite	**I_{Cu2O}/I_C ratio**	**Crystallite size, nm**	**NP diameter, nm**	**SSA, m^2g^{-1}**
1	2.3	40	12-55	207
2	49.1	36	5-85	65
3	1.5	36	8-60	215

The specific surface area of the obtained composites was 207 m^2/g, 65 m^2/g, 215 m^2/g for *composites 1*, *2* and *3*, respectively. Such high specific surface areas are related to carbon nanotubes, which possessing large SSA, since pristine MWCNTs SSA is equal to 116 m^2/g. Additionally, during the functionalisation step, the SSA increases up to 265 m^2/g, caused by the incorporation of functional groups, as well as the shortening of the tubes. The measured values for composites follow the same trend observed in XRD patterns: the higher the intensity measured with XRD, the higher the Cu_2O amount, and the lower the SSA.

12.2. Composites based on Activated Carbon Fibres

Preparation of Cu/ ACFs-based composites included one synthesis route, adsorption of aqueous copper ion, studied in details to obtain maximum copper adsorption on ACFs' surface.

Copper ion adsorption

Figure 49 presents results of preliminary Cu^{2+} adsorption equilibrium time study from 2 mmol $Cu(NO_3)_2 \cdot 5H_2O$ aqueous solution onto various activated carbon fibres (as-received, functionalised+ Soxhlet). Outcomes revealed that adsorption process is progressive with time, slowly saturating, obtaining similar level after 24 and 48 h, leading to the conclusion, that 24 h are enough to reach adsorption equilibrium. This time was used for the following studies.

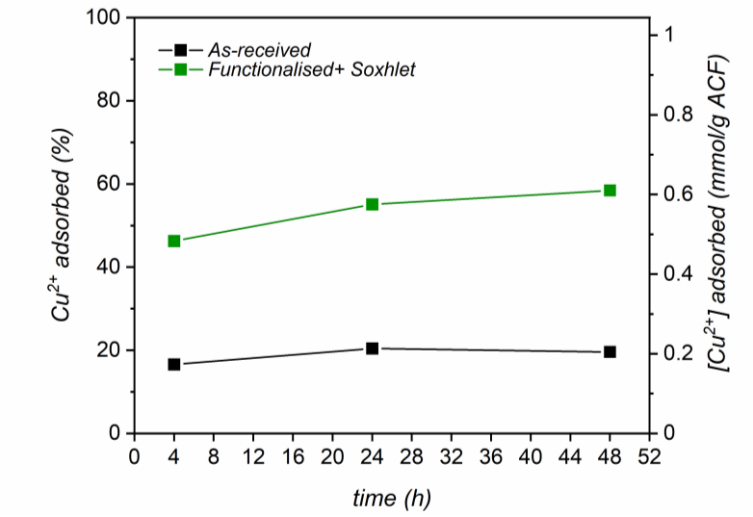

Figure 49 Results of equilibration time preliminary study of $Cu^{2+}_{(aq.)}$ adsorption from 2 mmol solution on various activated carbon fibres;

The amount of metal ions adsorbed on the ACFs surface was determined by the difference in metal ion concentration before and after adsorption using the following equation:

$$N_A = \frac{(C_{\text{init}} - C_e)V}{1000 W_c} \quad \text{Eq. 33}$$

where: N_A - the amount of metal ions adsorbed (mmol/g), C_{init} and C_e - the initial and equilibrium concentrations of metal ions (mmol), respectively, V - the volume of solution (L), W_c - the weight of ACFs (g).

Knowing the equilibration time, further studies of copper impregnation were performed. To quantify the adsorption capacity of copper ions onto activated carbon fibres, the Langmuir linear adsorption equation was applied in following form [270]:

$$n = \frac{n_{mKC}}{1+KC} \quad \text{Eq. 34}$$

where: n - the amount adsorbed (mmol/g), n_m - the maximum amount adsorbed (mmol/g), K - the adsorption constant (L/mmol), C - the solution concentration (mmol).

Figure 50 presents adsorption isotherms for as-received (Fig. 50a) and functionalised+ Soxhlet ACFs (Fig. 50b) at room temperature.

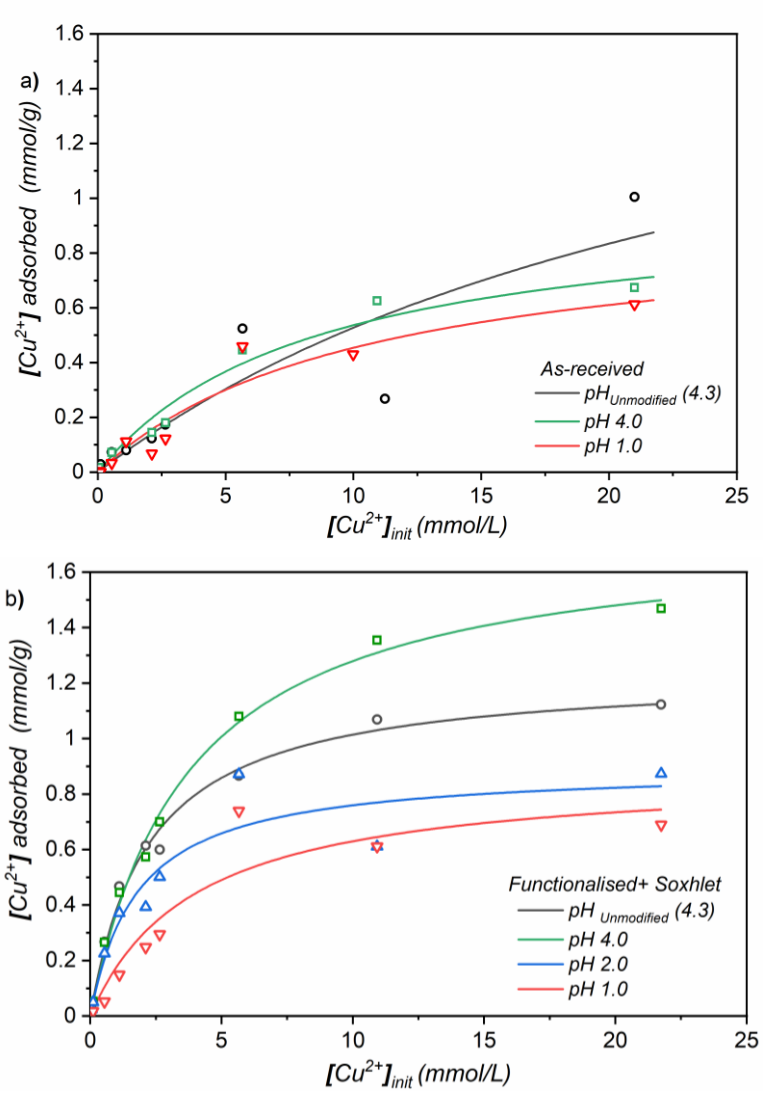

Figure 50 Adsorption isotherms of $Cu^{2+}_{(aq.)}$ adsorbed onto a) as-received activated carbon fibres; b) functionalised+ Soxhlet activated carbon fibres at 298 K;

The parameters derived from the Langmuir equation are collected in Table 20. The maximum amount of copper adsorbed (n_m) is higher for functionalised+ Soxhlet ACFs in comparison to as-received ones, which is ascribed to the presence of functional groups. An increase in n_m is observed and related to the higher solution pH_{init} than the pH_{PZC} of fibres. The adsorption constant (K) values are higher for functionalised+ Soxhlet ACFs that have more functional groups, which confirms such groups' affinity for metal ion adsorption [270]. Additionally, the results show that the Langmuir adsorption constant is not strongly dependent on the pH value. Lower K may also indicate lower adsorption capability of the $Cu^{2+}_{(aq.)}$ to the particular adsorbent.

Table 20 Adsorption parameters obtained from Langmuir equation for $Cu^{2+}_{(aq.)}$ ion adsorption;

ACFs type	**pH_{init}**	**Langmuir equation**		
		n_m, mmol·g^{-1}	**K, L·mmol^{-1}**	**R^2**
As-received	unchanged (4.3)	2.00	0.036	0.941
	4.0	0.99	0.118	0.975
	1.0	0.93	0.095	0.934
Functionalised + Soxhlet	unchanged (4.3)	1.24	0.451	0.993
	4.0	1.75	0.269	0.996
	2.0	0.90	0.551	0.921
	1.0	0.88	0.251	0.919

A higher copper ion uptake was noted for functionalised+ Soxhlet ACFs vs as-received ones, which is connected with the material surface charge and presence of functional groups that enhance metal ion adsorption and accessibility to internal porosity [213]. The most optimum synthesis conditions obtained for functionalised+ Soxhlet fibres are: $[Cu]_{init}$=20 mmol and pH_{init} equal to 4.0. The amount of copper adsorbed by functionalised+ Soxhlet ACFs under given synthesis conditions were 9.3 wt.%, while for as-received ones 4.3 wt.%.

The received data reveal that higher initial concentrations of copper ions led to an increase in copper ion adsorption, as a result of more efficient utilisation of sorption sites, due to an increased driving force by a greater concentration gradient [278].

For as-received ACFs, the higher copper adsorption was observed for pH_{init}=4.3, which was the highest tested that did not cause formation of $Cu(OH)_2$ precipitation. Under the tested conditions, copper species start to precipitate and form insoluble products at pH 6.0, as indicated in Figure 22.

The measured pH_{PZC} of the analysed ACFs is equal to 5.8 and 1.5 for as-received ACFs and functionalised+ Soxhlet ACFs, respectively. Promoted adsorption was observed for activated carbon fibres that possess a lower point of zero charge and higher amounts of functional groups, which is in line with the study of Jia et al. [279]. It is indicated that surface acidic oxygen functional groups decrease the adsorption enthalpy when aqueous metal ions interact with functional groups [279]. It has also been reported that adsorption of Cu^{2+} ions from aqueous solution can be linearly dependent on the amount of functional groups. However, from these relationships the contribution of particular functional groups onto metal ions adsorption were not determined [279,280].

Additionally, it was observed that solution pH affects adsorption of metal ions. At $pH_{init} < pH_{PZC}$, the surface of carbon is positively charged, while it is negatively charged at $pH_{init} > pH_{PZC}$, thus when $pH_{init} > pH_{PZC}$, adsorption of metal cations will be favoured via the electrostatic mechanism. Adsorption of Cu^{2+} ions leads to changes in final pH of the solution, usually to its decrease, due to proton release. The pH decrease is caused by the release of hydrogen ions from the surface functional groups during the ion exchange [213,270]. For low solution initial pH (e.g. pH_{init}=1.0), no significant pH change in equilibrium state was observed. Figure 51 presents the displacement of the protons originated from the functional groups on the functionalised+ Soxhlet activated carbon fibres surface by the adsorbed copper ions. For functionalised+ Soxhlet ACFs there is a clear correlation between released hydrogen and adsorbed copper ions, however, only if $pH_{init} > pH_{PZC}$ of fibres and until certain copper initial concentration, here $[Cu]_{init}$=5 mmol. At pH_{init}=1.0 no dependency was observed, due to positive surface charge of functionalised+ Soxhlet ACF ($pH_{init} < pH_{PZC}$ of fibres). Furthermore, it is possible that at higher pH (here pH_{init}=4.0), copper ions are adsorbed to nitrogen functional groups by a coordination mechanism, as at low pH nitrogen groups might be protonated [270]. As-received ACFs exhibited no correlation, as they possess too little amounts of functional groups.

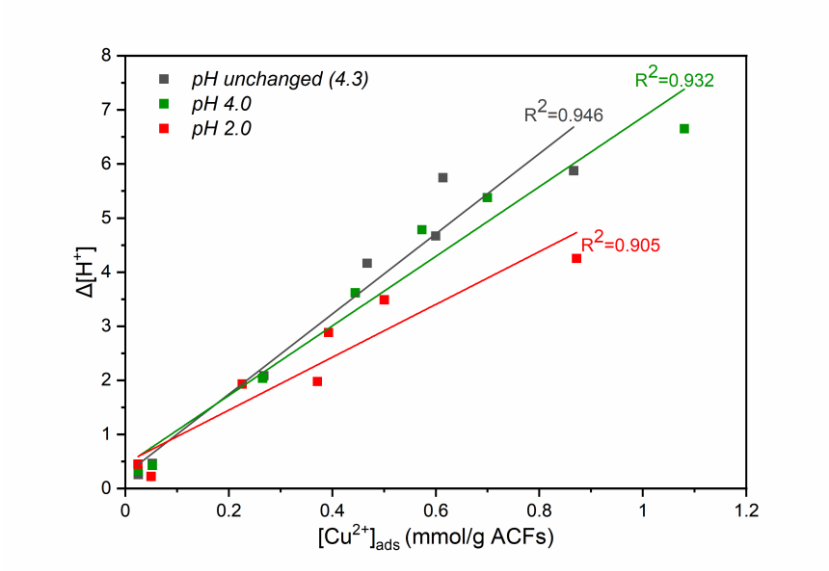

Figure 51 [H^+] displacement vs. [Cu^{2+}] adsorbed on functionalised+ Soxhlet activated carbon fibres;

Displacement of protons from functionalised+ Soxhlet ACFs surface has a linear relationship with the amount of $Cu^{2+}_{(aq.)}$ species adsorbed. This correlation is essential in understanding the adsorption mechanism. Such phenomena indicate that the sorption is attributed to chemical interactions between copper ions and carbon substrate functional groups by ion exchange with displacement of protons and coordination adsorption mechanisms. It suggests that the following surface structures might be formed during copper adsorption [213]:

$$> C - COOH + Cu^{2+} \rightarrow C - COOCu^{+} + H^{+} \quad \text{Eq. 35}$$

$$(> C - COOH)_2 + Cu^{2+} \rightarrow (> C - COO)_2 Cu + 2H^{+} \quad \text{Eq. 36}$$

$$> C - OH + Cu^{2+} \rightarrow > C = O \cdot Cu^{+} + H^{+} \quad \text{Eq. 37}$$

$$> N: + Cu^{2+} H_2O \rightarrow > N - Cu(OH)^{+} + H^{+} \quad \text{Eq. 38}$$

When adsorption is mainly controlled by electrostatic interactions, the amount of adsorbed species is dependent on their speciation in solution, adsorbent surface heterogeneity, accessibility of species to porous structures and interactions between adsorbate and adsorbent.

Copper species may differ with sizes and, in turn, accessibility to carbon structures. Species with smaller radii are able to diffuse with water into parts of the porous structure and be adsorbed. Within the considered pH range, mainly Cu^{2+} species occur, which ionic radius is equal to 0.70 Å [281], the radius of other possible species hydrated copper ion $Cu(H_2O)_6^{2+}$ is 0.62-0.94 Å [282], therefore they can easily be adsorbed into the pores of activated carbon fibres (Table 17). Such phenomena might be confirmed with the BET/ BJH method.

Continuing composite fabrication, a series of six composites was prepared: (i) two Cu-impregnated samples without thermal treatment ($CuACF_{AR}$ and $CuACF_{FUN+SOX}$); (ii) two N_2 thermal treated samples ($NCuACF_{AR}$ and $NCuACF_{FUN+SOX}$) under N_2 atmosphere at 350 °C; and (iii) two H_2/Ar treated samples at 350 °C ($HCuACF_{AR}$ and $HCuACF_{FUN+SOX}$). The selected temperatures allowed for the reduction of CuO or Cu_2O to Cu under H_2/Ar atmosphere and enhanced impregnation [283].

Figure 52 and Figure 53 present the XPS spectra of prepared functionalised+ Soxhlet and as-received ACFs-based composites: C 1s, O 1s, N 1s (Figure 52a and Figure 53a), Survey, Cu 2p and Cu LVV XANES (Figure 52b and Figure 53b). The peak areas obtained within the XPS study were converted to atomic percentage (at.%), which provides more visible trends and better understanding of the data (Table 21).

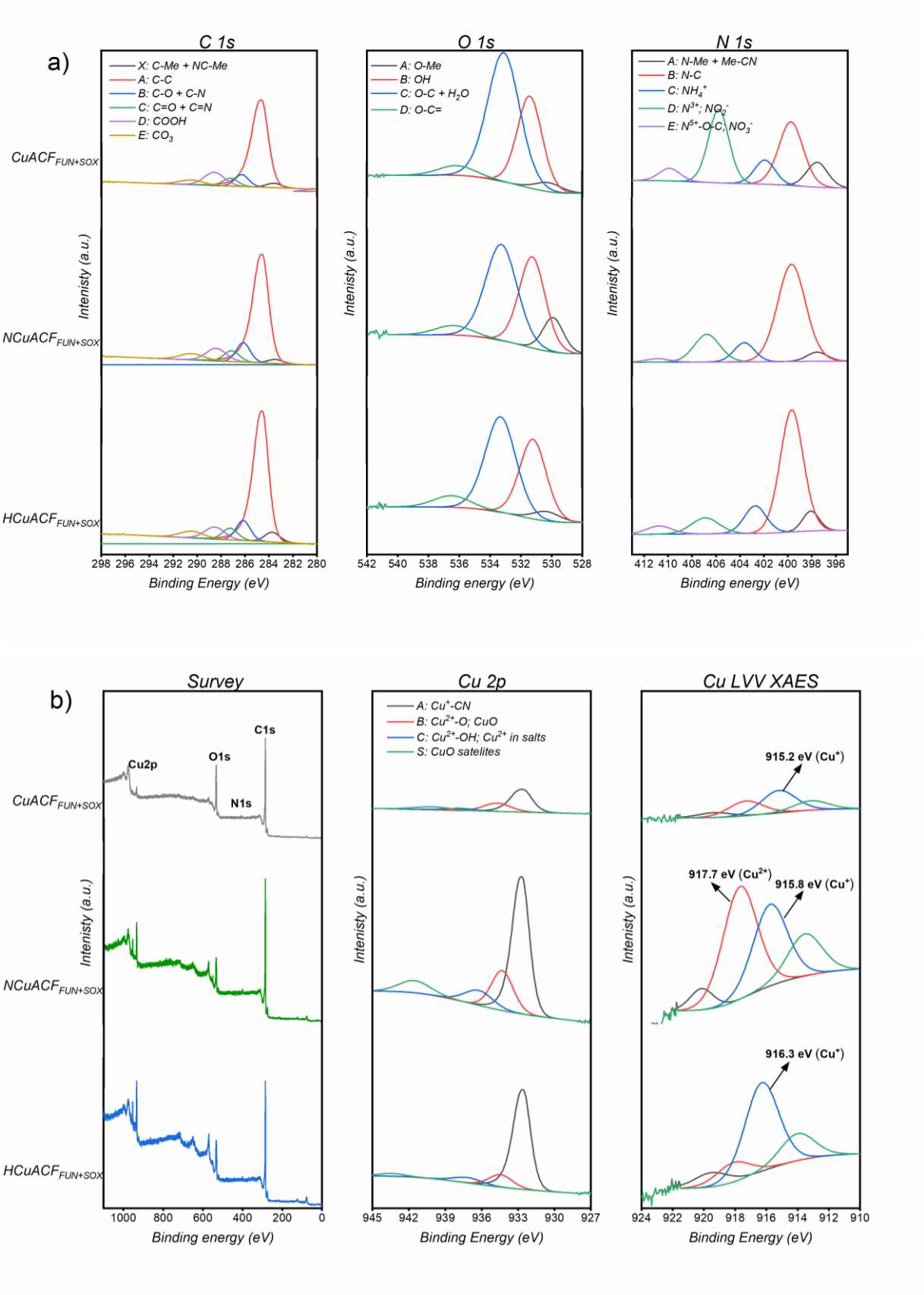

Figure 52 XPS spectra a) C 1s, O 1s, N 1s; b) Survey, Cu 2p, Cu LVV XANES of functionalised+ Soxhlet ACFs-based composites;

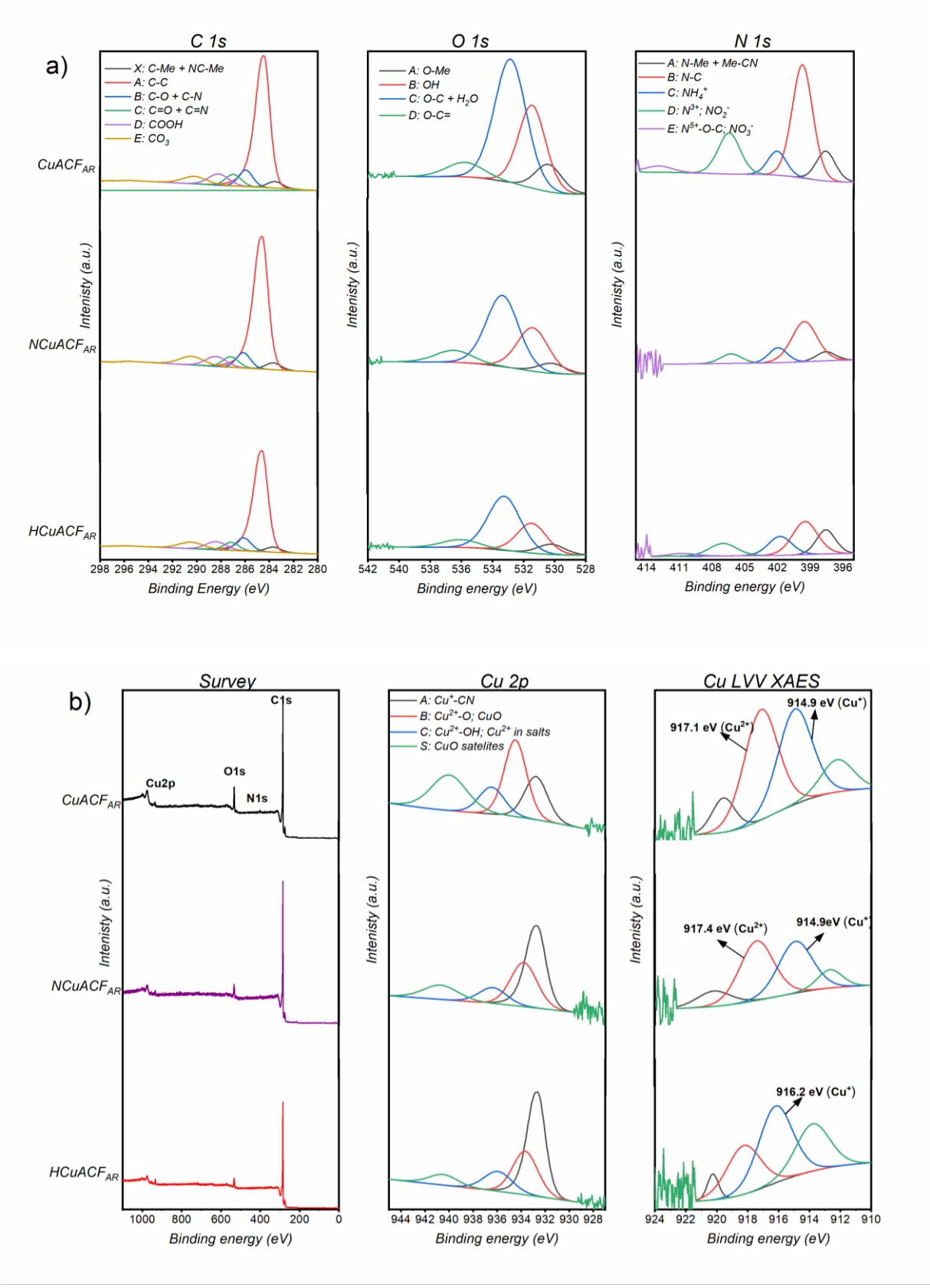

Figure 53 XPS spectra a) C 1s, O 1s, N 1s; b) Survey, Cu 2p, Cu LVV XANES of as-received ACFs-based composites;

Table 21 The XPS results, where the peak areas were converted to atomic percentage;

C 1s						
Composite type	**A: C-C**	**B: C-O + C-N**	**C: C=O + C=N**	**D: COOH**	**E: CO_3**	**X: C-Me + NC-Me**
$CuACF_{AR}$	63.33	8.18	5.19	7.00	4.65	4.25
$NCuACF_{AR}$	66.25	6.84	5.17	6.41	6.60	2.98
$HCuACF_{AR}$	65.55	8.02	4.93	6.75	6.47	3.19
$CuACF_{FUN+SOX}$	54.50	5.69	4.11	9.22	3.89	2.33
$NCuACF_{FUN+SOX}$	56.14	8.05	4.94	7.60	4.53	1.77
$HCuACF_{FUN+SOX}$	59.00	7.77	4.93	6.65	4.42	4.04

O 1s				
Composite type	**A: O-Me**	**B: OH**	**C: O-C + H_2O**	**D: O-C=**
$CuACF_{AR}$	0.74	2.29	4.00	0.54
$NCuACF_{AR}$	0.31	1.55	2.65	0.50
$HCuACF_{AR}$	0.41	1.30	2.59	0.42
$CuACF_{FUN+SOX}$	0.63	5.85	10.65	0.90
$NCuACF_{FUN+SOX}$	1.49	4.96	6.35	0.72
$HCuACF_{FUN+SOX}$	0.47	3.87	5.34	0.77

N 1s					
Composite type	**A: N-Me + Me-CN**	**B: N-C**	**C: NH_4^+**	**D: N^{3+}-O; NO_2^-**	**E: N^{5+}-O-C; NO^{3-}**
$CuACF_{AR}$	0.05	0.42	0.09	0.07	0.03
$NCuACF_{AR}$	0.01	0.16	0.02	0.04	0.00
$HCuACF_{AR}$	0.01	0.02	0.01	0.02	0.00
$CuACF_{FUN+SOX}$	0.35	0.63	0.34	0.26	0.06
$NCuACF_{FUN+SOX}$	0.11	0.68	0.18	0.13	0.00
$HCuACF_{FUN+SOX}$	0.18	0.73	0.14	0.28	0.05

Cu 2p				
Composite type	**A: Cu^+-CN**	**B: Cu^{2+}-O, CuO**	**C: Cu^{2+}-OH, Cu^{2+} in salts**	**X: Cu-C**
$CuACF_{AR}$	0.11	0.18	0.05	0.00
$NCuACF_{AR}$	0.11	0.07	0.03	0.00
$HCuACF_{AR}$	0.18	0.10	0.05	0.00
$CuACF_{FUN+SOX}$	0.41	0.18	0.05	0.00
$NCuACF_{FUN+SOX}$	1.44	0.51	0.24	0.16
$HCuACF_{FUN+SOX}$	1.04	0.17	0.09	0.08

XPS analysis indicates changes introduced through copper ion adsorption synthesis onto the surfaces of the activated carbon fibres. The study revealed that for functionalised+ Soxhlet carbon fibres, copper is bonded to oxygen and nitrogen functional groups, but preferentially to CN groups. Copper ion species are adsorbed to oxygen functional groups mainly by the ion exchange mechanism, while adsorption to nitrogen groups might involve a coordination mechanism, as suggested in [213,270].

Heat treatment of composites led to the conversion of the functional groups and changes in copper bonding. Thermal treatment causes a conversion of functional groups, e.g. COOH into C=O, C-O, as the stability of functional groups is thermally dependent. The decomposition temperature of carboxylic acid is in the range of 250-400 °C [284,285], therefore, degradation of carboxylic functional groups might occur during thermal treatment in N_2 and H_2/Ar atmosphere at 350 °C. Lactone groups decompose at 400-650 °C, while phenol ones at 350-650 °C [284,285]. Thus, during thermal treatment, re-organisation of bonding types between copper and fibres takes place.

In the case of as-received ACFs-based composites, copper is bonded to carbon functional groups, which presence is very limited, as well as to the fibres' surfaces via Van der Waals forces.

Since copper adsorbs not only to the hydroxyl or carboxylic groups, but also to nitrogen functional groups, which makes the system more complex, a detailed nitrogen group characterisation is very important for future studies. XPS describes only the surface of ACFs composites, as the thickness of the analysed layer was 3 nm. This means that, this method does not give an insight about phenomena occurring inside the pores.

All composites were analysed via the XRD technique. For as-received ACFs-based composites, as well as functionalised+ Soxhlet without thermal treatment, no copper species were detected. The reason could be that the amount of adsorbed copper was not high enough to be detected using XRD or copper was adsorbed mainly into the pores of carbon fibres or the copper species were in amorphous phase. Figure 54 presents XRD patterns of $CuACF_{FUN+SOX}$, $NCuACF_{FUN+SOX}$, $HCuACF_{FUN+SOX}$ composites, while Table 22 shows the calculated crystallite size of detected copper species.

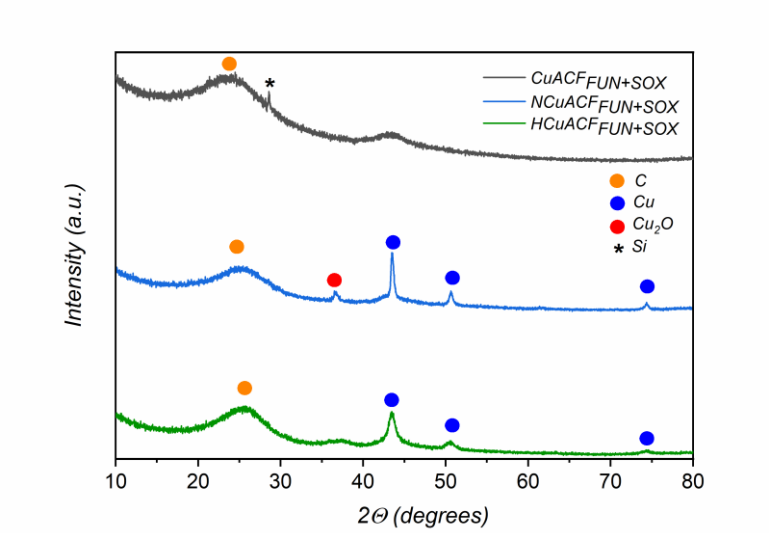

Figure 54 XRD patterns of ACFs-based composites (Si peak comes from the sample holder);

$NCuACF_{FUN+SOX}$ contains mainly Cu and low amounts of Cu_2O with crystallite size of 21.2 nm and 14.8 nm, respectively. $HCuACF_{FUN+SOX}$ reveals the presence of Cu with crystallite size of 10.5 nm.

Table 22 Crystallite size calculated based on Scherrer equation of ACFs-based composites;

ACFs composite	**Crystallite size, nm**	
	Cu	**Cu_2O**
$CuACF_{FUN+SOX}$	-	-
$NCuACF_{FUN+SOX}$	21.2	14.8
$HCuACF_{FUN+SOX}$	10.5	-

The obtained values are in accordance with results of pore volume and specific surface area measurement collected in Table 23. As-received ACFs-based composites reveal similar SSA to as-received ACFs (1677 m^2/g). Composites based on functionalised+ Soxhlet ACFs exhibit decrease in SSA in regard to their carbon substrate used for their synthesis (1652 m^2/g): 584 m^2/g, 464 m^2/g and 632 m^2/g for $CuACF_{FUN+SOX}$, $NCuACF_{FUN+SOX}$, $HCuACF_{FUN+SOX}$, respectively. This is due to the introduction of copper species via synthesis onto fibre surfaces and into the pores. Pore blockage caused a decrease in total pore volume, micropore volume and specific surface area values. The SSA values are in accordance with the amount of adsorbed copper ion, as well as the size of copper species, the lower the size of Cu or Cu_2O particles, the higher the specific surface area.

Table 23 Pore volumes and specific surface areas of ACFs-based composites;

ACFs composite	Pore volume, cm^3g^{-1}		V_{CO2}/V_{N2}	SSA, m^2g^{-1}
	V_{CO2}[a]	V_{N2}[b]		
$CuACF_{AR}$	0.157	0.460	0.342	1691
$NCuACF_{AR}$	0.169	0.455	0.370	1665
$HCuACF_{AR}$	0.173	0.464	0.372	1719
$CuACF_{FUN+SOX}$	0.067	0.160	0.420	584
$NCuACF_{FUN+SOX}$	0.088	0.130	0.680	464
$HCuACF_{FUN+SOX}$	0.077	0.181	0.425	635

a obtained from an intercept of DR plot
b obtained from Langmuir model at $p/p^0 = 1$

Figure 55 shows CO_2 (Fig 55a) and N_2 (Fig 55b) adsorption isotherms.

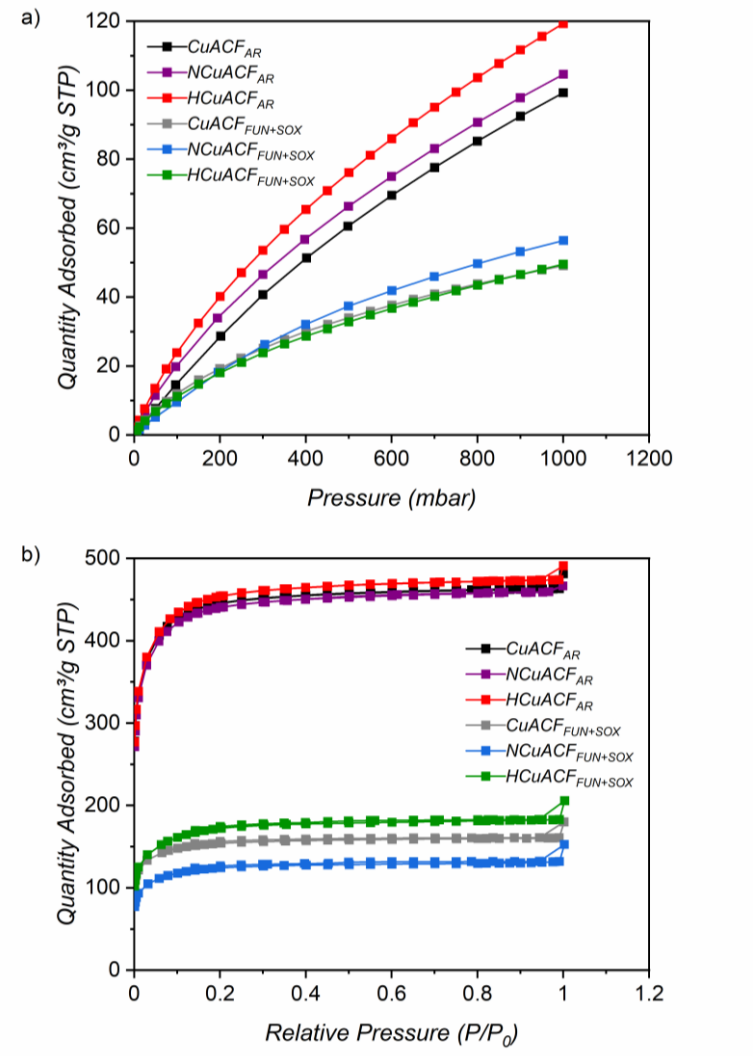

Figure 55 a) CO_2 adsorption isotherm; b) N_2 adsorption isotherm of ACFs-based composites;

For the functionalised+ Soxhlet composites, micropore volume (V_{CO2}) decreased by ~50-60 %, while total pore volume (V_{N2}) decreased by ~40 % in comparison to the characteristic of functionalised+ Soxhlet fibres. This is explained by adsorbed copper ions that caused pore blockage. These phenomena confirm that copper species were adsorbed either on ACFs surface or in the pores. The total pore volume of as-received ACFs-based composites remained at the same level in regard to respective activated carbon fibres substrate, while the micropore volume is slightly higher. The reason for that is very small loading of metal that does not affect the pores.

SEM images of the fabricated composites are depicted in Figure 56. As-received ACFs-based composites reveal a low amount and homogeneity of copper coverage onto activated carbon fibres in comparison to functionalised+ Soxhlet based materials. $CuACF_{FUN+SOX}$ composite presents random and little distribution of copper species that can be partially observed only under higher magnifications. This might also explain the lack of detection of copper species during XRD for this sample. $NCuACF_{FUN+SOX}$ exhibits dense coverage of granular-shape copper species, which size is much higher in comparison to $HCuACF_{FUN+SOX}$, which is covered by fine Cu particles, giving an impression of a more uniformly covered surface.

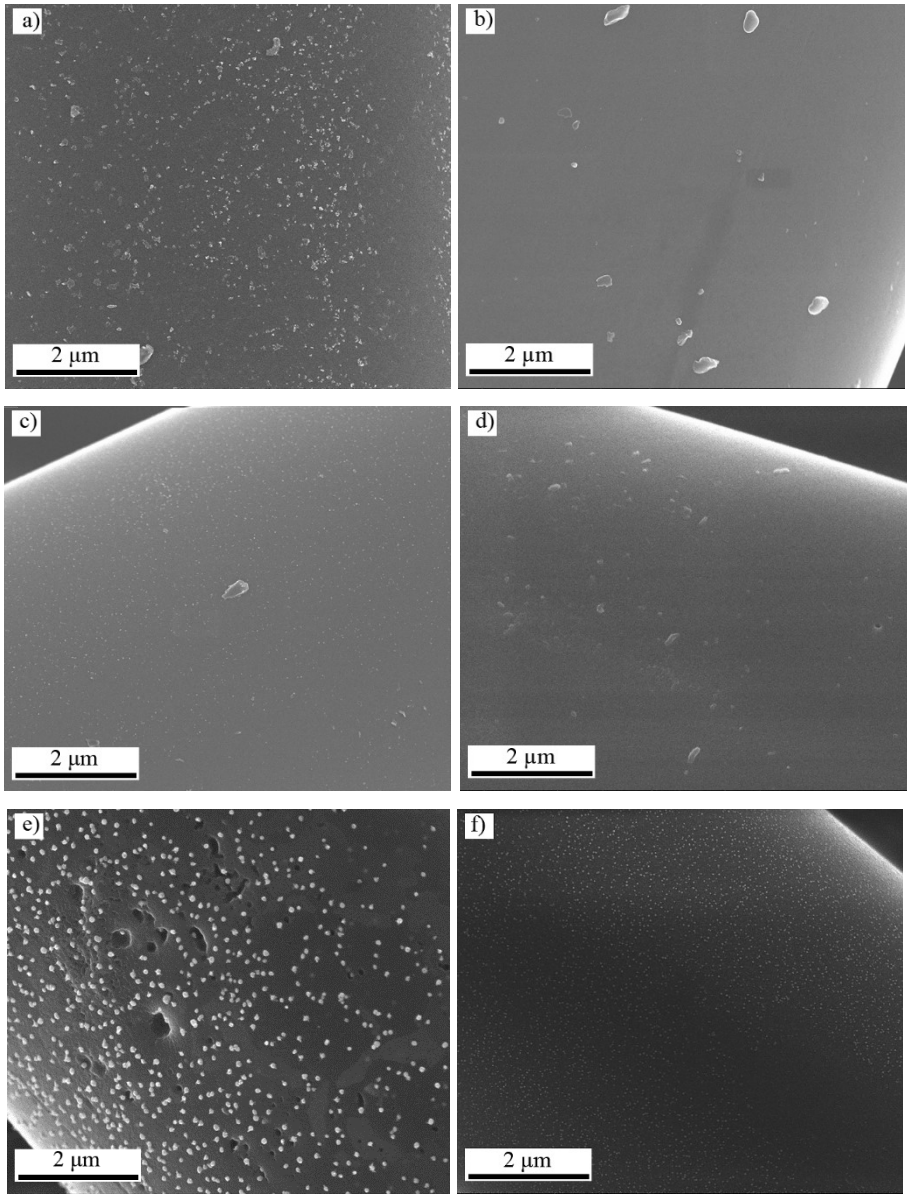

Figure 56 SEM images of ACFs-based composites a) $CuACF_{AR}$; b) $NCuACF_{AR}$; c) $HCuACF_{AR}$; d) $CuACF_{FUN+SOX}$; e) $NCuACF_{FUN+SOX}$; f) $HCuACF_{FUN+SOX}$;

$CuACF_{FUN+SOX}$, $NCuACF_{FUN+SOX}$ and $HCuACF_{FUN+SOX}$ composites were selected for study of MS2 removal due to the highest amount of copper adsorbed and observed differences in morphology. Therefore, their point of zero charge was measured. Such parameter is helpful in explanation of mechanism driven virus removal. The obtained values are presented in Figure 57.

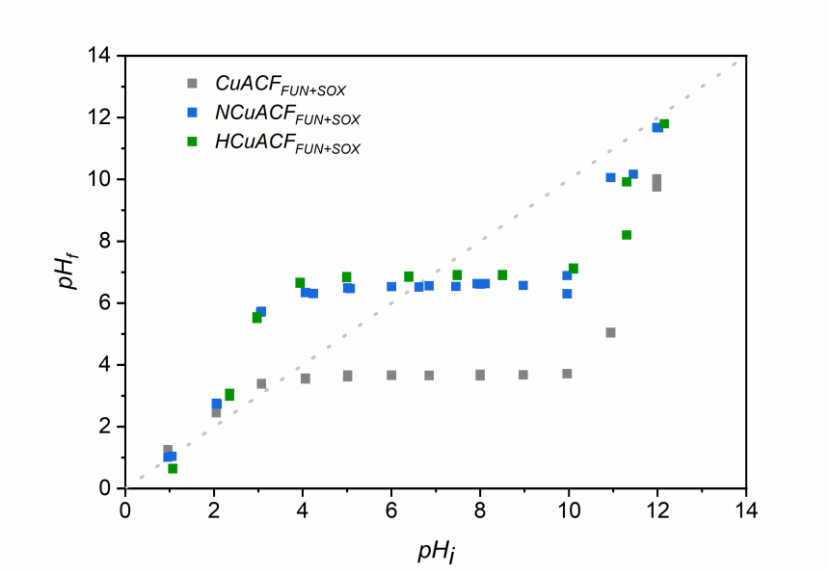

Figure 57 Graph of final pH vs. initial pH of ACFs-based composites;

The pH_{PZC} of $CuACF_{FUN+SOX}$, $NCuACF_{FUN+SOX}$ and $HCuACF_{FUN+SOX}$ is equal to 3.4, 6.5 and 6.9, respectively. The pH_{PZC} of functionalised+ Soxhlet ACFs (1.5) was shifted towards higher values due to the incorporation of copper species during the synthesis step. The thermal treatment procedure also had an impact, as pH_{PZC} of thermally treated composites is higher. This is linked with the decomposition of functional groups during thermal treatment and different bonds forming between fibres and adsorbed copper species.

12.3. Conclusions of composites synthesis

The composites based on multi-walled carbon nanotubes were prepared with following synthesis routes: adsorption of aqueous copper ion, adsorption of copper(II) hydroxide and adsorption of copper complex. All synthesis procedures resulted in three materials characterised by uniformly distributed nanosized Cu_2O particles on the MWCNTs surface. Main differences between obtained materials were the amount of adsorbed copper species and associated with that specific surface area.

Preparation of ACFs-based composites was done with one synthesis, adsorption of aqueous copper ion. The procedure was studied in details to obtain maximum copper uptake on the activated carbon fibres, as adsorption is dependent on many factors, i.e. metal ions concentration, solution pH, contact time, adsorbent surface functionality. Taking into the account above mentioned, $ACF_{FUN+SOX}$ were the most efficient in synthesis, adsorbing 9.3 wt% of copper from

aqueous solution. Study revealed that adsorption is attributed to the chemical interactions between copper ions and carbon substrate oxygen functional groups by the ion exchange with displacement of protons, and the coordination adsorption mechanism to nitrogen functional groups. As a result, copper species were adsorbed to the surface and into the pores of ACFs, leading to decrease in total pore volume, micropore volume and specific surface area. Additionally, the composites point of zero charge increased, while thermal treatment shifted it even slightly further. The composites thermal treatment also affected the morphology of copper, as well as the type and strength of bonding between metal and carbon fibres.

13. Conditioning and MS2 bacteriophage removal efficiency studies

13.1. Conditioning and stability test of Multi-walled Carbon Nanotubes-based composites

The aim of the study was to evaluate potential release/ dissolution of copper species into the permeate to determine the stability of the composites and understand the long-term viability of materials. The filter material was rinsed for 24 h with 0.01 M NaCl at pH 5.0 and pH 7.0, while the copper concentration was monitored in regularly collected permeate samples using ICP-MS.

The results of filter material conditioning are presented in Figure 58. Figure 58a shows a dynamic change of copper concentration in the permeate as a function of the filtered volume for the three composites at pH 5.0. The concentration of Cu dissolved in the permeate for *composite 1* and *3* gradually declines from initial value of 200-400 µg/L to less than 35 µg/L after filtration of 6 L of fluid, as shown in Figure 58a. This tendency is also noticeable in the cumulative copper mass graph (Fig. 58c), presenting permeate mass stabilisation at around 1000 and 800 µg for *composite 1* and *3*, respectively. In comparison, copper release in *composite 2* does not decrease until the end of rinsing, as shown in Figure 58a. This trend is also visible in Figure 58c, which is nearly double the value observed for *composite 1* and *3*. The high Cu release may be attributable to the mass of copper(I) oxide nanoparticles, which is the highest in *composite 2* in comparison to the others (Table 19 and Figure 47). Moreover, for *composite 2* the interaction between Cu_2O-NPs and carbon nanotubes are expected to be weaker than for other composites, increasing the probability of oxide dissolution. Nonetheless, the copper concentration detected in the permeate for all composites was lower than the limit value for drinking

water (<2 mg/L) guided by the WHO [191], making these materials viable for drinking water production applications.

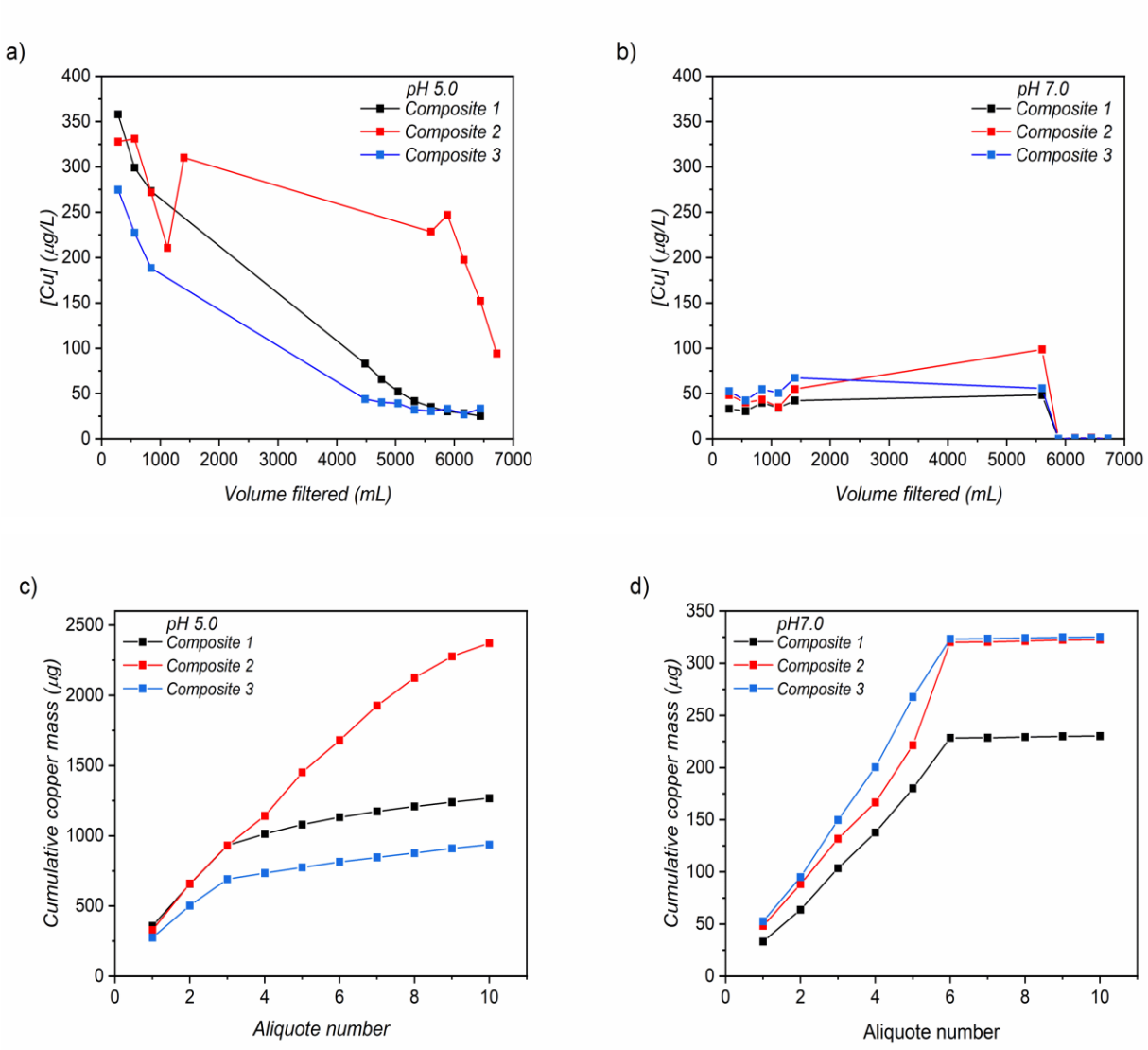

Figure 58 Stability test results at pH 5.0 (a and c) and pH 7.0 (b and d) of the MWCNTs-based composites*;

*The presented data come from duplicate measurements, statistics and standard error cannot be presented. The results of the first tests are comparable to the effects of the second round tests.

Further studies revealed the stability of the filter material being affected by pH with a clear increase in copper dissolution at pH 5.0 in comparison to pH 7.0. This is associated with higher solubility of Cu_2O at acidic pH in regard to neutral [186,199]. As depicted in Figure 58b, Cu concentration in the permeate of the three composites was nearly 7 times lower for the first millilitres of water passed at pH 7.0 relative to the first flush at pH 5.0. The copper detected in the permeate, in the first flush, is expected to be Cu_2O-NPs, although it is not possible to exclude the presence of dissolved copper. ICP-MS protocol applied in this study cannot differentiate

between copper forms in the permeate, so further tests would be required. However, it is possible to apply single-particle ICP-MS, which differentiates between dissolved metal ions and nanoparticles or centrifugation at high speed to divide the permeate fraction [286]. At pH 7.0, the copper dissolution dynamic for three composites was also filtered water-volume dependent. The concentration increased during the first litres, reaching a plateau after 24 h (approximately 6 L passed). Filter conditioning prior to application may therefore rinse out excess/ or non-bonded Cu_2O nanoparticles, stabilising the material. The copper release trend and reached maximum values were similar for *composite 2* and *3*, reaching a plateau of 325 µg after filtering approx. 6 L of water through the filters (Fig 58d). In comparison, the cumulative copper mass loss for *composite 1* was 225 µg. Having in mind that Cu dissolution is higher at pH 5.0, one possible explanation of this behaviour difference is disparity in interactions between Cu_2O and MWCNTs. They are weaker in the case of synthesis route 2 and 3 relative to route 1. Correlating this elucidation with the proposed syntheses mechanisms (Figure 47), for *composite 1* the direct adsorption of copper ions on the MWNCT surface (route 1) could lead to stronger interactions between the obtained Cu_2O-NPs and MWCNTs, as copper(I) oxide nanoparticles nucleate directly on carbon surfaces. Concerning route 2, Cu_2O-NPs were produced in excess in relation to MWCNTs, leading to the remove of excess and non-bonded metal oxide nanoparticles. Furthermore, the interactions are anticipated to be weaker than for *composite 1*, enhancing the release possibility of Cu_2O-NPs for *composite 2* into the permeate. In the case of route 3, the complex ions are bonded via amide group, which might decompose during the thermal treatment, decreasing the interaction between Cu_2O-NPs and MWCNTs and facilitating NP detachment. This might clarify the higher stability of *composite 1* in comparison to *composite 2* and *composite 3*. It should be noted that the detected copper concentrations are 100 times below the copper limit in drinking water recommended by the WHO.

13.2. Conditioning and stability test of Activated Carbon Fibres-based composites

The stability of the obtained composites was monitored during cartridge conditioning for 24 h at pH 5.0 and pH 7.0 with 0.01 M NaCl. It allowed evaluating the copper bonding strength and its potential release from composites, which is crucial for the assessment of material stability and cartridge long-term efficiency.

Figure 59 shows results of 24 h stability tests performed at pH 5.0 (Fig. 59a) and pH 7.0 (Fig. 59b). The presented values depict the cumulative mass of desorbed copper in the total collected permeate volume. It can be observed, that the amount of released copper gradually decreased and stabilised only for composites that were not thermally treated. Thermally treated composites exhibited not only higher levels of released copper but also the amount of dissolved copper was constantly increasing. This could be explained by the weaker bonding strength between copper and carbon fibres in thermally treated samples. The study revealed that the stability of composites is affected by the pH of the used media for composite rinsing. A higher copper release was observed at pH 5.0 in regard to pH 7.0, which is linked to the enhanced copper solubility under acidic pH conditions [187].

ACFs composites testing at pH 5.0

Figure 59a shows the dynamic release of copper as a function of filtered volume of all six tested composites at pH 5.0. The stability curves of $CuACF_{AR}$ and $CuACF_{FUN+SOX}$ composites reach a plateau after passing ~3000 mL of solution and exhibited a total copper release of 584 µg and 628 µg, respectively, which represents 2 and 5 wt.% of total copper content. The $CuACF_{FUN+SOX}$ composite within the first 450 mL of water passing released almost 60 % of total lost copper amount. This phenomenon can indicate that weakly bonded copper particles are released first and then those that dissolve due to acidic pH.

$NCuACF_{AR}$, $HCuACF_{AR}$, $NCuACF_{FUN+SOX}$ and $HCuACF_{FUN+SOX}$ followed similar trend of copper release, which was progressively increasing with each water volume passed through the cartridges. This can indicate that either the copper species were not properly or weakly bonded to ACFs and/or the stabilisation test was performed not long enough to reach a plateau. It leads to the conclusion that further or even constant copper dissolution might be expected. The highest amount of dissolved copper was observed for $NCuACF_{FUN+SOX}$ and $HCuACF_{FUN+SOX}$ composites, equal to 2292 µg (8 wt.%) and 2088 µg (7 wt.%), respectively. For $NCuACF_{AR}$ and $HCuACF_{AR}$ losses of 1385 µg (11 wt.%) and 1167 µg (13 wt.%), respectively, was noted. For ACF_{AR}-based composites, copper probably adsorbed to fibres' surfaces via Van der Waals forces, as ACF_{AR} do not have functional groups, which could more strongly bond copper species.

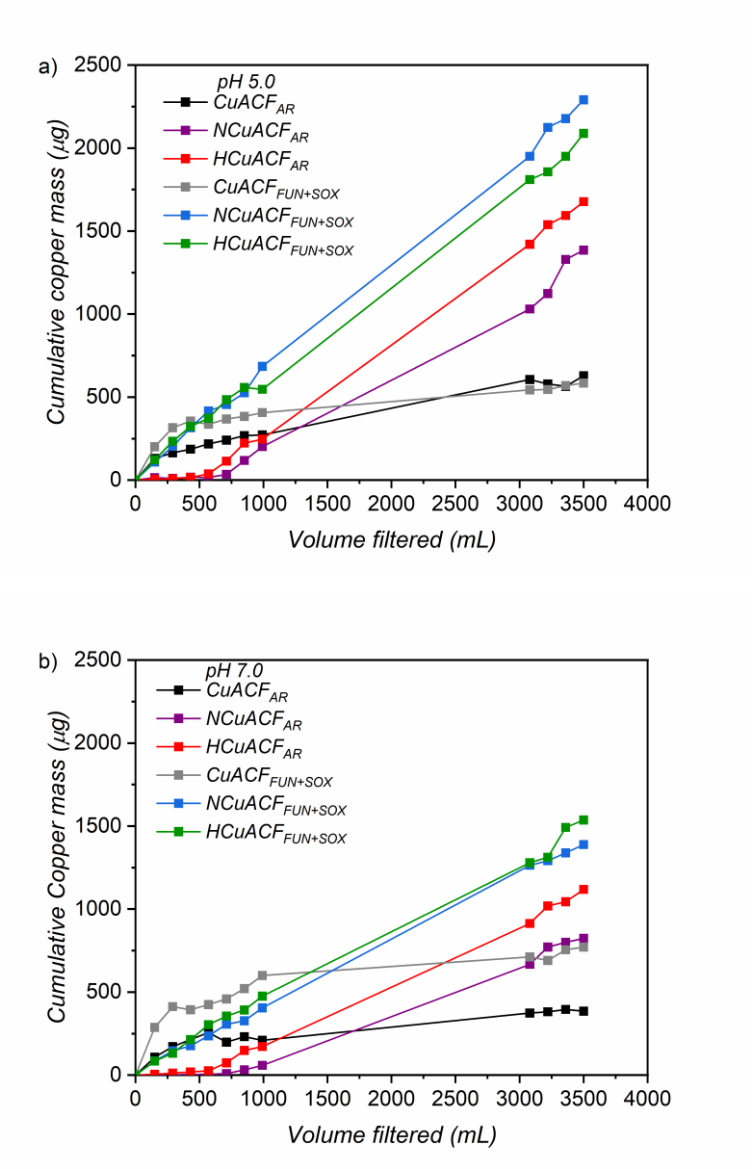

Figure 59 Stability test results at a) pH 5.0 and b) pH 7.0 of the ACFs-based composites*;
*The presented data come from duplicate measurements, statistics and standard error cannot be presented. The results of the first tests are comparable to the effects of the second round tests.

ACFs composites testing at pH 7.0

Figure 59b presents the results of material conditioning at pH 7.0. An overall decrease of copper release was observed in comparison to the study performed at pH 5.0. All of tested composites except CuACF$_{FUN+SOX}$ exhibited ~30-40 % less copper flushed out at pH 7.0 in regard to the pH 5.0. Although, for CuACF$_{FUN+SOX}$ at pH 7.0 was observed an increase of released copper of approximately 30 % concerning pH 5.0, the mass of copper released was equal to 771 µg, which makes up 3 wt.% of total copper content in the composite. CuACF$_{AR}$ desorbed 385 µg (3 wt.%) of copper. This result was according to expectations, because as-received fibres have much less functional groups that can strongly bond copper during adsorption. It might be possible that

some copper ions were weakly attached to fibres surface, and then easily released even under more favoured conditions of pH 7.0.

In the case of pH 7.0, thermally treated composites also revealed almost two times higher release of copper in regard to non-thermally treated composites. The $NCuACF_{FUN+SOX}$ and $HCuACF_{FUN+SOX}$ composites reached Cu release of 1389 µg (5 wt.%) and 1536 µg (6 wt.%), respectively, while $NCuACF_{AR}$ and $HCuACF_{AR}$ 823 µg (6 wt.%) and 118 µg (9 wt.%), respectively. The amount of released copper was constantly increasing and did not stabilise over time. This is another proof of the instability of thermally-treated composites, where the thermal process destroyed the bonds formed during adsorption between copper and the functional groups. Despite the fact that all composites exhibited copper release values within the limit guided by WHO for drinking water (<2 mg/L) [191], they are not suitable for water purification. The considered composites are not stable, as they are constantly releasing copper, which limits their lifetime and may have adverse health and environmental effects.

13.3. MS2 bacteriophage removal of Multi-walled Carbon Nanotubes and their composites

MS2 bacteriophages removal measurements were conducted twice, first prior to (day 1) and then after (day 2) filter material conditioning with 0.01 M NaCl at pH 5.0 and 7.0 for 24 h. The MS2 concentration was quantified directly after the permeate collection (t=0 h) and again after the permeate storage for 2 h (t=2 h) at room temperature. Additionally, the permeates were analysed in terms of copper concentration via ICP-MS. This approach was established to examine the effect of the virus progressive inactivation in permeate within time, that might be potentially caused/ enhanced by the presence of dissolved copper (colloidal copper /copper oxide particles) [287].

As-received MWCNTs

To determine the enhancement of virus removal due to MWCNT modification with Cu_2O in comparison with as-received MWCNTs, the MS2 bacteriophage solution was first filtered through an as-received MWCNT filter. The obtained $\log_{10}$ removal value was 0.1 and remained unaffected after 2 h at both pHs. This result was much lower than expected, assumed based on the results published in scientific papers, e.g. Brady-Estévez et al. obtained up to 8 LRV using MWCNTs filters, depending on the experiment conditions [129]. The discrepancies of virus removal values obtained in this work to other studies can be attributable to a number of different factors: (i) use of different types of MWCNTs, (ii) different filtration conditions (amount of

material, flux, pressure, water composition, virus-CNTs contact time) and/or (iii) different way of filter preparation. Commercially available multi-walled carbon nanotubes vary greatly not only between manufacturers, but also within production batches. MWCNTs differ with physical properties e.g. length, thickness, aspect-ratio, chemical composition, purity level, contamination content and homogeneity [288,289]. These differences lead to inequalities in material virucidal performance.

In another work, performed within MultiCarboVir project, we studied the competitive co-adsorption of MS2 bacteriophage and natural organic matter (NOM) onto as-received multiwalled carbon nanotubes, using batch equilibrium experiments. It gives an outlook into the applicability of MWCNT filters for virus removal in water containing natural organic matter as co-solute to MS2 bacteriophages [73]. Batch studies (3 h of equilibration time, constant solution stirring) of 15 mg of as-received MWNCTs (the same amount as used for flow-experiment) in water (without other components) revealed 4 LRV at both tested pHs (5.2 and 7.7). This value is high in comparison to values obtained in the flow-filtration test, suggesting the importance and influence of contact time between the filter and viruses on their inactivation.

This large difference in LRV highlights two important points: (i) not each type of pristine MWCNT may be a relevant adsorbent for pollutants, and (ii) MS2 bacteriophage removal in the presented study is not expected to be a consequence of the MWCNTs alone, but rather of the attached copper(I) oxide nanoparticles or dissolved copper. Nevertheless, despite the fact that in this work the virucidal properties of MWCNTs were weak, it did not hinder the study aim. Consequently, the main role of MWCNTs was to act as a network/ structure to support copper(I) oxide nanoparticles, the primary virucide. The MWCNTs' high surface area and sorption capacity are beneficial due to potential for high adsorption of copper species. Potential virucidal properties of MWCNTs are an obvious advantage, even thought, the observed low inactivation rates did not negatively affect our main research question, and even helped to understand more clearly the influence of Cu_2O-NPs.

MWCNTs-based composites

Tests performed at pH 5.0

Figure 60a presents the results of virus removal for three composites, as well as the copper concentrations measured in the permeate after MS2 filtration at pH 5.0. The subset of test conducted on day 1 at t=0 h theoretically indicate MS2 removal due to electrostatic adsorption of bacteriophages onto positively charged material surface containing Cu_2O [35–38]. The filter material is positively charged, because Cu_2O-NPs were incorporated onto MWCNT surfaces

during the synthesis procedure. Copper(I) oxide ensures a positive surface charge within the verified pH range (5.0, 7.0) [290], leading to the conclusion that the point of zero charge of the composite is also positive. The isoelectric point of MS2 is equal to 4, indicating that electrostatic adsorption is possible under the studied conditions. The obtained LRVs were equal to 2.6, 6.1, 2.3 for the *composites 1*, *2* and *3*, respectively, suggesting surface adsorption of MS2. Those values were significantly higher than the removal noted for as-received MWNCTs–based filters, proving that the modification with Cu_2O-NPs increased the virucidal performance of MWCNTs. However, in the tests performed at t=2 h, the $\log_{10}$ removal increased to 5.0 LRV, >7.0 LRV and 5.0 LRV for *composites 1*, *2* and *3*, respectively. This denotes several potential mechanisms of virus removal/ inactivation: removal at the filter surface (e.g. by electrostatic adsorption), and continued virus inactivation in the permeate (due to presence of released Cu or Cu_2O-NPs) [38,291]. Armstrong et al. have noted an additional MS2 bacteriophage removal of 1.8 LRV in permeate stored for 6 hours containing copper concentration 7-10 times lower than in this work [196]. The increase LRV during the time of permeate storage emphasises the necessity for a time control to distinguish LRV attributable to removal by the filter from removal/inactivation due to virucidal properties of metals in the permeate. Permeate storage prior to evaluation of virus concentration may lead to overestimates of filter performance.

The virus removal test was performed once more on day 2, after filter conditioning. The influence of copper dissolution on virus removal was observed again. After the filter conditioning step, *composite 2* still exhibits a LRV higher than 4 and an associated copper concentration in the permeate equals to 2.23 mg/L. This is in line with the copper dissolution results that revealed continuous copper release from *composite 2* after 24 h of filter rinsing. However, two conclusions can be formed for *composite 1* and *3*. At day 2, t=0 h, both composites exhibited lower MS2 removal and lower Cu concentrations in the permeate in comparison to day 1, t=0 h. This might be explained by two possible mechanisms: (i) the conditioning process washed out the Cu_2O-NPs from the filter surfaces, lowering the adsorption capacity of *composites 1* and *3* and/or (ii) at least part of the virus removal is caused by the direct effect of dissolved copper even at t=0 h. *Composites 2* and *3* showed almost unchanged MS2 removal after two hours storage, 6.8 to 6.8 and 0.8 to 1.0 LRV, respectively, while the LRV of *composite 1* increased from 1.0 to 5.0, despite low copper concentration in the permeate (0.001 mg/L). This might imply that other factors, apart from copper presence in the permeate, result in increased virus inactivation. Amongst these factors, difference in copper(I) oxide nanoparticles properties due to various synthesis routes might also play a role in virus inactivation [292].

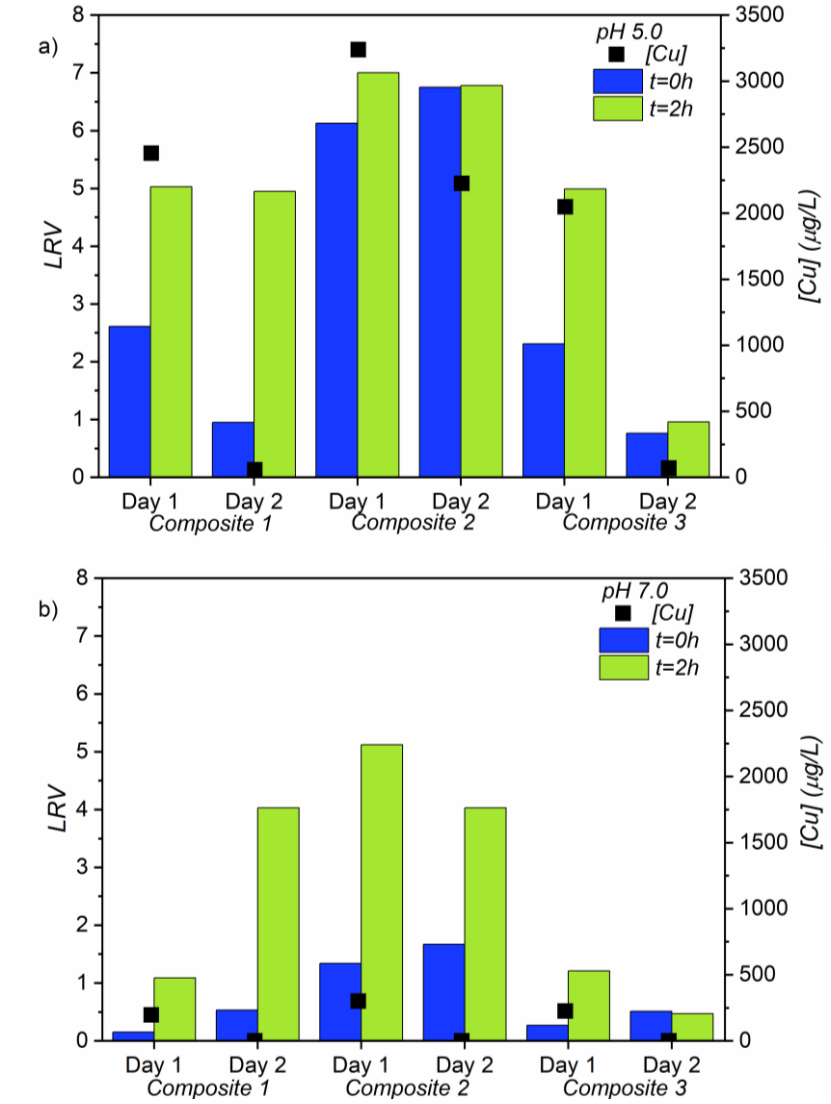

Figure 60 MS2 removal test results for *composite 1*, *composite 2* and *composite 3* at a) pH 5.0 and b) pH 7.0, and the associated copper concentrations detected in the permeate*;

*The presented data come from duplicate measurements, statistics and standard error cannot be presented. The results of the first tests are comparable to the effects of the second round tests.

Tests performed at pH 7.0

Figure 60b shows the outcomes from experiment performed at pH 7.0. Interestingly, at day 1 t=0 h, MS2 removal was in the range of 0.2-1.3 LRV for the three composites. Such low LRVs are similar to the results observed for as-received MWCNTs and considerably lower than the values noted at pH 5.0. The apparent virus removal mechanism by electrostatic adsorption was therefore low for all composites. This is also in line with the results from Figure 60a, showing a lower removal at t=0 h when Cu concentration in the permeate was lower. MS2 removal at t=0 h is mainly explained by the immediate effect of dissolved copper that led to bacteriophage inactivation, while the removal by adsorption onto the filter surface is limited.

Experiments at pH 7.0 reveal once again that virus removal tests for filters should take under consideration additional virus inactivation in the permeate. At pH 7.0, $\log_{10}$ removal increased for day 1 t=2 h in comparison to t= 0 h. This was surprising given that the permeate copper concentrations were low. Indeed, the removal of MS2 increased by 0.9, 3.8 and 0.9 LRV for com*posites 1*, *2* and *3*, respectively, while the associated Cu concentrations were equal to 0.196, 0.301 and 0.225 mg/L. Low Cu concentrations in the permeate are related to lower MS2 removal at t=2 h for *composite 1*. Moreover, for *composite 1* and *composite 2* at day 2 t=2 h an increase by 3.5 and 2.3 was observed, despite a copper concentration of 1 µg/L in the permeate. Notably, the Cu concentration in the permeate was not predictive of LRV values, therefore time-controlled virus removal tests should be performed to attest filter efficacy. The continued virus inactivation in the permeate implies that copper may be virucidal in low concentrations. Although a previously published work has suggested copper virucidal activity at concentrations of 300 µg/L [197], here virucidal effects were observed at even lower values. The Cu_2O-NPs interactions with MWCNTs and/or their physicochemical properties may affect the inactivation of viruses. For example, *composite 2* has a higher ratio of Cu_2O-NPs/ MWCNTs that facilitates/ increases the likelihood of oxide dissolution (in addition to the dissolution effect). There was observed not only the immediate (t=0 h) MS2 inactivation caused by copper presence, but also a LRV increase after 2 h due to above mentioned copper(I) oxide nanoparticles dissolution.

Overall, the obtained results suggest that the developed MWCNTs-based composites are not sufficient to provide safe drinking water through filtration (physical removal and/or adsorption processes) alone, as the method does not achieve adequate LRV. However, the composites ensure a mechanism for virus removal through the combined method of filtration and post-filtration virus inactivation. Therefore, the developed filters may be sufficient for application in combined treatment of filtration and post-filtration storage due to continued/ increased virus inactivation in the permeate over time, where water is stored prior to use. This is possible only under the condition that MWCNTs will stay on the filter and will not be released into the permeate. This is a crucial requirement as within the study performed by the project partner- Eawag, a risk of MWNCTs leakage was recognised. Presence of MWCNTs in drinking water might bring about serious health implications.

Importantly, the findings and proposed experimental procedure presented here clearly emphasise the necessity to establish a proper procedure for: (i) filter material conditioning (for material stabilisation), (ii) proper evaluation of virus removal capacity that takes into account continued virus inactivation in the permeate, and (iii) assessment of the potential metal dissolution and CNT liberation impact before using the filter materials in real applications.

13.4. MS2 bacteriophage removal of Activated Carbon Fibres and their composites

The study of MS2 bacteriophages removal efficiency were conducted after carbon substrate or composite conditioning with 0.01 M NaCl at pH 5.0 and 7.0 for 24 h. The MS2 concentration in the permeate was quantified directly after its collection (t=0 h) and again after permeate storage for 2 h (t=2 h) at room temperature. The collected permeate was analysed for copper concentration using the ICP-MS technique.

As-received ACFs and functionalised+ Soxhlet ACFs

For better understanding, both as-received and functionalised+ Soxhlet activated carbon fibres were evaluated for MS2 bacteriophage removal efficiency. Figure 61 shows the results of the MS2 removal study at pH 5.5 and 7.3. The obtained LRV for as-received ACFs at pH 5.5 was equal 2.7, while at pH 7.3, 1.7 LRV. The LRV values noted at t=0 h remained almost unchanged in comparison to the values obtained after 2 h of storage (t=2 h): 2.8 LRV and 1.7 LRV at pH 5.5 and 7.3, respectively. The detected copper concentration in the permeate was low: 1.2 µg/L at pH 5.5 and 2.0 µg/L at pH 7.3, which did not result in additional MS2 inactivation over time. Functionalised+ Soxhlet ACFs revealed slightly better antiviral properties. giving 3.3 LRV at pH 5.5 and 2.1 LRV at pH 7.3, which were 10 % higher after 2 h of permeate storage – 3.6 LRV at pH 5.5 and 2.4 LRV at pH 7.3. The measured Cu concentration in the permeate was also very low, being – 0.05 and 0.03 µg/L at pH 5.5 and 7.3, respectively. Higher virus removal at lower pH might be justified by MS2 tendency to agglomerate at more acidic pH [82].

Obtained results are below the target values recommended for technologies by both WHO and USEPA [74–76]. Notwithstanding, it is worth to underline that quite a low amount of material (300 mg) was used in this study, therefore at larger quantities higher performance is assumed, but still requires proving. The obtained LRV values from both as-received and functionalised+ Soxhlet activated carbon fibres are much higher than those showed by activated carbon in granular or powder form [40–42], confirming better material adsorption rate of viruses and, in turn, greater potential for water treatment application [154].

$ACF_{FUN+SOX}$ exhibited a 20 % higher $\log_{10}$ removal value at both pH than ACF_{AR}, which might suggest that the functionalisation process and introduced material changes (porosity opening, presence of functional groups) are profitable for viruses adsorption.

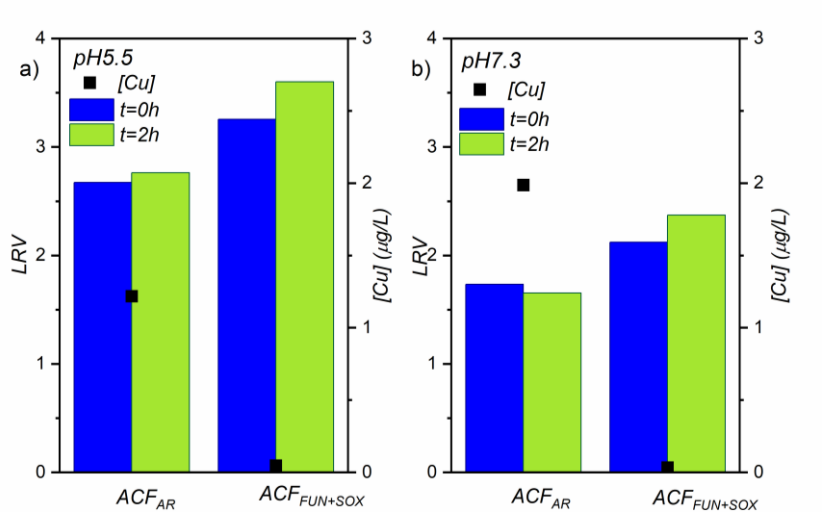

Figure 61 MS2 removal test results of as-received activated carbon fibres and functionalised+ Soxhlet activated carbon fibres at a) pH 5.5 and b) pH 7.3, and the associated copper concentrations detected in the permeate*;

*The presented data come from duplicate measurements, statistics and standard error cannot be presented. The results of the first tests are comparable to the effects of the second round tests.

Overall, the virus - adsorbent interactions are governed by electrostatic adsorption, Van der Waals forces as well as hydrogen bonding, hydrophobic and steric repulsions [71,221]. The hydrophobic effect contribution is expected to increase with decreasing polarity of the virus and adsorbent surfaces [71]. Furthermore, favourable contributions may arise when hydrogen bonds between donating and accepting moieties on the virus and adsorbent surfaces are formed. At the same time, hydrogen bonds are likely inhibited in aqueous systems, as water molecules are assumed to occupy a big portion of the H-bonding sites. Those interactions are dependent on the point of zero charge, the hydrophobic/ hydrophilic nature of virus and adsorbent, environmental physical (flow velocity, viscosity of fluid), chemical conditions (pH, ionic strength of solution, and presence of organic matter) and adsorbent surface topography.

We claim that depending on the considered material, particular forces have a more significant contribution in virus removal than others. Contribution of the following forces can be recognised in discussed cases: adsorption governed by Van der Waals forces, electrostatic forces, and hydrophobic repulsions. Adsorption by Van der Waals forces are influenced by fibres high specific surface area, as well as a high Hamaker constant [30,71]. Well-developed porous structure might also be profitable, however, in the considered case the pores diameter of ACFs is too small and the pores are not capable of retaining viruses (Table 17). The observed higher MS2 adsorption to ACF_{AR} at pH 5.5 in regard to pH 7.3 is in accordance with electrostatic adsorption [293]. At pH 5.5, an electrostatic interactions took place, as the point of zero charge of ACF_{AR}

is 5.8, while for MS2 is equal to 3.9, therefore the surfaces are oppositely charged, and dependent on the ionic strength within the aqueous medium double layer repulsion may occur. At pH 7.3, both as-received fibres and bacteriophages surfaces are negatively charged, hence electrostatic adsorption is assumed not to be dominant for retention. The same situation occurs at both tested pH conditions for $ACF_{FUN+SOX}$, the pH_{PZC} of which is 1.5, thus the surfaces possess negative charge. It can be deduced that electrostatic interactions are not the primary, predominant forces responsible for virus removal during filtration. Another force that has to be considered is the hydrophobic effect. Here the hydrophobic character of either MS2 or activated carbon fibres might be profitable for enhanced adsorption of bacteriophages [18,47,293]. This could be taken into consideration for ACF_{AR}, which possess low amounts of functional groups (0.46 mmol/g ACF) that should not affect the hydrophobicity. In the case of $ACF_{FUN+SOX}$, they have a high amount of functional groups (3.31 mmol/g ACF) that may change their character to hydrophilic. Carboxylic groups form intermolecular hydrogen bonding between the ends of functional groups when they are protonated, resulting in the decrease in hydrophilicity with decreasing pH [294,295]. Lim et al. discuss in this work the interactions between M13 bacteriophage and different functional groups [295]. Lim described that M13 bacteriophages have fewer chances to create hydrogen bonds with carboxylic groups in a short time unlike hydroxyl groups at lower pH [295]. It indicates that the presence and role of functional groups in virus interactions matter.

It can be assumed that MS2 bacteriophages were adsorbed on ACF surfaces, rather than being inactivated, because carbon itself is not recognised to possess antiviral characteristic and to interact with virus capsid, e.g. carbon is known as a bioinert material applied in implants [296]. The presented study did not reveal the strength of MS2 adsorption meaning reversibility of adsorption and desorption of MS2 into permeate might happen during further cartridge flushing. Potential desorption could be influenced by water pH change and presence of adsorbing ions, i.e. humic acids, phosphates, therefore this aspect requires further consideration if the ACFs are to be used for water treatment applications [293,297].

ACFs-based composites

At first, it is important to underline that for the preparation of MS2 bacteriophage test solutions, a Tris - (tris(hydroxymethyl)aminomethane) solution was used. Tris causes chelation of metal ions in the solution, which in the described study resulted in enhanced release of copper bonded to ACFs composites based on the formation of ligand complexes $(Cu(Tris)^{2+}$, $Cu(Tris)_2^{2+}$, $Cu(Tris)_4^{2+}$ or mixed one) [298]. As a consequence, high copper concentrations, up to 8.5 g, are

found in permeates. This indicated that the structure of the tested composites was affected, leading to continuous copper release during material rinsing with the above mentioned solution. The formed stable complexes with copper did not interact with MS2 bacteriophages present in the collected permeate and further MS2 inactivation over time was not observed. Therefore, despite observed high copper concentrations, almost no continuous increase of virus inactivation with storage took place. Another consequence of Tris application is change in solution ionic strength that also might lead to decrease in virus adsorption, as Tris may act as a competitive adsorbent.

Taking the above mentioned into account it is impossible to give a simple explanation for the mechanisms-driven virus removal or inactivation by composites, due to delicate test conditions that affect desired output of the studies. The received data presented on Figure 62.

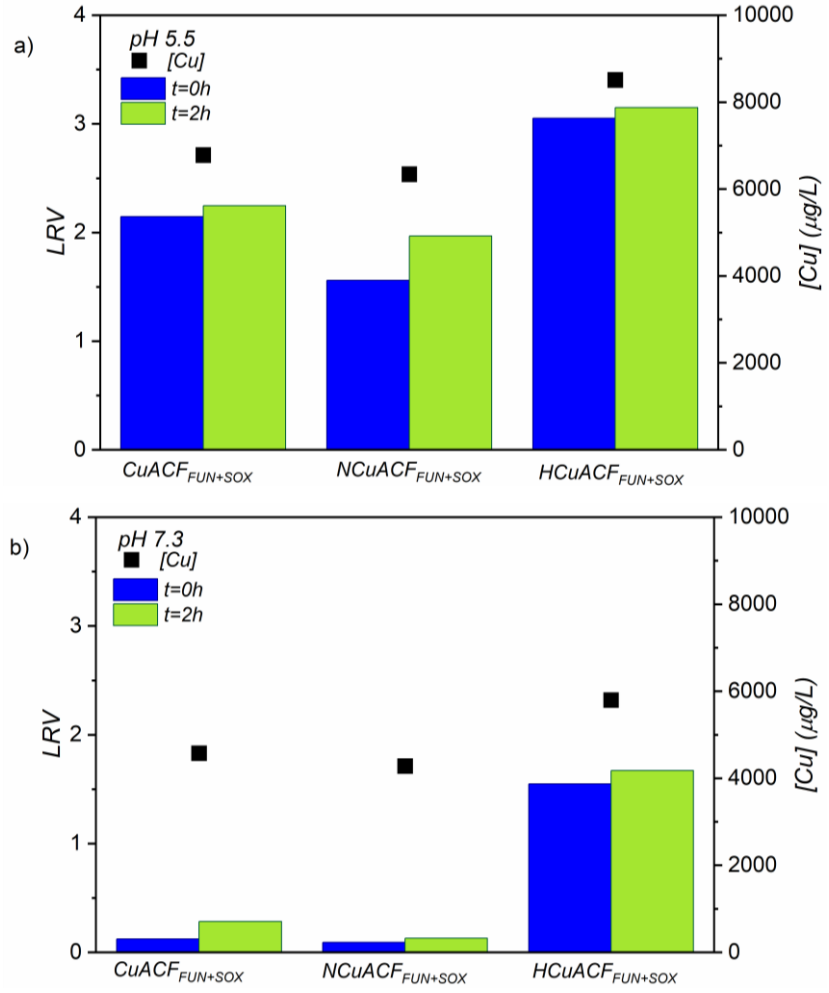

Figure 62 MS2 removal test results of ACFs-based composites at a) pH 5.5 and b) pH 7.3, and the associated copper concentrations detected in the permeate*;

*The presented data come from duplicate measurements, statistics and standard error cannot be presented. The results of the first tests are comparable to the effects of the second round tests.

The composite's structure was damaged due to constant copper release and complexing by Tris buffer interaction. Further flushing of cartridges with 3-6 L of media may result in total removal of copper species from the tested composites. Assuming that the data obtained from the composites cannot be fully interpreted, thus, a hypotheses may be proposed. It can be said that the observed MS2 bacteriophage removal is driven not only by electrostatic adsorption, which could occur only for $NCuACF_{FUN+SOX}$ and $HCuACF_{FUN+SOX}$ at pH 5.5 and for $HCuACF_{FUN+SOX}$ at pH 7.3, but also by other, not well defined mechanisms. Another justification can be found in immediate interactions between copper and MS2 bacteriophages onto the composites surface [299]. There should be taken into account influence of copper species morphology (size, shape, distribution onto fibres surface) onto virus inactivation [292]. Above mentioned explanations are only theoretical one and are out of the scope of performed study.

Such results raise doubts on the utilisation of copper species and their role in such applications. The performed investigation show that copper is an exceptionally delicate species for being applicable in water treatment technology, as it might be difficult to avoid its dissolution or complexation by compounds occurring in natural waters [300,301]. Moreover, copper species are prone to oxidation. Copper virucidal properties are indisputable, highly beneficial for virus inactivation. Copper species might be replaced with more chemically stable metal or metal oxides, such as MgO that also exhibits antiviral characteristic [37,146].
The conclusion is that activated carbon fibres modified with copper species should not be considered for water treatment applications. Activated carbon fibres themselves exhibit great potential, thus focus should be put on them. Fibres can be further tested by taking into account the following aspects: higher amounts of ACFs, larger volume of virus solution, evaluation of impact of different ions (e.g. Mg^{2+}, Cu^{2+}, Na^{+}) or natural organic matter on adsorption. There are also possible additional studies on fibre synthesis procedure to use recycled or environmental friendly substrates, develop favourable conditions for activation to obtain a material with tailored characteristic, e.g. greater porosity or specific surface area. Another possible point for improvement is functionalisation of activated carbon fibres to incorporate more functional groups to promote interaction between the material and viruses.

13.5. Conclusions of composites stability studies and MS2 removal tests

MWNCTs-based composites were tested in the form of flat, thin filter, while ACFs-based composites in the form of cartridge with certain bed height. Both filters and cartridges were rinsed for 24 h with 0.01 M NaCl at pH 5.0 and 7.0. The permeate was regularly collected and copper

concentration was monitored within ICP-MS measurement. The results show a dynamic change of cumulative copper mass in the permeate as a function of filtered volume. All composites exhibited measurable copper dissolution during conditioning, likely due to non-/weakly-bonded copper particles or their excessive amounts. Studies revealed the stability of composites being affected by pH with clear increase in copper dissolution at pH 5.0 in regard to pH 7.0. Although the detected copper concentrations in the permeate were below the limit recommended by WHO, not all of obtained materials are suitable for water treatment applications. The presented data indicates that only some of the composites, such as *composite 1 (Cu_2O/ MWCNTs)*, *composite 3 (Cu_2O/ MWCNTs)*, $CuACF_{AR}$ and $CuACF_{FUN+SOX}$ reached the plateau and stabilised over time. Other materials, such as c*omposite* 2 *(Cu_2O/ MWCNTs)* and remaining thermally treated ACFs-based composites: $NCuACF_{AR}$, $HCuACF_{AR}$ $NCuACF_{FUN+SOX}$, $CuACFFUN_{+SOX}$ revealed a constant copper release after 24 h of rinsing. It indicates that stabilisation test was performed not long enough or materials were unstable, thus further or even constant cooper dissolution might take place. Such behaviour eliminates above-mentioned materials from being applicable in water technologies.

The MS2 bacteriophage removal tests confirmed low LRV for as-received multi-walled carbon nanotubes in comparison to the results published elsewhere [24,129]. These discrepancies can be attributed to differences in type and characteristic of MWCNTs used, the manner of filter preparation, the amount of filter material and test conditions.

Overall, the MS2 removal results demonstrated that developed MWCNTs-based composites are not sufficient to provide safe drinking water through filtration alone, because the adequate efficiency level was not achieved. The composites provide a mechanism for virus removal through the combined treatment of filtration and post-filtration storage.

The as-received, as well as functionalised+ Soxhlet ACFs exhibited a great potential towards MS2 inactivation. Oxidised fibres reached a 20 % higher LRV than as-received ACFs, confirming an advantage of functionalisation process. The MS2 studies of ACFs-based composites revealed their inapplicability in water treatment and underlined sensitivity of copper species to water/ media composition.

The presented above findings and experimental procedures clearly indicate: (i) the necessity of material conditioning (for its stabilisation), (ii) an impact of permeate storage and composition on the viruses concentration.

Observed mechanisms responsible for MS2 inactivation are the electrostatic interactions, Van der Waals forces, steric and hydrophobic repulsion, as well as intimate contact between copper species and bacteriophages.

IV Summary and conclusions

The main goal of this PhD thesis was to understand the interactions between viruses (MS2 bacteriophages as a surrogates) and carbon-based adsorption material and develop an efficient adsorption material for water treatment with a focus on virus removal for point-of-use applications at the household scale. Many useful outcomes were found during the performed study, e.g. effective technologies for carbon substrates purification and functionalisation, distinctive synthesis routes to obtain copper-carbon composites and understanding the interactions between those materials and MS2 bacteriophages.

The subsequent findings of this PhD thesis are described in chronological order of the performed work: (i) functionalisation and characterisation of carbon substrates, (ii) synthesis of carbon composites, (iii) stability/ conditioning study, and (iv) MS2 bacteriophage removal test of fabricated composites, utilising multi-walled carbon nanotubes and activated carbon fibres.

Multi-walled carbon nanotubes

Within the scope of this work, a two-step process for MWNCT purification and functionalisation was established [227]. The treatment resulted in degradation of MWCNT structures leading to a lower degree of MWCNT agglomeration, tube shortening and breaking, as well as increase in specific surface area. An effective procedure was developed to remove residual catalyst contaminations (nearly 90 wt.% reduction of catalysts) and oxidise the carbon surface by incorporation of hydroxyl, carbonyl and carboxylic functional groups. The point of zero charge was shifted to more negative values due to the presence of acidic functional groups. Such modifications led to material chemical reactivity enhancement and increase in active sites.

Three Cu_2O/ MWCNTs composites were developed via three various synthesis methods: (i) adsorption of aqueous copper ion, (ii) adsorption of copper(II) hydroxide and (iii) adsorption of copper complex. All synthesis procedures resulted in the presence of uniformly distributed nanosized Cu_2O particles on the MWCNTs' surfaces. The main differences between obtained materials were the amounts of adsorbed copper species onto MWCNTs' surfaces and associated with that differences in specific surface area.

In contrary to the published results, MS2 removal test of as-received multi-walled carbon nanotubes revealed their low virucidal performance [24,129]. Those inequalities can be assigned to: MWCNTs type, filtration conditions (amount of material, flux, pressure, water composition and contact time between nanotubes and viruses), as well as the method of filter preparation. Moreover, the commercially available MWCNTs differ between manufacturers, as well as between

production batches. This significantly affects their characteristic (e.g., homogeneity, purity, chemical composition) and additionally introduces inequalities in virucidal characteristic, biological effects and toxicity, leading to the conclusion that MWCNTs do not possess uniform, repeatable characteristics. Within the MultiCarboVir project, an additional study was performed together with project partner – Eawag that suspected (however does not quantify) MWNCTs leakage from the filter into the permeate. This phenomenon increased the risk of health impact, which is not acceptable in water technologies, therefore the MWCNTs application in filtration is limited.

Despite the fact that pristine MWCNTs exhibited lower virucidal properties than expected, they were useful as support structures for Cu_2O nanoparticles. Furthermore, this study helped in understanding the virucidal properties of copper species that act as inactivator for viruses. The obtained results reveal that the developed MWCNTs-based composites are not effective in providing safe drinking water through filtration alone, due to physical removal and/or adsorption processes, as the method does not reach needed LRV. However, the composites ensure a mechanism for virus removal through combined treatment of filtration and post-filtration storage, due to increased virus inactivation in the permeate over time, where water is stored prior to use. Such utilisation might be considered only when both MWCNTs and copper are not released from the filter, optionally if the amount of copper released is below the recommended limits.

Performed work contributed in revision of the methods for filters testing in the aspect of virus removal and evaluation procedure of virus concentration. Studies on different filters allowed to deduce an essential approach to rate not only the proposed filter materials, but also all filters in general. This thesis discusses the importance of filter-material conditioning to remove any residuals and obtain a stable material under the tested conditions, due to potential dissolution/ desorption of filter elements that might influence either material performance and/or lifetime. An important aspect of the critical evaluation of virus removal methods is a proper examination of virus concentration. A crucial finding is that permeate storage affecting continued inactivation, which is usually not considered during material examination. For this reason the time control of sample analysis is essential. Additionally, the importance of permeate composition influence on LRV should be highlighted. All mentioned steps lead to improved, more reliable evaluation of the mechanisms behind the virus inactivation/ removal by the tested materials. We deducted that mechanism-driven virus removal by the proposed MWCNTs-based composites are very complex and include: (i) electrostatic adsorption of negatively charged viruses on the positively charged material (limited), (ii) immediate inactivation of viruses by copper(I)

oxide formation on filter surface, and (iii) continued inactivation in permeate due to the presence of dissolved copper species. An important note for future study is an application of single-particle ICP-MS or centrifugation at high speed to divide the permeate fraction in order to differentiate between dissolved metal ions and nanoparticles and their effect on virus inactivation. That might be helpful with determination of the exact mechanism and active form of metal responsible for inactivation.

Activated carbon fibres

Functionalisation of activated carbon fibres resulted in an increase in oxygen content on the surface and in the bulk. Oxygen and nitrogen functional groups were incorporated, with the greatest contribution coming from carboxylic groups. The total amount of functional groups increased nearly six times. The presence of functional groups caused a significant decrease in the fibres point of zero charge from 5.8 to 1.9. Although material structure and morphology was not significantly affected by acid treatment, a 25 % increase in microporosity was observed.

ACFs-based composites preparation comprised of just one synthesis route- adsorption of aqueous copper ion. The synthesis procedure was studied in details to achieve the greatest copper uptake on the activated carbon fibres. Adsorption is dependent on many factors, i.e. time, metal ion concentration and speciation, solution pH, contact time, adsorbent surface functionality and point of zero charge. The study proved that the presence of functional groups enhances ACFs reactivity, which resulted in greater adsorption of copper ions onto functionalised fibres in comparison to as-received ones. Taking into account above mentioned, the $ACF_{FUN+SOX}$ material were the most efficient substrate in synthesis, adsorbing 9.3 wt% of copper from aqueous solution As a result, six ACFs-based composites with distinctive characteristic were fabricated by mentioned synthesis method. Adsorption of aqueous copper ions was described by a Langmuir isotherm. Additionally, up to a certain copper initial concentration, a linear relationship of functional groups protons displacement with $Cu^{2+}_{(aq.)}$ was observed, which suggests that the copper adsorption was driven by the ion exchange mechanism to carboxylic groups and probably further through the coordination mechanism to nitrogen functional groups. Copper was incorporated not only onto the carbon materials' surfaces but also into their pores. Additionally, the composites' point of zero charge resulted in higher values than their carbon substrates due to the presence of copper species. The thermal treatments under various atmospheres affected the (potential further) interactions between activated carbon fibres and copper as well as formation of copper species with certain morphologies.

The conclusions drawn from the MWCNTs study regarding filter testing were implemented in all studies done with ACFs and ACFs-based composites in the form of cartridges. It might indicate the universality and practical application of such an approach.

The activated carbon fibres exhibited a great potential toward MS2 bacteriophage removal, reaching up to 3.6 LRV applying only 300 mg of material. Such values are much higher than results published for granular or powder forms of activated carbon (<1 LRV): Shimabuku et al. have used 150 g of GAC, while Hijnen et al. tested GAC in pilot scale [41,42]. Furthermore, functionalised ACFs fibres showed 20 % greater MS2 $\log_{10}$ removal of bacteriophages than as-received ones. This might indicate that characteristic properties introduced via functionalisation have a positive impact on virus adsorption. It is assumed that activated carbon fibres rather cause bacteriophages removal than inactivation, as carbon being not known as an antiviral material to interact with virus capsid. The recognised mechanisms responsible for virus removal are the following: electrostatic interactions, VdW forces, hydrophobic and steric repulsions. Performed studies demonstrate that the virus removal process is complex and cannot be simply explained by one certain mechanism, which is always acting. What should be considered is the contribution of various forces, the particular involvement of which type might vary, depending on the material characteristic, however, precise determination of that is a complex process that need additional experiments and combination of various techniques [222,302]. Figure 63 summarises the factors that influence interactions between adsorbent material and viruses.

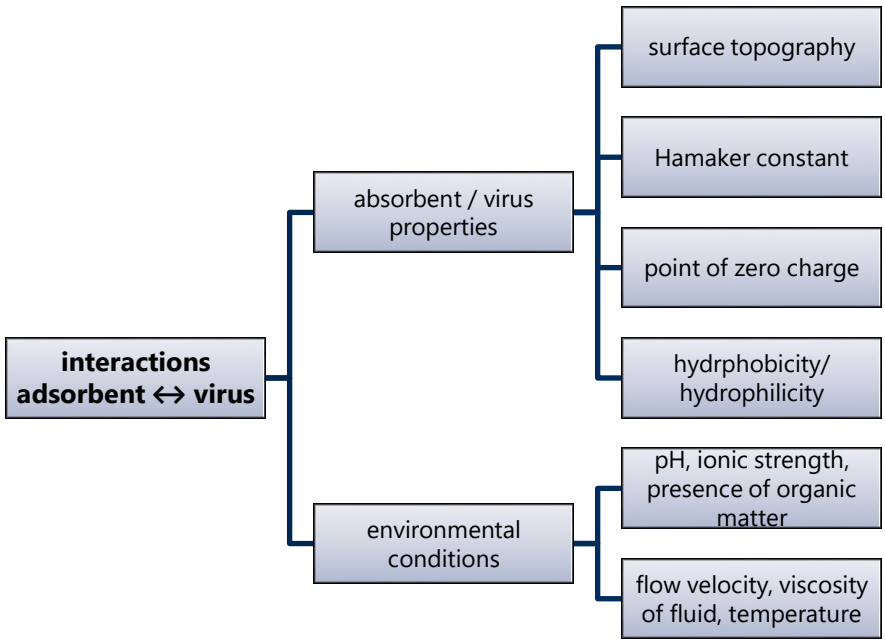

Figure 63 Dependence of interactions between adsorbent and virus [71,221];

The usage of the Tris solution as a dilution buffer for MS2 bacteriophages led to the complexation of copper on ACFs composites and, associated with that, their destruction by copper dissolution. It inhibited proper evaluation of the material's performance, as well as relevant mechanism responsible for the inactivation. The phenomenon of material instability and related constant copper species release indicates that activated carbon fibres modified with copper should not be considered further for water treatment applications. Copper species are too sensitive to other chemical compounds present in natural waters, which might enhance its solubility or release.

Future work on activated carbon fibres should evaluate further aspects of their virucidal characteristics. The following test conditions and variables are suggested for evaluation: bacteriophages that possess different isoelectric points, higher amounts of ACFs, greater volume of virus solution, different water compositions (presence of ions or natural organic matter). There are many perspectives for utilising of ACFs in water treatment technology not only for bacteria and viruses adsorption but also for other contaminations, e.g. heavy metals or dyes. There are possible also studies on activated carbon fibres synthesis from either recycled or environmental friendly, natural substrates. It allows to reduce the production cost, utilise waste and obtain activated carbon fibres with tailored characteristic. Further, to enhance the sorption capabilities of fibres, a chemically stable metal or metal oxide should be selected, e.g. MgO.

List of figures

List of tables

Publications of manuscript author

1. *K. Domagala*, M. Borlaf, J. Traber, D. Kata, T. Graule, Purification and Functionalisation of Multi-Walled Carbon Nanotubes, Mater. Lett. 253 (2019) 272–275. doi:10.1016/j.matlet.2019.06.085.
2. *K. Domagala*, M. Borlaf, M. Kata, T. Graule, Synthesis of Copper-based Multi-walled Carbon Nanotube Composites, Arch. Met. Mater. 65 (2020) 159–162. doi:10.24425/amm.2019.131109.
3. J.M. Mazurkow, N.S. Yüzbasi, *K. Domagala*, S. Pfeiffer, D. Kata, T. Graule, Nano-Sized Copper (Oxide) on Alumina Granules for Water Filtration: Effect of Copper Oxidation State on Virus Removal Performance, Environ. Sci. Technol. 54 (2020) 1214–1222. doi:10.1021/acs.est.9b05211.
4. *K. Domagala*, C. Jacquin, M. Borlaf, B. Sinnet, T. Julian, D. Kata, T. Graule, Efficiency and stability evaluation of Cu2O / MWCNTs filters for virus removal from water, Water Res. 179 (2020). doi:10.1016/j.watres.2020.115879.
5. C. Jacquin, D. Yu, M. Sander, *K. Domagala*, J. Traber, E. Morgenroth, T.R. Julian, Competitive co-adsorption of bacteriophage MS2 and natural organic matter onto multiwalled carbon nanotubes, Water Res. X. 9 (2020). doi:10.1016/j.wroa.2020.100058.
6. *K. Domagala*, J. Bell, S. Yüzbasi, B. Sinnet, D. Kata, T. Graule, Virus Deactivation in Drinking Water using Modified Activated Carbon Fibres, Environ. Sci. Technol., In progress, to be submitted in 03.2021.

References

[1] UNICEF, WHO, Progress on household drinking water, sanitation and hygiene 2000-2017. Special focus on inequalities, 2019.

[2] R.L.G. M. Kosek, C. Bern, The global burden of diarrhoeal disease, as estimated from studies published between 1992 and 2000, Biulletin World Heal. Organ. 81 (2014) 197–204. doi:10.1007/JHEP02(2015)121.

[3] United Nations, The United Nations World Water Development Report 2020. Water and Climate Change., Paris, 2020.

[4] S. Amrose, Z. Burt, I. Ray, Safe Drinking Water for Low-Income Regions, Annu. Rev. Environ. Resour. 40 (2015) 203–231. doi:10.1146/annurev-environ-031411-091819.

[5] R. Bain, R. Cronk, J. Wright, H. Yang, T. Slaymaker, J. Bartram, Fecal Contamination of Drinking-Water in Low- and Middle-Income Countries: A Systematic Review and Meta-Analysis, PLoS Med. 11 (2014). doi:10.1371/journal.pmed.1001644.

[6] C.K. Pooi, H.Y. Ng, Review of low-cost point-of-use water treatment systems for developing communities, Nat. Partn. Journals Clean Water. 1 (2018). doi:10.1038/s41545-018-0011-0.

[7] M.D. Sobsey, WHO, Managing water in the home : accelerated health gains from improved water supply, 2002. http://apps.who.int//iris/handle/10665/67319.

[8] S.C. Smith, D.F. Rodrigues, Carbon-based nanomaterials for removal of chemical and biological contaminants from water: A review of mechanisms and applications, Carbon N. Y. 91 (2015) 122–143. doi:10.1016/j.carbon.2015.04.043.

[9] V.K.K. Upadhyayula, S. Deng, M.C. Mitchell, G.B. Smith, Application of carbon nanotube technology for removal of contaminants in drinking water: A review, Sci. Total Environ. 408 (2009) 1–13. doi:10.1016/j.scitotenv.2009.09.027.

[10] T. Lee, C.H. Ooi, R. Othman, F.Y. Yeoh, Activated carbon fiber - The hybrid of carbon fiber and activated carbon, Rev. Adv. Mater. Sci. 36 (2014) 118–136.

[11] A.K. Haghi, S. Thomas, A. Pourhashemi, A. Hamrang, E. Klodzinska, Nanomaterials and Nanotechnology for Composites: Design, Simulation and Applications, Apple Academic Press Inc, Oakville, 2015.

[12] Y.T. Ong, A.L. Ahmad, S.H.S. Zein, S.H. Tan, A review on carbon nanotubes in an environmental protection and green engineering perspective, Brazilian J. Chem. Eng.

27 (2010) 227–242. doi:10.1590/S0104-66322010000200002.

[13] G. Borkow, R.W. Sidwell, D.F. Smee, D.L. Barnard, J.D. Morrey, H.H. Lara-Villegas, Y. Shemer-Avni, J. Gabbay, Neutralizing viruses in suspensions by copper oxide-based filters, Antimicrob. Agents Chemother. (2007). doi:10.1128/AAC.00125-07.

[14] A. Ananth, S. Dharaneedharan, M.S. Heo, Y.S. Mok, Copper oxide nanomaterials: Synthesis, characterization and structure-specific antibacterial performance, Chem. Eng. J. 262 (2015) 179–188. doi:10.1016/j.cej.2014.09.083.

[15] Y.J. Lee, S. Kim, S.H. Park, H. Park, Y.D. Huh, Morphology-dependent antibacterial activities of Cu2O, Mater. Lett. 65 (2011) 818–820. doi:10.1016/j.matlet.2010.12.023.

[16] K. Sunada, M. Minoshima, K. Hashimoto, Highly efficient antiviral and antibacterial activities of solid-state cuprous compounds, J. Hazard. Mater. 235–236 (2012) 265–270. doi:10.1016/j.jhazmat.2012.07.052.

[17] A. Bhatnagar, W. Hogland, M. Marques, M. Sillanpää, An overview of the modification methods of activated carbon for its water treatment applications, Chem. Eng. J. 219 (2013) 499–511. doi:10.1016/j.cej.2012.12.038.

[18] R.C. Bansal, M. Goyal, Activated Carbon Adsorption, Tylor & Francis, Boca Raton, 2005.

[19] T.J. Bandosz, Activated Carbon Surfaces in Environmental Remediation, Academic Press, New York, 2006.

[20] J. Perrich, Activated Carbon Adsorption for Wastewater Treatment, CRC Press, Boca Raton FL, 1981.

[21] J.W. Hassler, Purification With Activated Carbon, 3rd ed., Chemical Publishing Co., New York, 1974.

[22] E. Worch, Adsorption Technology in Water Treatment, de Gruyter, Berlin, 2012.

[23] M. Herzberg, D.F. Rodrigues, Carbon Nanotube Bacterial Cytotoxicity: Does the Type of Carbon Nanotubes Matter? Antibacterial Effects of Carbon Nanotubes: Size Does Matter !, Langmuir. (2008) 6409–6413. doi:10.1021Iia800951v.

[24] A. Srivastava, O.N. Srivastava, S. Talapatra, R. Vajtai, P.M. Ajayan, Carbon nanotube filters, Nat. Mater. 3 (2004) 610–614. doi:10.1038/nmat1192.

[25] A.S. Brady-Estévez, S. Kang, M. Elimelech, A single-walled-carbon-nanotube filter for

removal of viral and bacterial pathogens, Small. 4 (2008) 481–484. doi:10.1002/smll.200700863.

[26] X. Peng, Y. Li, Z. Luan, Z. Di, H. Wang, B. Tian, Z. Jia, Adsorption of 1,2-dichlorobenzene from water to carbon nanotubes, Chem. Phys. Lett. 376 (2003) 154–158. doi:10.1016/S0009-2614(03)00960-6.

[27] C. Lu, C. Liu, G.P. Rao, Comparisons of sorbent cost for the removal of Ni2+ from aqueous solution by carbon nanotubes and granular activated carbon, J. Hazard. Mater. 151 (2008) 239–246. doi:10.1016/j.jhazmat.2007.05.078.

[28] M. Rajabi, K. Mahanpoor, O. Moradi, Removal of dye molecules from aqueous solution by carbon nanotubes and carbon nanotube functional groups: Critical review, RSC Adv. 7 (2017) 47083–47090. doi:10.1039/c7ra09377b.

[29] A.S. Brady-Estévez, M.H. Schnoor, S. Kang, M. Elimelech, SWNT-MWNT hybrid filter attains high viral removal and bacterial inactivation, Langmuir. 26 (2010) 19153–19158. doi:10.1021/la103776y.

[30] S. Maurer, A. Mersmann, W. Peukert, Henry coefficients of adsorption predicted from solid Hamaker constants, Chem. Eng. Sci. 56 (2001) 3443–3453. doi:10.1016/S0009-2509(01)00033-1.

[31] J. Drzymala, Hydrophobicity and collectorless flotation of inorganic materials, Adv. Colloid Interface Sci. 50 (1994) 143–185. doi:10.1016/0001-8686(94)80029-4.

[32] P. Pour Shahid Saeed Abadi, M.R. Maschmann, S.M. Mortuza, S. Banerjee, J.W. Baur, S. Graham, B.A. Cola, Reversible tailoring of mechanical properties of carbon nanotube forests by immersing in solvents, Carbon N. Y. 69 (2014) 178–187. doi:10.1016/j.carbon.2013.12.004.

[33] M. Kawashita, S. Toda, H.M. Kim, T. Kokubo, N. Masuda, Preparation of antibacterial silver-doped silica glass microspheres, J. Biomed. Mater. Res. 66 (2003) 266–274. doi:10.1002/jbm.a.10547.

[34] Y.H. Kim, D.K. Lee, H.G. Cha, C.W. Kim, Y.S. Kang, Synthesis and Characterization of Antibacterial Ag−SiO2 Nanocomposite, J. Phys. Chem. 111 (2007) 3629–3635.

[35] G.P. Szekeres, Z. Nemeth, K. Schrantz, K. Nemeth, M. Schabikowski, J. Traber, W. Pronk, K. Hernadi, T. Graule, Copper-Coated cellulose-based water filters for virus retention, ACS Omega. 3 (2018) 446–454. doi:10.1021/acsomega.7b01496.

[36] Z. Németh, G.P. Szekeres, M. Schabikowski, K. Schrantz, J. Traber, W. Pronk, K. Hernádi, T. Graule, Enhanced virus filtration in hybrid membranes with MWCNT nanocomposite, R. Soc. Open Sci. 6 (2019) 181294. doi:10.1098/rsos.181294.

[37] B. Michen, J. Fritsch, C. Aneziris, T. Graule, Improved virus removal in ceramic depth filters modified with MgO, Environ. Sci. Technol. 47 (2013) 1526–1533. doi:10.1021/es303685a.

[38] R.B. Thurman, C.P. Gerba, The molecular mechanisms of copper and silver ion disinfection of bacteria and viruses, Crit. Rev. Environ. Control. 18 (1989) 295–315. doi:10.1080/10643388909388351.

[39] C.P. Gerba, M.D. Sobsey, C. Wallis, J.L. Melnick, Adsorption of Poliovirus onto Activated Carbon in Wastewater, Environ. Sci. Technol. 9 (1975) 727–731. doi:10.1021/es60106a009.

[40] J.T. Cookson, W.J. North, Adsorption of viruses on activated carbon. Equilibriums and kinetics of the attachment of Escherichia coli bacteriophage T4 on activated carbon, Environ. Sci. Technol. (1967). doi:10.1021/es60001a002.

[41] W.A.M. Hijnen, G.M.H. Suylen, J.A. Bahlman, A. Brouwer-Hanzens, G.J. Medema, GAC adsorption filters as barriers for viruses, bacteria and protozoan (oo)cysts in water treatment, Water Res. 44 (2010) 1224–1234. doi:10.1016/j.watres.2009.10.011.

[42] Q.L. Shimabuku, F.S. Arakawa, M. Fernandes Silva, P. Ferri Coldebella, T. Ueda-Nakamura, M.R. Fagundes-Klen, R. Bergamasco, Water treatment with exceptional virus inactivation using activated carbon modified with silver (Ag) and copper oxide (CuO) nanoparticles, Environ. Technol. (United Kingdom). 38 (2017) 2058–2069. doi:10.1080/09593330.2016.1245361.

[43] J. Margat, J. van der Gun, Groundwater around the World: A Geographic Synopsis, CRC Press, London, 2013.

[44] F.Y. Ramírez-Castillo, A. Loera-Muro, M. Jacques, P. Garneau, F.J. Avelar-González, J. Harel, A.L. Guerrero-Barrera, Waterborne pathogens: Detection methods and challenges, Pathogens. 4 (2015) 307–334. doi:10.3390/pathogens4020307.

[45] W.-S. Ryu, Chapter 1 - Discovery and Classification, in: Mol. Virol. Hum. Pathog. Viruses, Academic Press, 2017: pp. 3–20. doi:10.1016/b978-0-12-800838-6.00001-1.

[46] W.-S. Ryu, Chapter 2 - Virus Structure, in: Mol. Virol. Hum. Pathog. Viruses,

Academic Press, 2017: pp. 21–29. doi:10.1016/B978-0-12-800838-6.00002-3.

[47] J.F. Schijven, S.M. Hassanizadeh, Removal of viruses by soil passage: Overview of modeling, processes, and parameters, Crit. Rev. Environ. Sci. Technol. 30 (2000) 49–127. doi:10.1080/10643380091184174.

[48] WHO, Guidelines for drinking water quality, Geneva, 2011. https://apps.who.int/iris/bitstream/handle/10665/254637/9789241549950-eng.pdf?sequence=1.

[49] M.L. Pype, M.G. Lawrence, J. Keller, W. Gernjak, Reverse osmosis integrity monitoring in water reuse: The challenge to verify virus removal - A review, Water Res. 98 (2016) 384–395. doi:10.1016/j.watres.2016.04.040.

[50] B. Michen, T. Graule, Isoelectric points of viruses, J. Appl. Microbiol. (2010). doi:10.1111/j.1365-2672.2010.04663.x.

[51] A. Bosch, Human enteric viruses in the water environment: A minireview, Int. Microbiol. 1 (1998) 191–196. doi:10.2436/im.v1i3.39.

[52] M. Carrillo-Tripp, C.M. Shepherd, I.A. Borelli, S. Venkataraman, G. Lander, P. Natarajan, J.E. Johnson, C.I. Brooks, V.S. Reddy, VIPERdb: An enhanced and web API enabled relational database for structural virology, Nucleic Acids Res. 37 (2009) 436–442. doi:10.1093/nar/gkn840.

[53] T.-T. Fong, E.K. Lipp, Enteric Viruses of Humans and Animals in Aquatic Environments: Health Risks, Detection, and Potential Water Quality Assesment Tools, Microbiol. Mol. Biol. Rev. 69 (2014) 357–371. doi:10.1128/MMBR.69.2.357–37.

[54] A.M. Gall, B.J. Mariñas, Y. Lu, J.L. Shisler, Waterborne Viruses: A Barrier to Safe Drinking Water, PLOS Pathog. 11 (2015). doi:10.1371/journal.ppat.1004867.

[55] M. Exner, A. Kramer, L. Lajoie, J. Gebel, S. Engelhart, P. Hartemann, Prevention and control of health care-associated waterborne infections in health care facilities, Am. J. Infect. Control. 33 (2005) 26–40. doi:10.1016/j.ajic.2005.04.002.

[56] M.P. Zwart, L. Hemerik, J.S. Cory, J.A.G.M. De Visser, F.J.J.A. Bianchi, M.M. Van Oers, J.M. Vlak, R.F. Hoekstra, W. Van Der Werf, An experimental test of the independent action hypothesis in virus-insect pathosystems, Proc. R. Soc. B Biol. Sci. 276 (2009) 2233–2242. doi:10.1098/rspb.2009.0064.

[57] WHO, Guidelines for Drinking-water Quality. Volume 1 Recommendations, 2006.

https://www.who.int/water_sanitation_health/dwq/gdwq0506.pdf.

[58] K.T. Park, J. Hwang, Filtration and inactivation of aerosolized bacteriophage MS2 by a CNT air filter fabricated using electro-aerodynamic deposition, Carbon N. Y. 75 (2014) 401–410. doi:10.1016/j.carbon.2014.04.019.

[59] B. Hu, H. Guo, P. Zhou, Z.L. Shi, Characteristics of SARS-CoV-2 and COVID-19, Nat. Rev. Microbiol. (2020). doi:10.1038/s41579-020-00459-7.

[60] Y.R. Guo, Q.D. Cao, Z.S. Hong, Y.Y. Tan, S.D. Chen, H.J. Jin, K. Sen Tan, D.Y. Wang, Y. Yan, The origin, transmission and clinical therapies on coronavirus disease 2019 (COVID-19) outbreak - an update on the status, Mil. Med. Res. 7 (2020) 11. doi:10.1186/s40779-020-00240-0.

[61] S. Su, G. Wong, W. Shi, J. Liu, A.C.K. Lai, J. Zhou, W. Liu, Y. Bi, G.F. Gao, Epidemiology, Genetic Recombination, and Pathogenesis of Coronaviruses, Trends Microbiol. 24 (2016) 490–502. doi:10.1016/j.tim.2016.03.003.

[62] L. Casanova, W.A. Rutala, D.J. Weber, M.D. Sobsey, Survival of surrogate coronaviruses in water, Water Res. 43 (2009) 1893–1898. doi:10.1016/j.watres.2009.02.002.

[63] K.R. Wigginton, Y. Ye, R.M. Ellenberg, Emerging investigators series: The source and fate of pandemic viruses in the urban water cycle, Environ. Sci. Water Res. Technol. 1 (2015) 735–746. doi:10.1039/c5ew00125k.

[64] L.C. Marr, J.W. Tang, J. Van Mullekom, S.S. Lakdawala, Mechanistic insights into the effect of humidity on airborne influenza virus survival, transmission and incidence, J. R. Soc. Interface. 16 (2019). doi:10.1098/rsif.2018.0298.

[65] P.M. Gundy, C.P. Gerba, I.L. Pepper, Survival of Coronaviruses in Water and Wastewater, Food Environ. Virol. 1 (2009) 10–14. doi:10.1007/s12560-008-9001-6.

[66] J.W. Tang, The effect of environmental parameters on the survival of airborne infectious agents, J. R. Soc. Interface. 6 (2009) 737–746. doi:10.1098/rsif.2009.0227.focus.

[67] M.L. Rapp, T. Thiel, R.J. Arrowsmith, Model system using coliphage φX174 for testing virus removal by air filters, Appl. Environ. Microbiol. 58 (1992) 900–904. doi:10.1128/aem.58.3.900-904.1992.

[68] N. Kawabata, I. Ujino, Removal of virus from air by filtration using a composite

microporous membrane made of crosslinked poly(N-benzyl-4-vinylpyridinium chloride), React. Funct. Polym. 37 (1998) 213–218. doi:10.1016/s1381-5148(97)00133-8.

[69] J. Hyun, S.G. Lee, J. Hwang, Application of corona discharge-generated air ions for filtration of aerosolized virus and inactivation of filtered virus, J. Aerosol Sci. 107 (2017) 31–40. doi:10.1016/j.jaerosci.2017.02.004.

[70] P. Roelants, B. Boon, W. Lhoest, Evaluation of a commercial air filter for removal of viruses from the air., Appl. Microbiol. 16 (1968) 1465–1467. doi:10.1128/aem.16.10.1465-1467.1968.

[71] A. Armanious, M. Aeppli, R. Jacak, D. Refardt, T. Sigstam, T. Kohn, M. Sander, Viruses at Solid-Water Interfaces: A Systematic Assessment of Interactions Driving Adsorption, Environ. Sci. Technol. 50 (2016) 732–743. doi:10.1021/acs.est.5b04644.

[72] J.N. Ryan, M. Elimelech, Colloid mobilization and transport in groundwater, Colloids Surfaces A Physicochem. Eng. Asp. 107 (1996) 1–56. doi:10.1016/0927-7757(95)03384-X.

[73] C. Jacquin, D. Yu, M. Sander, K. Domagala, J. Traber, E. Morgenroth, T.R. Julian, Competitive co-adsorption of bacteriophage MS2 and natural organic matter onto multiwalled carbon nanotubes, Water Res. X. 9 (2020) 100058. doi:10.1016/j.wroa.2020.100058.

[74] A. Antony, J. Blackbeard, G. Leslie, Removal efficiency and integrity monitoring techniques for virus removal by membrane processes, Crit. Rev. Environ. Sci. Technol. 42 (2012) 891–933. doi:10.1080/10643389.2011.556539.

[75] A. Bennett, Maintaining the integrity of filtration systems, Filtr. Sep. 42 (2005) 30–33. doi:10.1016/S0015-1882(06)70843-6.

[76] WHO, International Scheme to Evaluate Household Water Treatment Technologies Harmonized Testing Protocol: Technology Non-Specific Version 2.1, gene, 2018. www.who.int/entity/household_water/scheme/HarmonizedTestProtocol.pdf?ua=1.

[77] C. Ferguson, A.M. De Roda Husman, N. Altavilla, D. Deere, N. Ashbolt, Fate and transport of surface water pathogens in watersheds, Crit. Rev. Environ. Sci. Technol. 33 (2003) 299–361. doi:10.1080/10643380390814497.

[78] W. Grabow, Bacteriophages: Update on application as models for viruses in water,

Water SA. 27 (2001) 251–268. doi:10.4314/wsa.v27i2.4999.

[79] S.M. Goyal, C.P. Gerba, G. Bitton, Phage Ecology, in: Wiley Ser. Ecol. Appl. Microbiol., John Wiley and Sons, New York—Chichester—Brisbane—Toronto—Singapore, 1987: p. 321.

[80] M.D. Sobsey, Methods to Identify and Detect Microbial Contaminants in Drinking Water, in: Natl. Res. Counc. Identifying Futur. Drink. Water Contam., The National Academies Press, 1999. doi:doi.org/10.17226/9595.

[81] V. Tanchou, Review of methods for the rapid identification of pathogens in water samples, 2014. doi:10.2788/18775.

[82] W.-S. Ryu, Chapter 4 - Diagnosis and Methods, in: Mol. Virol. Hum. Pathog. Viruses, Academic Press, 2017: pp. 47–62. doi:10.1016/b978-0-12-800838-6.00004-7.

[83] S. Watts, T.R. Julian, K. Maniura-Weber, T. Graule, S. Salentinig, Colloidal Transformations in MS2 Virus Particles: Driven by pH, Influenced by Natural Organic Matter, ACS Nano. 14 (2020) 1879–1887. doi:10.1021/acsnano.9b08112.

[84] O. Kavvada, A. Horvath, J.R. Stokes-Draut, T.P. Hendrickson, W.A. Eisenstein, K.L. Nelson, Assessing location and scale of urban nonpotable water reuse systems for life-cycle energy consumption and greenhouse gas emissions, Environ. Sci. Technol. 50 (2016) 13184–13194. doi:10.1021/acs.est.6b02386.

[85] WHO, Results of round II of the WHO international scheme to evaluate household water treatment technologies, 2019. http://www.who.int/household_water/scheme/household-water-treatment-report-round-1/en/#.VtmmIDJjI5c.mendeley.

[86] B. Oram, UV Disinfection Drinking Water Treatment, Drink. Water Treat. with UV Irradiat. (n.d.). Drinking Water Treatment with UV Irradiation (accessed July 15, 2020).

[87] WHO, Results of round I of the WHO International Scheme to Evaluate Household Water Treatment Technologies, 2016. http://www.who.int/household_water/scheme/household-water-treatment-report-round-1/en/#.VtmmIDJjI5c.mendeley.

[88] K. Sirikanchana, J.L. Shisler, B.J. Mariñas, Effect of exposure to UV-C irradiation and monochloramine on adenovirus serotype 2 early protein expression and DNA

replication, Appl. Environ. Microbiol. 74 (2008) 3774–3782. doi:10.1128/AEM.02049-07.

[89] M. Al-Abri, B. Al-Ghafri, T. Bora, S. Dobretsov, J. Dutta, S. Castelletto, L. Rosa, A. Boretti, Chlorination disadvantages and alternative routes for biofouling control in reverse osmosis desalination, Npj Clean Water. 2 (2019). doi:10.1038/s41545-019-0033-2.

[90] C. Tian, R. Liu, H. Liu, J. Qu, Disinfection by-products formation and precursors transformation during chlorination and chloramination of highly-polluted source water: Significance of ammonia, Water Res. 47 (2013) 5901–5910. doi:10.1016/j.watres.2013.07.013.

[91] P. Benech, J.M. Duchamp, Textile Materials in Liquid Filtration Practices: Current Status and Perspectives in Water and Wastewater Treatment, in: Text. Adv. Appl., 2017: pp. 293–320. doi:http://dx.doi.org/10.5772/intechopen.69462.

[92] A.R. Bielefeldt, K. Kowalski, C. Schilling, S. Schreier, A. Kohler, R. Scott Summers, Removal of virus to protozoan sized particles in point-of-use ceramic water filters, Water Res. 44 (2010) 1482–1488. doi:10.1016/j.watres.2009.10.043.

[93] H. Wang, T. Narihiro, A.P. Straub, C.R. Pugh, H. Tamaki, J.F. Moor, I.M. Bradley, Y. Kamagata, W.T. Liu, T.H. Nguyen, MS2 bacteriophage reduction and microbial communities in biosand filters, Environ. Sci. Technol. 48 (2014) 6702–6709. doi:10.1021/es500494s.

[94] I. Bradley, A. Straub, P. Maraccini, S. Markazi, T.H. Nguyen, Iron oxide amended biosand filters for virus removal, Water Res. 45 (2011) 4501–4510. doi:10.1016/j.watres.2011.05.045.

[95] L. Gutierrez, X. Li, J. Wang, G. Nangmenyi, J. Economy, T.B. Kuhlenschmidt, M.S. Kuhlenschmidt, T.H. Nguyen, Adsorption of rotavirus and bacteriophage MS2 using glass fiber coated with hematite nanoparticles, Water Res. 43 (2009) 5198–5208. doi:10.1016/j.watres.2009.08.031.

[96] F. Tepper, L. Kaledin, Argonide Corp., Sanford, FL, Particle removal efficiency of nano alumina fiber filters, (2005).

[97] M. Metzger, M. Peiker, S. Faust, S. Ebert, D. Müller, S. Winterfeld, N. Mang, Evaluating Adsorptive Filtration As a Unit Operation for Virus Removal, Bioprocess Int. (2015). https://bioprocessintl.com/downstream-processing/filtration/evaluating-

adsorptive-filtration-unit-operation-virus-removal/.

[98] M.D. Sobsey, B.L. Jones, Concentration of poliovirus from tap water using positively charged microporous filters, Appl. Environ. Microbiol. 37 (1979) 588–595. doi:10.1128/aem.37.3.588-595.1979.

[99] J.M. Brown, PhD Thesis: Effectivness of ceramic filtration for drinking water treatment in Cambodia, 2007.

[100] M. Wegmann, B. Michen, T. Graule, Nanostructured surface modification of microporous ceramics for efficient virus filtration, J. Eur. Ceram. Soc. 28 (2008) 1603–1612. doi:10.1016/j.jeurceramsoc.2007.11.002.

[101] M. Wegmann, B. Michen, T. Luxbacher, J. Fritsch, T. Graule, Modification of ceramic microfilters with colloidal zirconia to promote the adsorption of viruses from water, Water Res. 42 (2008) 1726–1734. doi:10.1016/j.watres.2007.10.030.

[102] D.R. Lide ed., CRC Handbook of Chemistry and Physics, Internet V, CRC Press, Boca Raton FL, 2005. http://www.hbcpnetbase.com.

[103] L.K.B. Prelas, M. A. G. Popovici, Handbook of Industrial Diamonds and Diamond Films, Marcel Dekker INC., New York, 1998.

[104] P. Delhaes, Graphite and Precursors, Overseas Oublishers Association, Amsterdam, 2001.

[105] IUPAC, Compendium of Chemical Terminology 2nd ed., Blackwell Scientific Publications, Oxford, 1979. doi:https://doi.org/10.1351/goldbook.F02547.

[106] B.D. Malhotra, M.A. Ali, Functionalized Carbon Nanomaterials for Biosensors Fundamentals and Applications, in: Chapter 2 - Funct. Carbon Nanomater. Biosens., Matthew Deans, 2018: pp. 75–103. doi:10.1016/b978-0-323-44923-6.00002-9.

[107] J. Robertson, Amorphous carbon, Adv. Phys. 35 (1986) 317–374. doi:10.1080/00018738600101911.

[108] S. Lijima, Helical microtubules of graphitic carbon, Lett. to Nat. 354 (1991) 56–58.

[109] A. Eatemadi, H. Daraee, H. Karimkhanloo, M. Kouhi, N. Zarghami, A. Akbarzadeh, M. Abasi, Y. Hanifehpour, S.W. Joo, Carbon nanotubes: Properties, synthesis, purification, and medical applications, Nanoscale Res. Lett. 9 (2014) 1–13. doi:10.1186/1556-276X-9-393.

[110] A.D. Dobrzańska, D. Cichocki, MWCNTs manufactured by CCVD method, Carbon Nanotechnol. (2014) 1–30. http://www.onecentralpress.com/carbon-nanotechnology/.

[111] D.K. Patel, H. Kim, S.D. Dutta, K. Ganguly, K. Lim, Carbon Nanotubes-Based Nanomaterials and Their Agricultural and Biotechnological Applications, Materials (Basel). 13 (2020). doi:doi:10.3390/ma13071679.

[112] K. Sears, L. Dumée, J. Schütz, M. She, C. Huynh, S. Hawkins, M. Duke, S. Gray, Recent developments in carbon nanotube membranes for water purification and gas separation, Materials (Basel). 3 (2010) 127–149. doi:10.3390/ma3010127.

[113] T. Poore, Image of 3D Model of Multi-walled Carbon Nanotube, (2007). https://www.archimorph.com/200709073ds-max-drawing-and-rendering-of-a-multi-wall-nanotube (accessed March 14, 2020).

[114] A. Szabó, C. Perri, A. Csató, G. Giordano, D. Vuono, J.B. Nagy, Synthesis methods of carbon nanotubes and related materials, Materials (Basel). 3 (2010) 3092–3140. doi:10.3390/ma3053092.

[115] A. Szabó, E. Kecsenovity, Z. Pápa, T. Gyulavári, K. Németh, E. Horvath, K. Hernadi, Influence of synthesis parameters on CCVD growth of vertically aligned carbon nanotubes over aluminum substrate, Sci. Rep. 7 (2017) 1–11. doi:10.1038/s41598-017-10055-0.

[116] A. Yahyazadeh, B. Khoshandam, Carbon nanotube synthesis via the catalytic chemical vapor deposition of methane in the presence of iron, molybdenum, and iron–molybdenum alloy thin layer catalysts, Results Phys. 7 (2017) 3826–3837. doi:10.1016/j.rinp.2017.10.001.

[117] A.F. Trompeta, M.A. Koklioti, D.K. Perivoliotis, I. Lynch, C.A. Charitidis, Towards a holistic environmental impact assessment of carbon nanotube growth through chemical vapour deposition, J. Clean. Prod. 129 (2016) 384–394. doi:10.1016/j.jclepro.2016.04.044.

[118] L. Wood, ResearchAndMarkets.com, Global Nanotubes Market - Segmented by Product type, Application, End-user Industry and Region - Growth, Trends, and Forecast (2018 – 2023), (2018). https://www.businesswire.com/news/home/20180509006235/en/Global-Nanotubes-Market-2018-Forecast-2023--, published 05.2018, accessed 27.11.2019 (accessed November 27, 2019).

[119] Z. Wu, P.K. Shaw, A. Holian, R.F. Hamilton, S. Mitra, Effect of MWCNT size, carboxylation, and purification on in vitro and in vivo toxicity, inflammation and lung pathology, Part. Fibre Toxicol. 10 (2013) 57. doi:10.1186/1743-8977-10-57.

[120] E.R. Edwards, E.F. Antunes, E.C. Botelho, M.R. Baldan, E.J. Corat, Evaluation of residual iron in carbon nanotubes purified by acid treatments, Appl. Surf. Sci. 258 (2011) 641–648. doi:10.1016/j.apsusc.2011.07.032.

[121] T.A. Saleh, The influence of treatment temperature on the acidity of MWCNT oxidized by HNO3 or a mixture of HNO3/H2SO4, Appl. Surf. Sci. (2011). doi:10.1016/j.apsusc.2011.04.020.

[122] V. Datsyuk, M. Kalyva, K. Papagelis, J. Parthenios, D. Tasis, A. Siokou, I. Kallitsis, C. Galiotis, Chemical oxidation of multiwalled carbon nanotubes, Carbon N. Y. 46 (2008) 833–840. doi:10.1016/j.carbon.2008.02.012.

[123] Y.C. Chiang, W.H. Lin, Y.C. Chang, The influence of treatment duration on multi-walled carbon nanotubes functionalized by H2SO4/HNO3 oxidation, Appl. Surf. Sci. 257 (2011) 2401–2410. doi:10.1016/j.apsusc.2010.09.110.

[124] L. Stobinski, B. Lesiak, L. Kövér, J. Tóth, S. Biniak, G. Trykowski, J. Judek, Multiwall carbon nanotubes purification and oxidation by nitric acid studied by the FTIR and electron spectroscopy methods, J. Alloys Compd. 501 (2010) 77–84. doi:10.1016/j.jallcom.2010.04.032.

[125] Y. Chen, Z. Li, Y. Zhao, Purification and dispersibility of multi-walled carbon nanotubes in aqueous solution, Russ. J. Phys. Chem. A. (2016). doi:10.1134/S0036024416130227.

[126] K. Domagala, M. Borlaf, M. Kata, T. Graule, Synthesis of Copper-based Multi-walled Carbon Nanotube Composites, Arch. Met. Mater. 65 (2020) 157–162. doi:10.24425/amm.2019.131109.

[127] F. Morales-Lara, M.J. Pérez-Mendoza, D. Altmajer-Vaz, M. García-Román, M. Melguizo, F.J. López-Garzón, M. Domingo-García, Functionalization of multiwall carbon nanotubes by ozone at basic pH. Comparison with oxygen plasma and ozone in gas phase, J. Phys. Chem. C. 117 (2013) 11647–11655. doi:10.1021/jp4017097.

[128] R. Saito, G. Dresselhaus, Physical Properties of Carbon Nanotubes, Imperial College Press, London, 1998. doi:10.1016/s0368-3273(15)30035-3.

[129] A.S. Brady-Estévez, M.H. Schnoor, C.D. Vecitis, N.B. Saleh, M. Elimelech, Multiwalled carbon nanotube filter: Improving viral removal at low pressure, Langmuir. 26 (2010) 14975–14982. doi:10.1021/la102783v.

[130] R.F. Rajter, R.H. French, W.Y. Ching, W.C. Carter, Y.M. Chiang, Calculating van der Waals-London dispersion spectra and Hamaker coefficients of carbon nanotubes in water from ab initio optical properties, J. Appl. Phys. 101 (2007) 1–6. doi:10.1063/1.2709576.

[131] Y.H. Li, J. Ding, Z. Luan, Z. Di, Y. Zhu, C. Xu, D. Wu, B. Wei, Competitive adsorption of Pb2+ , Cu2+ and Cd2+ ions from aqueous solutions by multiwalled carbon nanotubes, Carbon N. Y. 41 (2003) 2787–2792. doi:10.1016/S0008-6223(03)00392-0.

[132] Q.L. Li, D.X. Yuan, Q.M. Lin, Evaluation of multi-walled carbon nanotubes as an adsorbent for trapping volatile organic compounds from environmental samples, J. Chromatogr. A. 1026 (2004) 283–288. doi:10.1016/j.chroma.2003.10.109.

[133] F. Su, C. Lu, S. Hu, Adsorption of benzene, toluene, ethylbenzene and p-xylene by NaOCl-oxidized carbon nanotubes, Colloids Surfaces A Physicochem. Eng. Asp. 353 (2010) 83–91. doi:10.1016/j.colsurfa.2009.10.025.

[134] V.V. Kumar, S.P. Anthony, Antimicrobial studies of metal and metal oxide nanoparticles, Elsevier Inc., 2016. doi:10.1016/b978-0-323-42861-3.00009-1.

[135] O. Akhavan, R. Azimirad, S. Safa, M.M. Larijani, Visible light photo-induced antibacterial activity of CNT-doped TiO2 thin films with various CNT contents, J. Mater. Chem. 20 (2010) 7386–7392. doi:10.1039/c0jm00543f.

[136] F. Yang, Q. Jiang, W. Xie, Y. Zhang, Effects of multi-walled carbon nanotubes with various diameters on bacterial cellular membranes: Cytotoxicity and adaptive mechanisms, Chemosphere. 185 (2017) 162–170. doi:10.1016/j.chemosphere.2017.07.010.

[137] A.S. Brady-Estévez, T.H. Nguyen, L. Gutierrez, M. Elimelech, Impact of solution chemistry on viral removal by a single-walled carbon nanotube filter, Water Res. 44 (2010) 3773–3780. doi:10.1016/j.watres.2010.04.023.

[138] F. Ahmed, C.M. Santos, J. Mangadlao, R. Advincula, D.F. Rodrigues, Antimicrobial PVK: SWNT nanocomposite coated membrane for water purification: Performance and toxicity testing, Water Res. 47 (2013) 3966–3975. doi:10.1016/j.watres.2012.10.055.

[139] S. Mallakpour, E. Khadem, Carbon nanotube–metal oxide nanocomposites: Fabrication, properties and applications, Chem. Eng. J. 302 (2016) 344–367. doi:10.1016/j.cej.2016.05.038.

[140] W.A. Wani, S. Prashar, S. Shreaz, S. Gómez-Ruiz, Nanostructured materials functionalized with metal complexes: In search of alternatives for administering anticancer metallodrugs, Coord. Chem. Rev. 312 (2016) 67–98. doi:10.1016/j.ccr.2016.01.001.

[141] D.J. Guo, H.L. Li, High dispersion and electrocatalytic properties of platinum on functional multi-walled carbon nanotubes, Electroanalysis. 17 (2005) 869–872. doi:10.1002/elan.200403164.

[142] X. Qin, X. Gao, H. Liu, H. Yoan, Electrochemical Hydrogen Storage of Multiwalled Carbon Nanotubes, Electrochem. Solid-State Lett. 3 (2000) 532–535.

[143] B.C. Satishkumar, A. Govindaraj, M. Nath, C.N.R. Rao, Synthesis of metal oxide nanorods using carbon nanotubes as templates, J. Mater. Chem. 10 (2000) 2115–2119. doi:10.1039/b002868l.

[144] W. Wang, P. Serp, P. Kalck, J.L. Faria, Photocatalytic degradation of phenol on MWNT and titania composite catalysts prepared by a modified sol-gel method, Appl. Catal. B Environ. 56 (2005) 305–312. doi:10.1016/j.apcatb.2004.09.018.

[145] Y. You, J. Han, P.C. Chiu, Y. Jin, Removal and inactivation of waterborne viruses using zerovalent iron, Environ. Sci. Technol. 39 (2005) 9263–9269. doi:10.1021/es050829j.

[146] R.V. P. Vilagines, B. Sarrette, Preformed magnesium hydroxide precipitate for second-step concentration of enteroviruses from drinking and surface waters., Can J Microbiol. 28 (1982) 783–787.

[147] H. Pang, F. Gao, Q. Lu, Morphology effect on antibacterial activity of cuprous oxide, Chem. Commun. (2009) 1076–1078. doi:10.1039/b816670f.

[148] M. Yusuf, Silver Nanoparticles: Synthesis and Applications, in: Handb. Ecomater., 2019: pp. 2343–2356. doi:10.1007/978-3-319-68255-6.

[149] T.R. Sinclair, A. Patil, B.G. Raza, D. Reurink, S.K. van den Hengel, S.A. Rutjes, A.M. de Roda Husman, H.D.W. Roesink, W.M. de Vos, Cationically modified membranes using covalent layer-by-layer assembly for antiviral applications in drinking water, J.

Memb. Sci. 570–571 (2019) 494–503. doi:10.1016/j.memsci.2018.10.081.

[150] S. Biniak, M. Pakula, A. Swiatkowski, Chemistry and Physics of Carbon A Series of Advances, Marcel Dekker INC., New York, 2001. doi:10.1021/ja015236x.

[151] IUPAC, Recommendations for the characterization of porous solids, Pure Appl. Chem. 66 (1994) 1739–1758. doi:http://dx.doi.org/10.1351/pac199466081739.

[152] Dxdcarbon.com, Images of Activated Carbon, (2020). https://www.dxdcarbon.com/product-category/activated-carbon (accessed July 27, 2020).

[153] V. Karelid, G. Larsson, B. Bjorlenius, Pilot-scale removal of pharmaceuticals in municipal wastewaterComparison of granular and powdered activated carbon treatment atthree wastewater treatment plants.pdf, J. Environ. Manage. 193 (2017) 491–502. doi:doi.org/10.1016/j.jenvman.2017.02.042.

[154] N.H. Phan, S. Rio, C. Faur, L. Le Coq, P. Le Cloirec, T.H. Nguyen, Production of fibrous activated carbons from natural cellulose (jute, coconut) fibers for water treatment applications, Carbon N. Y. 44 (2006) 2569–2577. doi:10.1016/j.carbon.2006.05.048.

[155] C. Brasquet, P. Le Cloirec, Adsorption onto activated carbon fibers: Application to water and air treatments, Carbon N. Y. 35 (1997) 1307–1313. doi:10.1016/S0008-6223(97)00079-1.

[156] P. Le Cloirec, C. Brasquet, E. Subrenat, Adsorption onto fibrous activated carbon: Applications to water treatment, Energy and Fuels. 11 (1997) 331–336. doi:10.1021/ef9601430.

[157] T.A. Langston, R.D. Granata, Influence of nitric acid treatment time on the mechanical and surface properties of high-strength carbon fibers, J. Compos. Mater. 48 (2014) 259–276. doi:10.1177/0021998312470471.

[158] S. Manocha, Porous Carbon, Sadhan. 28 (2003) 335–348. doi:10.1016/B978-008044163-4/50007-3.

[159] P.L. Walker, Chemistry and physics of carbon: a series of advances, 2nd. editi, Dekker, New York, 1966.

[160] L. Quanming, Z. Wanxi, Study on PAN-based activated carbon fiber prepared by different activation methods, in: 2009 Asia-Pacific Power Energy Eng. Conf., 2009.

doi:10.1109/APPEEC.2009.4918829.

[161] G.G. Stavropoulos, A.A. Zabaniotou, Minimizing activated carbons production cost, Fuel Process. Technol. 90 (2009) 952–957. doi:10.1016/j.fuproc.2009.04.002.

[162] A. Celzard, A. Albiniak, M. Jasienko-Halat, J.F. Marêché, G. Furdin, Methane storage capacities and pore textures of active carbons undergoing mechanical densification, Carbon N. Y. 43 (2005) 1990–1999. doi:10.1016/j.carbon.2005.03.022.

[163] A. Sakoda, T. Nomura, M. Suzuki, Activated carbon membrane for waste treatments: Application to decolorization of coke furnace wastewater, Adsorption. 3 (1997) 93–98. doi:10.1007/bf01133010.

[164] S. Tiwari, J. Bijwe, Surface Treatment of Carbon Fibers - A Review, Procedia Technol. 14 (2014) 505–512. doi:10.1016/j.protcy.2014.08.064.

[165] M.K. Almutairi, R.A. Felemban, S.E. Pasha, The Effect of Different Surface Treatments of Carbon Fibers and Their Impact on Composites, Egypt. J. Hosp. Med. 70 (2018) 1275–1281. doi:10.12816/0044635.

[166] A.R. Yeddou, S. Chergui, A. Chergui, F. Halet, A. Hamza, B. Nadjemi, A. Ould-Dris, J. Belkouch, Removal of cyanide in aqueous solution by oxidation with hydrogen peroxide in presence of copper-impregnated activated carbon, Miner. Eng. 24 (2011) 788–793. doi:10.1016/j.mineng.2011.02.012.

[167] J.P. Chen, S. Wu, Simultaneous adsorption of copper ions and humic acid onto an activated carbon, J. Colloid Interface Sci. 280 (2004) 334–342. doi:10.1016/j.jcis.2004.08.029.

[168] S.L. Bazana, Q.L. Shimabuku-Biadola, F.S. Arakawa, R.G. Gomes, E.S. Cossich, R. Bergamasco, Modified activated carbon with silver–copper mixed oxides nanoparticles for removal of heavy metals from water, Int. J. Environ. Sci. Technol. 16 (2019) 6727–6734. doi:10.1007/s13762-019-02260-3.

[169] J. Wang, F. Zhao, Y. Hu, R. Zhao, R. Liu, Modification of activated carbon fiber by loading metals and their performance on SO2 removal, Chinese J. Chem. Eng. 14 (2006) 478–485. doi:10.1016/S1004-9541(06)60102-X.

[170] P. Jain, A. Kumar, N. Verma, R.K. Gupta, In-situ synthesis of TiO2 nanoparticles in ACF: Photocatalytic degradation under continuous flow, Sol. Energy. 189 (2019) 35–44. doi:10.1016/j.solener.2019.07.042.

[171] M. Bikshapathi, S. Singh, B. Bhaduri, G.N. Mathur, A. Sharma, N. Verma, Fe-nanoparticles dispersed carbon micro and nanofibers: Surfactant-mediated preparation and application to the removal of gaseous VOCs, Colloids Surfaces A Physicochem. Eng. Asp. 399 (2012) 46–55. doi:10.1016/j.colsurfa.2012.02.023.

[172] A. Chakraborty, D. Deva, A. Sharma, N. Verma, Adsorbents based on carbon microfibers and carbon nanofibers for the removal of phenol and lead from water, J. Colloid Interface Sci. 359 (2011) 228–239. doi:10.1016/j.jcis.2011.03.057.

[173] B.L.T. Lau, G.W. Harrington, M.A. Anderson, I. Tejedor, Removal of nano and microparticles by granular filter media coated with nanoporous aluminium oxide, Water Sci. Technol. 50 (2004) 223–228. doi:10.2166/wst.2004.0717.

[174] H. Le Pape, F. Solano-Serena, P. Contini, C. Devillers, A. Maftah, P. Leprat, Evaluation of the anti-microbial properties of an activated carbon fibre supporting silver using a dynamic method, Carbon N. Y. 40 (2002) 2947–2954. doi:10.1016/S0008-6223(02)00246-4.

[175] G. Nangmenyi, W. Xao, S. Mehrabi, E. Mintz, J. Economy, Bactericidal activity of Ag nanoparticle-impregnated fibreglass for water disinfection, J. Water Health. 7 (2009) 657–663. doi:10.2166/wh.2009.107.

[176] S. Singh, H.C. Joshi, A. Srivastava, A. Sharma, N. Verma, An efficient antibacterial multi-scale web of carbon fibers with asymmetrically dispersed Ag-Cu bimetal nanoparticles, Colloids Surfaces A Physicochem. Eng. Asp. 443 (2014) 311–319. doi:10.1016/j.colsurfa.2013.11.041.

[177] L.E. Murr, Handbook of Materials Structures, Springer Reference, 2015.

[178] H. Warlimont, W. Martienssen, Springer Handbook of Condensed Mater and Materials Data, Springer Berlin Heidelberg, Heidelberg, 2005.

[179] O. Madelung, Semiconductors: Data Handbook, 3rd ed., Springer, 2004. doi:10.1007/978-3-642-18865-7.

[180] N. Kallay, Z. Torbic, E. Barouch, The Determination of Isoelectric Point for Metalic Surfaces, Interface. 118 (1987).

[181] Q. Zhang, K. Zhang, D. Xu, G. Yang, H. Huang, F. Nie, C. Liu, S. Yang, CuO nanostructures: Synthesis, characterization, growth mechanisms, fundamental properties, and applications, Prog. Mater. Sci. (2014).

doi:10.1016/j.pmatsci.2013.09.003.

[182] C. Xiang, G.M. Kimball, R.L. Grimm, B.S. Brunschwig, H.A. Atwater, N.S. Lewis, 820 mV open-circuit voltages from Cu2O/CH3CN junctions, Energy Environ. Sci. 4 (2011) 1311–1318. doi:10.1039/c0ee00554a.

[183] M. O-Keeffe, Infrared Optical Properties of Cuprous Oxide, J. Phys. Chem. 39 (1963). doi:doi.org/10.1063/1.1734530.

[184] M. Kosmulski, Compilation of PZC and IEP of sparingly soluble metal oxides and hydroxides from literature, Adv. Colloid Interface Sci. 152 (2009) 14–25. doi:10.1016/j.cis.2009.08.003.

[185] R.D. Schmidt-Whitley, M. Martinez-Clemente, A. Revcolevschi, Growth and microstructural control of single crystal cuprous oxide Cu2O, J. Cryst. Growth. 23 (1974) 113–120. doi:10.1016/0022-0248(74)90110-9.

[186] I.T. Vargas, D.A. Fischer, M.A. Alsina, J.P. Pavissich, P. Pablo, G.E. Pizarro, Copper corrosion and biocorrosion events in premise plumbing, Materials (Basel). 10 (2017) 1–30. doi:10.3390/ma10091036.

[187] B. Beverskog, I. Puigdomenech, Revised Pourbaix Diagrams for Copper at 25 to 300°C, J. Electrochem. Soc. 144 (1997) 3476–3483.

[188] R. Dortwegt, E. V. Maughan, The chemistry of copper in water and related studies planned at the advanced photon source, in: Proc. IEEE Part. Accel. Conf., 2001: pp. 1456–1458. doi:10.1109/pac.2001.986712.

[189] J.P. Loveland, J.N. Ryan, G.L. Amy, R.W. Harvey, The reversibility of virus attachment to mineral surfaces, Colloids Surfaces A Physicochem. Eng. Asp. 107 (1996) 205–221. doi:10.1016/0927-7757(95)03373-4.

[190] World Health Organisation, pH in drinking-water, 2007. http://www.who.int/water_sanitation_health/dwq/chemicals/ph_revised_2007_clean_version.pdf.

[191] WHO, Copper in Drinking-water, WHO/SDE/WSH/03.04/88, 2004. doi:10.1111/1467-8292.00035.

[192] D. Bunderat, Wasser in öffentlich zugänglichen Bädern und Duschanlagen SR-Nummer 817.022.12, 2016. https://www.admin.ch/opc/de/classified-compilation/20143400/index.html.

[193] G. Ren, D. Hu, E.W.C. Cheng, M.A. Vargas-Reus, P. Reip, R.P. Allaker, Characterisation of copper oxide nanoparticles for antimicrobial applications, Int. J. Antimicrob. Agents. 33 (2009) 587–590. doi:10.1016/j.ijantimicag.2008.12.004.

[194] G. Grass, C. Rensing, M. Solioz, Metallic copper as an antimicrobial surface, Appl. Environ. Microbiol. 77 (2011) 1541–1547. doi:10.1128/AEM.02766-10.

[195] K.R. Wigginton, T. Kohn, Virus disinfection mechanisms: The role of virus composition, structure, and function, Curr. Opin. Virol. 2 (2012) 84–89. doi:10.1016/j.coviro.2011.11.003.

[196] A.M. Armstrong, M.D. Sobsey, L.M. Casanova, Disinfection of bacteriophage MS2 by copper in water, Appl. Microbiol. Biotechnol. 101 (2017) 6891–6897. doi:10.1007/s00253-017-8419-x.

[197] T.A. Dankovich, J.A. Smith, Incorporation of copper nanoparticles into paper for point-of-use water purification, Water Res. 63 (2014) 245–251. doi:10.1016/j.watres.2014.06.022.

[198] J.I. Nieto-Juarez, K. Pierzchla, A. Sienkiewicz, T. Kohn, Inactivation of MS2 coliphage in Fenton and Fenton-like systems: Role of transition metals, hydrogen peroxide and sunlight, Environ. Sci. Technol. 44 (2010) 3351–3356. doi:10.1021/es903739f.

[199] Z. Wang, A. Von Dem Bussche, P.K. Kabadi, A.B. Kane, R.H. Hurt, Biological and environmental transformations of copper-based nanomaterials, ACS Nano. 7 (2013) 8715–8727. doi:10.1021/nn403080y.

[200] S. Amram, M. Chevion, G. Czapski, Roles of Copper and O2 in the Radiation-Induced Inactivation of T7 Bacteriophage, Radiat. Reserach. 99 (1984) 562–572.

[201] S. Amram, J. Aronovitch, D. Godinger, C. M, G. Czapski, On the cytotoxicity of vitamin C and metal ions. A site-specific Fenton mechanism, Eur J Biochem. 137 (1983) 119–124. doi:doi: 10.1111/j.1432-1033.1983.tb07804.x.

[202] E. Lund, The Significance of Oxidation in Cheical Inactivation of Poliovirus, Arch. Ges. Virusforsch. 12 (1962). https://fdocuments.in/document/the-significance-of-oxidation-in-chemical-inactivation-of-poliovirus.html.

[203] M. Plastourgou, M.R. Hoffmann, Transformation and Fate of Organic Esters in Layered-Flow Systems: The Role of Trace Metal Catalysis, Environ. Sci. Technol. 18

(1984) 756–764. doi:10.1021/es00128a007.

[204] R. Martin, Y. Mariam, Interaction between metal ions and nucleic bases, nucleosides, and nucleotides in solution, in: Met. Ions Biol. Syst., Vol. 8, Sigel, H., Ed., Marcel Dekker, New York, 1979.

[205] D. Hutchinson, Metal chelators as potential antiviral agents, Antivir. Res. 5 (1985) 193–205. doi:doi: 10.1016/0166-3542(85)90024-5.

[206] K. Wong, A.R. Morgan, W. Paranchych, Controlled cleavage of phage R17 RNA within the virion by treatment with ascorbate and copper (II), Can. J. Biochem. 52 (1974) 950–958. doi:doi: 10.1139/o74-133.

[207] J. Rifkind, Y. Shin, J. Heim, G. Eichhorn, Cooperative disordering of single-stranded polynucleotides through copper crosslinking, Biopolymers. 15 (1976) 1879–1902. doi:doi: 10.1002/bip.1976.360151002.

[208] C. Zimmer, G. Luck, H. Fritzsche, H. Triebel, DNA-copper (II) complex and the DNA conformation, Bio. 10 (1971) 441–463. doi:doi: 10.1002/bip.360100303.

[209] J. Huff, K. Sastry, M. Gordon, Wacker W., The action of metal ions on tabacco mosaic virus ribonucleic acid, Biochemistry. 3 (1964) 501–506. doi:doi: 10.1021/bi00892a006.

[210] C. Tien, Adsorption Calculations and Modelling, Butterworth-Heinemann, 1994. doi:10.1016/B978-0-7506-9121-5.50001-X.

[211] L. Liu, X.B. Luo, L. Ding, S.L. Luo, Chapter 4 - Application of Nanotechnology in the Removal of Heavy Metal From Water, in: Nanomater. Remov. Pollut. Resour. Reutil., In Micro a, Elsevier Inc., 2019: pp. 83–147. doi:10.1016/B978-0-12-814837-2.00004-4.

[212] D. Evans, H. Wennerstrom, The Colloidal Domain: Where Physics, Chemistry, Biology and Technology Meet, 2nd ed., Willey-VCH, 1999.

[213] S. Biniak, M. Pakuła, G.S. Szymański, A. Świątkowski, Effect of activated carbon surface oxygen- and/or nitrogen-containing groups on adsorption of copper(II) ions from aqueous solution, Langmuir. 15 (1999) 6117–6122. doi:10.1021/la9815704.

[214] C. Moreno-Castilla, M.A. Ferro-García, J.P. Joly, I. Bautista-Toledo, F. Carrasco-Marín, J. Rivera-Utrilla, Activated Carbon Surface Modifications by Nitric Acid, Hydrogen Peroxide, and Ammonium Peroxydisulfate Treatments, Langmuir. 11 (1995) 4386–4392. doi:10.1021/la00011a035.

[215] C. Baes, R. Mesmer, The hydrolysis of cations, John Wiley & Sons, New York, 1976.

[216] C.P. Gerba, W.Q. Betancourt, Viral Aggregation: Impact on Virus Behavior in the Environment, Environ. Sci. Technol. 51 (2017) 7318–7325. doi:10.1021/acs.est.6b05835.

[217] J.M. Mazurkow, N.S. Yüzbasi, K.W. Domagala, S. Pfeiffer, D. Kata, T. Graule, Nano-Sized Copper (Oxide) on Alumina Granules for Water Filtration: Effect of Copper Oxidation State on Virus Removal Performance, Environ. Sci. Technol. 54 (2020) 1214–1222. doi:10.1021/acs.est.9b05211.

[218] S. Kang, M. Herzberg, D.F. Rodrigues, M. Elimelech, Antibacterial effects of carbon nanotubes: Size does matter!, Langmuir. 24 (2008) 6409–6413. doi:10.1021/la800951v.

[219] D. Sano, R.M. Pintó, T. Omura, A. Bosch, Detection of oxidative damages on viral capsid protein for evaluating structural integrity and infectivity of human norovirus, Environ. Sci. Technol. 44 (2010) 808–812. doi:10.1021/es9018964.

[220] G. Gelardi, R.J. Flatt, Working mechanisms of water reducers and superplasticizers, Elsevier Ltd, 2016. doi:10.1016/B978-0-08-100693-1.00011-4.

[221] H. Malte, The DLVO theory in microbial adhesion, Colloids Surfaces B Biointerfaces. 14 (1999) 105–119. http://www.sciencedirect.com/science/article/pii/S0927776599000296.

[222] J. Israelachvili, Intermolecular and Surface Forces, 3rd ed., Academic Press, 2011. doi:https://doi.org/10.1016/B978-0-12-375182-9.10025-9.

[223] F.L. Leite, C.C. Bueno, A.L. Da Róz, E.C. Ziemath, O.N. Oliveira, Theoretical models for surface forces and adhesion and their measurement using atomic force microscopy, Int. J. Mol. Sci. 13 (2012) 12773–12856. doi:10.3390/ijms131012773.

[224] P.S. Sit, Studying molecular-scale protein-surface interactions in biomaterials, in: Charact. Biomater., Woodhead Publishing, 2012: pp. 182–223. doi:10.1533/9780857093684.182.

[225] A.K. Da Silva, O. V. Kavanagh, M.K. Estes, M. Elimelech, Adsorption and aggregation properties of norovirus GI and GII virus-like particles demonstrate differing responses to solution chemistry, Environ. Sci. Technol. 45 (2011) 520–526. doi:10.1021/es102368d.

[226] J.A. Redman, S.B. Grant, T.M. Olson, M.E. Hardy, M.K. Estes, Filtration of recombinant norwalk virus particles and bacteriophage MS2 in quartz sand: Importance of electrostatic interactions, Environ. Sci. Technol. 31 (1997) 3378–3383. doi:10.1021/es961071u.

[227] K. Domagala, M. Borlaf, J. Traber, D. Kata, T. Graule, Purification and Functionalisation of Multi-Walled Carbon Nanotubes, Mater. Lett. 253 (2019) 272–275. doi:doi.org/10.1016/j.matlet.2019.06.085.

[228] G. Zhang, S. Sun, D. Yang, J.P. Dodelet, E. Sacher, The surface analytical characterization of carbon fibers functionalized by H2SO4/HNO3 treatment, Carbon N. Y. 46 (2008) 196–205. doi:10.1016/j.carbon.2007.11.002.

[229] A. Cuesta, P. Dhamelincourt, J. Laureyns, A. Martínez-Alonso, J.M.D. Tascón, Raman microprobe studies on carbon materials, Carbon N. Y. 32 (1994) 1523–1532. doi:10.1016/0008-6223(94)90148-1.

[230] E. Stupnisek-Lisac, M. Karsulin, H. Takenouti, Passivation of Iron, Nickel and Cobalt in Concentrated Nitric Acid Solutions, in: Passiv. Met. Semicond., 2013. doi:10.1016/b978-0-444-42252-1.50054-0.

[231] H.H. Uhlig, T.L. O'Connor, Nature of the Passive Film on Iron in Concentrated Nitric Acid, J. Electrochem. Soc. (2007). doi:10.1149/1.2429913.

[232] M. V. Lopez-Ramon, F. Stoeckli, C. Moreno-Castilla, F. Carrasco-Marin, On the characterization of acidic and basic surface sites on carbons by various techniques, Carbon N. Y. 37 (1999) 1215–1221. doi:10.1016/S0008-6223(98)00317-0.

[233] M.A. Salam, M.S.I. Makki, M.Y.A. Abdelaal, Preparation and characterization of multi-walled carbon nanotubes/chitosan nanocomposite and its application for the removal of heavy metals from aqueous solution, J. Alloys Compd. 509 (2011) 2582–2587. doi:10.1016/j.jallcom.2010.11.094.

[234] L. Wang, N. Liu, Z. Guo, D. Wu, W. Chen, Z. Chang, Q. Yuan, M. Hui, J. Wang, Nitric acid-treated carbon fibers with enhanced hydrophilicity for Candida tropicalis immobilization in xylitol fermentation, Materials (Basel). 9 (2016). doi:10.3390/ma9030206.

[235] Z. Wu, C.U. Pittman, S.D. Gardner, Nitric acid oxidation of carbon fibers and the effects of subsequent treatment in refluxing aqueous NaOH, Carbon N. Y. 33 (1995) 597–605. doi:10.1016/0008-6223(95)00145-4.

[236] M.M. Mesquita, M. Emelko, Bacteriophages as Surrogates for the Fate and Transport of Pathogens in Source Water and in Drinking Water Treatment Processes, Bacteriophages. (2012). doi:10.5772/34024.

[237] IAWPRCStudyGroup, Bacteriophages as model viruses in water quality control, Water Res. 25 (1991) 529–545. doi:10.1016/0043-1354(91)90126-B.

[238] B. Michen, F. Meder, A. Rust, J. Fritsch, C. Aneziris, T. Graule, Virus removal in ceramic depth filters based on diatomaceous earth, Environ. Sci. Technol. 46 (2012) 1173–1177. doi:10.1021/es2030565.

[239] EPA, Method 1602 : Male-specific (F+) and Somatic Coliphage in Water by Single Agar Layer (SAL) Procedure April 2001. EPA Document 821-R-01-029, 2001.

[240] S. Tanuma, C.J. Powell, D.R. Penn, Calculations of electron inelastic mean free paths. V. Data for 14 organic compounds over the 50–2000 eV range, Surf. Interface Anal. 21 (1994) 165–176. doi:https://doi.org/10.1002/sia.740210302.

[241] J.A. Leiro, M.H. Heinonen, T. Laiho, J.G. Baitrev, Core-level XPS spectra of fullerene, highly oriented pyrolitic graphite, and glassy carbon, J. Electron Spectrosc. Relat. Phenom. 128 (2003) 205–213.

[242] A. Yoshida, I. Tanahashi, A. Nishino, Effect of concentration of surface acidic functional groups on electric double-layer properties of activated carbon fibers, Carbon N. Y. 28 (1990) 611–615. doi:10.1016/0008-6223(90)90062-4.

[243] A.M. Oickle, S.L. Goertzen, K.R. Hopper, Y.O. Abdalla, H.A. Andreas, Standardization of the Boehm titration: Part II. Method of agitation, effect of filtering and dilute titrant, Carbon N. Y. (2010). doi:10.1016/j.carbon.2010.05.004.

[244] S.L. Goertzen, K.D. Thériault, A.M. Oickle, A.C. Tarasuk, H.A. Andreas, Standardization of the Boehm titration. Part I. CO2 cexpulsion and endpoint determination, Carbon N. Y. 48 (2010) 1252–1261. doi:10.1016/j.carbon.2009.11.050.

[245] M. Voll, H.P. Boehm, Basische Oberflächenoxide auf Kohlenstoff-IV. Chemische Reaktionen zur Identifizierung der Oberflächengruppen, Carbon N. Y. 9 (1971) 481–488. doi:10.1016/0008-6223(71)90028-5.

[246] H.P. Boehm, Some aspects of the surface chemistry of carbon blacks and other carbons, Carbon N. Y. 32 (1994) 759–469. doi:10.1016/0008-6223(94)90031-0.

[247] J. Schönherr, J. Buchheim, P. Scholz, P. Adelhelm, Boehm Titration Revisited (Part

II): A Comparison of Boehm Titration with Other Analytical Techniques on the Quantification of Oxygen-Containing Surface Groups for a Variety of Carbon Materials, J. Carbon Res. 4 (2018). doi:10.3390/c4020022.

[248] J.M. Solar, C.A. Leon, K. Osseo-Asare, L.R. Radovic, On the importance of the electrokinetic properties of carbons for their use as catalyst supports, Carbon N. Y. 28 (1990) 369–375. doi:10.1016/0008-6223(90)90010-V.

[249] A.C. Lau, D.N. Furlong, T.W. Healy, F. Grieser, The electrokinetic properties of carbon black and graphitized carbon black aqueous colloids, Colloids and Surfaces. 18 (1986) 93–104. doi:10.1016/0166-6622(86)80196-2.

[250] S. Brunauer, P.H. Emmett, E. Teller, Adsorption of Gases in Multimolecular Layers, J. Am. Chem. Soc. 60 (1938) 309–319. doi:10.1021/ja01269a023.

[251] I. Langmuir, The constitution and fundamental properties of solids and liquids. Part I. Solids, J. Am. Chem. Soc. 38 (1916) 2221–2295. doi:10.1021/ja02268a002.

[252] M.M. Dubinin, Microporous Structures and Absorption, Carbon N. Y. 21 (1983) 359–366.

[253] J. Garrido, A. Linares-solano, J.M. Martìn-Martìnez, M. Molina-Sabio, F. Rodrìguez-Reinoso, R. Torregrosa, Use of N2 vs CO2 in the Characterization of Activated Carbons, Langmuir. 3 (1987) 76–81. doi:10.1021/la00073a013.

[254] A.L. Patterson, The scherrer formula for X-ray particle size determination, Phys. Rev. 56 (1939) 978–982. doi:10.1103/PhysRev.56.978.

[255] L.S. Oliveira, J.F.G. Alba, V.L. Silva, R.T. Ribeiro, E.H.L. Falcão, M. Navarro, The effect of surface functional groups on the performance of graphite powders used as electrodes, J. Electroanal. Chem. 818 (2018) 106–113. doi:10.1016/j.jelechem.2018.04.022.

[256] H. Wu, W. Lu, Y. Chen, P. Zhang, X. Cheng, Application of Boehm Titration for the Quantitative Measurement of Soot Oxygen Functional Groups, Energy & Fuels. 34 (2020) 7363–7372. doi:10.1021/acs.energyfuels.0c00904.

[257] H.O. Rike Yudianti, Lucia Indrarti, Thermal Behavior of Purified Multi Walled Carbon Nanotube, J. Appl. Sci. 10 (2010) 1978–1982. doi:10.3923/jas.2010.1978.1982.

[258] M. Chen, H.W. Yu, J.H. Chen, H.S. Koo, Effect of purification treatment on adsorption characteristics of carbon nanotubes, Diam. Relat. Mater. 16 (2007) 1110–1115.

doi:10.1016/j.diamond.2006.12.061.

[259] J.-S. Roh, Structural Study of the Activated Carbon Fiber using Laser Raman Spectroscopy, Carbon Lett. 9 (2008) 127–130. doi:10.5714/cl.2008.9.2.127.

[260] A.C. Ferrari, S.E. Rodil, J. Robertson, S.E. Rodil, J. Robertson, Interpretation of infrared and Raman spectra of amorphous carbon nitrides, Phys. Rev. B - Condens. Matter Mater. Phys. 67 (2003) 1–20. doi:10.1103/PhysRevB.67.155306.

[261] S. Osswald, M. Havel, Y. Gogotsi, Monitoring oxidation of multiwalled carbon nanotubes by Raman spectroscopy, J. Raman Spectrosc. (2007). doi:10.1002/jrs.1686.

[262] P. Puech, M. Kandara, G. Paredes, L. Moulin, E. Weiss-Hortala, A. Kundu, N. Ratel-Ramond, Plewa. J. M., R. Pellenq, M. Monthioux, Analyzing the Raman Spectra of Graphenic Carbon Materials from Kerogens to Nanotubes: What Type of Information Can Be Extracted from Defect Bands?, C J. Carbon Res. 5 (2019). doi:10.3390/c5040069.

[263] A. Lazzarini, A. Piovano, R. Pellegrini, G. Leofanti, G. Agostini, S. Rudić, M.R. Chierotti, R. Gobetto, A. Battiato, G. Spoto, A. Zecchina, C. Lamberti, E. Groppo, A comprehensive approach to investigate the structural and surface properties of activated carbons and related Pd-based catalysts, Catal. Sci. Technol. 6 (2016) 4910–4922. doi:10.1039/c6cy00159a.

[264] N. Iwashita, C.R. Park, H. Fujimoto, M. Shiraishi, M. Inagaki, Specification for a standard procedure of X-ray diffraction measurements on carbon materials, Carbon N. Y. 42 (2004) 701–714. doi:10.1016/j.carbon.2004.02.008.

[265] I.Y. Stein, A.J. Constable, N. Morales-Medina, C. V. Sackier, M.E. Devoe, H.M. Vincent, B.L. Wardle, Structure-mechanical property relations of non-graphitizing pyrolytic carbon synthesized at low temperatures, Carbon N. Y. 117 (2017) 411–420. doi:10.1016/j.carbon.2017.03.001.

[266] Y. Otake, R.G. Jenkins, Characterization of oxygen-containing surface complexes created on a microporous carbon by air and nitric acid treatment, Carbon N. Y. 31 (1993) 109–121. doi:10.1016/0008-6223(93)90163-5.

[267] J.J. Ternero-Hidalgo, J.M. Rosas, J. Palomo, M.J. Valero-Romero, J. Rodríguez-Mirasol, T. Cordero, Functionalization of activated carbons by HNO3 treatment: Influence of phosphorus surface groups, Carbon N. Y. 101 (2016) 409–419. doi:10.1016/j.carbon.2016.02.015.

[268] P. Chingombe, B. Saha, R.J. Wakeman, Surface modification and characterisation of a coal-based activated carbon, Carbon N. Y. 43 (2005) 3132–3143. doi:10.1016/j.carbon.2005.06.021.

[269] P. Vinke, M. van der Eijk, M. Verbree, A.F. Voskamp, H. van Bekkum, Modification of the surfaces of a gasactivated carbon and a chemically activated carbon with nitric acid, hypochlorite, and ammonia, Carbon N. Y. 32 (1994) 675–686. doi:10.1016/0008-6223(94)90089-2.

[270] B. Xiao, K.M. Thomas, Adsorption of aqueous metal ions on oxygen and nitrogen functionalized nanoporous activated carbons, Langmuir. 21 (2005) 3892–3902. doi:10.1021/la047135t.

[271] A.N.A. El-Hendawy, Influence of HNO3 oxidation on the structure and adsorptive properties of corncob-based activated carbon, Carbon N. Y. 41 (2003) 713–722. doi:10.1016/S0008-6223(03)00029-0.

[272] B.K. Kim, S.K. Ryu, B.J. Kim, S.J. Park, Adsorption behavior of propylamine on activated carbon fiber surfaces as induced by oxygen functional complexes, J. Colloid Interface Sci. 302 (2006) 695–697. doi:10.1016/j.jcis.2006.07.028.

[273] M.A. Álvarez-Merino, V. López-Ramón, C. Moreno-Castilla, A study of the static and dynamic adsorption of Zn(II) ions on carbon materials from aqueous solutions, J. Colloid Interface Sci. 288 (2005) 335–341. doi:10.1016/j.jcis.2005.03.025.

[274] J. Jang, H. Yang, Effect of surface treatment on the performance improvement of carbon fiber/polybenzoxazine composites, J. Mater. Sci. 35 (2000) 2297–2303. doi:10.1023/A:1004791313979.

[275] C. Moreno-Castilla, F. Carrasco-Marín, F.J. Maldonado-Hódar, J. Rivera-Utrilla, Effects of non-oxidant and oxidant acid treatments on the surface properties of an activated carbon with very low ash content, Carbon N. Y. 36 (1998) 145–151. doi:10.1016/S0008-6223(97)00171-1.

[276] J. Wang, Z. Li, S. Li, W. Qi, P. Liu, F. Liu, Y. Ye, L. Wu, L. Wang, W. Wu, Adsorption of Cu(II) on Oxidized Multi-Walled Carbon Nanotubes in the Presence of Hydroxylated and Carboxylated Fullerenes, PLoS One. 8 (2013). doi:10.1371/journal.pone.0072475.

[277] X. Wang, F. Zhang, B. Xia, X. Zhu, J. Chen, S. Qiu, P. Zhang, J. Li, Controlled modification of multi-walled carbon nanotubes with CuO, Cu2O and Cu nanoparticles,

Solid State Sci. 11 (2009) 655–659. doi:10.1016/j.solidstatesciences.2008.10.009.

[278] V. Lyklema, Electric double layers, in: Fundam. Interface Colloid Sci., Academic Press, 1995. doi:10.1016/S1874-5679(06)80006-1.

[279] Y.F. Jia, K.M. Thomas, Adsorption of cadmium ions on oxygen surface sites in activated carbon, Langmuir. 16 (2000) 1114–1122. doi:10.1021/la990436w.

[280] C.A. Toles, W.E. Marshall, M.M. Johns, Surface functional groups on acid-activated nutshell carbons, Carbon N. Y. 37 (1999) 1207–1214. doi:10.1016/S0008-6223(98)00315-7.

[281] Ö. Yavuz, Y. Altunkaynak, F. Güzel, Removal of copper, nickel, cobalt and manganese from aqueous solution by kaolinite, Water Res. 37 (2003) 948–952. doi:10.1016/S0043-1354(02)00409-8.

[282] I. Persson, Hydrated metal ions in aqueous solution: How regular are their structures?, Pure Appl. Chem. 82 (2010) 1901–1917. doi:10.1351/PAC-CON-09-10-22.

[283] J.Y. Kim, J.A. Rodriguez, J.C. Hanson, A.I. Frenkel, P.L. Lee, Reduction of CuO and Cu2O with H2: H embedding and kinetic effects in the formation of suboxides, J. Am. Chem. Soc. 125 (2003) 10684–10692. doi:10.1021/ja0301673.

[284] V. Bernal, L. Giraldo, J. Moreno-Piraján, Physicochemical Properties of Activated Carbon: Their Effect on the Adsorption of Pharmaceutical Compounds and Adsorbate–Adsorbent Interactions, J. Carbon Res. 4 (2018). doi:10.3390/c4040062.

[285] G. De La Puente, J.J. Pis, J.A. Menéndez, P. Grange, Thermal stability of oxygenated functions in activated carbons, J. Anal. Appl. Pyrolysis. 43 (1997) 125–138. doi:10.1016/S0165-2370(97)00060-0.

[286] R. Álvarez-Fernández García, M. Corte-Rodríguez, M. Macke, K.L. Leblanc, Z. Mester, M. Montes-Bayón, J. Bettmer, Addressing the presence of biogenic selenium nanoparticles in yeast cells: Analytical strategies based on ICP-TQ-MS, Analyst. 145 (2020) 1457–1465. doi:10.1039/c9an01565e.

[287] K. Domagala, C. Jacquin, M. Borlaf, B. Sinnet, T. Julian, D. Kata, T. Graule, Efficiency and stability evaluation of Cu2O / MWCNTs filters for virus removal from water, Water Res. 179 (2020) 115879. doi:10.1016/j.watres.2020.115879.

[288] S.S. Poulsen, P. Jackson, K. Kling, K.B. Knudsen, V. Skaug, Z.O. Kyjovska, B.L. Thomsen, P.A. Clausen, R. Atluri, T. Berthing, S. Bengtson, H. Wolff, K.A. Jensen, H.

Wallin, U. Vogel, Multi-walled carbon nanotube physicochemical properties predict pulmonary inflammation and genotoxicity, Nanotoxicology. 10 (2016) 1263–1275. doi:10.1080/17435390.2016.1202351.

[289] S.S. Poulsen, A.T. Saber, A. Williams, O. Andersen, C. Købler, R. Atluri, M.E. Pozzebon, S.P. Mucelli, M. Simion, D. Rickerby, A. Mortensen, P. Jackson, Z.O. Kyjovska, K. Mølhave, N.R. Jacobsen, K.A. Jensen, C.L. Yauk, H. Wallin, S. Halappanavar, U. Vogel, MWCNTs of different physicochemical properties cause similar inflammatory responses, but differences in transcriptional and histological markers of fibrosis in mouse lungs, Toxicol. Appl. Pharmacol. 284 (2015) 16–32. doi:10.1016/j.taap.2014.12.011.

[290] H.Y. Jing, T. Wen, C.M. Fan, G.Q. Gao, S.L. Zhong, A.W. Xu, Efficient adsorption/photodegradation of organic pollutants from aqueous systems using Cu2O nanocrystals as a novel integrated photocatalytic adsorbent, J. Mater. Chem. A. 2 (2014) 14563–14570. doi:10.1039/c4ta02459a.

[291] H. Babich, G. Stotzky, H.L. Ehrlich, Environmental factors that influence the toxicity of heavy metal and gaseous pollutants to microorganisms, Crit. Rev. Microbiol. 8 (1980) 99–145. doi:10.3109/10408418009081123.

[292] L. Xiong, H. Yu, C. Nie, Y. Xiao, Q. Zeng, G. Wang, B. Wang, H. Lv, Q. Li, S. Chen, Size-controlled synthesis of Cu2O nanoparticles: Size effect on antibacterial activity and application as a photocatalyst for highly efficient H2O2 evolution, RSC Adv. 7 (2017) 51822–51830. doi:10.1039/c7ra10605j.

[293] R.C. Bales, S.R. Hinkle, T.W. Kroeger, K. Stocking, C.P. Gerba, Bacteriophage Adsorption during Transport through Porous Media: Chemical Perturbations and Reversibility, Environ. Sci. Technol. 25 (1991) 2088–2095. doi:10.1021/es00024a016.

[294] N. Winter, J. Vieceli, I. Benjamin, Hydrogen-bond structure and dynamics at the interface between water and carboxylic acid-functionalized self-assembled monolayers, J. Phys. Chem. B. 112 (2008) 227–231. doi:10.1021/jp0734833.

[295] C. Lim, J. Ko, D. Jeon, Y. Song, J. Park, J. Ryu, D.W. Lee, Probing molecular mechanisms of M13 bacteriophage adhesion, Commun. Chem. 2 (2019) 1–9. doi:10.1038/s42004-019-0198-0.

[296] T. Thamaraiselvi, S. Rajeswari, Biological evaluation of bioceramic materials-a review, Carbon N. Y. 24 (2004) 172.

[297] R.C. Bales, S. Li, K.M. Maguire, M.T. Yahya, C.P. Gerba, MS2 and Poliovirus transport in porous media: Hydrophobic effects and chemical perturbations, Water Resour. Res. 29 (1993) 957–963. doi:10.1029/92WR02986.

[298] B.E. Fischer, U.K. Haering, R. Tribolet, H. Sigel, Metal Ion /Buffer Interactions Stability of Binary and Ternary Complexes Containing 2-amino-2(hydroxymethyl)-1,3-propanediol (Tris) and Adenosine 5`-Triphosphate (ATP), Eur. J. Biochem. 94 (1979) 523–530. doi:doi.org/10.1111/j.1432-1033.1979.tb12921.x.

[299] V. Cagno, P. Andreozzi, M. D'Alicarnasso, P.J. Silva, M. Mueller, M. Galloux, R. Le Goffic, S.T. Jones, M. Vallino, J. Hodek, J. Weber, S. Sen, E.R. Janecek, A. Bekdemir, B. Sanavio, C. Martinelli, M. Donalisio, M.A.R. Welti, J.F. Eleouet, Y. Han, L. Kaiser, L. Vukovic, C. Tapparel, P. Král, S. Krol, D. Lembo, F. Stellacci, Broad-spectrum non-toxic antiviral nanoparticles with a virucidal inhibition mechanism, Nat. Mater. 17 (2018) 195–203. doi:10.1038/NMAT5053.

[300] T.R. Holm, Copper complexation by natural organic matter in contaminated and uncontaminated ground water, Chem. Speciat. Bioavailab. 2 (1990) 63–76. doi:10.1080/09542299.1990.11083126.

[301] J.D. Hem, Study and interpretation of the chemical characteristics of natural water, 3rd ed., US Geological Survey Water-Supply Paper, Alexandria, 1985.

[302] K. Kendall, M. Kendall, F. Rehfeldt, Adhesion of Cells, Viruses and Nanoparticles, 1st ed., Dordrecht: Springer Netherland, Web, 2011. doi:10.1007/978-90-481-2585-2_8.